The University Of Sheffield.

Proposed Framework of Building Nonlinear Models: A Study using the Bouc-Wen Hysteretic Model

By:

Anas Mohd Mustafah

A thesis submitted in partial fulfilment of the requirements for the degree of Doctor of Philosophy

The University of Sheffield

Faculty of Engineering

Department of Mechanical Engineering

30 September 2016

In the name of Allah, the Most Gracious, the Most Merciful

Abstract

Nonlinear models are useful tools in current engineering practice for benefits such as cost savings and improved safety features, especially for testing, designing and maintenance of engineering services. Such models have been widely used for understanding the physics of systems and structures, predictions of abnormalities, predictions of specific scenarios to enable control and for planning of production. Having the correct fit-for-purpose model is very important for the model to be utilised in any of the functions as required, which enables accurate understanding and predictions of the real system to be modelled.

The work presented in this thesis is concerned with proposing a framework for building a fit-for-purpose nonlinear model using the Bouc-Wen model of hysteresis as an example nonlinear model to be identified.

The proposed framework is presented with steps suggested for the understanding of the requirements and purpose of building a nonlinear model. This is the main idea of the thesis where sufficient initial understanding of a problem will lead to experimental design to be able to provide the right sets of data to fit the purpose of the model to be built.

Using a variant of the Differential Evolution algorithm, the inputs of data sets for identification or parameter estimation were investigated. The investigation compared the input magnitudes, input types and noise levels to show that the result of identification can be misleading without a real understanding of the model requirements. This shows the importance of the specification of model requirements suggested in the framework. A measure of Improvement Ratio is also suggested to improve confidence of nonlinear parameter estimation by way of evaluation against linear parameter estimates.

Finally, a Volterra series approximation method for nonlinear polynomial models is used to estimate the parameters of the Bouc-Wen hysteretic model. It is shown that only linear parameters can be identified accurately in the presence of noise. Another key finding relates the nonlinear parameters to parameters of a nonlinear polynomial model to show some physical resemblance to the nonlinear polynomial damping and stiffness term, further work is required to truly understand this.

Acknowledgements

The author would like to express his thanks to the following people for their support during this research:

Dr Graeme Manson, my brilliant supervisor. For his enthusiasm, ideas and support that has provided me with direction and allowed me to complete the research. My sincere thanks for all the guidance and knowledge that he has shared with me during the research.

My wife and children for their full support and understanding during the good and difficult times, and for believing in me and giving me the drive to fulfil this dream. To my Mother and Father for their support, advice and help throughout my study. To all my family for their continuous support, love and belief in me. For always being there by my side through all the ups and downs. I love you all.

Fellow friends and colleagues in Sheffield, Malaysia and everywhere else that have shared this journey with me.

University Putra Malaysia and Kementerian Pelajaran Tinggi Malaysia that sponsored me for the duration of this research and for giving me the chance to start my career in academia.

Table of Contents

Chapter 1

1 Proposed Framework for Building Nonlinear Models

1.1 Introduction

Nonlinear models are useful tools in the current engineering practice for benefits such as cost savings and improved safety features, especially for testing, designing and maintenance of engineering services. Such models have been widely used for understanding the physics of systems and structures, predictions of abnormalities, predictions of specific scenarios to enable control and for planning of production. Having the correct fit-for-purpose model is very important for the model to be utilized in any of the functions as required, which enables accurate understanding and predictions of the real system to be modelled.

A proposed framework for building a nonlinear model is presented here to show the steps involved in nonlinear model building. This thesis is concerned with the fitness for purpose of model building with a focus on the parameter estimation stage. The fitness for purpose presented here emphasises having the right level and types of input corresponding to the intended use of the model. This stems from

acknowledgement of the linearisation effect in a nonlinear system due to lack of forcing that may contribute to misleading nonlinear parameter estimates which would desensitise on the nonlinear parameter accuracy.

In this chapter, firstly a brief introduction to the purpose of nonlinear model building is presented. Then a proposed framework of building a nonlinear model is given followed by a brief explanation of each stage. Next the objectives of the thesis are given. Finally a summary of the following chapters is presented.

1.2 **Why is a computational model built?**

In July 1945, the first nuclear weapon atmospheric testing was conducted by the United States. Following that first event, more nuclear weapons testing was conducted via atmospheric testing, underwater testing, exoatmospheric testing and underground testing. The last known field testing was undertaken in 2006 by North Korea who has not signed the treaty calling for cessation of testing of nuclear weapons [1]. Figure 1.1 shows the number of nuclear weapon that are known by country [2]. The first three types of test were known to emit radioactive fallout causing harm to humans and nearby living things. Although these tests were usually done in isolated areas away from populations, atmospheric testing produces irradiated dust and debris which can be carried away to populated areas. Similarly, underwater testing causes damage to the underwater ecosystem and can irradiate ships and structures above water although not on a huge scale. Exoatmospheric testing causes a nuclear electromagnetic pulse which can penetrate back into the hemisphere. These tests were first banned in a treaty in 1963 signed by the United States, the United Kingdom and the Soviet Union, although some countries still continue to conduct such tests. China and France joined in to sign the treaty in 1996 to cease nuclear weapon testing. Underground testing was deemed to be the safest method and was not banned. However, when conducted near the surface, radiation still leaks above ground and still results in radiation harm.

Non-full scale testing and computational modelling of nuclear weapons now has taken over most of the testing conducted on nuclear weapons. For example, France who only indefinitely halted real

nuclear weapon testing in 1996 relies on simulation to maintain the reliability, safety and performance of the country's nuclear weapons [3]. The computational modelling still achieves the purpose of ensuring the performance of nuclear weapons whilst avoiding harmful live nuclear testing. Numerical models and simulation can be compared to data from past test for result validation.

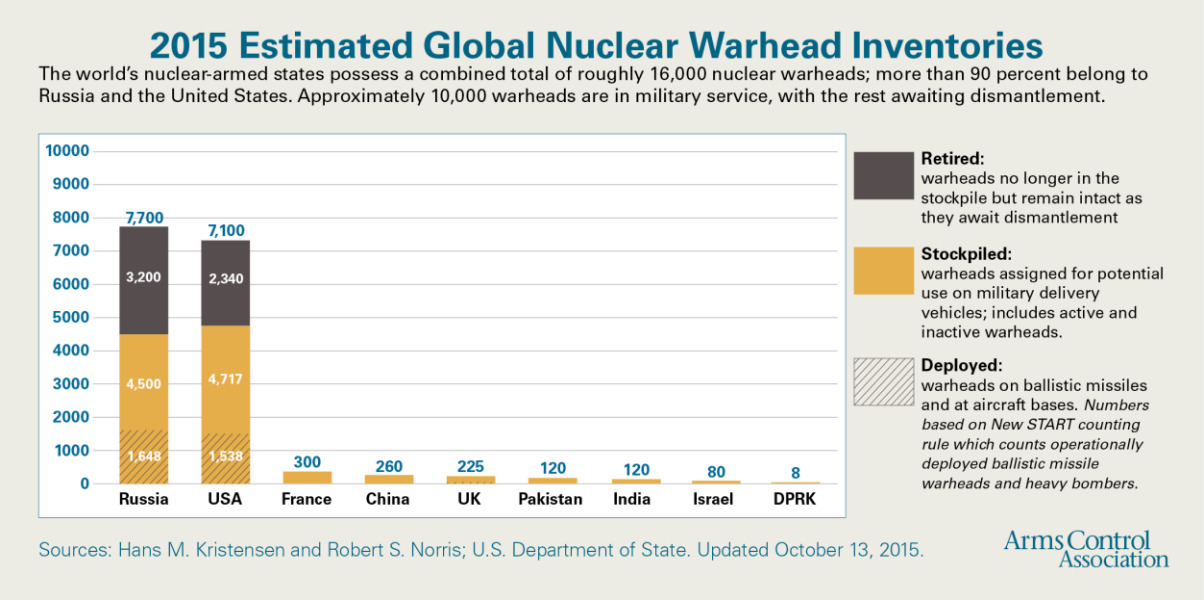

Figure 1.1: Nuclear warhead inventories by country [2]

In the aircraft industries, from initial design to being in service, a jet engine can cost almost a billion pounds. In engineering, to test a material and its design behaviour and efficiency can cost a huge amount of money. For example, it would be very costly to build an engine, test and rebuild it over and over. This is where computational modelling is useful to predict the behaviour and to analyse the designs of these expensive materials. With a model, various simulations can be performed to investigate its reliability, performance and any issues. It can also be used to simulate failures without having to destroy the actual product. For example, the Airbus A380 uses computational models to understand the dynamics and simulation of its wings, operational cost and efficiency of the whole aircraft and the design of the fuel management systems [4].

The two examples above show that computational models are a useful tool. With models, a significant cost reduction can be achieved and hazardous testing can be made safe. With the use of models, the

prediction of a system can be done without having to disturb the process or to stop the work of the actual real system or plant.

By having accurate models to represent these experiments and tests, stake holders can avoid having to face problems with cost, damage and safety issues. Data can be collected during the actual operation of a system. Models representing the whole system can be built using the collected data of the system. Simulations using the computational models representing the system can then be used to predict the behaviour and to monitor the condition of the system as required.

Generally the objectives of building models are:

- to understand the physics of a system or structure
- to identify nonlinearity
- to predict specific scenarios
- to predict damage, abnormalities or failure of systems
- to plan for future productions
- to simulate extreme events on a system

Models that have been properly established can be used for the tasks below as illustrated in Figure 1.2 [5]. In the figure, it can be seen that models can either be used to predict, simulate or optimise responses with input-output introduced to the model. This is done without comparison to any true system response. Models can also be used by comparing with a control true system to analyse the model performance, to be used as a control for a process or to detect fault when the model response shows an output response other than the expected nominal response.

Current advances in computer technologies have given engineers the ability to model very complex systems. Other than engineering applications, computational biologists have created many models of the human anatomy to study disease control and to understand the biomechanical functions of the human body. Although the computational cost and time is very high, the results obtained are still worth the time and effort. Other biological models have looked at animal motion and behavioural patterns, and also insect anatomy including the brain functions [6].

When first introduced, a weather model required six-weeks of calculation to produce a six-hour weather pattern in 1920 [7]. Current practice had been able to include much more input information such as physical processes, statistical relations between prediction and real weather patterns, and can predict much farther into the future [8].

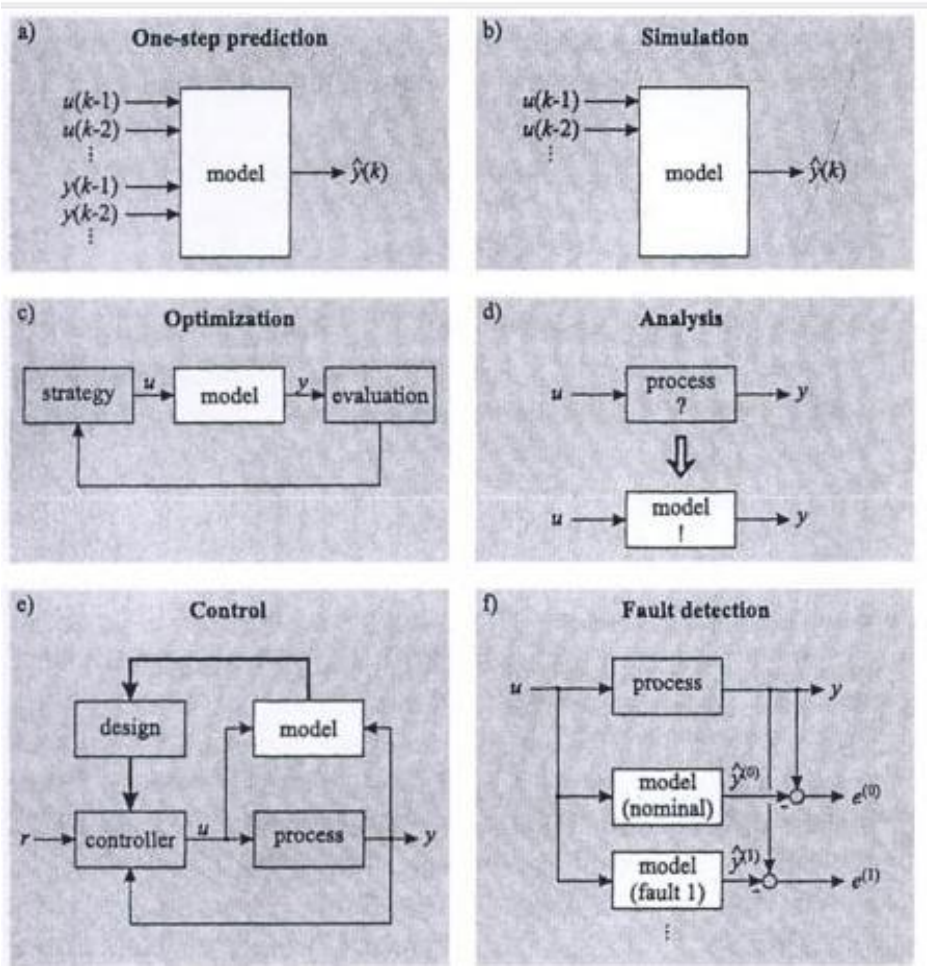

Figure 1.2: Objectives of building models [5]

where u is the system input
y is the system output
$\hat{y}$ is the predicted system output
k is the current state
e is the error between y and $\hat{y}$

1.3 **Is the model fit-for-purpose?**

In the previous section, the potential economic and safety benefits of using computational models over experimental testing were discussed. Whilst the benefits of computational models are easy to

comprehend, this potential is only truly realised if the computational model is capable of replicating the behaviour of the real structure, system or process.

In this thesis the focus is on parameter estimation. The fit-for-purpose nonlinear model term used here is a model that will fulfil its intended role in simulation or prediction of a system as good as or as close as possible to the real system it is representing with emphasises on the input of the data used for prediction. In general the model is expected to perform well under certain conditions that should have been specified at the initial stage of building the model. Since a nonlinear system can behave differently under different environments, the region of acceptable condition should be determined to avoid the model from failing to work.

The model can be used in day-to-day behaviour monitoring to diagnose deviations from normal operational behaviour or to predict response to extreme conditions or other purposes. The first will set up the model working under normal input excitation whilst the second will put the model in a very different input excitation mode from the normal working condition. This should also be taken into considerations when building the model to obtain a fit-for-purpose model. If a model is intended to perform under different conditions, the model should be built using data collected under those conditions under which it is required to perform. That is why a model should be built with the full knowledge of its purpose.

When the exact purpose of building a model is clear, only then can the assessment of the fitness-for-purpose of a model be done.

1.4 **How computational models are built**

The previous section considered the issue of the fitness-for-purpose of models whilst this section will briefly discuss the procedure of building a model, namely System Identification. This will first be considered for building of linear models before studying the procedure for nonlinear models.

The action of building a computational model relies on simplification, as almost all real world systems are known to be nonlinear. Simplification can be taken as far as necessary with the resulting

model still being a good representation of the real world system and which can perform as expected under a range of predetermined conditions. The simplest form for a model which is relatively easy to understand and widely used in engineering teaching is the linear model. Linear models have been largely used in dynamical systems. However with the growing importance of precision and the availability of superior machines, nonlinear modelling is a growing field of interest.

A nonlinear effect can be introduced to a test rig or experimental set up in many ways such as presented in Section 2.4 of reference [9]. A selection is listed below:

- Misalignment
- Exciter problem
- Looseness
- Pre-loads
- Cable rattle
- Overloads/offset loads
- Temperature effect
- Impedance mismatching
- Poor transducer mounting

There are many model testing and parameter estimation algorithms currently available for model building due to continuous advances in technology. Nonlinear modelling grows from the understanding of linear modelling. Hence it still has some characteristics influenced by linear modelling.

This affiliation between nonlinear modelling and linear modelling sometimes can be blurry and linearisation can be introduced unintentionally. When this happens, it can lead to having a model that may not perform as expected when the model is being used in a real world system environment. An example is when doing nonlinear detection with the use of random input. Often the frequency response function (FRF) of a nonlinear structure would appear undistorted due to randomness of the

amplitude and phase of the input excitation. In Section 2.6.4 of reference [9], this is expected even with a band-limited random signal.

1.4.1 Building Linear Models (Linear System Identification)

System identification in its simplest form is an action of matching a predicted response to an actual response from experimental data which have both been excited by the same input. The predicted response can be calculated analytically and most current practice uses a computer programming language for simulating the system as complicated and costly calculation can be done rather efficiently using a computer. Figure 1.3 below shows a standard system identification workflow. The error between the predicted response and the real or experimental response is used to tune parameters of the predicted system until the error is minimised, thus matching the predicted system to the real system.

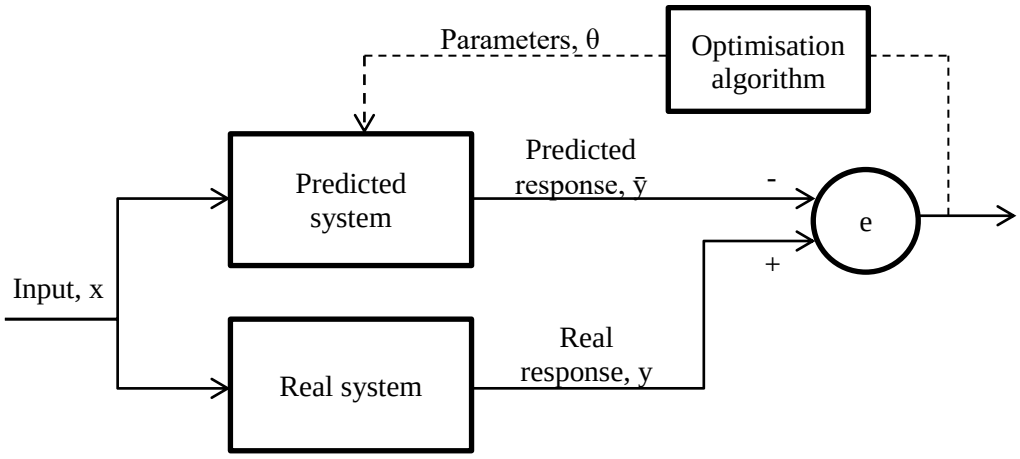

Figure 1.3: System identification workflow

A linear system is largely used to model physical characteristics, material behaviour or phenomena found naturally in the world. A linear system is simple to understand as it exhibits a linear behaviour that can be accurately predicted. The four properties that shows a system is linear are [9]:

1. Superposition
2. Homogeneity
3. Reciprocity
4. Harmonic distortion

A linear system follows the principle of superposition, which means that the response of a linear system can be formed by the summation of responses of its subsystems. The individual response when each input is applied separately can be summed to give a total response and total input. So the system S, in Figure 1.4 below is a linear system as it follows the principle of superposition.

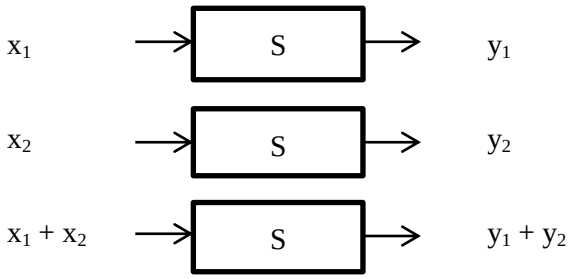

Figure 1.4: Principle of superposition

One of the other behaviours of a linear system is that it shows homogeneity, which is a form of superposition. Homogeneity holds when $x(t) \rightarrow y(t)$ implies $\alpha x(t) \rightarrow \alpha y(t)$ for all values of α. From this homogeneity effect, linear system identification is not affected by the magnitude level of the input. Given any input level, the identification should always give the correct system.

Reciprocity requires superposition to be conditional of a linear system as some symmetrical nonlinearity also can show reciprocity. A system which results in the response *y(t),* at some point B to an input, *x(t)*, applied at some point A is said to show reciprocity if the same input, *x(t)*, applied at point B results in the same response, *y(t)*, at point A.

Harmonic distortion is easiest to identify as it can be seen in the waveform of the output usually observed by oscilloscope during experiments or on the plot when doing simulation. Harmonic distortion is observed when a sine or cosine waves pass through a system, resulting in distortion in the output. The output or response will be the same monoharmonic wave at the same frequency.

Since a linear system has the four properties as above, once a linear system had been identified through any type of input of any level, the identified system should respond as expected to any other type of input of any level. That is why random input (of any level) tends to be used in linear system

identification. A random signal is the most efficient way to excite across all frequencies in a short amount of time.

The most famous method for linear system identification is modal parameter estimation or modal analysis [10]. Modal analysis can identify a system with any type of input and level of inputs. It uses modal parameters such as natural frequencies, mode shapes and damping ratios. This great generality is the reason why it is so famous. A full description of modal analysis can be found in [11]. The Ibrahim time domain method [12], eigensystem realisation algorithm [13], stochastic subspace identification method [14], polyreference least-square complex frequency domain method [15] are some of the examples of approaches of modal analysis.

1.4.2 Building Nonlinear Models (Nonlinear System Identification)

Nonlinearity is a common natural occurrence. In engineering and mathematically it had been addressed by the linearisation method since 1963 [16]. In the past few decades many other theories have come up as the importance of addressing nonlinearity has grown. In structural dynamic areas, new materials that introduce nonlinear behaviour due to being lighter and more flexible have become increasingly important. Dry friction is an example of a system that causes a nonlinearity behaviour that cannot be avoided. Even at a very low level of excitation, the nonlinearity will still be present and must be addressed. In [17] it has been shown that with even minor free-play in the bearing of a rotordynamic system, this can lead to major nonlinear instabilities in the form of a chaotic explosion that could potentially be catastrophic. This is presented by large-amplitude chaotic motions with frequencies close to linearised critical.

A nonlinear system does not fulfil the four behaviours that hold for a linear system. In terms of response, a nonlinear system exhibits a response that is usually nonharmonic. Any disturbance in the harmonic excitation can be seen quite clearly which can be the simplest method of identifying the presence of nonlinearity in a system and structures.

Homogeneity too does not hold for nonlinearity. For example, a small amplitude oscillation which can be understood by linear dynamics breaks down at higher amplitude levels. Increasing input type and levels would change the output observed for a nonlinear system.

Since a nonlinear system does not follow the principle of superposition, it leads to complexities of nonlinear system identification. Those challenges include identifying which nonlinear behaviour is predominant, then to have the predicted model correctly regenerate the same nonlinear dynamics as identified. Another challenge is to have the nonlinear system identification techniques work on a wide-class of dynamic nonlinearity. However attempts have been made in the development of principles of superposition for nonlinear systems such as suggested in Section 2.1 of reference [18] and in reference [19] for example.

The powerful theory of modal analysis for linear systems is sometimes used in nonlinear systems without modification. This could be useful for a restricted system. However, as nonlinear Frequency Response Functions (FRF) are subjected to shape changes when the excitation type or levels are altered, this would not be useful to classify a wider nonlinear system with accuracy. These are clear limitations of the linear method for a nonlinear class of system. The random input that is notably useful in linear system identification may not be the best solution for nonlinear system identification. This also leads to an investigation into the beneficial use of harmonic excitation due to its ability to excite nonlinearity in a system.

1.5 Proposed framework for model building

Given the discussion presented in the previous three sections, it is clear that in order to build a fit-for-purpose nonlinear model or, at least to understand the limitations of the nonlinear model that was built, it is necessary to have a proper framework.

The author would like to propose to initiate a guide, where relevant, for new users, clients and stakeholders of model building for nonlinear systems, to assist input readiness for modelling a fit-for-purpose predicted system models. Figure 1.5 shows the proposed steps in nonlinear system identification. Most academic papers when looking at nonlinear system identification have only

focused on model selection and parameter estimation part in the proposed framework. Although these could be taken as the core of system identification, the author has the impression that the other steps, which are still important, are being neglected. This would result in predicting a model that may not be fit for the purpose intended by the stakeholder.

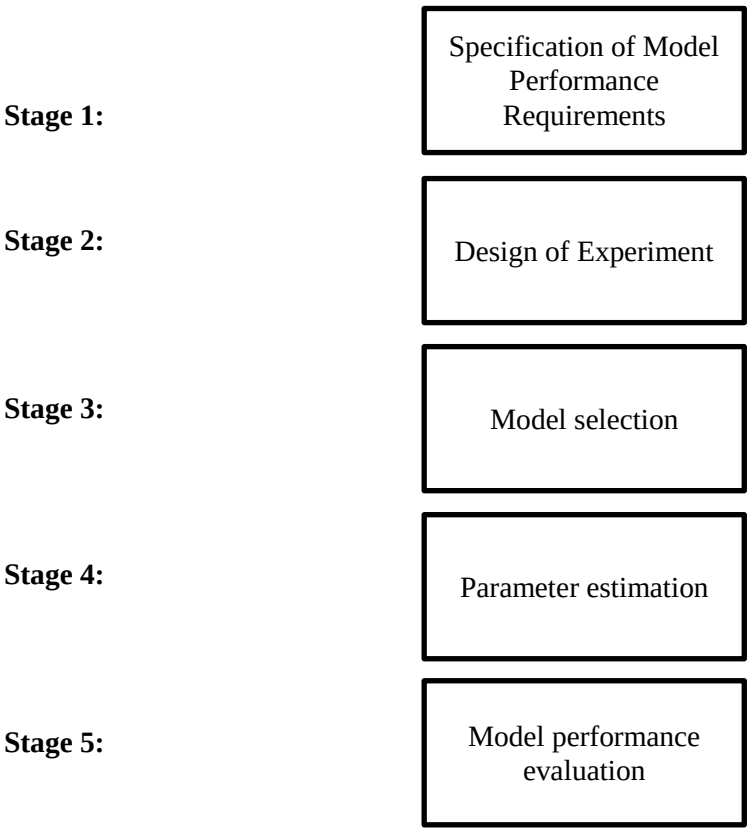

Figure 1.5: Proposed framework of building a nonlinear model

1.5.1 Specification of Model Performance Requirements

A model performance specification is a set of objectives that a stakeholder should set for a nonlinear predicted model. This is the first part of model quality where the input choice relations to data collection can affect the model to be identified [20]. The author wishes to stress that a predicted model should always be able to perform the best it can for the true purpose of the system it is representing. The main point to be brought up here is the true purpose of the predicted model which means that the predicted model can perform as expected in its working environment, rather than only in an experimental or simulated environment. The model performance specification should be set before attempting to perform other stages in nonlinear system identification. There should be clear

objectives to be determined by the stakeholders for the predicted model. The objectives would include:

1. Range of inputs for the real system
2. Type of inputs for the real system
3. Whether the real system would be susceptible to extremes cases
4. Other requirements by the stakeholder

Meeting the set objectives requires stakeholders to provide appropriate data sets for the parameter estimation stage. The data should cover all necessary input ranges and types. For example, if the predicted model is going to work in an environment with high input magnitude, the data should be based on a high input magnitude as well. This is since a higher magnitude of input will have a more pronounced effect of nonlinearity and could even potentially introduce different types of nonlinearity than at low magnitudes. If this is not the case, and data with low input magnitude is used instead, some or all the nonlinear parameters will not be predicted correctly. This will lead to the predicted system failing to match the true system performance in the required environment. Thus knowing the expected true system environment is essential in the next stages of nonlinear system identification. This will lead to decisions in the design of the experiment and will be good criteria for evaluation in the end, at the model performance evaluation stage.

1.5.2 Design of experiments

Design of experiments should take into account the model performance specification that had been established. In an ideal situation, it should consider all ranges and types of inputs that the true system the model is representing is going to experience. Experiments should be setup to include all scenarios according to the true working environment for the predicted model. The data available should give the system identification enough incentive to predict accurately all associated parameters of the predicted model. Thus, this will lead to a robust predicted model that will perform well for the system identified.

However, most times there will be limitations in a real situation when designing experiments. Such limitations are in general based on resources availability, time limits and cost restrictions. Where there are limitations, not all the scenarios for the required data for building a predicted model can be produced. In essence it is crucial to keep a balance between having enough experimental data to keep the cost minimal while at the same time obtaining a robust enough prediction out of it.

Most research papers make use of random inputs since it covers various frequencies and control is simpler with only the magnitude to adjust. For a nonlinear system, a higher input magnitude will have a higher effect of system nonlinearity. For a nonlinear predicted model which is expected to work in a high amplitude environment, experiments for system identification should also use high input magnitude whenever possible. By using high amplitude random signals, the data produced for parameter optimisation would result in a more a robust predicted model. This comes from the fact that nonlinear properties have been amplified in the data, and a parameter optimisation algorithm would have a better incentive at finding the nonlinear parameters.

Using sinusoidal input on the other hand requires a choice of frequency, magnitude and a combination of signals. It requires more control and knowledge such as determining the undamped natural frequency to obtain a better output signal. However, such input gives more information that can be related between the input and output of a data. Information such as system harmonics and restoring forces can be extracted and may be used to further understand the system to be identified.

1.5.3 Model selection and parameter estimation

Figure 1.6: Single output single input system

For the single input single output (SISO) model shown in Figure 1.6, determination of a function, *S* which maps an input, *x(t)* to an output, *y(t)* is model selection. Given information on the system, an experienced expert can determine the structure of the system, *S*. For example, if the system is known

to be a single degree-of-freedom nonlinear system with cubic stiffness, a structural form of equation 1.1 is expected.

$$m\ddot{u} + c\dot{u} + ku + k_3u^3 = F(t) \tag{1.1}$$

where *u* is the input, *F(t)* is the response and overdot denotes derivatives

In this case, after knowing the model structure, it will only leave the expert the parameter estimation problem of *m*, *c*, *k* and k_3 to identify the system. At present there are a huge number of parameter estimation methods available. Some examples of parameter estimation are the least square method, recursive least squares method, Masri-Caughey method [21], Hilbert transform [22], and differential evolutions. A review of the parameter estimation method can be found in the survey paper in reference [10].

In this thesis, the author will discuss further and show examples of parameter estimation methods of Self-adaptive Differential Evolutions and the Volterra series in later chapters.

1.5.4 Model performance evaluation

Based upon the model performance specification, the performance requirements of a predicted model can be measured. This will assist in evaluating the success of the whole model building process. A predicted model which was built under all relevant conditions of its true system would be a good prediction and hence be a robust model fit for its purpose, whilst a predicted model that does not have relevant data for estimation can be considered as unsatisfactory. Such a model is input-dependent and would only perform in a limited suitable environment. This is similar to the model validation stated in [23], where it assures quality before the predicted model is put in use. Model validation is about finding the fault in the model and proving the model is wrong by working the model with various other data sets [24] including data from different input types. The model is only considered as validated when there are no faults with the tests. This was briefly demonstrated for the harmonic inputs parameter estimation in section 4.5 of this thesis, though it was done to compare the robustness of the inputs rather than validation of the model.

1.5.5 Improvement Ratio

Current practice at Stage 3 of the proposed framework introduced earlier usually relies only on the error between a real system and an estimated system. The error is the main measure of success of most parameter estimation algorithms. Minimisation of error should lead to having two similar systems - that is the estimated system will improve by trying to mimic the real system continuously with each algorithm generation.

In real problems with unknown system parameters, it would be necessary to rely only on the error given by the parameter estimation algorithm to tell if the estimated system is representative of the real system or otherwise. This may sometimes be misleading as revealed in later chapters.

The author would like to propose the Improvement Ratio, which is a dimensionless measure to show improvement of a predicted nonlinear model over a predicted linear model. This would be mostly applicable to a system that may be susceptible to linearisation. Where no good linear model can be predicted due to the highly nonlinear behaviour of a system, the Improvement Ratio would not be required. The Improvement Ratio value will be calculated in later chapters and shows the improvement value seen for a predicted nonlinear model over a predicted linear model.

The Improvement Ratio is used to increase confidence in the nonlinear model that was chosen. Both the nonlinear model and the linear model are identified using the same parameter estimation algorithm with the same data set. By using the linear model as a basis in the parameter estimation algorithm, the Improvement Ratio allows comparison between the error of the predicted linear model and the error of the predicted nonlinear model. The Improvement Ratio suggested here is only valid for data that could be fitted with the linear model. This can be due to linerisation due to signal types or low excitation data. The procedure is given in Figure 1.7 and the Improvement Ratio is given by:

$$Improvement\ Ratio = \frac{Linear\ Model\ Error - Nonlinear\ Model\ Error}{Nonlinear\ Model\ Error}$$

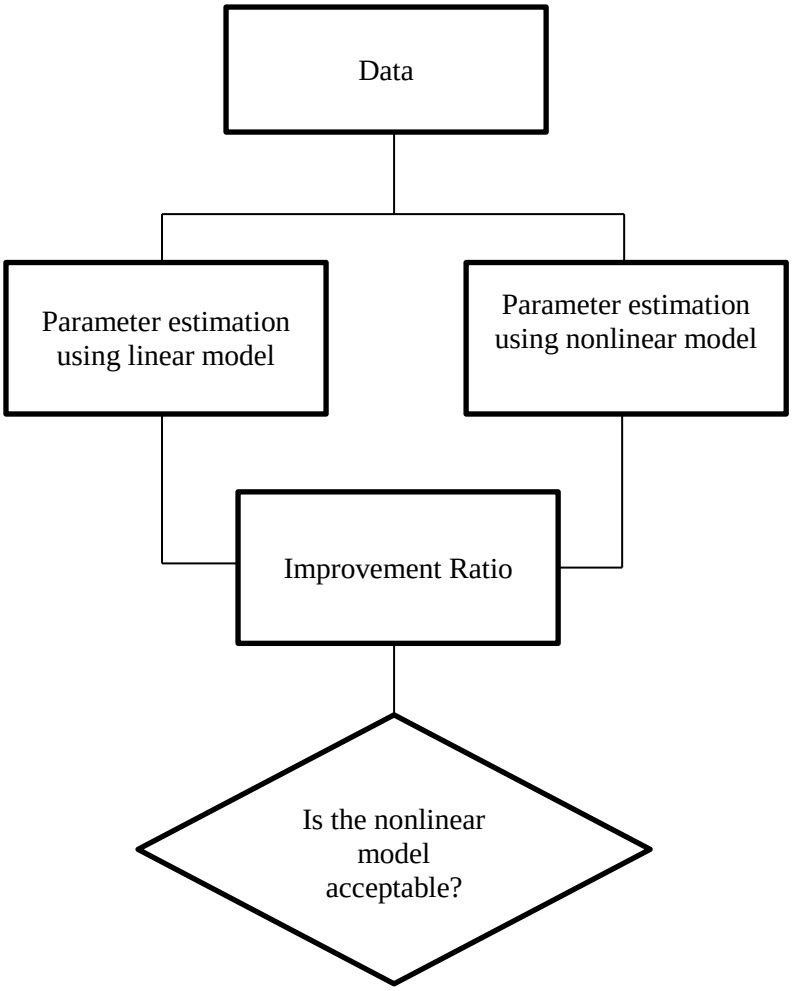

Figure 1.7: Steps of comparison of Improvement Ratio between nonlinear and linear predicted models

The Improvement Ratio should be positive. A negative value would mean that the predicted linear model would be more suited to the data. This would mean that the nonlinear model of choice might be wrong. With a low Improvement Ratio, the question could be asked whether the nonlinear model is necessary or is a linear model sufficient. In this case, the designer would also be alerted to check if the data is representative of the real system environment. Improvement Ratio will be demonstrated for the system identification problems presented in this thesis.

1.5.6 Current practise in model building

Most papers referred to and encountered by the author usually only look at optimising the experimental data against the predicted model data. This is done via a certain chosen criteria value or objective function to come to a conclusion whether an optimisation or parameter estimation method has been successful or has failed. The conclusion would usually be based on the premise of commenting that the method has been successful with a value of precision based on the value of the

error obtained from the objective functions. A value of less than 5 would be acceptable with less than 1 viewed as excellent [25]. Then the predicted model would be accepted as representing the whole true system.

Rarely has it been seen that previous papers have looked at other criteria such as the availability and completeness of input data and the actual objectives of the predicted model. What is the purpose of building the model? Where will the models be used? What is the actual working environment of the system that the model is representing? The results from these models will work well to some degree. However the estimated model may not be suited for the actual real purpose of the system it is representing and may fail to work completely when in actual use.

The focus has usually been on Stage 3 and Stage 4. Rarely, some studies talk about Stage 2 regarding the design of the experiments. Whilst it is true that these stages are the core of model building, however this still lacks the main objectives of model building which is to build a model to accurately represent a system. The problem with this approach is that unless the purpose for building a model has been set clearly set, the designer will not be able to know when that purpose has been achieved. To truly realise this, the model built must be set with a model performance specification. Referring to the proposed framework, without Stage 1, there will be no assessment to be done at Stage 5. The predicted model could possibly perform exceptionally well in the region associated with the available data with which the system identification was implemented. However if the true system actually sees different input than the data used in terms of type, magnitude or frequency range, the predicted model will still fail to model certain part of the system due to the limitation of information. This then will result in failure in use.

The author does not seek to say that such identification is incorrect but is concerned about the completeness of the results obtained. Even in the early part of the author's research, comments were made on some parameters from the Bouc-Wen equation regarding their insensitivity [26]. Further investigation on the matter shed some light and new perspective on the availability of input data rather than just on the system parameter themselves.

A high Improvement Ratio gives confidence of the predicted nonlinear model that has been identified. It shows that the nonlinearity behaviour of the real system is present and has been picked up by the parameter estimation algorithm. The Improvement Ratio will be used in later chapters concerning parameter identification.

1.5.7 Real world limitations

Building a model in a real world situation differs significantly from simulated work where parameters are known specifically and the point of having less information would grant confidence to the model built. With simulated work, the parameters are known where result of parameter estimation can be referred to the true chosen parameter, for example with percentage error of an estimated model against a true model.

While in reality, when estimating parameters for a model the results cannot be compared to a 'true model'. Under the false confidence of obtaining a model from identifying a system with inadequate information this could lead to a disastrous result if modelled wrongly. A real world system is modelled based on the dynamics that can be picked up from the system and this can differ significantly under different conditions. Thus it would be of utmost importance to have as much information as possible of the system in its working environment in order to build a representative model of the system that would promote confidence.

Ideally for building a model, the best way to capture all the required information needed is by running many experiments and tests. However, realistically, cost and time will be the limiting factors. Thus planning is essential in maximising the amount of information that can be obtained from the limited amount of testing available. This is the balance between having enough experiments and tests to keep the cost minimal while at the same time obtaining a robust enough predicted model out of the exercise. It is similar to the operational evaluation in structural health monitoring (SHM) term [27].

There are also circumstances where data is directly given for model building, without being able to design the experiments. This data may come from the stakeholders directly and no further testing is allowed. In such cases, if the data captures all forces and environmental effects that the real system is

being subjected to in daily operations, then the model building process can proceed. The model performance requirements should have been met, and the outcome will be a good predicted model. However if in such cases, the data has not captured all forces and environmental effects that the real system is being subjected to in daily operations, the model performance evaluation will fail to meet the requirements. The predicted model, may perform well in an environment similar to the data used, but might not be a good prediction for the whole system it is representing.

1.5.8 Domain of applicability of a Model

Figure 1.8 shows a chart of scenarios of communication between a stakeholder and expert that are being proposed. This scenario looks at the situation where experts are given a set or sets of data for model prediction. In such circumstances, data may have been acquired via experimental work, collected during the lifetime of the real system in real time, or after the failure of a system.

The typical process for model building starts with the acquisition of data. Then a model is predicted based on the system behaviour. This can be done via physical modelling, where experienced experts will determine the type of system behaviour and find its association with the known model. This can also be done with mathematical modelling, where in this case some parameters may not have a physical meaning. With a form of model selected, experts will use a parameter estimation algorithm to predict the parameter values and compare the objective functions or cost value i.e. root mean square error of the displacement of the predicted model against the real system. When the root mean square error is less than 5, the predicted model is accepted as a good prediction.

At the starting point of interaction where data is handed over, the model performance specification should be discussed. At this point the expert should learn of the objectives of the predicted model. If the data given is not comprehensive enough to meet the model performance specification, additional data should be requested.

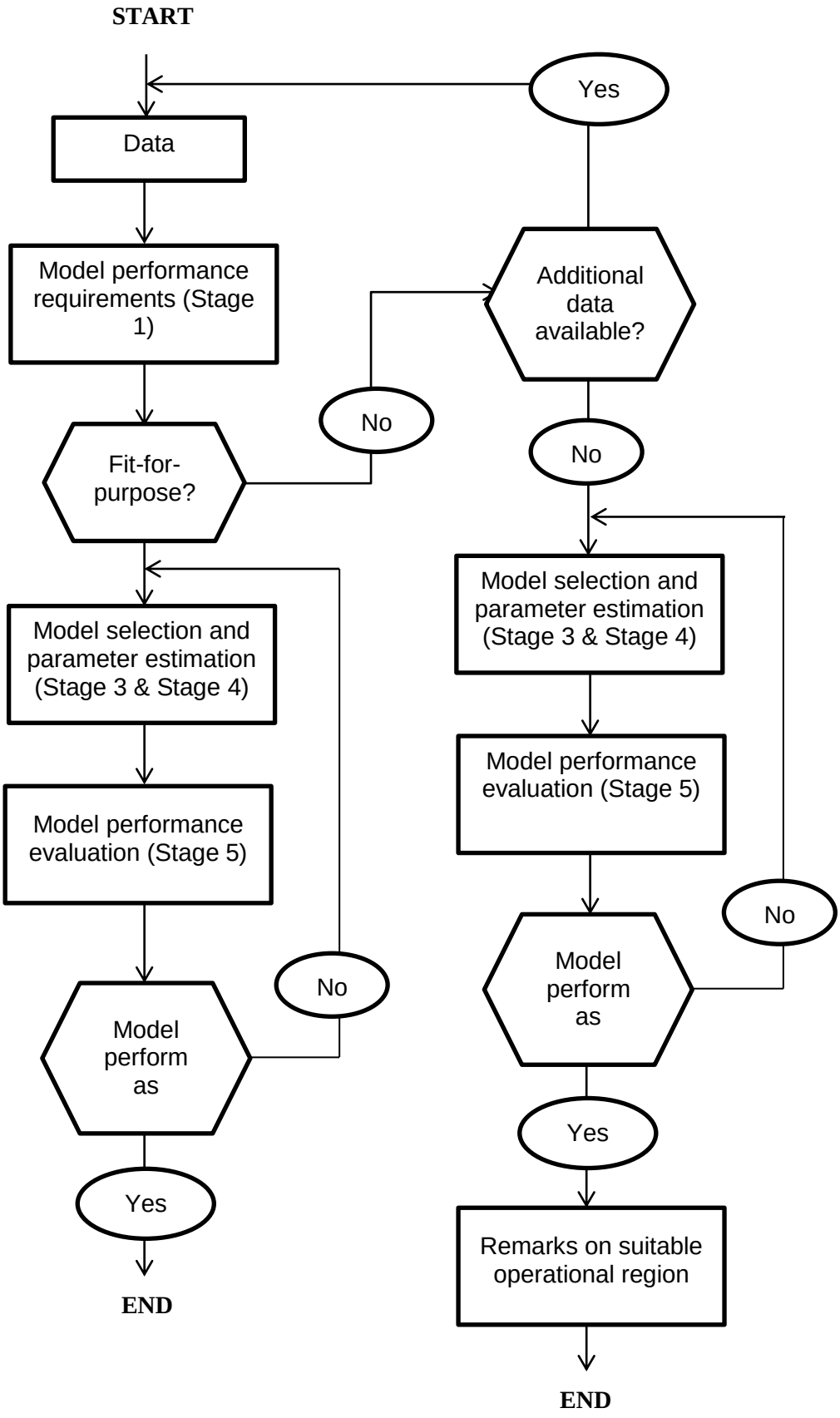

Figure 1.8: Communication between stakeholder and expert, where data is provided without control of design of experiments.

Experts should have the right to decline the model building request should the data available be incomplete. If no additional data is available and the stakeholder still wants to proceed with the model building, the expert should provide a model performance evaluation note or rules regarding the suitable operational conditions of the predicted model based on the available data for model building. This will be a user manual for the use the predicted model and should note on the input type and range and also the environmental conditions under which the predicted model will be valid. Outside of this condition, the predicted model may not be fit, up to the point of total failure.

1.6 **Objectives**

The aim of this work is to investigate how the choice of input excitation, system identification strategy and measure of system identification success affects the fitness-for-purpose of nonlinear models within the framework discussed in the previous section.

To achieve the above aims, the thesis uses the Bouc-Wen hysteresis models as an example of a nonlinear system of interest. The Bouc-Wen hysteresis models have been used in much of the literature and are a familiar model within author's research group. This model has been shown to be capable of representing behaviour often observed in real-life applications. The optimisation methods of choice in the thesis are the population-based optimisation approach, specifically the Differential Evolution and the functional series approximation approach, namely the Volterra series. A variation of the Differential Evolution, the Self-adaptive Differential Evolution is used in the thesis as the parameter estimation algorithm of choice to achieve the objective of input choice and measuring the system identification success.

The Bouc-Wen hysteresis model is investigated by using varying levels of random excitations and some types of harmonic excitation. The effects of the various input excitations and the resulting predicted models are observed to see the behaviour of the fit-for-purpose models. The thesis also investigates the substance of additional confidence to assist the mean-square error as a measure of system identification success for nonlinear systems. This is where the Improvement Ratio is calculated and observed.

The final objective of the thesis is to find the relationship between parameters of the Bouc-Wen hysteretic model to the parameters of the nonlinear polynomial model via use of Volterra series approximation.

1.7 **Summary by chapter**

Chapter 2

Chapter two presents and discusses the Bouc-Wen model equations as the model of interest in this thesis. In this chapter a Simulink model for the Bouc-Wen model that is used in the optimisation algorithm throughout the thesis is also shown. Then the general behaviour of the Bouc-Wen model is observed by comparing responses to low and high amplitude levels. Finally, the specific behaviour of each parameter is observed.

Chapter 3

Chapter three firstly describes the use of the Self-adaptive Differential Evolution for parameter estimation of the Bouc-Wen model using data with random input. The chapter looks at parameter estimation with data from varying amplitude random excitation with and without noise.

Finally, this chapter discusses how the Self-adaptive Differential Evolution works in improving the parameter estimation exercise with the adaptation variant compared to the original Differential Evolution.

Chapter 4

Chapter four describes the use of Self-adaptive Differential Evolution for parameter estimation of the Bouc-Wen model using data with single sinusoidal, multiple sinusoidal and chirp input. Similar to the previous chapter, parameter estimation results from data with low and high excitation levels are compared with and without the addition of noise. A region of stability of the parameters for the sinusoidal input is also described.

A conclusion is drawn comparing the results from random, multi sinusoidal and chirp excitation data. A sensitivity analysis between the results using Self-adaptive Differential Evolution is also discussed. Finally the sensitivity analysis is also shown for each parameter of the Bouc-Wen model.

Chapter 5

Chapter five introduces the Volterra series approximation using Higher-order Frequency Response Functions for derivations of nonlinear polynomial model parameters using the harmonic probing method. This chapter looks at the linear and nonlinear polynomial model separately. The effect of noise on the derivations is also discussed.

Chapter 6

Chapter six compares the Bouc-Wen model directly with the nonlinear polynomial model with Volterra series approximation using Higher-order Frequency Response Functions and harmonic probing equations for the nonlinear polynomial model instead of Bouc-Wen model itself. The derivations for the linear parameters and the nonlinear parameters are undertaken separately. This chapter also discusses the Bouc-Wen model nonlinear parameter behaviour. From the results, this chapter attempts to find the relation of the parameters of the Bouc-Wen model to the parameters of the nonlinear polynomial model.

Chapter 7

Chapter seven draws together the key conclusions from the chapters in the thesis and states if the set objectives have been met. This chapter also presents suggestions for future work.

Chapter 2

2 The Bouc-Wen model of hysteretic systems

2.1 **Introduction**

In the previous chapter, a framework for building nonlinear models was proposed. For the purpose of illustrating the problems and findings in this thesis, the nonlinear model of interest used throughout this thesis is the Bouc-Wen model of hysteretic system. The model is described in this chapter.

In this chapter the general behaviour of the classic Bouc-Wen model is investigated in response to harmonic and random excitations. The specific responses to these input types with low and high excitation levels on the Bouc-Wen system is also investigated here. This will be necessary in order to explain the role and effect of the excitation type and level in the nonlinear system identification process as applied in the subsequent chapters to address the problems in the section of the proposed framework for building nonlinear models.

Firstly, the behaviour of the classic Bouc-Wen model is investigated by looking at the model response information at a single frequency of harmonic excitation at low and high levels of amplitude. Then the system is investigated over a range of frequencies, again comparing the low and high levels of excitation. This is to understand the excitation levels and harmonic frequencies necessary to really excite the nonlinearity of the system. Finally, the parameters of the Bouc-Wen model are investigated while specifically looking at the behaviour of two hysteretic parameters γ and β. This will look at how changes in the parameters affect the nonlinearity of the system at different amplitudes under sinusoidal and random input.

2.2 **Hysteresis in general**

In the most general sense, hysteresis is the behaviour of a system that shows the effect of memory. The memory effect can be caused by energy stored, a transition lag or magnetisation, depending on the system. Then it can be said that hysteretic system behaviour is affected both by its current state and its past state or history. There are many different fields of study that involve hysteretic systems. Some of the fields where hysteresis is observed are economics, mechanics, magnetism, structural engineering and biology. In economics for example, hysteresis can relate to the unemployment effect on its own progression [28] and have an effect on the inflation of currency as discussed in [29]. In mechanics, the effect of hysteresis is observed in the basic stress-strain relationship of material. In 1887, reports of the British Association on the Advancement of Science, described hysteresis as the lag in the change of a quality [30], where the material qualities do not have the same value during loading and unloading. In the field of magnetism, the magnetisation and demagnetisation of most ferrous materials will show a hysteresis effect [31]. In [32], some examples of mathematical models for hysteresis in magnetisation and relays such as the Preisach type model and the Prandtl-Ishlinkii operator are discussed.

In structural engineering, recent hysteresis work has been done on a mild steel damper due to the property of a mild steel damper to exhibit substantial energy dissipation when subjected to earthquake vibrations [33]. Hysteresis is also of interest in modelling wooden material under vibrations, for example modelling of wood joints due to their dependence on the preceding input and response

(memory effect) [34]. The aerodynamic force and moments of two models of rectangular wings in a subsonic wind tunnel has also been shown to exhibit hysteretic property in [35]. When subjected to vibration, the elasto-plasticity properties of the material of the vibrating components can introduce hysteretic nonlinearity behaviour [36]. One of the more popular models of hysteresis in structural engineering is the Bouc-Wen model. The Bouc-Wen model of hysteretic system is widely considered because it represents a wide class of hysteresis in structural engineering.

2.3 **The Bouc-Wen hysteresis model**

One of the most popular hysteresis models was proposed by R. Bouc in 1967. The initial model was then further generalized by Yi-Kwei Wen about nine years later. The Bouc-Wen model is a versatile model that can accurately describe a hysteretic system in structural engineering.

The Bouc-Wen model is a hysteretic nonlinear model for a dynamical system that is used in this thesis as an example of a nonlinear system to be modelled. It is a well-accepted model for hysteretic systems. In 1967, Bouc introduced his first model for a hysteretic system [37]. In 1971, he submitted a report to *Centre de Recherches Physiques* on the same proposed model [38]. In 1976, the model by Bouc was generalised by Wen [39]. With the generalisation, the differential equation model can be used analytically to model a range of hysteretic systems. This is possible due to the model ability of the model to produce a hysteretic loop shape that captures the behaviour of various ranges of systems. It had been shown that the Bouc-Wen model shows softening, hardening and is quasi-linear with different parameter combinations. In 1981 and 1985, the initial model with six hysteretic parameters was extended to 13 hysteretic parameters to include pinching and degradation in the hysteretic loop by Wen with Baber and Noori [40], [41].

The Bouc-Wen model and its variant can be found in many literatures since the generalisation by Wen, and appeared to gain increasing popularity after 2004 with an increasing number of literatures using the model for a wide variety of hysteretic systems. Some of the literature on the application of the Bouc-Wen model are concerned with a magnetorheological fluid damper in [42], in [43] on the identification of the Bouc-Wen model and in [44] on experimental modelling of a magnetorheological

damper. The study of the model on mild steel damper in [33] also worked on the parametric identification of the Bouc-Wen model.

Some other applications of the Bouc-Wen model considered piezoelectric actuators. They included [45], a study of control of the hysteretic Bouc-Wen model, Bouc-Wen modelling in a piezoelectric actuator in [46] and for actuator dynamics and control in [47]. Finally concerning the research of earthquakes, [48] showed a study of the identification of the Bouc-Wen model for inelastic structures and [49] presented an extended Bouc-Wen model identification for seismic protection using hysteretic devices.

2.3.1 Bouc-Wen hysteresis equation

The general classical Bouc-Wen model, given in equations (2.1), (2.2) and (2.3), consists of five hysteresis parameters - *A*, α, β, γ, and n - which give the basic hysteresis loop. Some academic works would also consider not including α as it is only a ratio between the hysteretic part and the linear stiffness part. By doing this, the stiffness, k can be accommodated by the term $A\dot{u}$ in Equation 2.3.

$$m\ddot{u} + c\dot{u} + R_T = F(t) \tag{2.1}$$

$$R_T = \alpha k u + (1-\alpha)kz \tag{2.2}$$

$$\dot{z} = A\dot{u} - \beta|\dot{u}||z|^{n-1}z - \gamma\dot{u}|z|^n \tag{2.3}$$

where R_T is the restoring force

z is a hysteresis term sometimes called hysteretic displacement

Further extensions by Baber, Wen and Noori [40], [41] to the Bouc-Wen model introduced degradation and pinching shapes in the hysteresis loop which resulted in a total of 13 hysteretic parameters. The 13 parameters are given by Equations (2.4) to Equation (2.11) which modifies the $\dot{z}$ term in Equation (2.3) to Equation (2.4). The 13 parameter for hysteresis are *A*, α, β, γ, and n from the classical model. δ_ν and δ_η in Equation (2.5) and Equation (2.6) which give the strength and stiffness degradation respectively. q, p, ζ_s, ψ, δ_ψ and λ from Equation (2.8) to Equation (2.11)

contributes to the pinching of the hysteresis loop. The hysteresis term z is not measurable, thus presenting a challenge in system identification.

$$\dot{z} = h\left(\frac{A\dot{u} - \nu\left(\beta|\dot{u}||z|^{n-1}z + \gamma\dot{u}|z|^{n}\right)}{\eta}\right) \tag{2.4}$$

$$\nu = 1 + \delta_{\nu}\varepsilon \tag{2.5}$$

$$\eta = 1 + \delta_{\eta}\varepsilon \tag{2.6}$$

$$\varepsilon = \int_0^t z\dot{u}dt \tag{2.7}$$

$$h = 1 - \zeta_1 e^{\frac{-[z\,\mathrm{sgn}(u) - qz_u]^2}{{\zeta_2}^2}} \tag{2.8}$$

$$\zeta_1 = \zeta_s\left[1 - e^{(-p\varepsilon)}\right] \tag{2.9}$$

$$\zeta_2 = \left(\psi + \delta_{\psi}\varepsilon\right)(\lambda + \zeta_1) \tag{2.10}$$

$$z_u = \left(\frac{A}{\nu(\beta+\gamma)}\right)^{1/n} \tag{2.11}$$

Other types of Bouc-Wen model alternatives have also been published such as that proposed by Sivaselvan and Reinhorn [50] for seismic analysis and design and by Charalampakis and Koumousis [51] that adhere to plasticity postulates. However this will not be discussed further in this thesis. Figure 2.1 shows examples of the classical and extended Bouc-Wen hysteresis models under sinusoidal force input. The difference due to pinching and degradation can be seen. Again, this pinching and degradation is captured by the additional parameters in the extended Bouc-Wen equation.

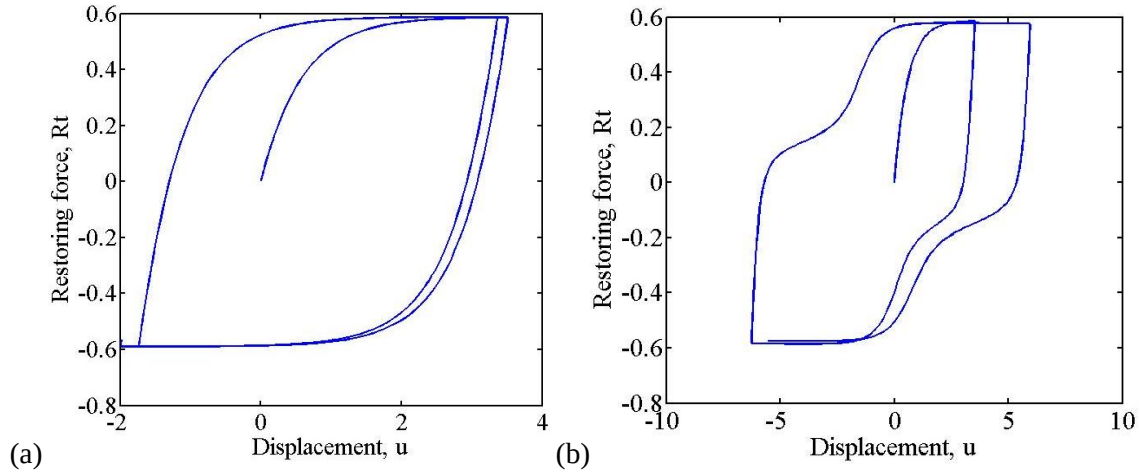

Figure 2.1: (a) Classical Bouc-Wen hysteresis model; (b) Extended Bouc-Wen hysteresis model.

2.4 **Behaviour of the Bouc-Wen model**

This section is intended to aid the understanding of the Bouc-Wen model behaviour by using sine and random input excitation at low and high amplitudes. Parameters of the model are also investigated separately in order to further understand the system behaviour.

2.4.1 Bouc-Wen classic model system information

The model parameters used in the investigation of the behaviour of Bouc-Wen model in this section are shown in Table 2.1.

The parameter values were obtained from identification of the El Centro 1940 Earthquake data available online [52] that was used in the book by Anil Chopra [53] and other journal papers such as [48] and [54] with some modification to suit the purpose of this research. El Centro earthquake was the first earthquake where useful data for engineering purposes had been recorded. The data was collected by a strong motion seismograph attached to the concrete floor of the El Centro Terminal Substation building which acts as the modern shaker table experiment data collection. The data used was the processed and reviewed data by California Geological Survey (CGS) operated California Strong Motion Instrumentation Program (CSMIP) available online in reference [55].

For the above nonlinear system, the underlying linear system natural frequency, ω_n was 17.6 rad/s corresponding to 2.8 Hz. The underlying linear system was under damped with damping ratio of 0.02.

Parameter	Value	Units
m	1	kg
c	0.7037	Ns/m
k	309.51	N/m
α	0.01	-
β	150	1/m
γ	20	1/m
A	1	-
n	2	-

Table 2.1: Parameter values of Bouc-Wen classical model

These system properties obtained from the underlying linear system can be used only as a reference as no such data exists for a nonlinear system. The investigation reported in this section was conducted using a sinusoidal force input i.e. $u(t) = X \sin(\omega t)$.

The system is simulated using 4th order Runge-Kutta numerical integration via Simulink for a single degree-of-freedom circuit of the classic hysteretic system. The simulation step size is 0.01s for a total time of 500 s per generation giving 50000 points of data. The plot for displacement and velocity is shown for 2000 points of data from initiation until 20s. For the restoring force and frequency spectrum plot, the plot uses points at steady state.

2.4.1.1 **System response in a single frequency excitation**

Although excitation of nonlinear systems at a single frequency returns limited response information, it is a worthwhile exercise to demonstrate the different effects of low and high amplitude forcing upon the system response. It is widely known that, for most nonlinear systems, excitation at low amplitude usually results in the response of the system appearing mostly linear. It is reasonable to expect that a nonlinear system identification approach conducted using low amplitude data is not capable of returning a good estimate of the system. By correctly identifying the linear parameters of a system could result in a low error between actual and predicted data without having a good estimate of the nonlinear parameters.

In this work the forcing frequency, ω that was used was at 0.933 Hz corresponding to 1/3 of the undamped natural frequency of the underlying linear system. This was chosen due to the excitation frequency being able to excite the best response to give clear comparisons of the system. Figure 2.2 to Figure 2.6 show the comparison of the system response when excited at a low amplitude of 0.1 N and a high amplitude of 10 N. Figure 2.2 and Figure 2.3 shows displacement and velocity versus time respectively. Due to the relatively low damping ratio of the underlying linear system, the transient response has decayed by around 10 cycles leaving the steady state response. Nonlinear behaviour can be seen in Figure 2.3(b) with distortion appearing in the steady state velocity plot. This is seen again in Figure 2.4(b) with the distortion of the phase plane. Harmonic distortion is the simplest way to detect nonlinearity arising from the principle of superposition. Since the input to the system is a simple sine wave, the distortion presented here is clearly a sign of nonlinearity. The cause of the distortion could be higher harmonics appearing in the response. Looking at Figure 2.5, hysteretic nonlinearity can already be identified at the 10 N amplitude, compared to a mostly linear behaviour for the 0.1 N amplitude. This is shown by the hysteretic loop that appears in the higher amplitude plot. In Figure 2.6, it can be seen that the harmonics for the low amplitude shows a huge drop between the 1st and 3rd harmonics compared to the high amplitude which is only around a factor of 1.

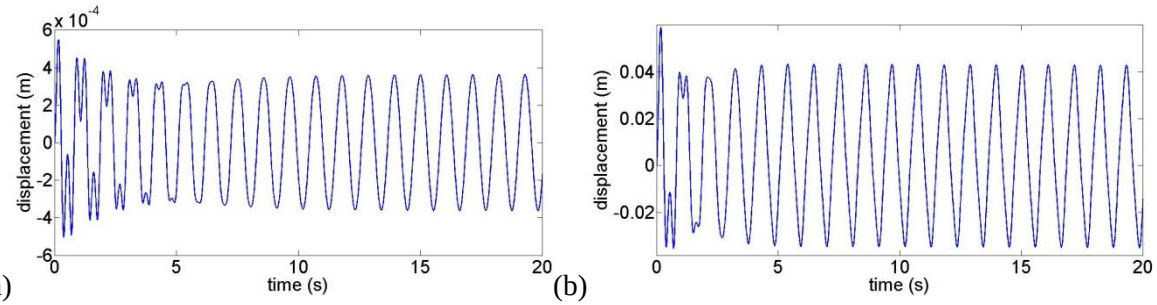

(a) (b)

Figure 2.2: Plot of displacement versus time (a) low amplitude (b) high amplitude

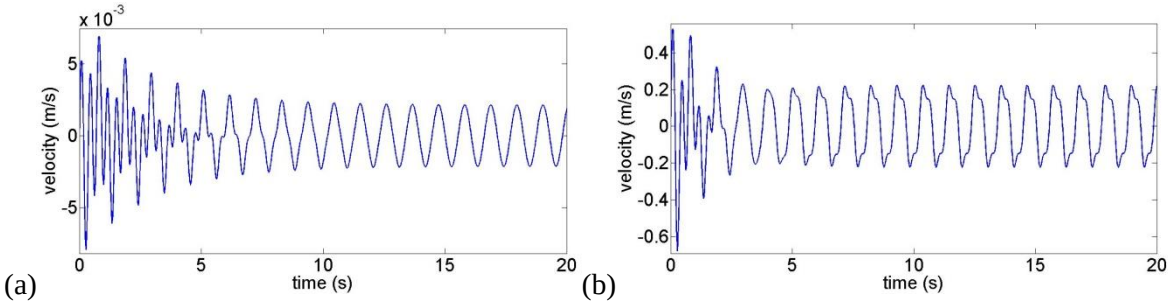

(a) (b)

Figure 2.3: Plot of velocity versus time (a) low amplitude (b) high amplitude

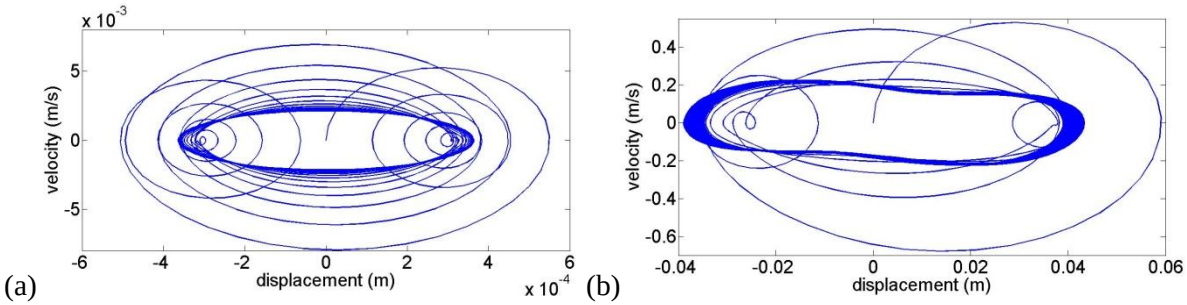

(a) (b)

Figure 2.4: Phase plane plot of velocity versus displacement (a) low amplitude (b) high amplitude

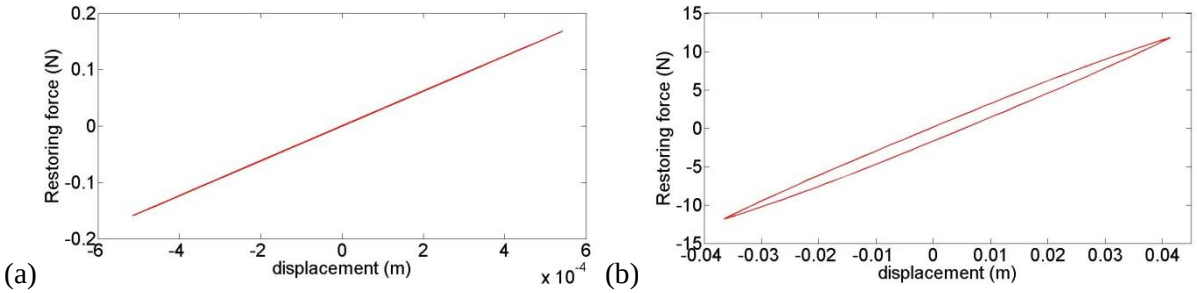

(a) (b)

Figure 2.5: Plot of restoring force versus displacement (a) low amplitude (b) high amplitude

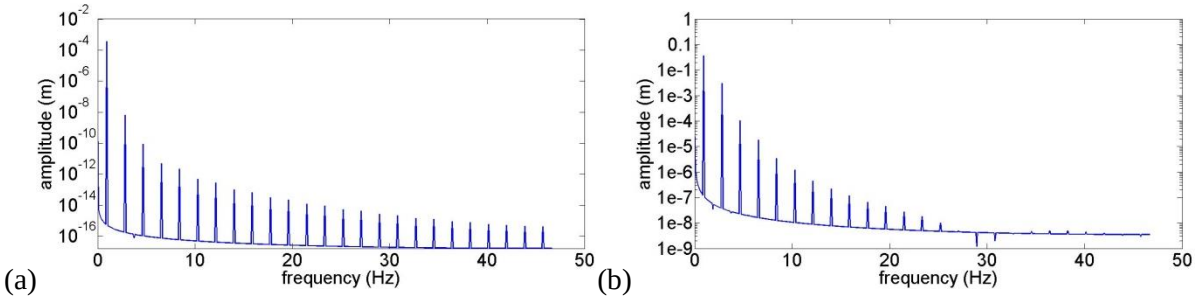

(a) (b)

Figure 2.6: Frequency spectrum plot (a) low amplitude (b) high amplitude

2.4.1.2 System response at other single frequency excitation

In the previous subsection the excitation frequency was done only at 0.933 Hz, due to showing a good nonlinear excitation at that particular frequency and close to its proximity. The low excitation amplitude did not show any changes as near linear behaviour was observed throughout. At an amplitude of 10 N, most single excitation frequencies are expected to show the behaviour of hysteretic nonlinearity as in the above observations. Here some other frequencies, relative to the undamped natural frequency of the underlying linear system are observed at high amplitude excitation. Only some plots are shown and discussed here so as not to digress.

The frequencies shown here are 2.8Hz, 2.5Hz and 1.4Hz corresponding to one, 1.25 times and half of the undamped natural frequency of the underlying linear system. Figure 2.7 shows the plot for 2.8Hz excitation frequency. The transient response decayed very quickly compared to previously after only 2 cycles compared to previously. However, nonlinearity cannot be detected as no distortion to the steady state response is observed. Figure 2.8 shows the plots at 3.5Hz excitation frequency. Nonlinear behaviour is observed for both the velocity versus time plot and the frequency spectrum plot.

Figure 2.9 shows the plots at 1.4Hz excitation frequency. The velocity plot does not show any sign of distortion while the frequency spectrum drops for more than a factor while both show very little sign of nonlinearity. In all the frequency spectrum plots, it can be seen that the peaks skip the even harmonics of the system with a very small peak visible, while at the odd harmonics, peaks are seen clearly. This behaviour is seen throughout at other single frequencies. The particular hysteretic system sets of parameters appear to confirm that the system investigated in this work shows mostly only odd harmonics behaviour.

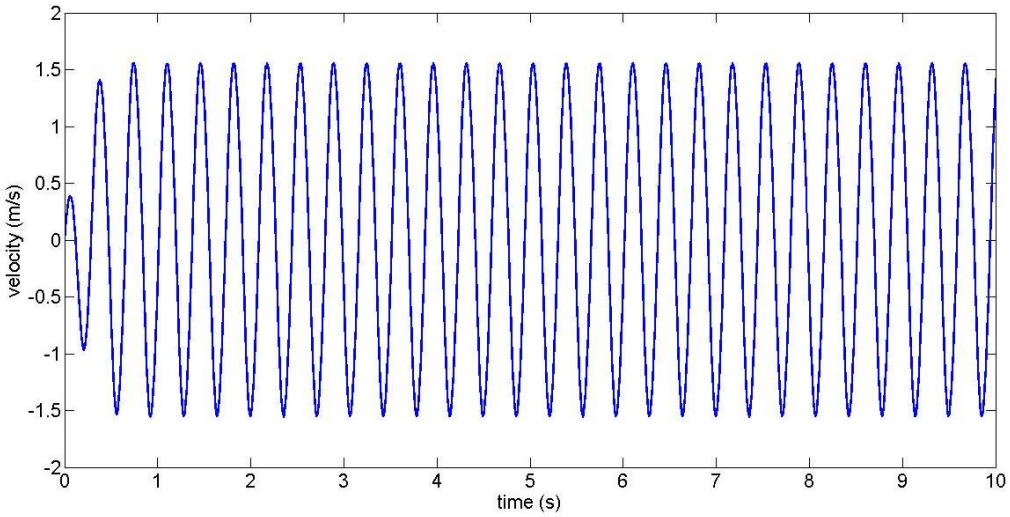

Figure 2.7: Plots of velocity versus time at 2.8Hz excitation frequency

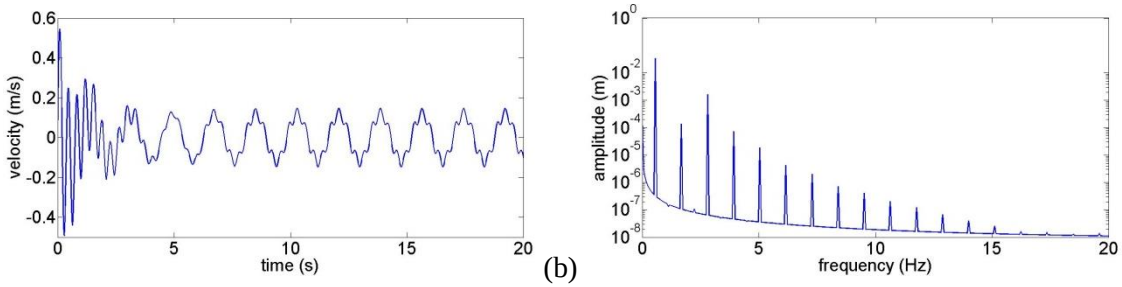

(a) (b)

Figure 2.8: Plots at 3.5 Hz excitation frequency (a) velocity versus time (b) frequency spectrum

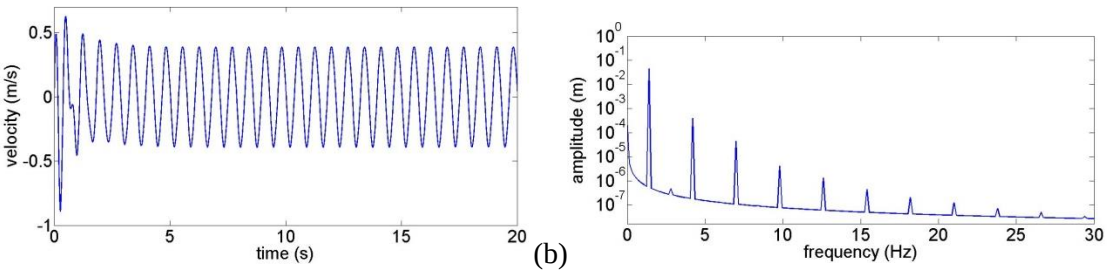

(a) (b)

Figure 2.9: Plots at 1.4 Hz excitation frequency (a) velocity versus time (b) frequency spectrum

2.4.1.3 System response over frequency range

The previous subsections only examined the response of the classic Bouc-Wen model at a single frequency. The work in this subsection will examine the behaviour of the system across a range of frequencies between 0.1 Hz to 5 Hz, thereby passing through the undamped natural frequency of the underlying linear system. This was conducted by running a series of simulations with increasing frequencies and recording the response over the frequency range. Only the steady state response was used here while the transient response was discarded. This was done to allow visualization over the whole frequency range. The same low and high excitation amplitudes of 0.1 N and 10 N used in the single frequency investigation were again used here.

An elementary approach of using a Bode plot and a Nyquist plot in the Argand plane, as seen in Figure 2.10 to Figure 2.14, was used here to visualise the effect of the nonlinearity. The figures also separately show the real and imaginary plot for the sake of visualisation.

Figure 2.10 shows the response of $\Lambda(\Omega)$ and Figure 2.11 shows the phase of $\Lambda(\Omega)$ at low and high amplitude in the same plot. $\Lambda(\Omega)$ is known as the composite FRF - since this is a nonlinear problem; obtained from simulation in Matlab. It is given by,

$$\Lambda(\Omega) = \frac{\mathrm{Y}(\Omega)}{X(\Omega)} e^{i\Omega \mathrm{t}}$$

This is obtained from simulation in Matlab by recording time histories of the steady state response, $\mathrm{Y}(\Omega)$ and input $\mathrm{X}(\Omega)$ over a range of frequencies with a fixed frequency increment. The ratio $\mathrm{Y}(\Omega)$ /$\mathrm{X}(\Omega)$ is then Fourier transformed to give the value of the composite FRF. Figure 2.12 to Figure 2.14 show the other system information of $\Lambda(\Omega)$ at low and high amplitude side by side.

In Figure 2.10, a comparison between linear and nonlinear can be seen quite clearly. At low amplitude, a distinct high peak can be seen in the plot but when the system is subjected to the 10 N excitation amplitude, a nonlinear behaviour similar to stiffness softening is seen with the peak shifting towards the lower frequency region. The clear damping effect is seen with the resonance peak

broadening and this is also evident in Figure 2.11 with the phase passing the -90^{o} gradually starting at 2 Hz to 3.5 Hz for the higher excitation amplitude system.

In Figure 2.12, the almost circular locus of the low amplitude Nyquist plot shows the typical behaviour of a near linear system compared to the non-circular locus effect of nonlinearity at high amplitude. Figure 2.13 and Figure 2.14 show the same linear versus nonlinear behaviour as well. Here the broader peak and trough show the effects of nonlinearity at higher amplitude. The more observant reader may also notice in Figure 2.11 and Figure 2.14(b), the effects of odd harmonics which can be seen as small peaks at 1/3 of the undamped natural frequency of the underlying linear system.

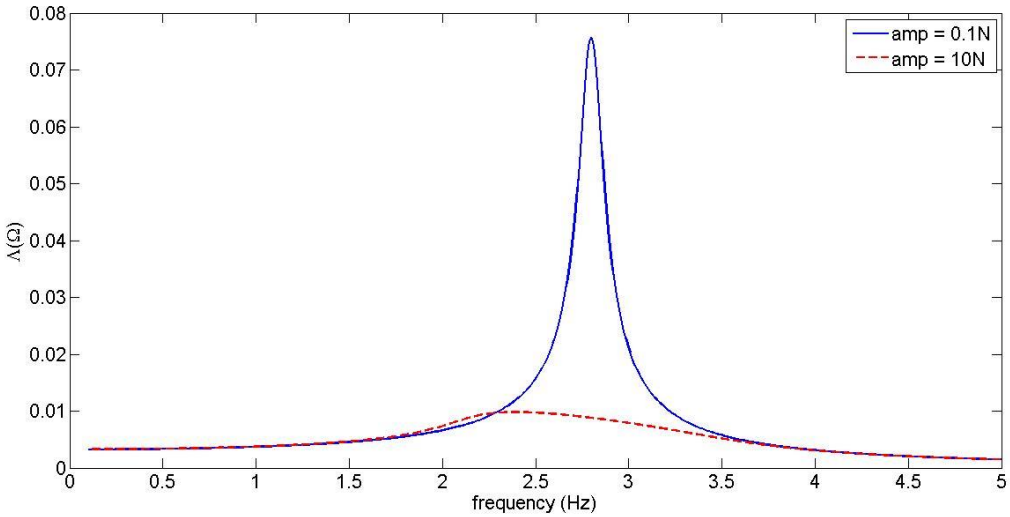

Figure 2.10: Λ(Ω) vs frequency plot for low and high amplitude

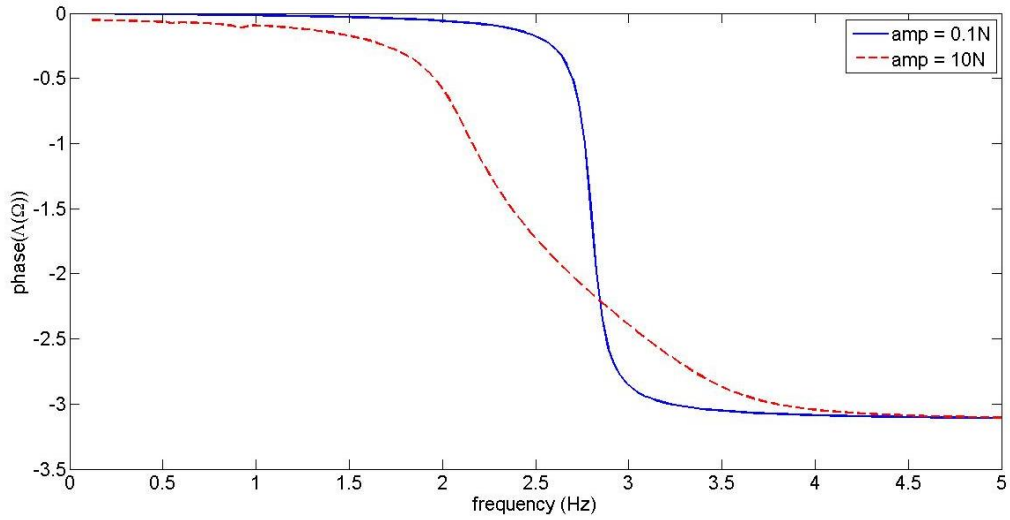

Figure 2.11: Plot of phase of Λ(Ω) versus frequency

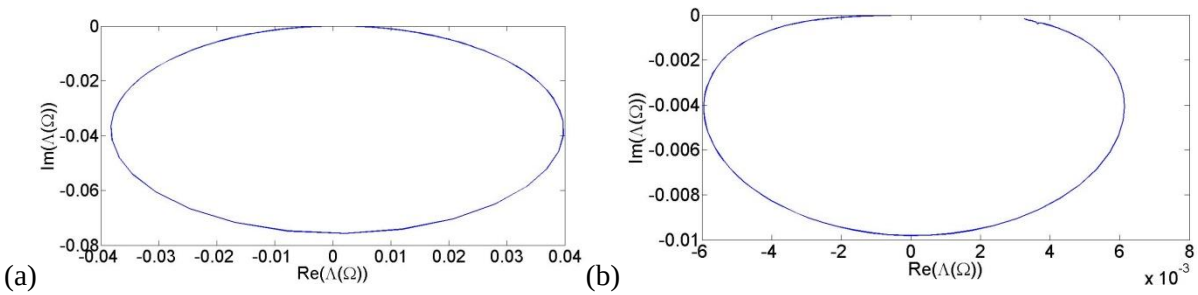

Figure 2.12: Nyquist plot of Λ(Ω) (a) low amplitude (b) high amplitude

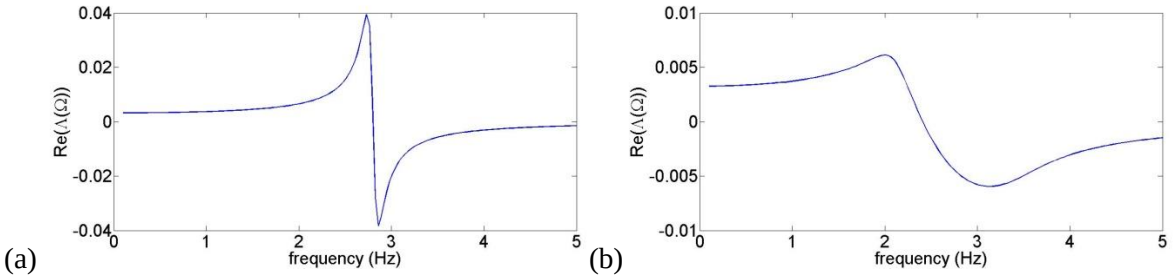

Figure 2.13: Plot of real part of Λ(Ω) versus time (a) low amplitude (b) high amplitude

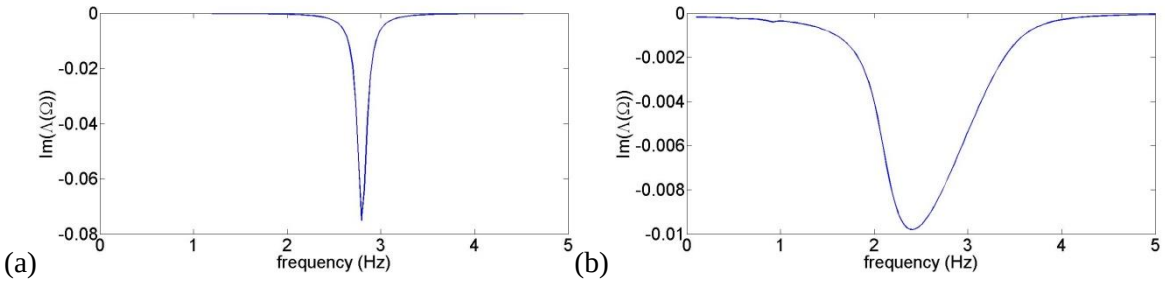

Figure 2.14: Plot of imaginary part of Λ(Ω) versus time (a) low amplitude (b) high amplitude

2.4.2 Parameters of Bouc-Wen model

The last subsection reviewed single frequency excitation and excitation over frequencies to gain an understanding of the particular set of Bouc-Wen parameters used in this work. It was shown that a 10 N amplitude of sinusoidal excitation at the right frequencies would trigger the nonlinearity of the system while at an amplitude of 0.1 N the behaviour tends to be mostly linear.

In this subsection, the behaviour of the system was investigated by varying each parameter separately to gain an understanding of the role of the hysteretic parameters. The investigation of the Bouc-Wen

model parameters behaviour was conducted via Matlab simulation using the same Simulink model as used previously with the same sets of parameters.

Since the Bouc-Wen model was derived from a linear model, the effect of the linear parameters *m*, *c*, and *k* behave exactly as expected from a single degree-of-freedom linear system of mass, damping and stiffness.

The effect of parameters *A* and α on the system response can be understood by looking at the model equation. Both parameters are independent of the value of the hysteretic displacement, *z* and so are less complicated in nature. The parameter *A* is a multiplier value to the linear stiffness and it affects the system response similarly to the linear stiffness, *k*, while α is the ratio that can act as a switch between a purely linear system and a nonlinear system. Both of these values are dimensionless.

From the equation it can be seen that for a true system that has parameter α at a value of 0, the system will not be affected by the value of linear stiffness, *k*. With α value set to 0 in a parameter estimation exercise, any linear stiffness value will be incorporated into the value of parameter *A* instead. This was done in the work in [56] for the purpose of simplifying the parameter estimation process by removing the parameters *k* and α from the equation. With α equals to 1, the system is a purely linear system without the hysteretic nonlinearity presence.

Figure 2.15 to Figure 2.17 shows the $\Lambda(\Omega)$ plot, restoring force plot and phase plane plot with increasing value of n. For the particular set of parameters in this work, a value of n of 1 is not possible as it results in calculation error. So the investigation only looked at values of *n* between 2 and 6. With increasing n, the system behaviour tends to approach the behaviour of a mostly linear system and this can be seen very clearly in Figure 2.16 and Figure 2.17 where only when the value of *n* is at 2 does the system response show a nonlinear behaviour. The cause of this can be referred to from Equation (2.3) of the Bouc-Wen model equation. For the current set of parameters of the system presented in this thesis, the value of *z* in the system is always a positive number less than one. By increasing the power for the term *z* will lead to the 2nd and 3rd term with the nonlinear hysteretic parameter, γ and β to tend to zero. Hence the system tends to behave more linearly with increasing values of *n*.

Throughout the remaining work in this thesis, the value of n is set to a value of 2. This is done to simplify the parameter estimation process as a non-integer value of n could introduce problems for the optimisation algorithm. In [25], n was similarly set to the value of 2. The work in [25] considers the situation where n is in a small range of integers between 1 and 4. This stems from the work in [57] using a cross-validation method of selection.

The investigation of the effects of altering γ and β will be presented in the next part. The investigation will look at different levels of forcing with sinusoidal and random input and how the changes in γ and β affect the system. This relates back to the main idea of the thesis, where it is necessary to determine the required range of forcing experienced by a system to match the data used in model building. Without doing so, some parameters maybe ignored by the parameter estimation algorithm and it will render the model building process inadequate and a waste of valuable time and resources.

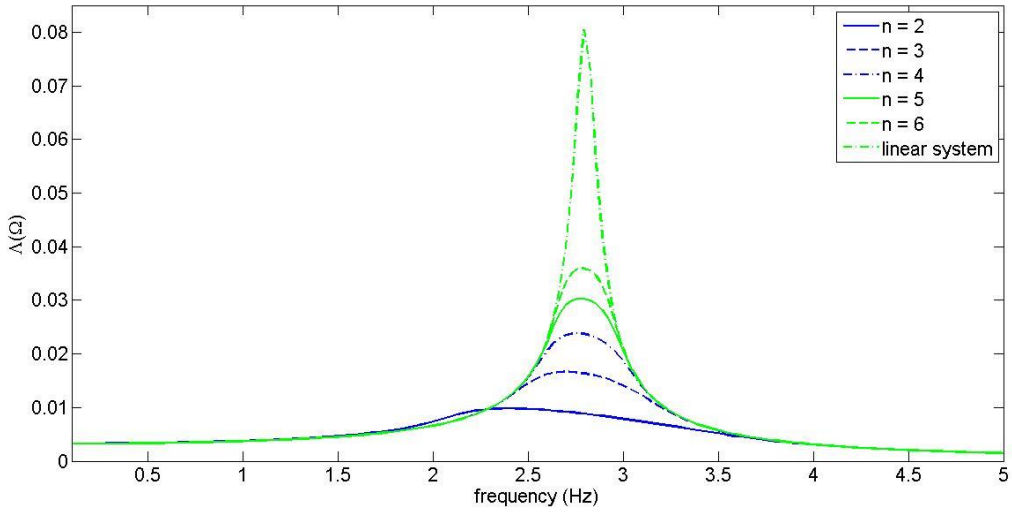

Figure 2.15: Λ(Ω) vs frequency plot with increasing value of n at 10 N amplitude

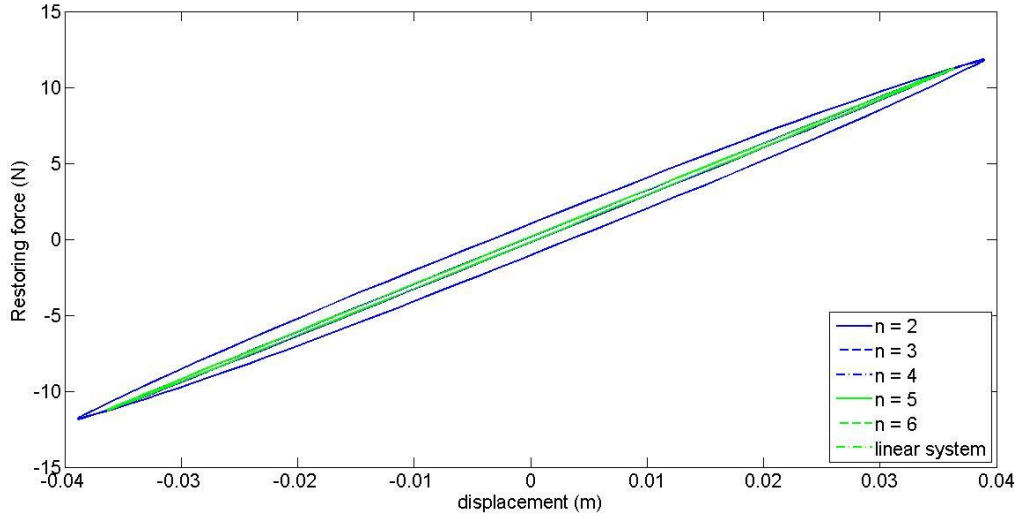

Figure 2.16: Restoring force vs displacement plot with increasing value of n at 10 N amplitude

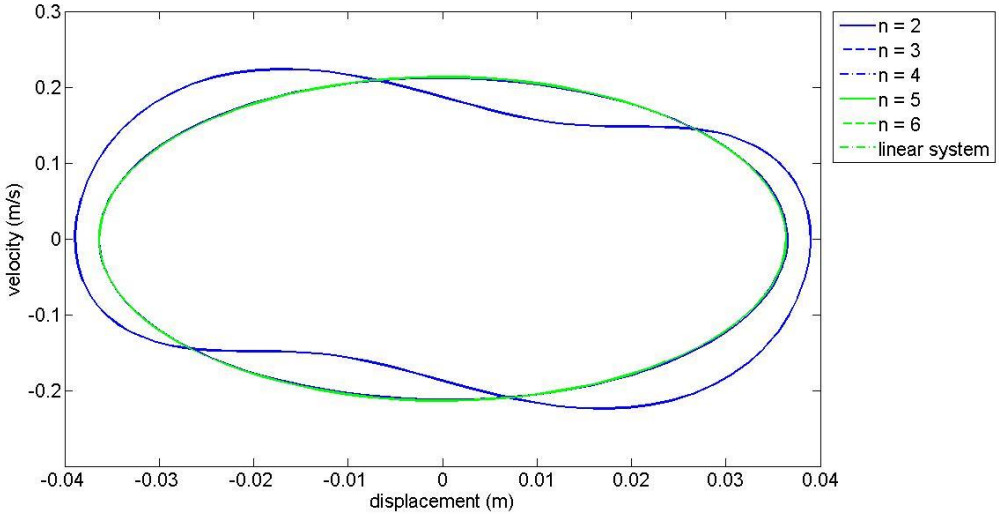

Figure 2.17: Phase plane plot with increasing value of n at 10 N amplitude

2.4.2.1 **Effect of varying gamma, γ**

In the simulation, all parameters were set to the values as in Table 2.1 except for γ which was increased from 0 to 200 in increments of 50. In Figure 2.18, in order to show a clear view of how γ affects the restoring force vs displacement plot, the simulation was conducted at a forcing amplitude of 10 N and a forcing frequency equal to the undamped natural frequency, ω_n of the underlying linear system. Here the low amplitude plot at 01N for restoring force versus displacement is not shown since no changes were observed in the plot with increasing value of γ.

Increasing γ, reduces both the minimum and maximum restoring force and displacement of the system. The entire restoring force loop can be seen to shrink as well as γ increases. The loop also appears to tilt clockwise with increasing γ showing the increasing effect of softening.

Figure 2.19 and Figure 2.20 show the difference between low amplitude and high amplitude of the phase plane plot respectively. Comparison of these two plots shows clear evidence of the need to have sufficiently high amplitude in order to differentiate between different nonlinear parameter values. As shown here, at low amplitude, regardless of the value of γ, very little difference can be observed in the phase plane plot. If conducting parameter optimisation using data from low amplitude such as this, the data itself would not give a sufficiently good incentive for finding the correct nonlinear parameter. If the true system is usually subjected to higher amplitude forcing than that used in acquiring the data for parameter identification, this would then lead to identifying the wrong parameters for the true system.

In many cases, nonlinear system identification has been done by using data obtained from random input excitation. This was due to the fact that nonlinear system identification stems directly from linear system identification in which random excitation works very well. The work here will investigate the system response under random excitation with changing the nonlinear parameter, γ to observe the nonlinear behaviour.

Figure 2.21 to Figure 2.32 show the behaviour under random forcing. The random input was generated with a zero mean and a variance of 0.1 N, 10 N and 100 N. In Matlab, the seed for all simulation was maintained to keep the same value for each of the inputs. The simulation was conducted using the same Simulink model as used previously, with input block changed from sinusoidal to random excitation.

Figure 2.21 to Figure 2.23 show the displacement versus time plot and Figure 2.24 to Figure 2.26 show the velocity versus time plot. For random input, changing variance from 0.1 N to 10 N did not translate to much difference in both displacement and velocity response. Only at variance of 100 N can a clear difference, in both displacement and velocity, be identified in relation to the changes in the nonlinear parameter.

In the phase plane plot of Figure 2.27 to Figure 2.29, although variations in response are seen in the 10 N excitation plot with increasing γ, the value is small with the shape mostly remaining the same. When looking at the 100 N random excitation, the variations are seen in both magnitude and shape of the phase plane plot.

The results here show that when using random excitation, a much higher amplitude would be required to obtain a nonlinear behaviour in the response. There is a tendency for random excitation even at larger amplitude to linearise the response of a system. This should be noted when performing system identification to avoid neglecting the nonlinearity of a system in any system to be identified.

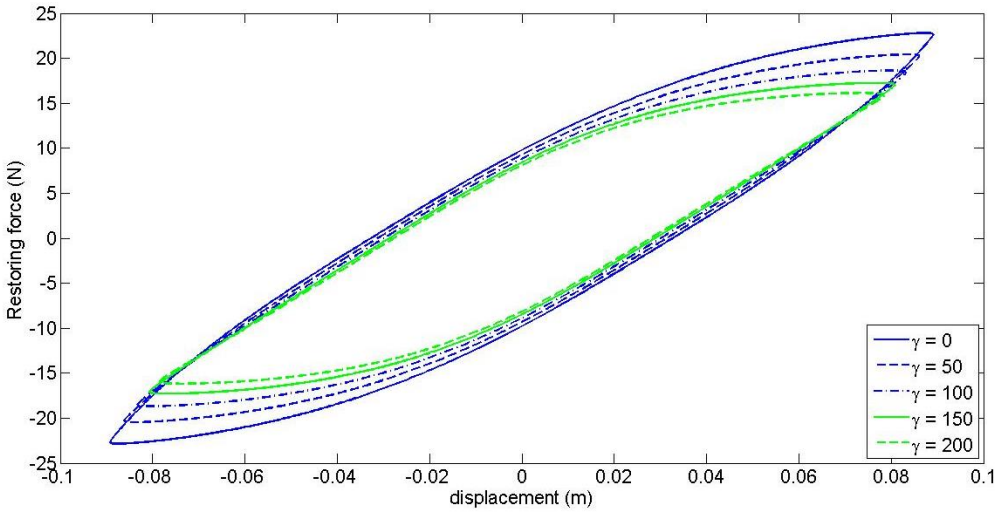

Figure 2.18: Restoring force vs displacement plot under sinusoidal input of 10 N amplitude with increasing γ

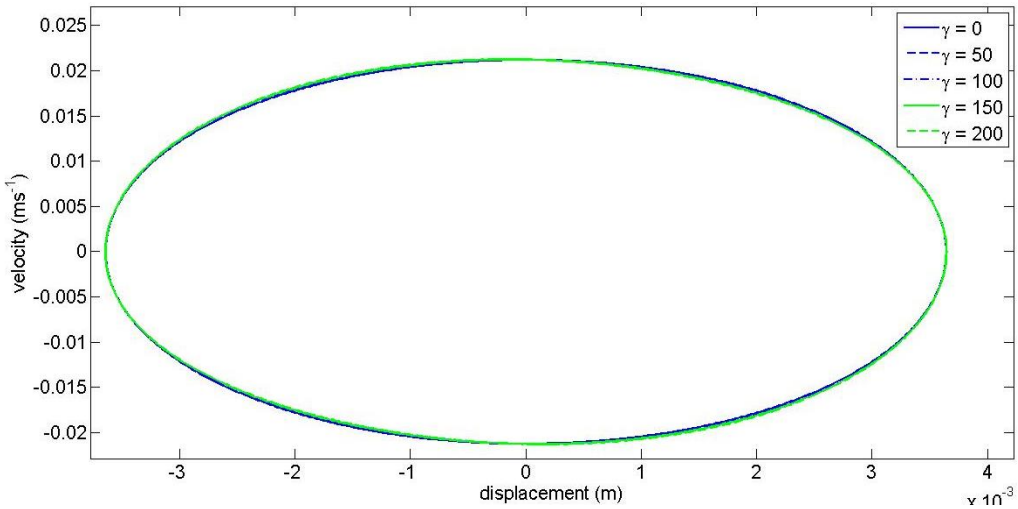

Figure 2.19: Phase plane plot under sinusoidal input of 0.1 N amplitude with increasing γ

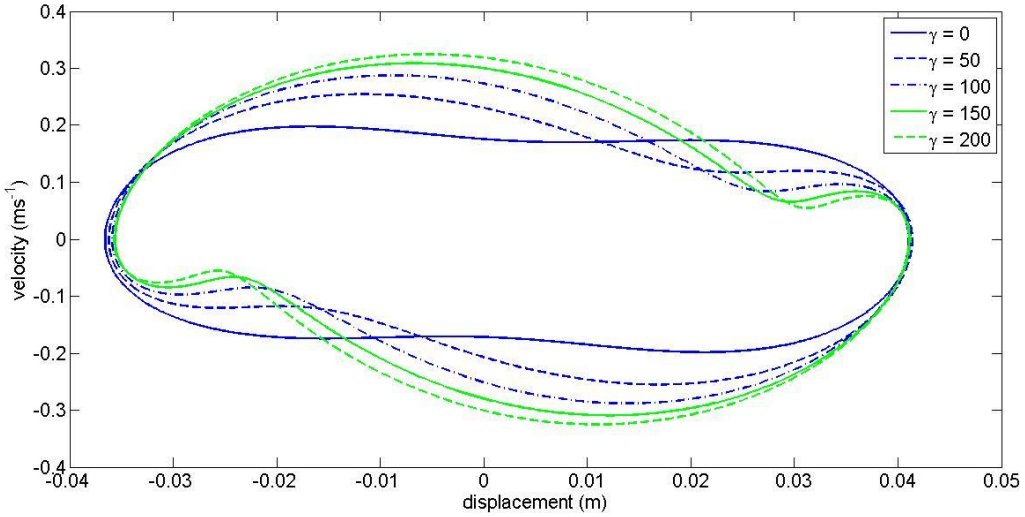

Figure 2.20: Phase plane plot under sinusoidal input of 10 N amplitude with increasing γ

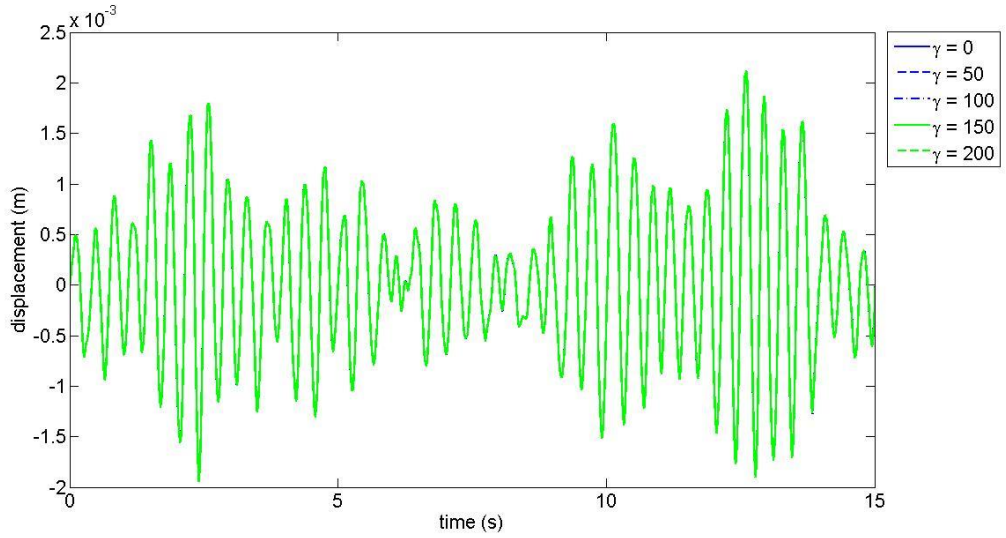

Figure 2.21: Displacement vs time plot under random input of 0.1 N variance with increasing γ

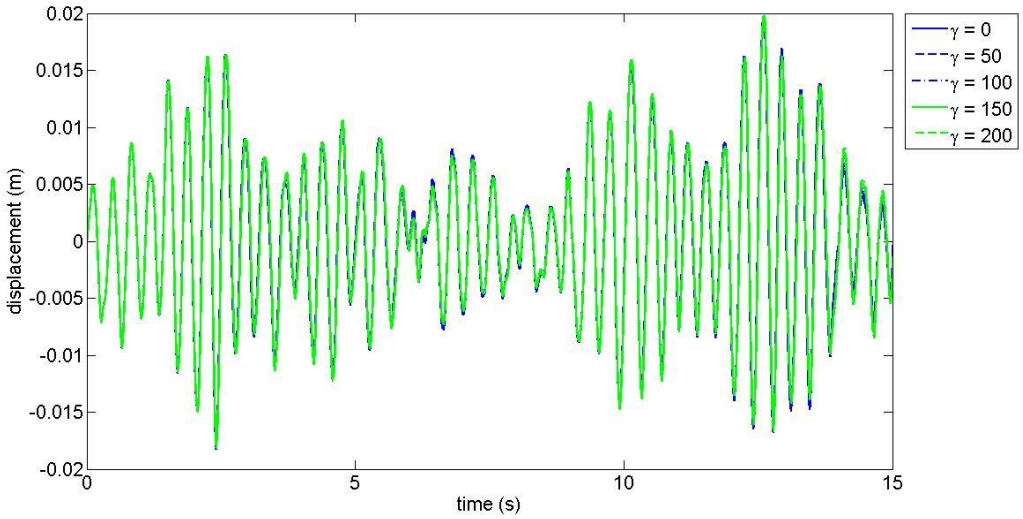

Figure 2.22: Displacement vs time plot under random input of 10 N variance with increasing γ

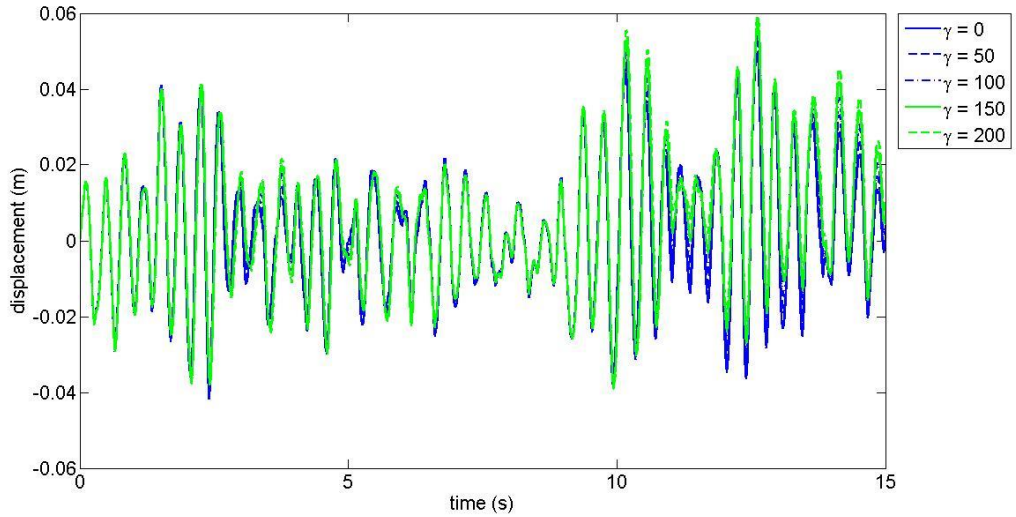

Figure 2.23: Displacement vs time plot under random input of 100 N variance with increasing γ

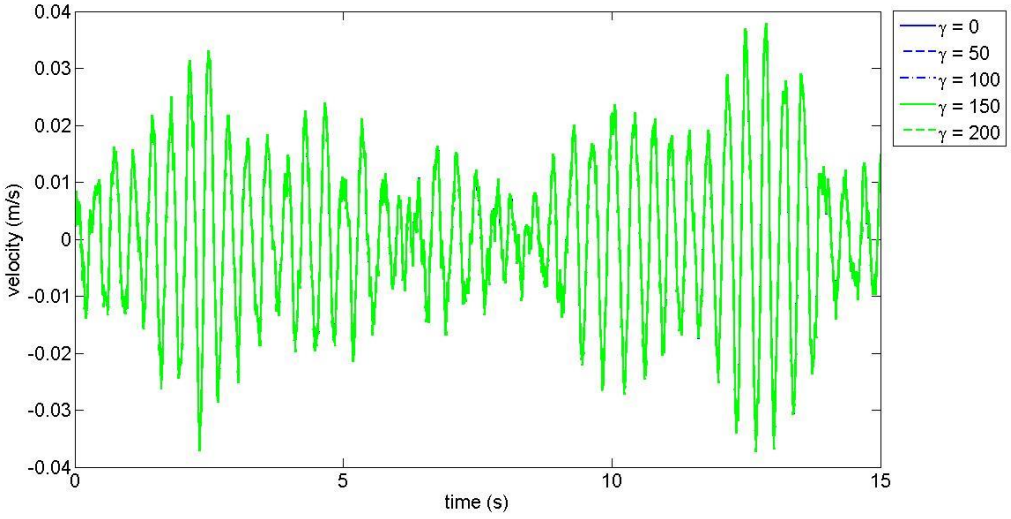

Figure 2.24: Velocity vs time plot under random input of 0.1 N variance with increasing γ

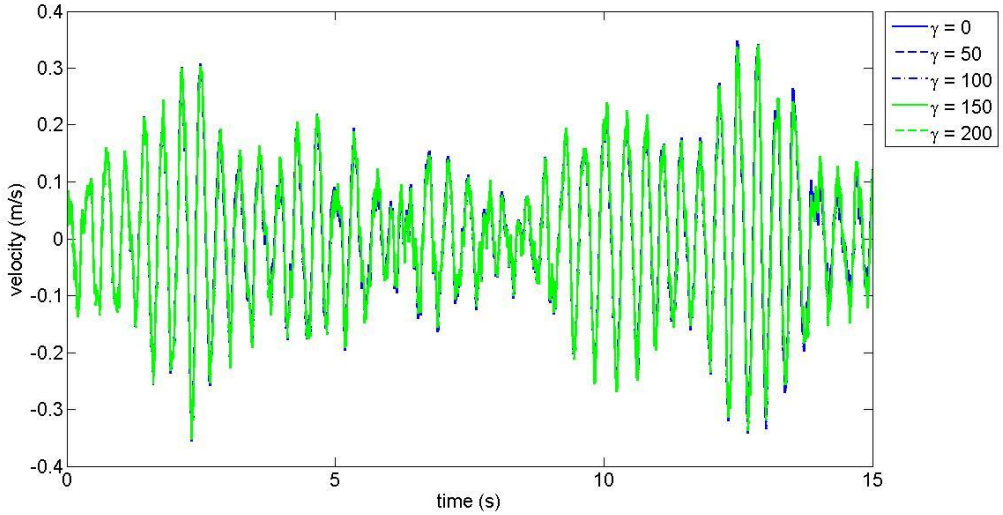

Figure 2.25: Velocity vs time plot under random input of 10 N variance with increasing γ

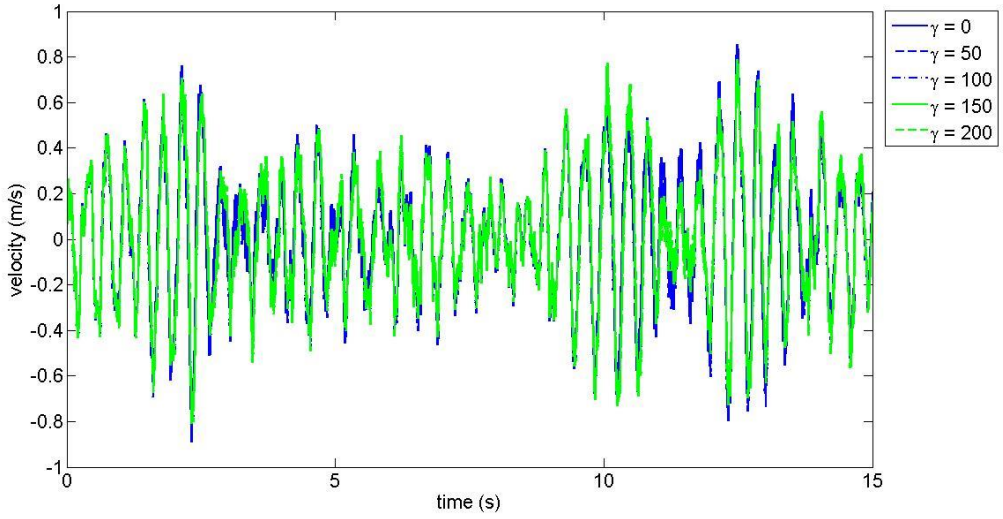

Figure 2.26: Velocity vs time plot under random input of 100 N variance with increasing γ

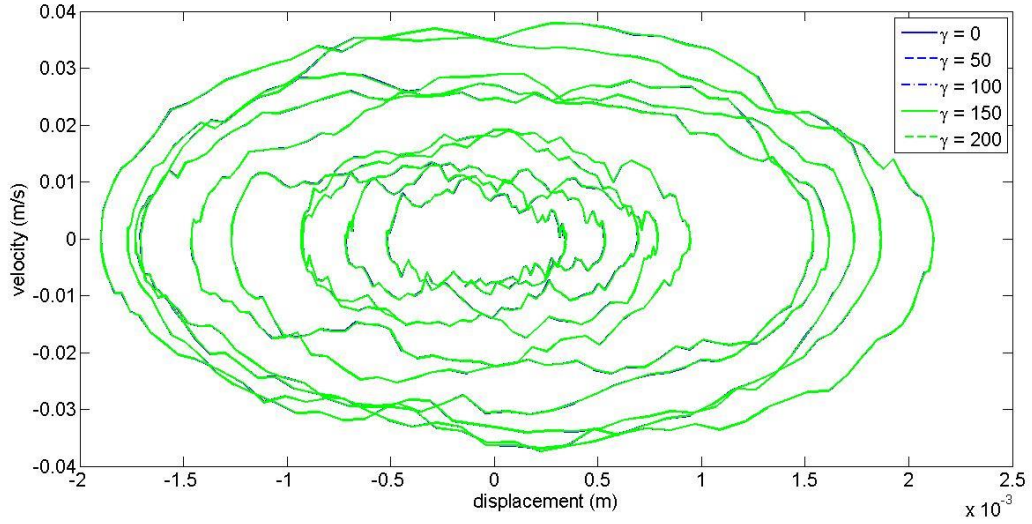

Figure 2.27: Phase plane plot under random input of 0.1 N variance with increasing γ

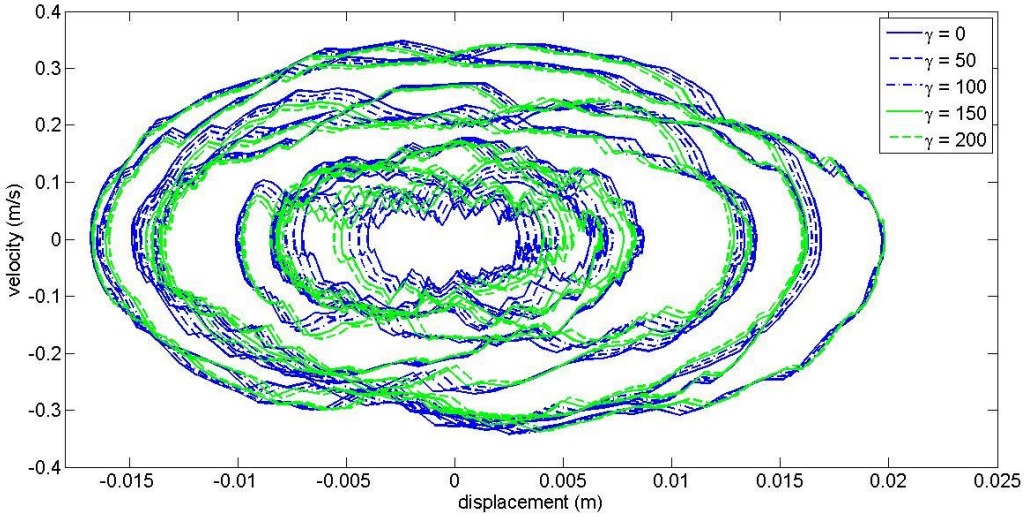

Figure 2.28: Phase plane plot under random input of 10 N variance with increasing γ

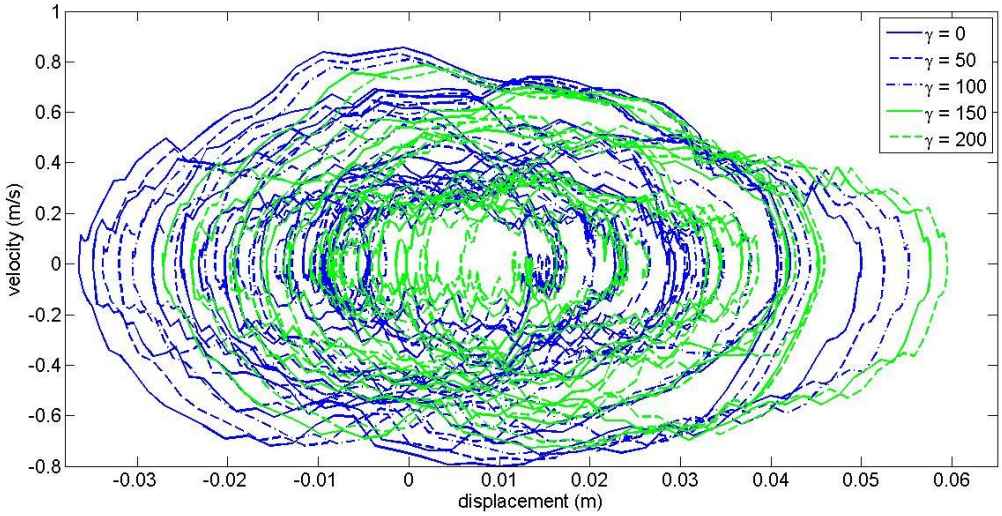

Figure 2.29: Phase plane plot under random input of 100 N variance with increasing γ

2.4.2.2 **Effect of Varying Beta, β**

The Bouc-Wen hysteretic model can demonstrate both hardening and softening behaviour with different combinations of β and γ. Figure 2.30 shows the different behaviour. Hardening usually occurs with negative values of γ.

Similarly to the previous investigation of γ, the parameters values for investigation of β were set as per Table 2.1 except for β. The value of β was increased from 0 to 200 in increments of 50.

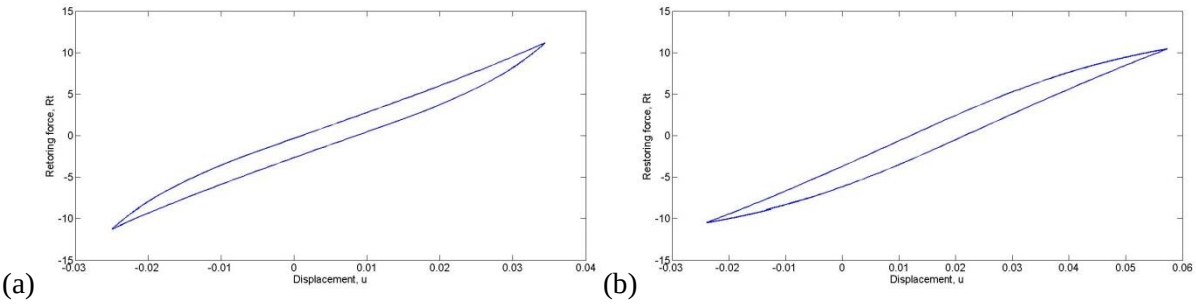

(a) (b)

Figure 2.30: (a) Hardening behaviour (b) Softening behaviour

In Figure 2.31, it can be seen that increasing β reduces the maximum restoring force and displacement within the hysteresis loop. However, compared to the γ changes, here the loop width does not shrink with increasing β. With $\beta = 0$ however, the shape of the loop is totally different with a thinner width, both maximum and minimum stretched and a skewed tip of the loop can be seen. When γ dominates β, the skewed shape of the loop tips tends to occur.

Similarly, comparing sinusoidal input at amplitude 0.1 N and 10 N in Figure 2.32 and Figure 2.33, the effect due to the increase in β can be seen much clearer at the higher amplitude. The higher amplitude will again lead to data which will provide a greater incentive for the parameter optimisation algorithm when building models, thereby resulting in a more accurate model prediction.

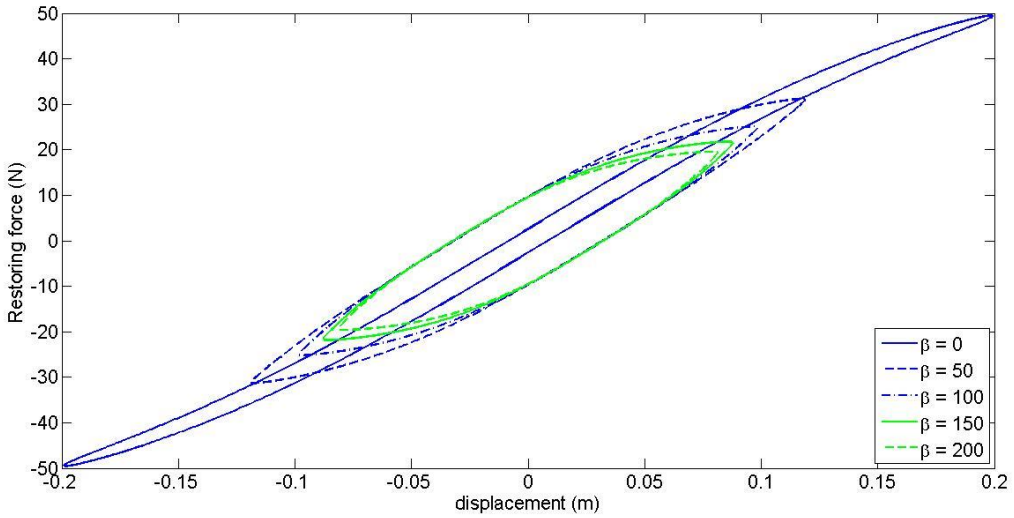

Figure 2.31: Restoring force vs displacement plot under sinusoidal input of 10 N amplitude with increasing β

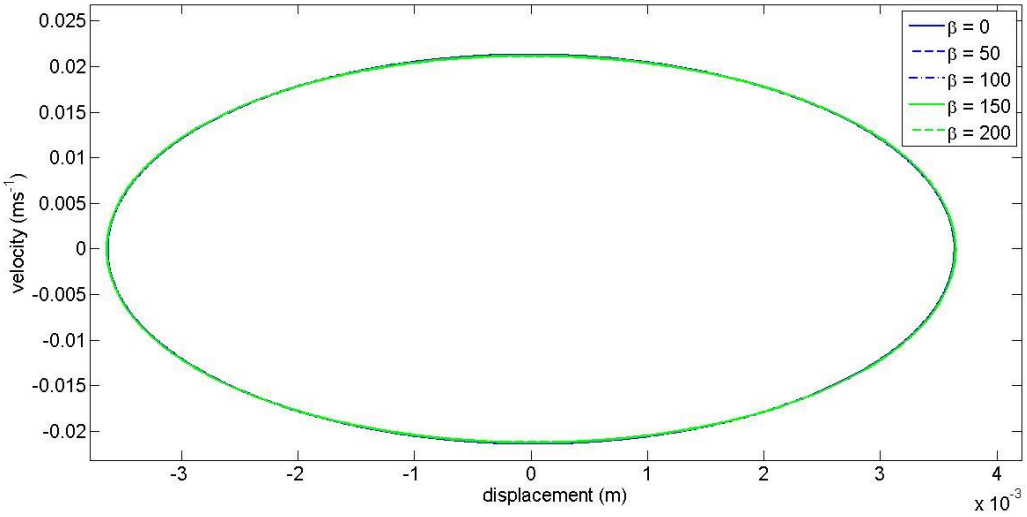

Figure 2.32: Phase plot under sinusoidal input of 0.1 N amplitude with increasing β

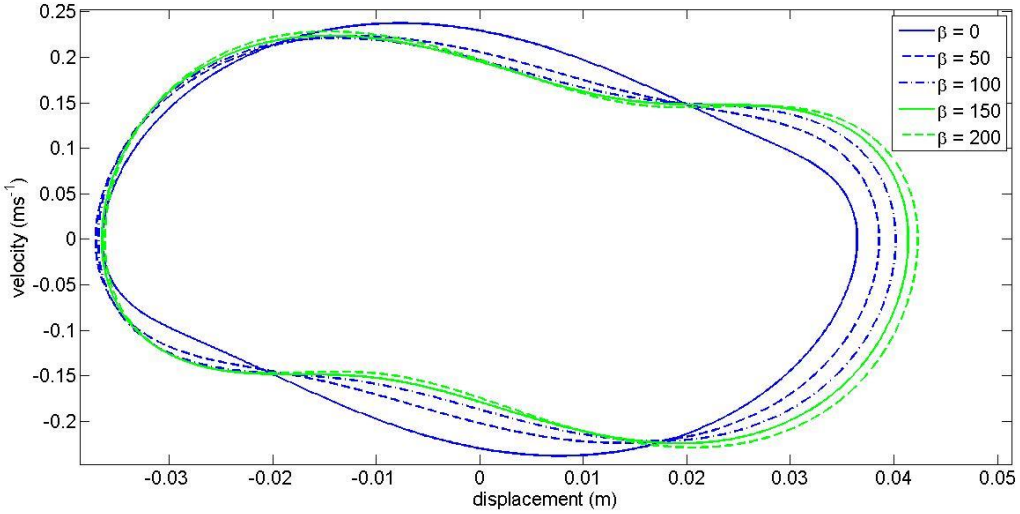

Figure 2.33: Phase plane plot under sinusoidal input of 10 N amplitude with increasing β

Under random input, changes from 0.1 N variance to 10 N variance does not show much difference with increasing β. However the difference is slightly better when compared to the effect of increasing γ with small differences starting to show in the 10 N variance plot. Clear changes can be easily spotted in the 100 N variance plot. Similarly to the previous subsection observation, the random excitation requires even larger amplitude for pushing the nonlinearity of a system.

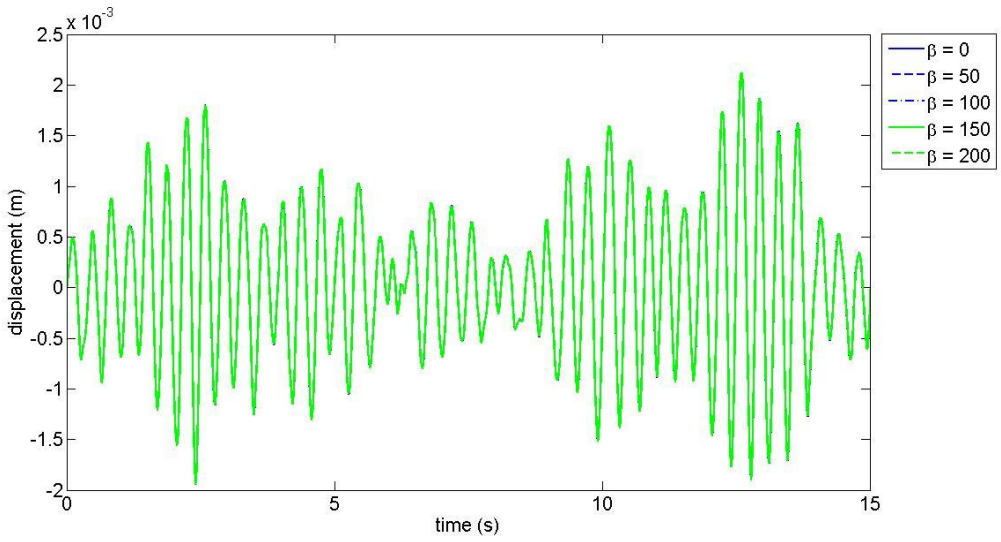

Figure 2.34: Displacement vs time plot under random input of 0.1 N variance with increasing β

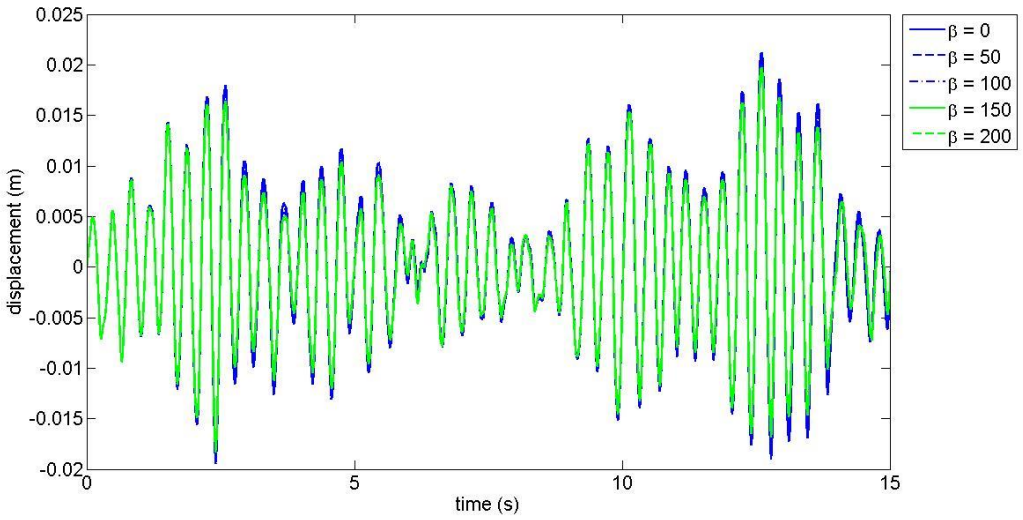

Figure 2.35: Displacement vs time plot under random input of 10 N variance with increasing β

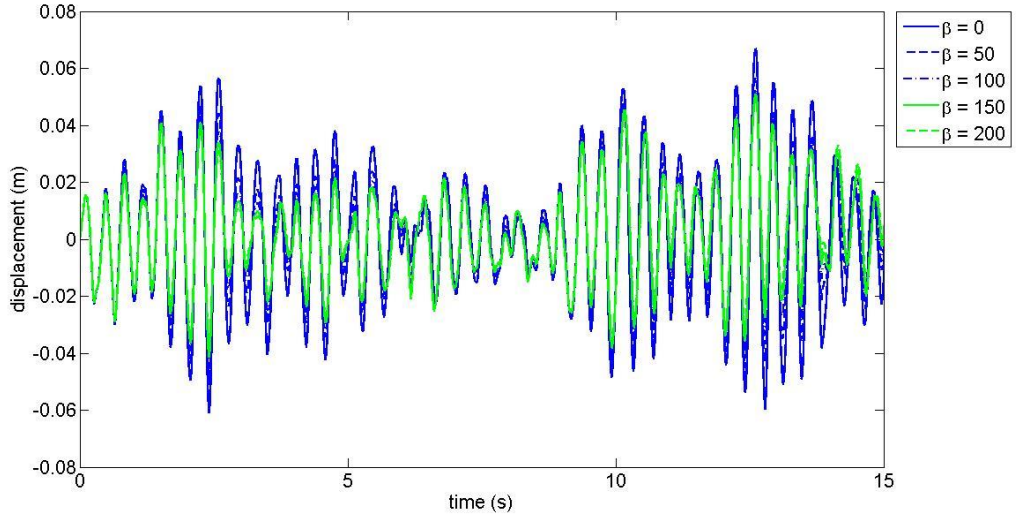

Figure 2.36: Displacement vs time plot under random input of 100 N variance with increasing β

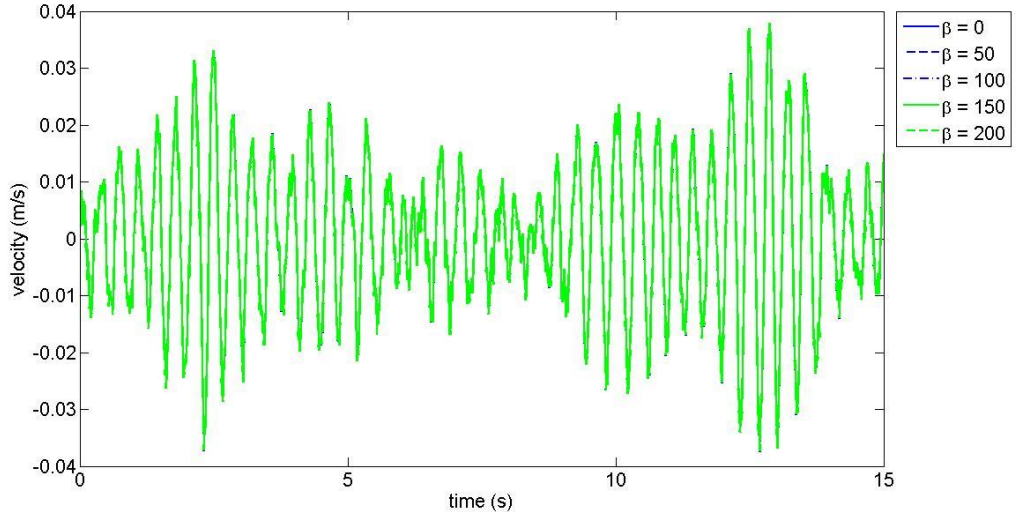

Figure 2.37: Velocity vs time plot under random input of 0.1 N variance with increasing β

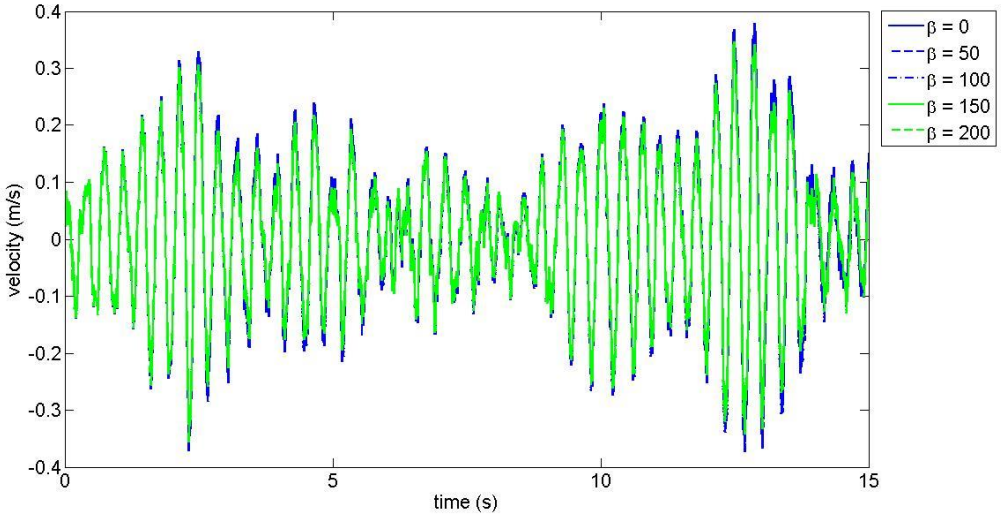

Figure 2.38: Velocity vs time plot under random input of 10 N variance with increasing β

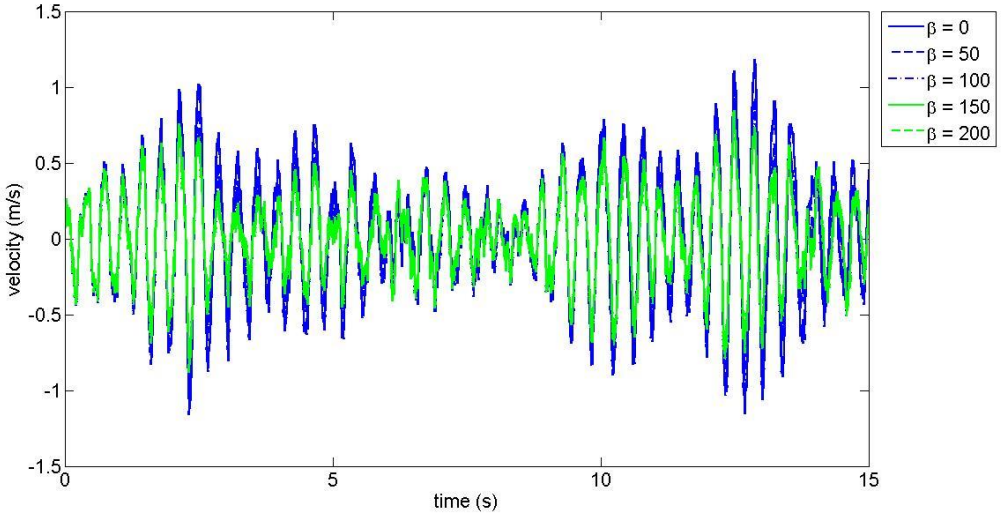

Figure 2.39: Velocity vs time plot under random input of 100 N variance with increasing β

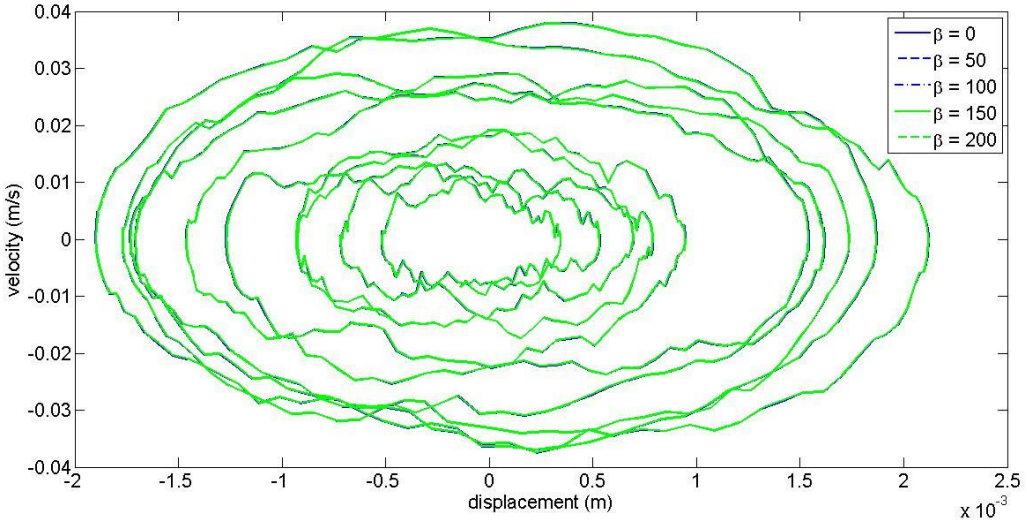

Figure 2.40: Phase plane plot under random input of 0.1 N variance with increasing β

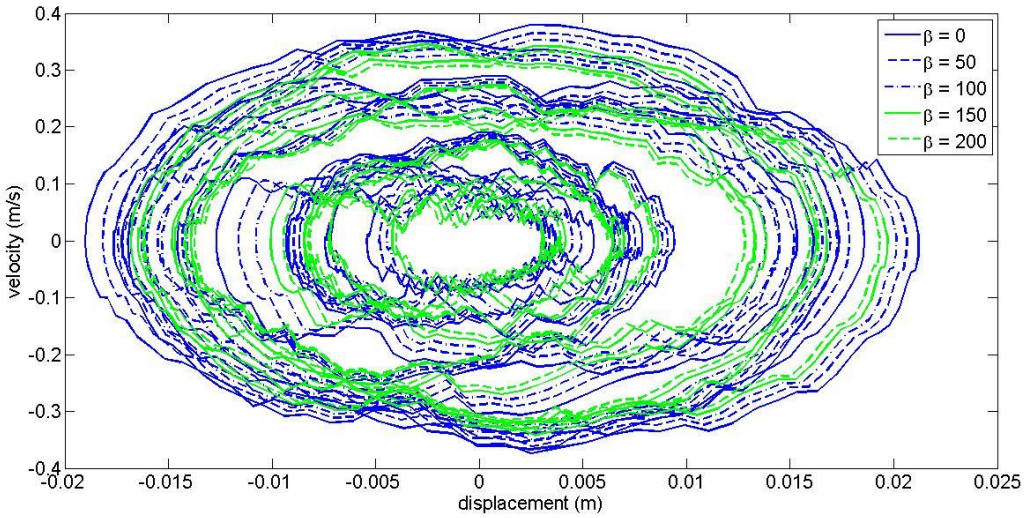

Figure 2.41: Phase plane plot under random input of 10 N variance with increasing β

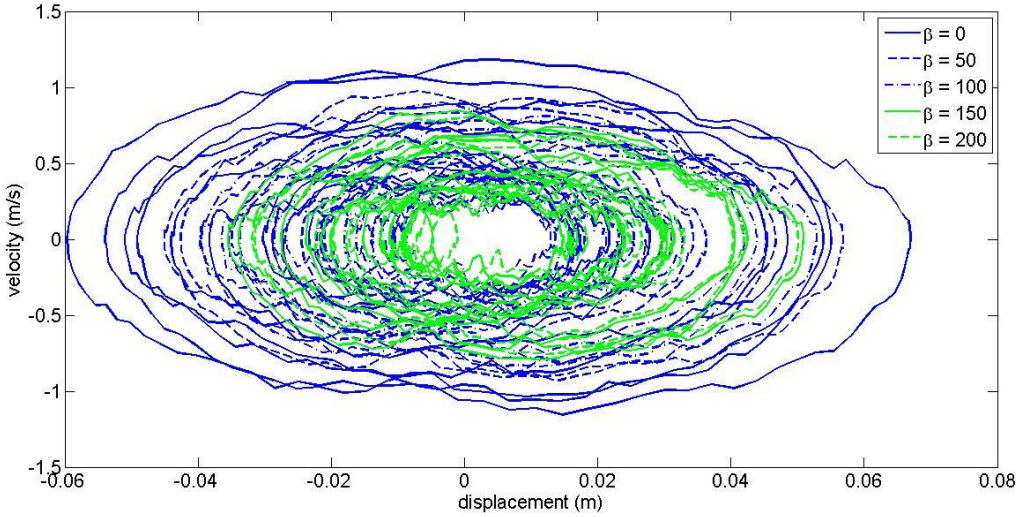

Figure 2.42: Phase plane plot under random input of 100 N variance with increasing β

2.5 **Discussion**

In this chapter, the Bouc-Wen model of a hysteretic system has been introduced and investigated with sinusoidal and random input excitations at low and high input excitation levels. The behaviour of the Bouc-Wen model was shown to be mostly linear when subjected to low amplitude input and at some single frequency harmonic inputs. The nonlinear behaviour was suppressed under these conditions due to the system not being sufficiently excited. It was also shown in this chapter that the Bouc-Wen model with the specific parameters used in the thesis showed odd order harmonics. This odd harmonics behaviour will be further investigated in Chapter 5 and Chapter 6.

Experimental data obtained using sinusoidal input requires more information to control, for example in the case of the model in this thesis. Better response was only seen at the odd harmonics i.e. one third and one fifth of the underlying linear model undamped natural frequency as shown here. At other frequencies, especially at even harmonics, less nonlinear information was shown by the system. Hence in using sinusoidal input, it is important to have an understanding of the system. However, with sinusoidal input, more information on the output of a system could be understood by direct relations to its input from the data. It is possible to relate the output behaviour to the exact frequency that caused that behaviour. This would allow better understanding of the model to be built.

On the other hand, using random input was simpler with only the variance of the input to be determined. Most academic papers on parameter optimisation use random input for data generation due to its simplicity. Model building for a nonlinear system also stems from linear system optimization which uses random input for the data generation. This extension was mainly the reason random input was still preferred other than having a single input that was expected to cover wide range of frequencies. Random input also introduced a linearisation effect, so a much higher excitation amplitude (variance) on the random input signal was required. This was shown in this chapter where the increase from 0.1 N to 10 N did not show much difference with the varying nonlinear parameter γ and β in the investigations. Nonlinear behaviour only started to show at the 100 N excitation amplitude.

Here some examples of the importance of properly setting the specification of model performance requirements (Stage 1) from the proposed framework for building model in Chapter 1 were shown. If a system to be modelled needs to perform under a high excitation environment, data for the model building should truly represent this. Only by doing this will the predicted model be able to properly represent the actual system under the same condition. Even with a true system that works under a low forcing environment, by providing the right data, parameter optimisation cost could be saved. No unnecessary time should be spent to identify parameters that the system would not be sensitive to.

Predicted models should truly represent the real system in order to improve safety and reduce cost. That is why it is very important to set the specification of model performance requirement right and then designing experiments that would provide data with ample information for the optimization.

The same Bouc-Wen model will be used in parameter optimisation investigation in the following chapters to further investigate optimisation results under the different input excitation types and excitation levels.

Chapter 3

3 Nonlinear Parameter Estimation using Random Excitation

3.1 Introduction

In the previous chapter, the Bouc-Wen model of hysteretic systems was introduced and the behaviour of the system was investigated for both sinusoidal and random input excitation. The same model with the same parameters as investigated in the previous chapter will be used here as an example model for investigation of nonlinear parameter estimation.

In this chapter, parameter estimation is conducted on data from a random input of low and high levels of excitation to represent mostly linear and nonlinear systems. This is done to show that using estimated data without having the proper input can lead to inaccurate estimation of the parameters. Extended data is used to investigate whether it could provide more information for the system identification algorithm in order to improve its estimation. The Improvement Ratio is also calculated

to improve confidence in the parameter estimation by showing the percentage of cost function improvement of an estimated nonlinear system over an estimated linear system.

Firstly, Self-adaptive Differential Evolution (SADE) is implemented to identify the parameters of the Bouc-Wen model using data from random input of low and high excitation levels. The results of the parameter estimation are compared to show the effect of the different inputs on the parameter estimation result. For each of the parameter estimation results, the Improvement Ratio is calculated. Then an additional investigation using extended random input data is also conducted to investigate whether it would contribute to improve the parameter estimation. Finally, the chapter will also discuss how SADE adapts to improve the estimation of the parameters compared to DE.

3.2 **Bouc-Wen parameter estimation**

The parameter estimation exercise in this chapter was conducted using Self-Adaptive Differential Evolution (SADE) algorithm written in Matlab with Simulink. A population size of 35, that is 5*D (where D is the number of parameters to be identified), was used to create the initial population matrix. The four strategies that were used were Rand/1, Rand/2, Current to Best/2 and Current to Rand/1. The strategies were initially set with 25% probability of use each. After the initial 20 generations, this probability was updated according to number of successful trial. With each updates, the strategy with the higher success rate would be more favoured in the next generations. The details on the strategies are further explained in Appendix A. The crossover ratio and mutation factor hyperparameters were set at initial values of Cr= 0.5 and Fr= 0.9. Both hyperparameters value was allowed to update every 10 generations to give fair evaluation of trials before updating.

The parameter estimation exercise was conducted for a low variance level (= 0.1), medium level (= 10) and high variance level (= 100) with 1000 generations as a maximum limit. The parameter estimation usually will have reached optimum estimation value within 400-500 generations. These exercises were repeated for 100 runs for each variance level. The Simulink circuit was similar to the one used in previous chapter with the investigation of Bouc-Wen model of a hysteretic system as shown in Figure 3.1. In this chapter only random input excitation data had been investigated as shown

by the random block in the Simulink circuit. The signal used was generated with a sampling time of 0.0025s taking 2000 points of simulated data for identification purposes. The random input block was fixed to start with seed of 0. The same parameters as in Chapter 2 were used for the Bouc-Wen model as shown in Table 3.1.

Parameter	Value	Units
m	1	kg
c	0.7037	Ns/m
k	309.51	N/m
α	0.01	-
β	150	1/m
γ	20	1/m
A	1	-
n	2	-

Table 3.1: Parameters of the Bouc-Wen model

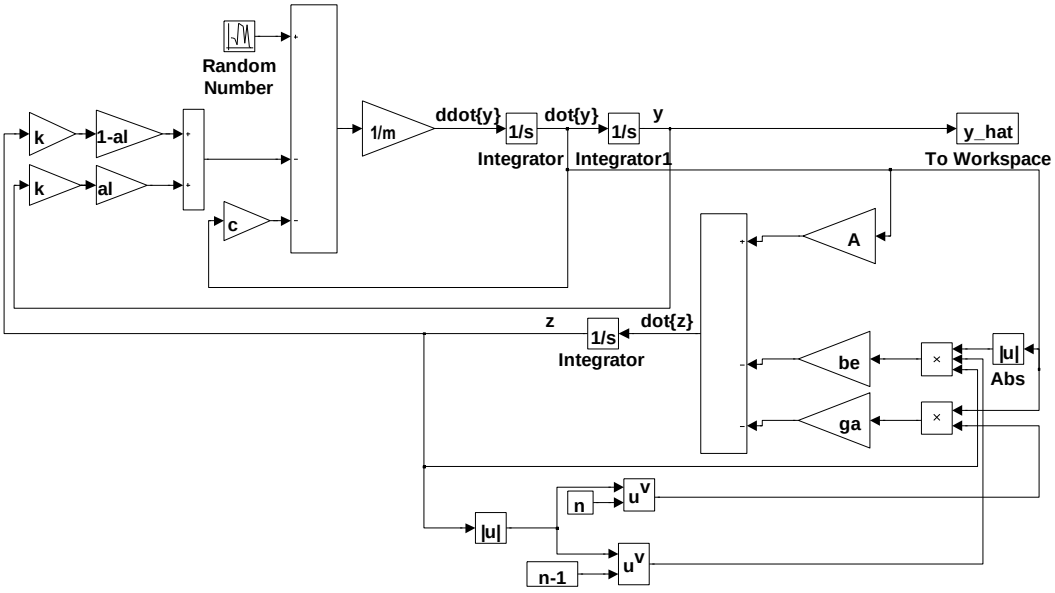

Figure 3.1: Simulink circuit for the Bouc-Wen model

The results below only consider runs which gave MSE values of less than 5% to remove outliers. Only 12 out of the total of 300 runs did not converge as expected. This would be due to the challenges faced by the use of inverse identification method where the parameter estimation can get trapped at

around the false minima. This would happen when the parameter optimisation would not be able to make the next generation estimation that could jump out of the false minima area.

Figure 3.2 shows the plot of output signals obtained from the Bouc-Wen system at three levels of excitation with input variance 0.1, 10 and 100 with a set-up as shown in the Simulink model above. Figure 3.3 shows a zoomed in plot of the output signals. It may be observed that with the variance level at 100, the output signal started to show distinct nonlinearity behaviour that could be picked up by a parameter estimation algorithm. It is expected that these would result in a more precise parameter estimation compared to a parameter estimation undertaken at the low variance level of 0.1. The results for the parameter estimations are shown in Table 3.2, Table 3.3 and Table 3.4 below:

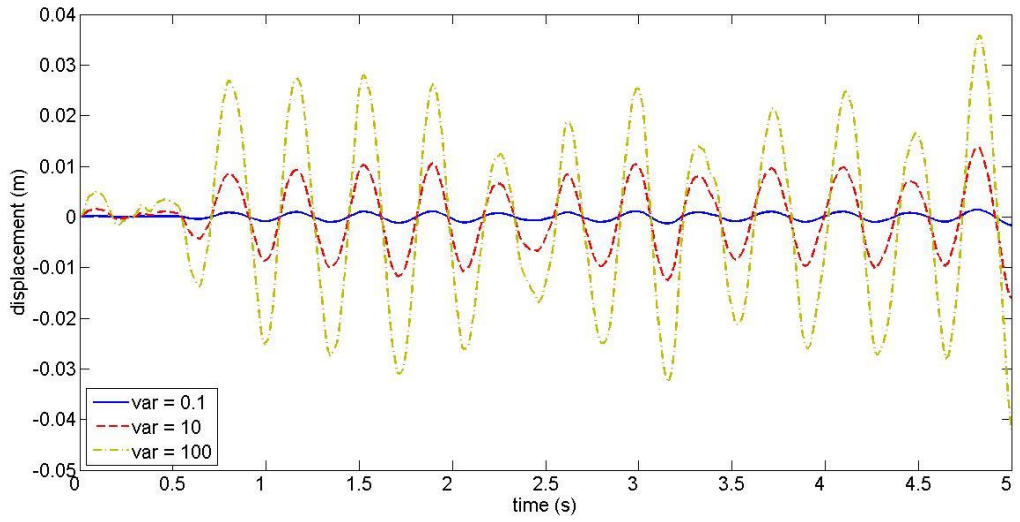

Figure 3.2: Output displacement responses from a random input with three variance levels

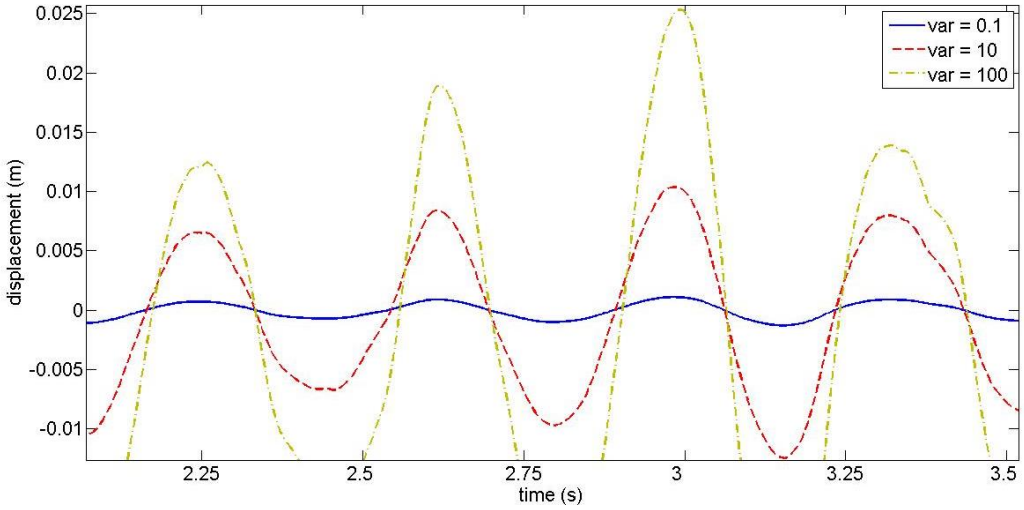

Figure 3.3: Zoomed in plot of output displacement responses from a random input with three variance levels

	Real Parameter	Best Estimated Parameter	% Error	Mean Estimated Parameter	Standard Deviation
m	1	1	2.44E-06	1.0001	0.0010
c	0.7037	0.7037	4.50E-05	0.7038	0.0005
k	309.51	309.51	1.47E-06	313.7903	13.6628
α	0.01	0.1744	1.64E+03	0.4775	0.2610
A	1	1	0.00E+00	0.9442	0.1586
β	150	179.9427	19.9618	242.5512	55.0132
γ	20	23.9349	19.6743	21.3328	11.1762

Table 3.2: Parameter estimation result with variance = 0.1

	Real Parameter	Best Estimated Parameter	% Error	Mean Estimated Parameter	Standard Deviation
m	1	1	1.62E-06	0.9997	5.30E-04
c	0.7037	0.7037	3.74E-05	0.7014	0.01
k	309.51	309.515	1.60E-03	317.0893	20.207
α	0.01	0.0101	1.0599	0.1485	0.1523
A	1	1	1.60E-03	0.9679	0.0849
β	150	150.0193	1.29E-02	197.3601	61.5648
γ	20	20.0052	2.58E-02	17.2099	7.8486

Table 3.3: Parameter estimation result with variance = 10

	Real Parameter	Best Estimated Parameter	% Error	Mean Estimated Parameter	Standard Deviation
m	1	1	4.16E-10	0.9999	0.0011
c	0.7037	0.7037	5.54E-09	0.7027	0.0053
k	309.51	309.51	1.82E-08	319.1399	16.5742
α	0.01	0.01	9.80E-07	0.0126	0.0109
A	1	1	1.83E-08	0.9715	0.0452
β	150	150	3.56E-08	155.5928	9.0546
γ	20	20	9.40E-08	19.5301	4.0461

Table 3.4: Parameter estimation result with variance = 100

From the results in the tables above, the best estimated parameter correspond to MSEs of 1.78e-13, 2.26e-21 and 4.20e-21 for the variance levels 0.1, 10 and 100 respectively. Moving forward, only the low level and high level variance random excitations will continue to be investigated as the medium level variance of 10 did not provide any additional insights for comparisons.

It can be observed in the best estimated parameter column that the parameter estimations at the low and high variance levels were giving exact predictions (very small insignificant error) for the linear parameters *m, c, k* and *A*. Parameter estimation for α, β and γ on the other hand was significantly worse for the low variance estimation with 20% error for both β and γ, whilst the α error was very large at over 16 times the real value. Although the errors on these parameters were very high for this simulation, the objective function (mean square error) was still impressively low giving the impression of an excellent estimation. Comparatively, for the high variance estimation, the best estimated parameters returned very low errors for the nonlinear parameters, α, β and γ.

However, since in a real model building problem, the true parameter value is unknown and no best estimated parameter can be expected, the data of a mean parameter value is often taken as the predicted parameter of the model identified. This presents another concern of using random excitation data where the standard deviations for the high variance level for *k*, β and γ are still quite high even without any presence of noise.

Further investigations that looked into the mean estimated parameters from Table 3.2 for the low variance estimation can be seen in Figure 3.4 to Figure 3.8. This is conducted to demonstrate the

effect when the model parameters identified from low excitation are used to try to predict the system behaviour under high excitation. Figure 3.4 shows that using the mean estimated parameters identified at 0.1 variance, the system output behaves similarly to a linear system of $m\ddot{u} + c\dot{u} + ku = F(t)$ with m = 1, c = 0.7037 and k = 309.51. As at low variance, the Bouc-Wen system does not show any nonlinear behaviour, the estimation algorithm manages to get the linear parameter right and could not determine any relevance for finding the real nonlinear parameter, hence the total neglect of α which is the ratio of linear and nonlinear. With low variance input such as this, α, β and γ could easily be any value as they do not dictate or contribute to the system behaviour at all.

Figure 3.5 shows the system using mean estimated parameters identified at 0.1 variance plotted at a variance of 100. Here however it looks like the estimation matches the true system response up until around 3.5s where it starts to show a slight variation. This is still is a very good prediction and the calculated mean square error (MSE) is under 5%. Looking at the higher amplitude (variance of 300) in Figure 3.6, the variation between the estimated system and the true system response still looks to be a good fit with an MSE of 3.45%.

The results here seem to show that, using grossly inaccurate nonlinear parameters does not have a significant effect upon the overall system response. If working on a real system without having known the real parameters, as in this exercise, it would seem that the predicted parameters were truly the real parameters of the system. It could almost be said here that the model behaviour is insensitive to the nonlinear parameters.

Figure 3.7 shows the plot of MSE against increasing variance level with estimated parameters identified from a low variance (= 0.1) and a high variance (= 100). The MSE at each variance level are calculated for both the identified estimated parameters to investigate how the MSE for random excitation is dependent upon variance levels. Looking at the plot for the mean estimated parameters identified from the low variance level estimation, it can be seen that the MSE does in fact stay below 5 up to variance level of 500.

The same investigation using mean estimated parameters identified from low and high level variances have been used to fit to an extended data set. This is to see if the same behaviour would hold for any random input excitation and not just limited to the previous set of data only. The MSEs were calculated from 30 different sets of random excitation data with the variance kept at the same levels. The average MSE was calculated and plotted against variance level. In Figure 3.8, it can be seen that the previous behaviour does not hold for the model using mean estimated parameters identified from low variance level when using the extended data sets. The MSE now is over 5% for almost all variance levels slightly above 100.

Meanwhile, the MSE for the mean estimated parameters identified from the 100 variance level shows the same pattern as in the previous investigation with MSEs less than 5% starting at a variance level of 100 and higher.

Since it is difficult to determine the frequency effect of random input on the resulting output, the next subsection investigates whether parameter estimation using an extended data set would improve the parameter estimation accuracy and fitting of identified parameters of the estimated system to the real system.

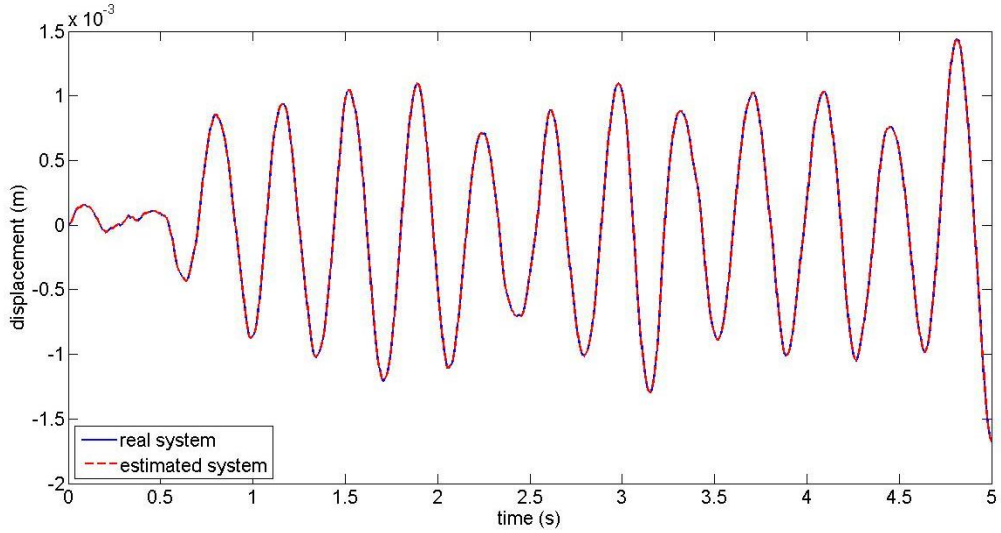

Figure 3.4: Response plot of linear system and estimated system from var. = 0.1

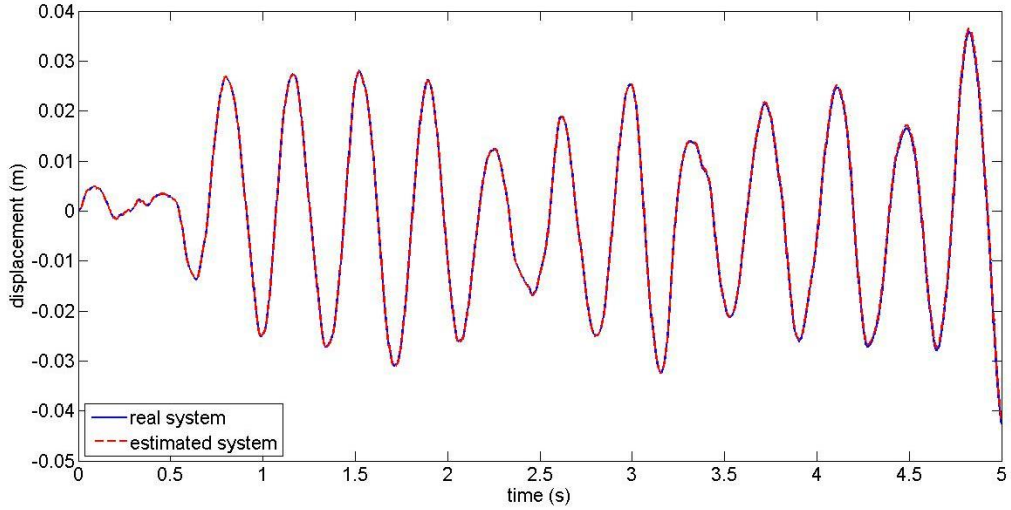

Figure 3.5: Response plot at var =100 of Bouc-Wen system and estimated system from var. = 0.1

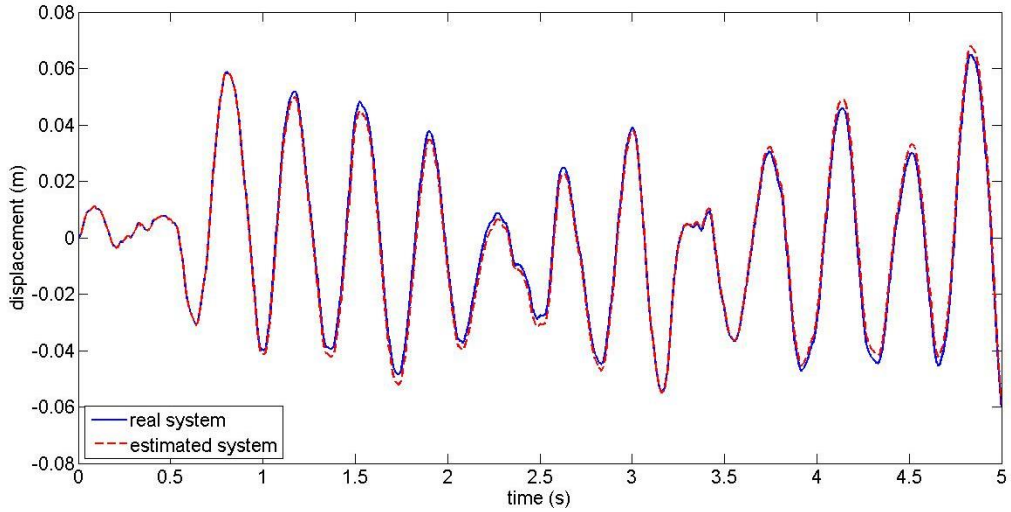

Figure 3.6: Response plot at var. = 300 of Bouc-Wen system and estimated system from var. = 0.1

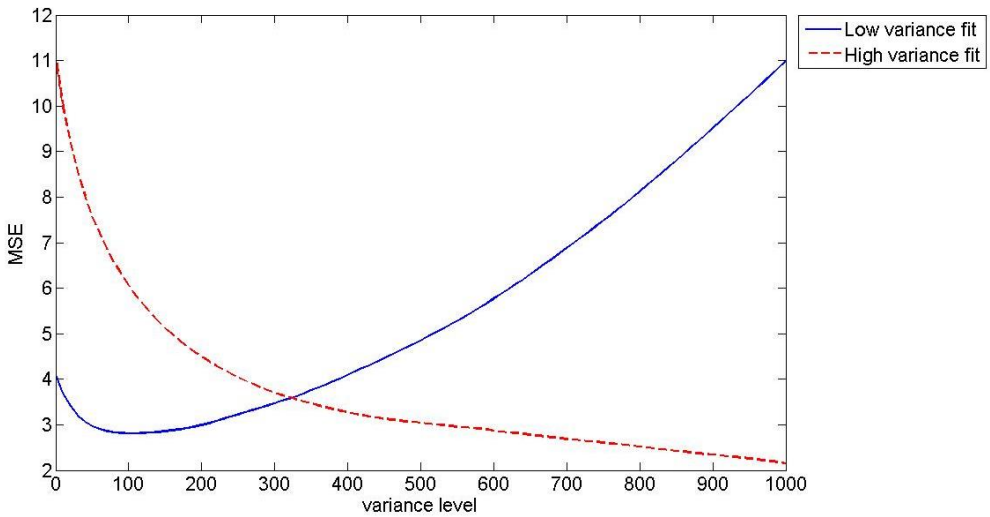

Figure 3.7: MSE for fitting estimated parameters to one data set against variance level

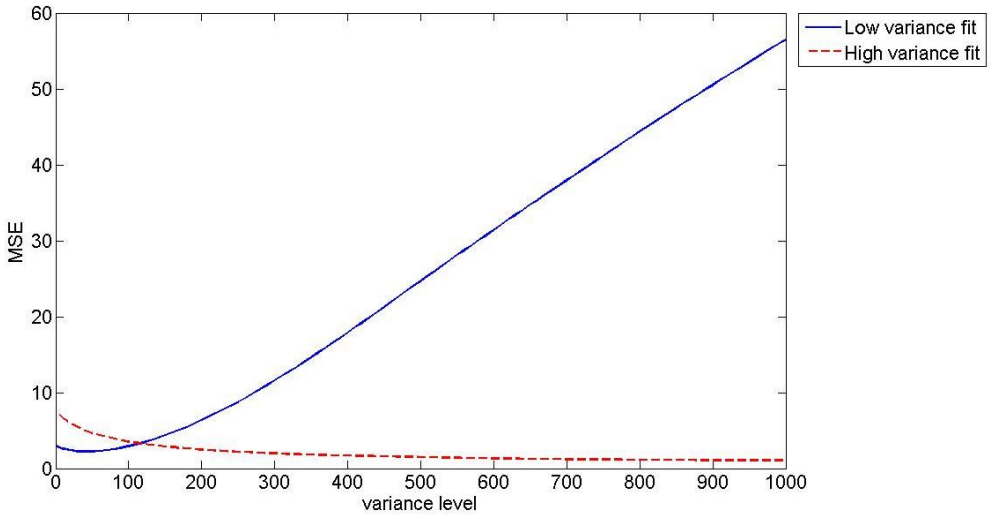

Figure 3.8: MSE for fitting estimated parameters to extended data set against variance level

3.2.1 Extended data set

Using an extended data set, a similar exercise as above was conducted. Five sets of random excitation data were used here with each data set sets to run for 20 runs with a maximum of 1000 generations per run. Similar parameters for the SADE were used for the population size, strategy choice and crossover ratio and mutation factor hyperparameters in order to have a direct comparison with the previous investigation. The purpose of using extended data sets was to see if any improvement in accuracy can be gained for parameter estimation using random excitation data to minimise the linearisation effect.

Table 3.4 and Table 3.5 show the results for low and high levels of variance respectively. The mean estimated parameter and standard deviation in the table come from the average of all the total of 100 runs. The MSEs for the best estimated parameters associated with the tables are 2.67E-15 and 4.90E-25 respectively.

Fitting the mean estimated parameter identified from the low and high variance levels from the tables, the MSE against variance level was plotted as in Figure 3.9. Both were fitted using 30 different sets of random excitation data similar to Figure 3.8. No improvement was seen for the low variance level estimates due to the signal being mostly linear and still neglecting the nonlinear parameters. However, for the estimated parameters from the high variance level, the MSE stayed below 0.1% even at a low

variance level thus showing an improved fitting compared to the estimation using single data sets. This result shows that by having extended data sets an improvement in parameter estimation can be obtained. The improved estimation at a high variance level of 100 allows the estimated parameters to be fitted to all levels of variance compared to the previous result.

	Real Parameter	Best Estimated Parameter	% Error	Mean Estimated Parameter	Standard Deviation
m	1	1	0	1.0002	0.0017
c	0.7037	0.7037	0	0.7039	0.0006
k	309.51	309.6897	0	322.491	24.7400
α	0.01	0.015	50	0.4494	0.2589
A	1	0.9994	0	0.8823	0.2041
β	150	150.849	1	230.6049	60.7499
γ	20	20.1124	1	21.9828	10.5786

Table 3.4: Parameter estimation result with variance = 0.1 using extended data set

	Real Parameter	Best Estimated Parameter	% Error	Mean Estimated Parameter	Standard Deviation
m	1	1	0	1.0001	0.0010
c	0.7037	0.7037	0	0.7025	0.0046
k	309.51	309.51	0	319.7865	17.3175
α	0.01	0.01	0	0.0140	0.0151
A	1	1	0	0.9699	0.0470
β	150	150	0	156.2187	10.2873
γ	20	20	0	20.1435	1.9815

Table 3.5: Parameter estimation result with variance = 100 using extended data set

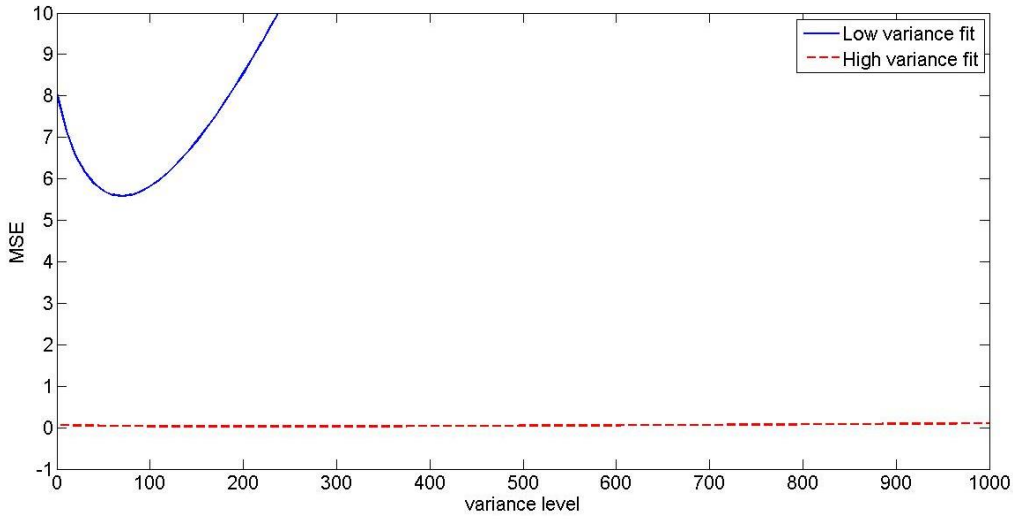

Figure 3.9: MSE for fitting estimated parameters identified using extended data set against variance levels

The Improvement Ratio as suggested in Chapter 2 was also compared here as shown again in Equation 3.1 to remind the reader. Linear parameter estimation was conducted for both low and high variance level data with the extended data set. Linear parameter estimation means that only the *m*, *c* and *k* value were fitted to the data during the parameter optimisation process. In both cases, the linear fitting estimation gives a MSE value of lower than 5%. The linear fitting MSE value was 1.02E-06 and 0.5754 for low and high variance data respectively with an Improvement Ratio of 3.83E+08 and 1.17E+24 respectively. For the high variance data, the Improvement Ratio was significantly greater compared to the Improvement Ratio of the low variance data. This would provide more confidence in the nonlinear model estimation.

$$Improvement\ Ratio = \frac{Linear\ Model\ Error - Nonlinear\ Model\ Error}{Nonlinear\ Model\ Error} \tag{3.1}$$

3.3 **Bouc-Wen parameter estimation with noise**

In this section, the investigation as above was carried out in the presence of output noise added to the data. The noise was added at a level of 5% root mean-square value of the output signal. For the model that corresponds to the parameters in this thesis, 10% noise was not feasible as it would cause the parameter estimation to not be able to converge to a MSE of 5%, hence the resulting estimated parameters did not represent the model as expected.

The result for parameter estimation for one data set for the low and high input excitation is given in Table 3.6 and Table 3.7 respectively. The best estimated parameter corresponds to 0.2516 for the low input excitation estimation and 0.2476 for the high input excitation estimation. Although the MSE are quite similar, the percentage errors of the nonlinear parameter against the true parameter values are quite different with high error on the low input excitation estimates. Similarly as in the data without noise estimation, only under the high input excitation estimation was the nonlinear parameters identified appropriately.

The results identified using the extended data set for low and high input excitation is given in Table 3.8 and Table 3.9 respectively. The best parameter estimates corresponds to a MSE of 0.2495 and

0.2586 respectively. Similar to the above findings, only the parameter estimation using high input excitation data returned all the estimated parameters as expected with low errors for both linear and nonlinear parameter estimates.

To calculate the Improvement Ratio, a linear model of *m*, *c* and *k* was used in the parameter estimation exercise. This was only calculated for the extended set since the MSE were quite similar for both methods. The cost function MSE of 0.2494 was obtained for low input excitation for the linear fitting with an Improvement Ratio of 0.0004, while for the high input excitation the MSE was 2.0606 with Improvement Ratio of 6.9683. This shows that, although using low input excitation for the parameter estimation may give a good MSE, but looking at the Improvement Ratio, it clearly shows that there is almost no benefit of using the Bouc-Wen model as the selected model over a basic linear model in this particular parameter estimation exercise. With the use of the Improvement Ratio here, a concern could be raised about such a low Improvement Ratio, prompting the user to revisit either the model selection step or redesign the experiments to provide a more suitable data for estimation.

With the identified mean estimated parameters from both single data set and the extended data set, the MSE against increasing variance level was plotted in Figure 3.10 and Figure 3.11 respectively. It was observed that no improvement was obtained using the extended data set here in the presence of noise, contrary to the previous observation with data without noise. The same observation on the importance of the having suitable input data was sustained here with the model using the mean estimated parameters from the low input excitation data giving an MSE over 5% for all variance levels.

	Real Parameter	Best Estimated Parameter	% Error	Mean Estimated Parameter	Standard Deviation
m	1	0.9984	1.64E-01	0.9983	0.0004
c	0.7037	0.6992	6.33E-01	0.7004	0.0008
k	309.51	309.096	1.34E-01	313.6494	5.9907
α	0.01	0.1054	9.54E+02	0.673	0.3906
A	1	0.9997	3.12E-02	0.7765	0.2683
β	150	300	1.00E+02	250	100.0000
γ	20	30	5.00E+01	15.05	17.2628

Table 3.6: Parameter estimation result with variance = 0.1 with presence of noise

	Real Parameter	Best Estimated Parameter	% Error	Mean Estimated Parameter	Standard Deviation
m	1	0.9981	1.95E-01	0.9981	0.0001
c	0.7037	0.7253	3.06E+00	0.7258	0.0011
k	309.51	309.0981	1.33E-01	312.8921	8.2612
α	0.01	0.01	4.45E-11	0.01	0.0000
A	1	1	0.00E+00	0.9881	0.0258
β	150	145.4897	3.01E+00	147.1609	3.6318
γ	20	25.2159	2.61E+01	24.3383	1.9778

Table 3.7: Parameter estimation result with variance = 100 with presence of noise

	Real Parameter	Best Estimated Parameter	% Error	Mean Estimated Parameter	Standard Deviation
m	1	1.0012	1.22E-01	0.9998	0.0019
c	0.7037	0.7015	3.07E-01	0.7043	0.0029
k	309.51	309.8752	1.18E-01	314.914	11.5723
α	0.01	1	9.90E+03	0.7339	0.3793
A	1	0.5039	4.96E+01	0.7712	0.3021
β	150	101.2924	3.25E+01	173.6901	78.3907
γ	20	11.148	4.43E+01	16.8155	12.4712

Table 3.8: Parameter estimation result with variance = 0.1 using extended data set with presence of noise

	Real Parameter	Best Estimated Parameter	% Error	Mean Estimated Parameter	Standard Deviation
m	1	0.9985	1.49E-01	0.9995	0.0016
c	0.7037	0.7055	2.54E-01	0.7007	0.0053
k	309.51	311.6322	6.86E-01	321.6677	21.5586
α	0.01	0.0127	2.73E+01	0.0148	0.0065
A	1	0.9923	7.71E-01	0.9644	0.0578
β	150	152.7135	1.81E+00	158.2198	10.3329
γ	20	27.1196	3.56E+01	17.1469	5.8069

Table 3.9: Parameter estimation result with variance = 100 using extended data set with presence of noise

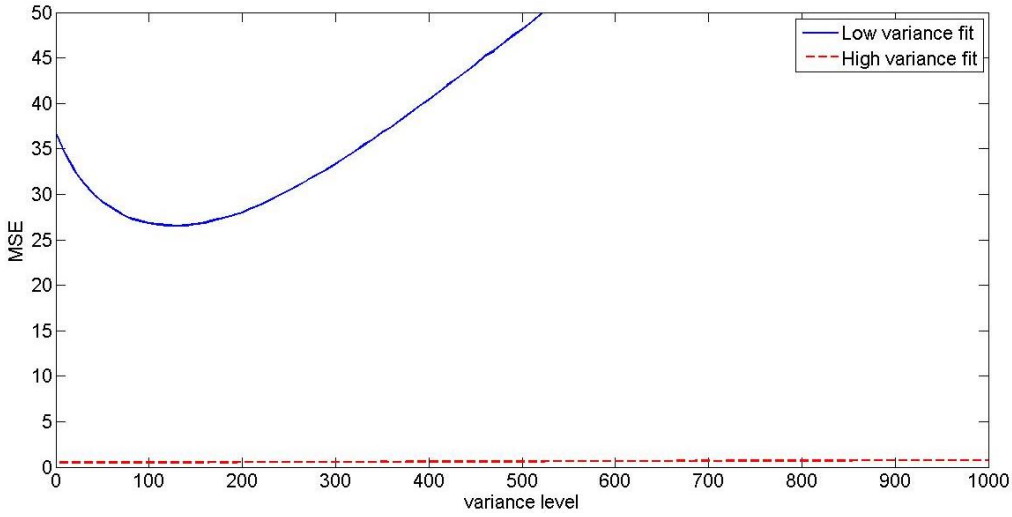

Figure 3.10: MSE for fitting estimated parameters identified using single data set with noise against variance levels

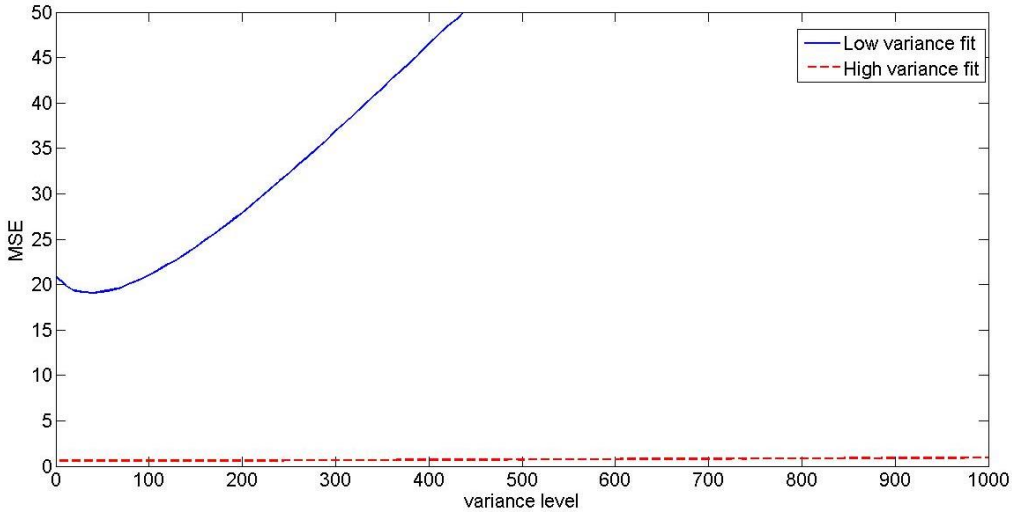

Figure 3.11: MSE for fitting estimated parameters identified using extended data set with noise against variance levels

3.4 **SADE strategies and hyperparameters**

In this section the behaviour of SADE itself is observed. The SADE ability to adapt its optimisation parameter is interesting and has been observed to show similar patterns during the optimisation exercises conducted in this chapter. These adaptations of strategy choices, crossover ratio and mutation factor hyperparameters resulted in improved efficiency for the optimisation process in which new generation populations were driven towards finding the optimum value more effectively with every adjustment to the SADE parameters.

3.4.1 Mutation strategy behaviour

Throughout the optimisation exercises in this chapter, a consistent adaption of the mutation strategy behaviour was observed with a typical plot being shown in Figure 3.12. The convergence points are usually different depending on the selected model and variance level. It was seen that initially, the preferred strategies were Rand/1 and Rand/2. At later generations the preference switched to Current to Best/2 and Current to Rand/1. It appeared that the SADE preference of strategy Rand/1 and Rand/2 initially was to allow a wider search area for the early investigation of the parameter values. When a more restricted search space of parameter values had been identified, the strategy switched to Current to Best/2 and Current to Rand/1 to allow the investigation to focus the search in the preferred space around the best parameter values and the current parent values which by that time would already be good estimates. This gives SADE its advantage of using multiple strategies without requiring the user to determine when to switch between these strategies.

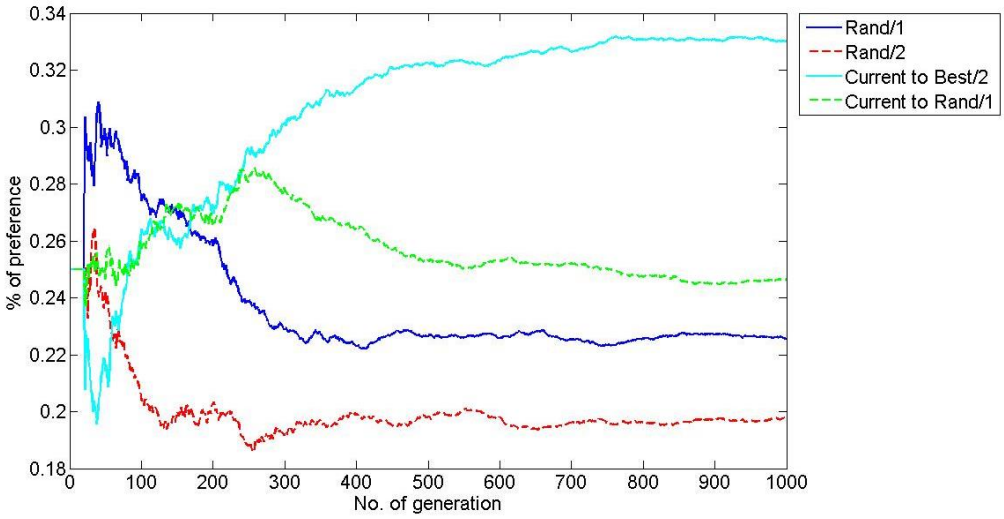

Figure 3.12: Behaviour of Mutation strategies on the classic Bouc-Wen model.

3.4.2 Crossover ratio, *Cr* and mutation factor, *Fr* behaviour

Cr and *Fr* were initially set to 0.5 and 0.9 respectively. This was suggested in [10] and [12] as values in a good range of *Cr* and *Fr*. For the classical Bouc-Wen model the *Cr* and *Fr* value shifts as shown in Figure 3.13 It can be seen that the *Cr* value steadily increases to 0.8-0.9. A high crossover ratio, *Cr*,

means that the trial vector will have higher chances of selecting parameters from the mutation vector rather than the parent vector. This gives more exploration possibility for the SADE.

On the other hand, the value of *Fr* quickly declines and remains steady between 0.15 - 0.3. A low mutation factor, *Fr*, means that the mutation vectors will not differ significantly from the original parent vectors. The explanation for this behaviour is similar to that in Section 3.4.1, where once a suitable region of parameter values had been found, the low *Fr* value gives focus to explore in the preferred search space local to the current parent value. This behaviour has been consistently observed for almost all optimisation conducted in this chapter, for both *Cr* and *Fr* values.

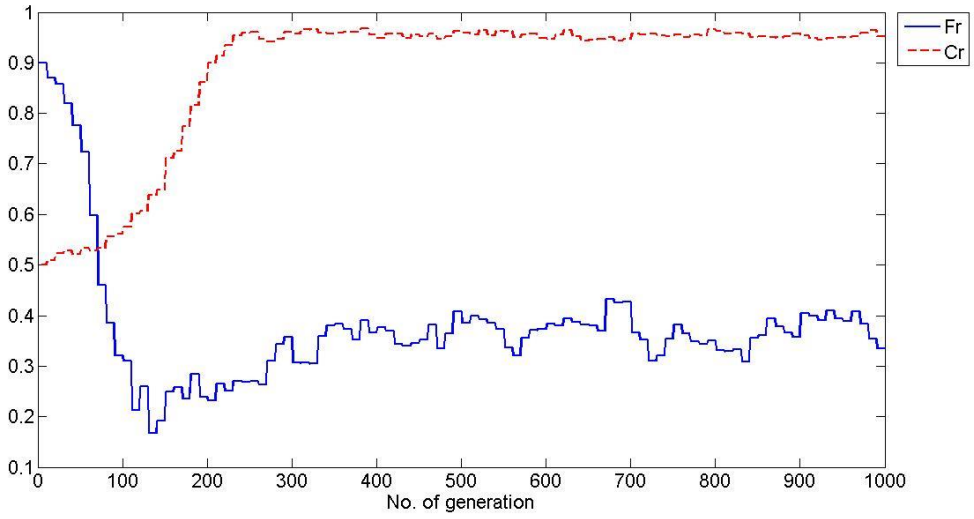

Figure 3.13: Behaviour of *Cr* and *Fr* in classic Bouc-Wen model.

3.5 **Discussion**

In this chapter, a parameter estimation algorithm of Self-adaptive Differential Evolution (SADE) had been introduced and implemented in the parameter estimation of the Bouc-Wen model of a hysteretic system under random inputs at low and high excitation levels with a variance of 0.1 and 100 respectively.

The results showed that whilst obtaining an impressively low cost function value associated with excellent fit, the nonlinear parameters do not match the true system parameters when using random input with low variance. This is due to the mostly linear system that does not give incentive to the

SADE algorithm to identify the nonlinear parameters after identifying the linear parameters. This again stressed the importance of having to set a proper specification for the model performance requirements when building a model for a nonlinear system or structure. If the real system was required to perform in a high amplitude input environment, experiments should be designed to meet this criterion. If this is not done so, and the experiments are instead designed with low input amplitude, the parameter estimation may falsely give an excellent estimate for that particular data set. When the model is built it will then fail to perform as expected when used in the actual required condition.

With the use of extended data, although significant improvement was shown for the data without noise investigation, the same was not observed for data in the presence of noise. It was concluded that it is unnecessary to use an extended data set for SADE compared to using a smaller amount of sampling data for the purpose of parameter estimation in the real environment where noise is always expected.

Observation of the Improvement Ratio trends showed that ranges of the Improvement Ratio value when optimisation was performed on data without noise was rather high with the value of up to 3E8 when the parameter estimation did not have a nonlinear incentive with a low input excitation data. Then when the optimisation was given incentive to find the nonlinear parameters with a high excitation level, the Improvement Ratio significantly went up to around 1E24. In the presence of noise, the Improvement Ratio provided clear information by showing almost no improvement of the estimation using a low input excitation of 0.0004 compared to 6.9683 for the estimation using a high input excitation. Around a 700% improvement was obtained by performing parameter estimation using the high excitation level data compared to only 0.4% improvement with low excitation level data over a simple linear system. This again showed the importance of having the right data for nonlinear system identification.

Observation of the SADE behaviour showed that the algorithm worked well with strategy choices and crossover ratio and mutation factor hyperparameters values adapted during the parameter estimation

process. It allows for faster and more efficient parameter estimation. At the initial stage of the parameter estimation, a wider search space was preferred. Then the preference shifted to focus on the best elements both when creating the mutation matrix and when choosing the elements in the crossover procedure as the estimation became better.

In the next chapter, an investigation using SADE will be undertaken with sinusoidal input signals and chirp input signals on the same Bouc-Wen model of a hysteretic system. The next chapter will also look at comparisons of nonlinear parameter estimation with data generated from different input types.

Chapter 4

4 Nonlinear Parameter Estimation using Harmonic Excitation

4.1 Introduction

In the previous chapter, SADE was implemented using a simulated signal using data from random input. With random input, an output signal was expected to contain a lot of information that would be picked up by a parameter estimation algorithm. However, amongst the information it contains, most of it would be not be as useful as expected for nonlinear parameter identification purposes. The main reason for this was due to the lack of sufficiently strong excitation of the nonlinearity coming from data with random excitation. This was shown in the previous chapter where estimation with random data sets returned estimated parameters that could not be fitted to other data sets and to the same random excitation at a different excitation amplitude level.

Here, in this chapter, parameter estimation investigation is done to further understand any effect on the choice of input for the simulated signal on parameter estimation. The parameter estimation

algorithm, SADE is used on data with harmonic excitation which is sinusoidal input and chirp input here in the thesis. A sensitivity study is also conducted to determine the region of suitability (in terms of frequencies and amplitude level) for the multi sinusoidal investigation. It is expected that harmonic excitation would return a better parameter estimates due to the fact that it will concentrate more energy at specific frequencies and produce a stronger nonlinear behaviour for identification purposes. This in turn will result in better accuracy for nonlinear parameter estimation.

Firstly, a single sinusoidal input is considered. Here parameter estimation is investigated for the single sinusoidal input to understand its effect and limitations. Then the parameter sensitivity (in terms of parameter estimation) is investigated. This is done by varying one parameter and studying the effect on parameter estimation MSE for a single sinusoidal input across the frequency and amplitude range. Next, a simulated signal with multi sinusoidal input is investigated. This is to investigate the effect of additional information coming from the interaction frequencies of multiple sinusoidal signals. Here various frequency combinations of two sinusoidal signals are compared. Finally the effect of using chirp input is investigated. Chirp then takes this to its logical conclusion in that there is a complete range of frequencies excited but in a concentrated manner, in terms of total energy of the input. With chirp, the energy will be concentrated at a single frequency at any moment in time. Finally a comparison between the parameter estimation results using data from random, sinusoidal and chirp input is tabled. All of these are investigated on the Bouc-Wen system with the same parameters as in Chapter 2 and Chapter 3 for cases without noise and with noise.

4.2 **Single sinusoidal input**

Using the same setup with Matlab and Simulink, as discussed in Chapter 3 but with the substitution of the random input with sinusoidal input, the parameter estimation algorithm for Self-adaptive Differential Evolution (SADE) was used to estimate the parameters of the Bouc-Wen system with known parameters in the same manner as in the previous chapter.

In this section, a single sinusoidal input was used for generating data for the investigation. Two different frequencies were chosen. The first frequency was at the undamped natural frequency of the

underlying linear system at 17.6 rad/s and the other frequency was at 3 rad/s. The latter was a 'trial and error' frequency to investigate the effect of using a randomly chosen frequency value. The amplitude was set at low and high amplitudes of 0.1 N and 10 N respectively, similarly to the amplitudes applied in the previous chapter.

4.2.1 Signal without noise

Table 4.1 and Table 4.2 show the results for parameter estimation for low and high forcing amplitude respectively, when the forcing frequency was equal to the undamped natural frequency, ω_n of the underlying linear system. The mean square error (MSE) from the low and high amplitude excitation was 2.46E-11 and 1.76E-24 respectively. Clearly, both are exceptionally good predictions in terms of the MSE. However, it can be seen in the table that the nonlinear parameters for the first estimation exercise had very significant errors whilst the latter provided better estimates. This is as expected due to the mostly linear output data when the system was subjected to a low amplitude input.

Figure 4.1 shows the output comparison plot for the real system, estimated Bouc-Wen system and estimated linear system for sinusoidal inputs with a frequency of 17.6 rad/s and amplitude 10 N. The figure shows that a linear system could still fit well to the data here. The linear fit estimation for this data gives a good estimation with a MSE of 2.84E-04 for the low amplitude and 0.2915 for the high amplitude data. Looking at the Improvement Ratio for both cases here, the Improvement Ratios are 1.16E+07 for the low amplitude and 1.66E+23 for the high amplitude data.

	Real Parameter	Best Estimated Parameter	% Error	Mean Estimated Parameter	Standard Deviation
m	1	1	4.31E-05	0.9924	9.40E-03
c	0.7037	0.7037	2.31E-04	0.7215	1.16E-02
k	309.51	309.5102	7.14E-05	327.4456	2.51E+01
α	0.01	0.0363	2.63E+02	0.6211	2.77E-01
A	1	3	200	2.4	1.10E+00
β	150	154.1064	2.7376	188.2449	7.56E+01
γ	20	20.538	2.6899	20.3857	1.14E+01

Table 4.1: Estimation with sinusoidal inputs with frequency 17.6rad/s and amplitude 0.1 N

	Real Parameter	Best Estimated Parameter	% Error	Mean Estimated Parameter	Standard Deviation
m	1	1	5.54E-11	1	6.92E-04
c	0.7037	0.7037	2.00E-09	0.7028	1.04E-02
k	309.51	309.51	1.17E-10	310.5855	3.21E+00
α	0.01	0.01	1.21E-09	0.01	1.18E-06
A	1	1	6.69E-11	0.9966	1.02E-02
β	150	150	4.82E-10	150.613	1.97E+00
γ	20	20	3.88E-09	20.0185	7.53E-01

Table 4.2: Estimation with sinusoidal inputs with frequency 17.6rad/s and amplitude 10 N

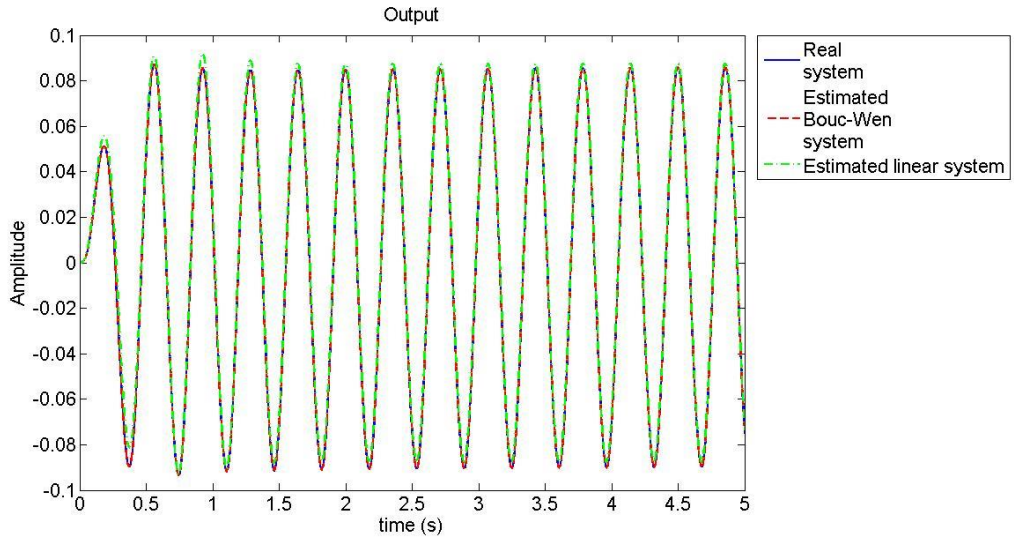

Figure 4.1: Output response plot of real and estimated systems for sinusoidal inputs with frequency 17.6rad/s and amplitude 10 N

Table 4.3 and Table 4.4 show the result for parameter estimation at a frequency of 3 rad/s at amplitude of 0.1 N and 10 N respectively. The parameter estimation gives a mean square error (MSE) of 3.23E-18 and 4.30E-23 respectively. Similar to the previous results, the estimated nonlinear parameter significantly improve in accuracy as the excitation amplitude increases due to the system nonlinear behaviour having greater influence at higher forcing.

Linear fitting still gives good estimates for both low and high amplitude with an MSE of 1.71E-08 and 1.2205 respectively. The Improvement Ratios show a similarity in trend to that shown with the 17.6 rad/s data with value of 5.28E+09 for the low amplitude and 2.84E+22 for the high amplitude.

Although the Improvement Ratio could potentially improve confidence in the nonlinear parameter model with a high Improvement Ratio value for the model here, it can still be argued based on the MSE that with the data from a single sinusoidal input, a linear model would be sufficient. The use of single sinusoidal input here seems to offer output data that is not exclusive to the Bouc-Wen system as it could be fitted to other models such as the linear model that has already been demonstrated. This generality of data arises from the lack of information from the single sinusoidal input due to limited information at a single excitation frequency.

	Real Parameter	Best Estimated Parameter	% Error	Mean Estimated Parameter	Standard Deviation
m	1	1	4.05E-09	1	3.06E-07
c	0.7037	0.7037	1.10E-07	0.7037	1.64E-06
k	309.51	309.5102	7.72E-05	309.5101	3.50E-04
α	0.01	0.1697	1.60E+03	0.3578	8.77E-02
A	1	3.078	207.8	2.625	1.20E+00
β	150	178.8626	19.2417	235.8231	3.43E+01
γ	20	23.8491	19.2457	26.6079	7.56E+00

Table 4.3: Estimation with sinusoidal inputs with frequency 3 rad/s and amplitude 0.1 N

	Real Parameter	Best Estimated Parameter	% Error	Mean Estimated Parameter	Standard Deviation
m	1	1	1.24E-10	1.0002	6.15E-04
c	0.7037	0.7037	6.39E-10	0.7044	2.30E-03
k	309.51	309.51	3.58E-09	319.4238	1.53E+01
α	0.01	0.01	8.39E-08	0.0105	1.90E-03
A	1	1	3.69E-09	0.9703	4.21E-02
β	150	150	5.07E-09	155.1421	8.36E+00
γ	20	20	1.25E-08	19.9761	1.18E+00

Table 4.4: Estimation with sinusoidal inputs with frequency 3 rad/s and amplitude 10 N

4.2.2 Signal with noise

The investigation looked at single sinusoidal excitation data with output noise of 5% to 20% of the output signal root mean-square (RMS) value. This was to observe the effect on parameter estimation of single sinusoidal input under the effect of noise and how it affected the estimated parameters, the MSE of the parameter estimation and the Improvement Ratio. Table 4.5 and Table 4.6 show the results for a sinusoidal excitation of frequency of 17.6 rad/s with 0.1 N and 10 N excitation amplitude

respectively and Table 4.7 and Table 4.8 show the results for a sinusoidal excitation of frequency of 3 rad/s with 0.1 N and 10 N excitation amplitudes respectively.

The MSE was as expected, where an increasing MSE trend showed with increasing output noise. This was observed for all four scenarios in the tables. Looking at the standard deviation of the parameters, it can be seen clearly seen that for the low amplitude excitation data, the standard deviation for the nonlinear parameters is always high. This is again due to the data showing a linear behaviour under low amplitude excitation. The standard deviation for the high amplitude excitation always remains low even when the noise causes the mean estimated nonlinear parameters to deviate from the actual value of the nonlinear parameters as seen especially for γ values in the tables. This may be cause by the generality introduced by the single sinusoidal input where only a single frequency and harmonic are the only source of information for the system.

As previously observed in last chapter, the Improvement Ratio gives a clearer comparison under the effect of noise. Here it can be seen that the Improvement Ratio for the low amplitude excitation data is very low for both excitation frequencies with zero Improvement Ratio for the 3 rad/s frequency excitation. For the 17.6 rad/s frequency, the linear fitting MSE are even better than the Bouc-Wen model MSE, although very marginal. This again pointed to having almost no benefits in the selection of the Bouc-Wen model as the predicted model compared to a simple linear model of m, c and k for the low amplitude excitation data.

The Improvement Ratio for the high amplitude excitation data decreased with the increase of noise. This may be due to the higher noise level making it difficult to fit the Bouc-Wen model to the single sinusoidal data which has been dominated by noise. The Improvement Ratios for the 3 rad/s excitation frequency were better compared to the 17.6 rad/s excitation frequency estimation. This could be caused by the stronger harmonics of the 3 rad/s frequency which also caused the linear fitting to fail to get an estimation of good fit for the 20% RMS noise.

The Improvement Ratio here showed that at higher amplitude excitation, a more nonlinear signal would result in significant Improvement Ratio value which could be useful in improving confidence in the parameter estimation exercise.

	Noise = 5% RMS		Noise = 10% RMS		Noise = 15% RMS		Noise = 20% RMS	
	MEP	SD	MEP	SD	MEP	SD	MEP	SD
m	0.990	1.83E-02	0.971	7.10E-03	1.010	1.55E-02	0.980	1.20E-02
c	0.721	1.78E-02	0.731	1.70E-02	0.709	3.36E-02	0.731	9.80E-03
k	315.713	2.04E+01	314.064	2.21E+01	315.387	2.75E+00	323.215	3.73E+01
α	0.583	5.03E-01	0.706	2.92E-01	0.650	5.55E-01	0.905	1.50E-01
A	0.856	2.27E-01	0.654	3.20E-01	0.644	3.15E-01	0.652	3.58E-01
β	169.061	1.13E+02	230.283	1.13E+02	184.659	1.03E+02	223.652	6.62E+01
γ	20.033	1.73E+01	20.033	1.73E+01	18.545	1.61E+01	12.480	1.10E+01
MSE	0.2499		0.9673		2.108		3.7559	
Linfit MSE	0.2501		0.9672		2.1101		3.7557	
I.Ratio	0.0008		0.0001		0.0010		0.0001	

Table 4.5: Estimation with single sinusoidal excitation with amplitude = 0.1 N and frequency = 17.6rad/s with noise

	Noise = 5% RMS		Noise = 10% RMS		Noise = 15% RMS		Noise = 20% RMS	
	MEP	SD	MEP	SD	MEP	SD	MEP	SD
m	1.013	6.90E-03	1.006	4.92E-05	1.040	8.11E-05	0.998	4.22E-04
c	0.425	1.21E-01	0.516	5.87E-04	0.254	6.47E-04	0.553	1.43E-02
k	354.501	1.44E+01	315.382	7.90E-03	322.202	2.63E-02	305.733	3.39E-01
α	0.0103	4.53E-04	0.010	3.85E-10	0.010	5.51E-08	0.010	5.16E-07
A	0.879	4.04E-02	1.000	1.61E-07	1.000	4.33E-05	1.000	1.14E-04
β	183.224	7.20E+00	157.741	2.16E-02	162.934	3.63E-02	161.490	7.16E-01
γ	18.636	4.39E+00	19.346	4.50E-02	21.144	6.50E-04	23.106	9.60E-03
MSE	0.2471		0.989		2.0363		3.8881	
Linfit MSE	0.5413		1.3085		2.3317		4.1856	
I.Ratio	1.1906		0.3231		0.1451		0.0765	

Table 4.6: Estimation with single sinusoidal excitation with amplitude = 10 N and frequency = 17.6rad/s with noise

	Noise = 5% RMS		Noise = 10% RMS		Noise = 15% RMS		Noise = 20% RMS	
	MEP	SD	MEP	SD	MEP	SD	MEP	SD
m	1.000	1.48E-07	0.998	3.27E-10	0.999	1.39E-09	0.997	1.54E-09
c	0.709	2.45E-09	0.701	8.85E-09	0.671	4.75E-09	0.689	2.14E-08
k	309.429	3.84E-05	309.322	2.79E-07	309.525	1.33E-06	308.847	5.25E-06
α	1.000	5.98E-11	1.000	9.79E-12	1.000	5.06E-09	1.000	2.05E-08
A	0.521	1.36E-01	0.701	2.27E-01	0.599	2.50E-02	0.584	4.91E-01
β	131.179	2.77E+01	108.139	8.63E+00	115.002	1.92E+01	236.052	5.61E+01
γ	11.784	9.61E+00	11.139	9.49E+00	15.523	9.48E+00	16.660	7.67E+00
MSE	0.2705		1.0317		2.3041		4.0332	
Linfit MSE	0.2705		1.0317		2.3041		4.0332	
I.Ratio	0		0		0		0	

Table 4.7: Estimation with single sinusoidal excitation with amplitude = 0.1 N and frequency = 3rad/s with noise

	Noise = 5% RMS		Noise = 10% RMS		Noise = 15% RMS		Noise = 20% RMS	
	MEP	SD	MEP	SD	MEP	SD	MEP	SD
m	1.000	1.28E-07	1.002	3.25E-06	1.005	3.14E-04	0.998	3.13E-08
c	0.696	3.47E-06	0.699	2.57E-05	0.497	2.41E-04	0.676	9.92E-08
k	317.223	7.22E+00	317.161	3.56E+00	327.477	1.16E+01	310.251	7.42E-06
α	0.015	3.35E-04	0.019	2.29E-04	0.048	1.10E-03	0.021	1.95E-07
A	0.977	2.24E-02	0.968	1.10E-02	0.947	3.56E-02	1.000	9.21E-13
β	155.165	3.58E+00	148.550	1.69E+00	174.683	6.72E+00	154.892	8.54E-05
γ	20.848	4.81E-01	21.873	1.45E-06	24.255	6.24E-01	28.978	2.97E-12
MSE	0.2483		1.0261		2.2522		4.143	
Linfit MSE	1.4607		2.1471		3.8598		-	
I.Ratio	4.8828		1.0925		0.7138		-	

Table 4.8: Estimation with single sinusoidal excitation with amplitude = 10 N and frequency = 3rad/s with noise

4.2.3 Sensitivity of Bouc-Wen parameters under sinusoidal input

The investigation of a good estimation region using sinusoidal input for the particular Bouc-Wen system used here is shown in Figure 4.2 to Figure 4.8. The figures show the value of the mean parameters across 10 runs at each frequency and amplitude with frequency ranges 1 rad/s to 25 rad/s with a step size of 0.5 rad/s and amplitude ranges 0.1 N to 20N. These figures are aimed at showing which value of amplitude and frequency are a good choice for doing parameter estimation using sinusoidal excitation where a flat region is a good region of choice of amplitude and frequency value.

The results will be used to determine the choice of amplitude and frequency for the multi sinusoidal section later.

In Figure 4.2 and Figure 4.3, it is shown that parameters *m* and *c* are easily identified with mostly flat regions and a good prediction close to the real parameter values with some small errors at lower amplitude regions. Parameter *k* in Figure 4.4 shows that at a low amplitude and low frequency region, there is a significant fluctuation of value. This is due to the stiffness parameter, *k* adapting to counter balance the effect of the nonlinear parameter at that region to keep the MSE low. Flat regions of parameter *k* can be seen at higher amplitudes and higher frequencies where nonlinearity behaviour can be recognised by the estimation algorithm and nonlinear parameters are settling close to their respective real values. Parameter *A*, α, β and γ in Figure 4.5 to Figure 4.8 shows mostly flat regions above an amplitude region of 5 N. At the low amplitude region it is expected for the parameters to be inaccurate as the nonlinearity behaviour of the Bouc-Wen system is undetected. Parameter β and γ also shows slight variability at around the low frequency region as seen in Figure 4.7 and Figure 4.8.

From these results, it can be observed that an amplitude of above 10 N results in good prediction for all parameters of the specific Bouc-Wen model used here. Since a multi sinusoidal signal will provide combinations of frequencies anyway, the frequency choice of the next section will have multiple sets to investigate the different combinations.

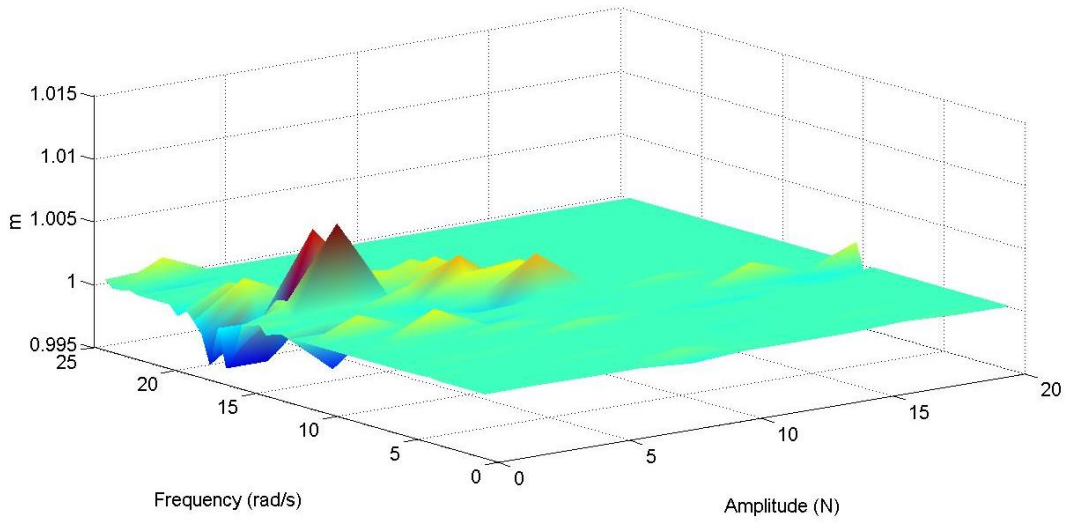

Figure 4.2: Estimation of parameter *m*, under sinusoidal input across amplitude and frequency values

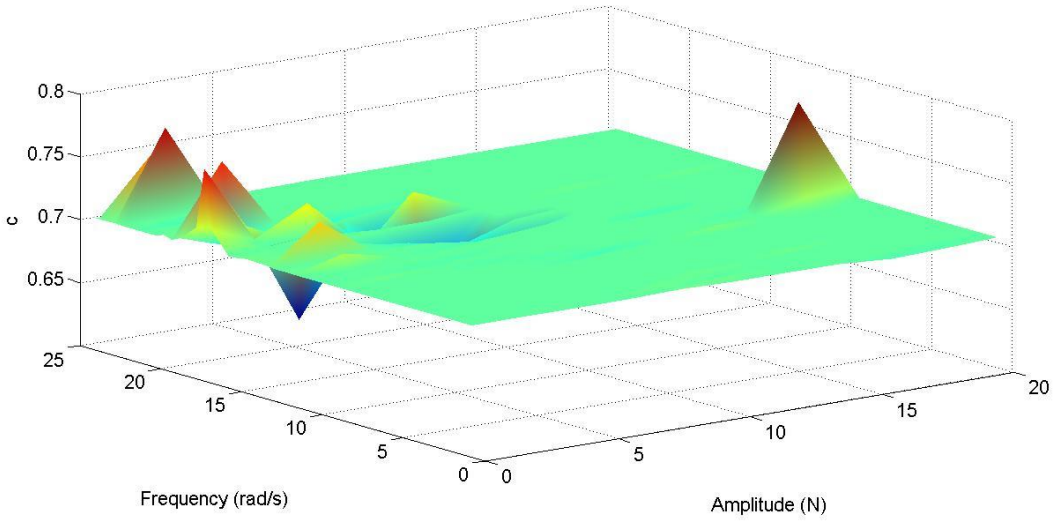

Figure 4.3: Estimation of parameter *c*, under sinusoidal input across amplitude and frequency values

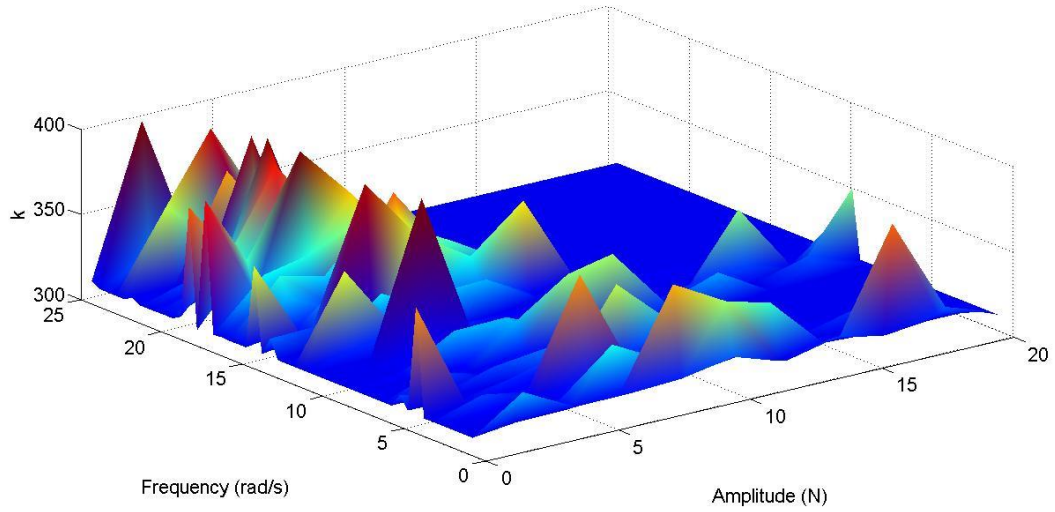

Figure 4.4: Estimation of parameter *k*, under sinusoidal input across amplitude and frequency values

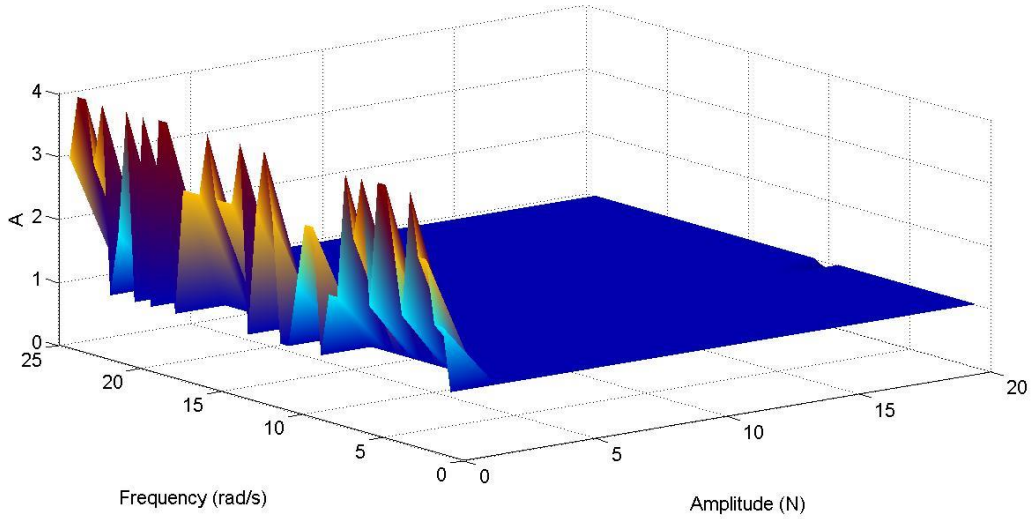

Figure 4.5: Estimation of parameter *A*, under sinusoidal input across amplitude and frequency values

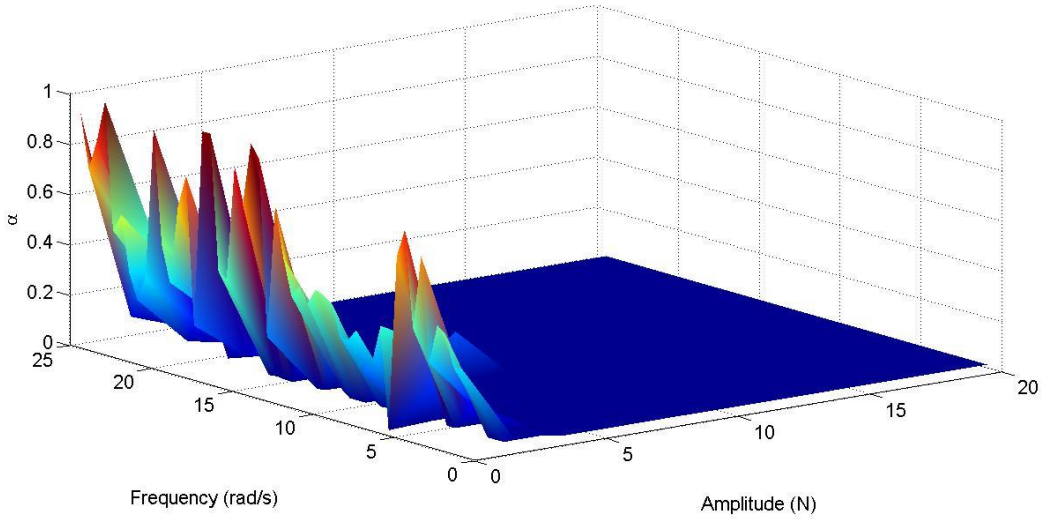

Figure 4.6: Estimation of parameter α, under sinusoidal input across amplitude and frequency values

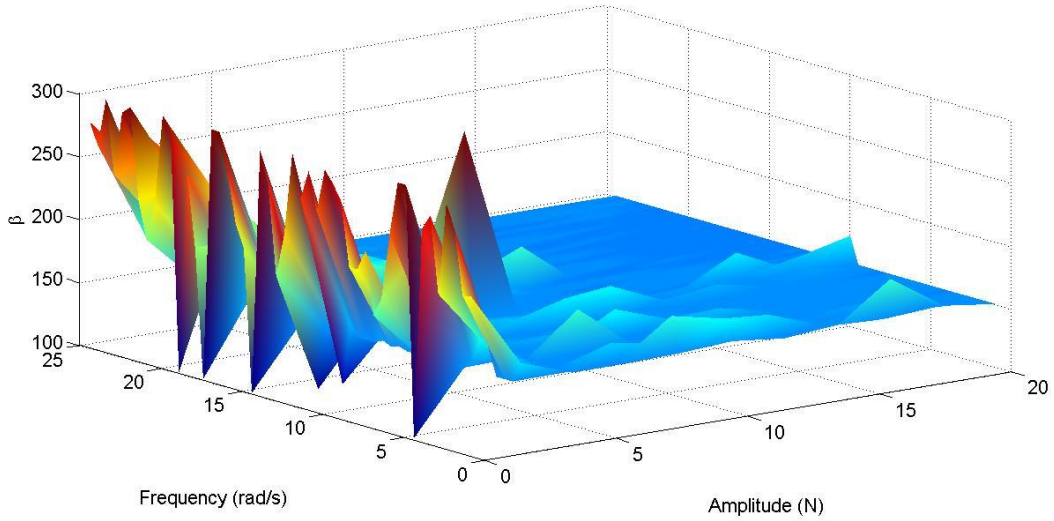

Figure 4.7: Estimation of parameter β, under sinusoidal input across amplitude and frequency values

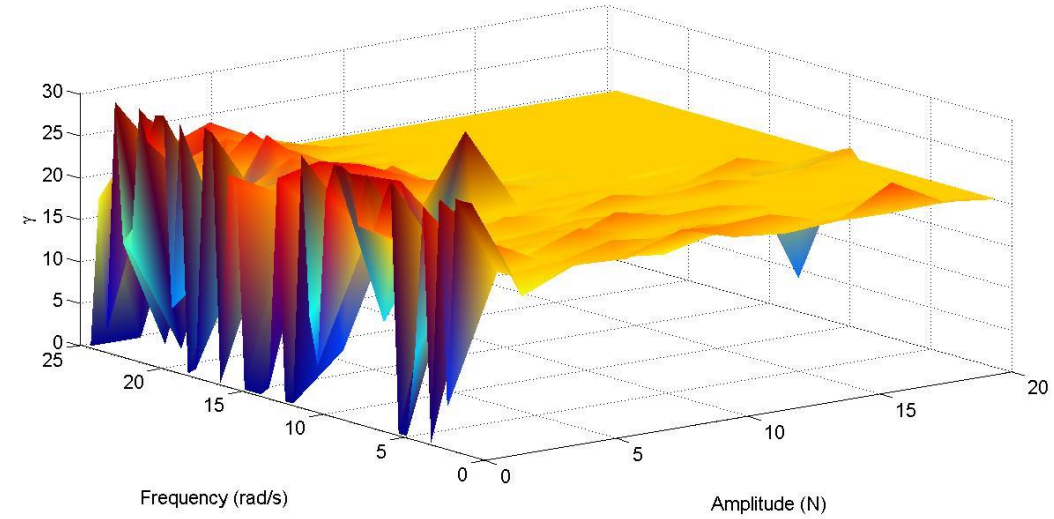

Figure 4.8: Estimation of parameter γ, under sinusoidal input across amplitude and frequency values

4.3 **Multiple sinusoidal input**

To further investigate the sinusoidal input, multiple sinusoidal inputs were used following on from the previous section. A single sinusoidal will mainly only return information at the forcing frequency and harmonics which is limited and may cause the nonlinearity of a system to be ignored. With two sinusoids, information at two forcing frequencies, two sets of harmonics and the sum and difference of the frequencies are obtained. From a nonlinear parameter estimation point of view, this should give

greater discrepancy (wrong values would result in poor MSEs) between different estimates of the nonlinear parameters. Using the same setup with Matlab and Simulink, SADE was used in the parameter estimation of the known Bouc-Wen system with parameters similar to the previous chapter.

In the previous chapter, using extended random excitation data yielded better parameter estimates (at least for the data without noise). Following on from that, five sets of multi sinusoidal signals were used for each of the parameter estimation exercises. For each signal set, 20 runs of SADE were performed and assessed to obtain the parameter estimation values. That means the mean estimated parameters come from the average of all five sets, meaning a total of 100 runs for each scenario.

The input signals used two sine inputs, both with amplitude of 10 N. This arose from the sensitivity observation from the previous subsection, where at 10 N amplitude the data had a good presence of nonlinearity. The frequency was set whereby one sine source was fixed, while the other was increased gradually to obtain the five sets of input. The first frequency would allow for control if necessary whilst the second would act as a mixing frequency to create a diverse input. Figure 4.9 shows the sinusoidal combination example that was presented in the plot of Figure 4.10 (a).

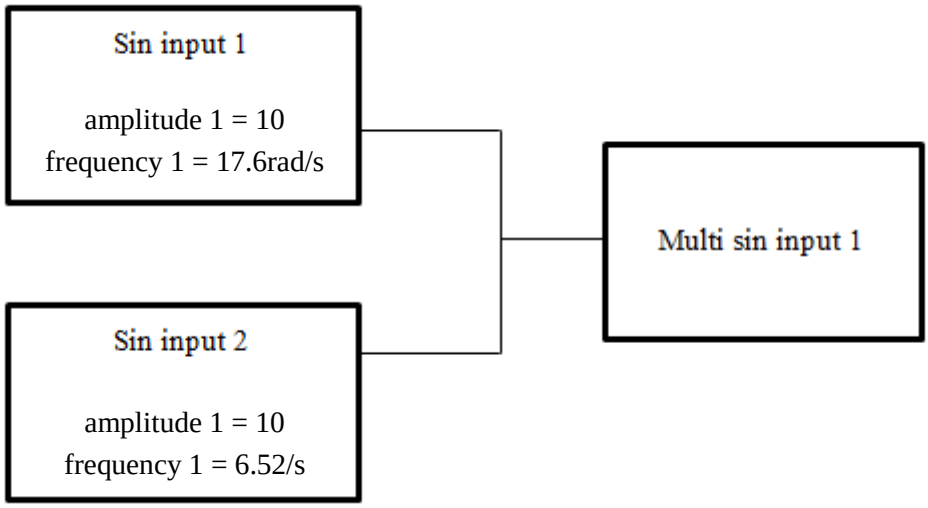

Figure 4.9: Example of multi sinusoidal combination to create input signal

The input and output of the signals that were used are shown in Figure 4.10 for frequency 1 = 17.6 rad/s, Figure 4.11 for frequency 1 = 8 rad/s and Figure 4.12 for frequency 1 = 3 rad/s where (a) to (e)

represent set 1 to set 5 respectively. The selection of frequency 1 of 8 rad/s and 3 rad/s was done to investigate the effect of using input with frequencies that do not excite at the natural frequency of the underlying linear system for exploratory investigation. The result could give insights into the design of experiments for frequency choices of the input signal. The value of frequency 2 used are listed below in Table 4.9. As can be seen in the table, the signals vary from one another and were expected to produce different results in the parameter estimation.

Set	1	2	3	4	5
Frequency 2	$\omega_n/0.3$	$\omega_n/0.9$	$\omega_n/1.5$	$\omega_n/2.1$	$\omega_n/2.7$
Frequency 2 in rad/s	58.67	19.56	11.73	8.38	6.52

Table 4.9: Values of frequency 2 for the 5 sets of input signals.

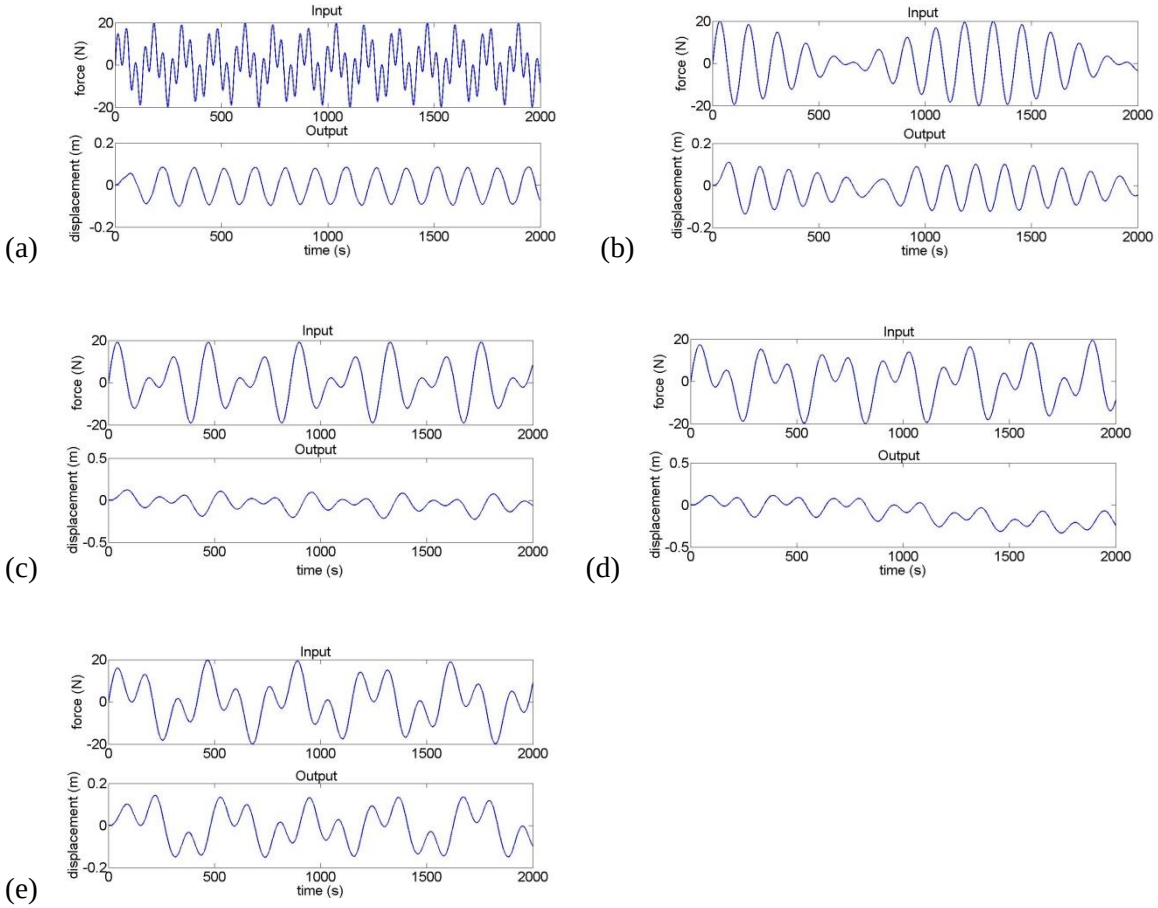

Figure 4.10: Input output plot of multi sinusoidal with amplitude = 10 N, frequency 1 = 17.6 rad/s and frequency 2 (a) 58.67 rad/s (b) 19.56 rad/s (c) 11.73 rad/s (d) 8.38 rad/s and (e) 6.52 rad/s

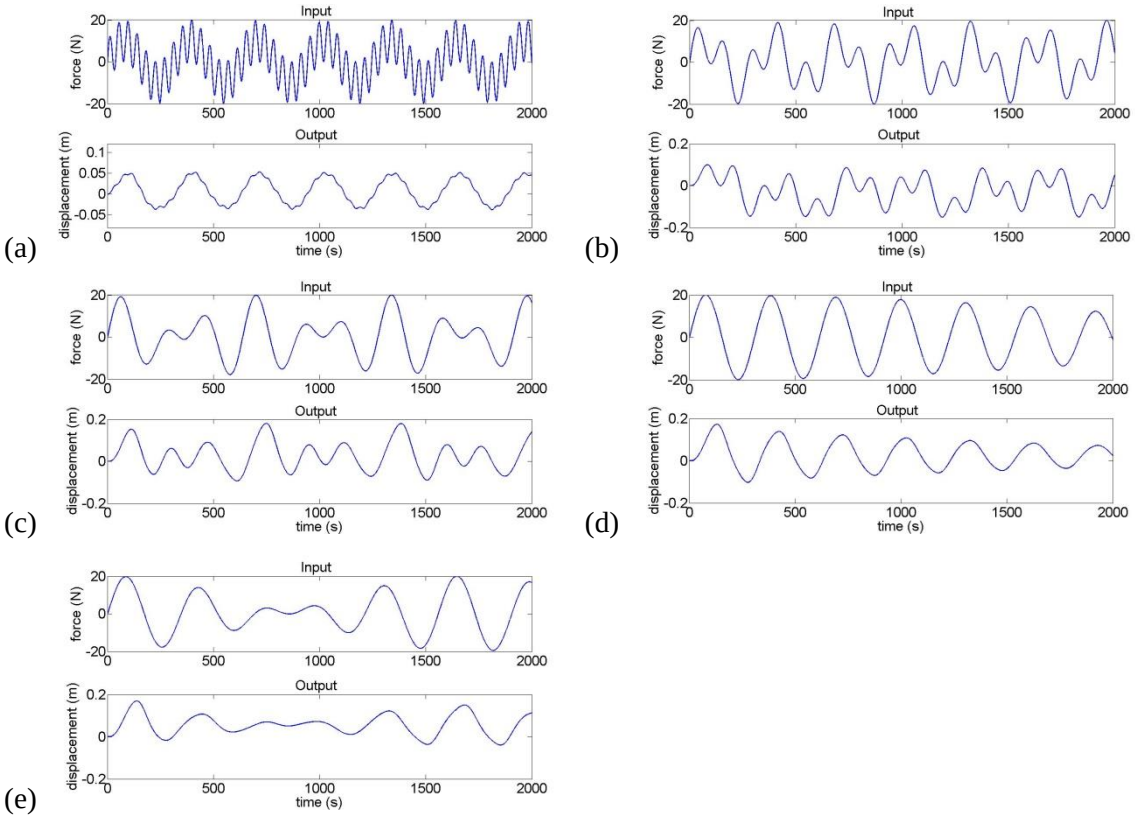

Figure 4.11: Input output plot of multi sinusoidal with amplitude = 10 N, frequency 1 = 8 rad/s and frequency 2 (a) 58.67 rad/s (b) 19.56 rad/s (c) 11.73 rad/s (d) 8.38 rad/s and (e) 6.52 rad/s

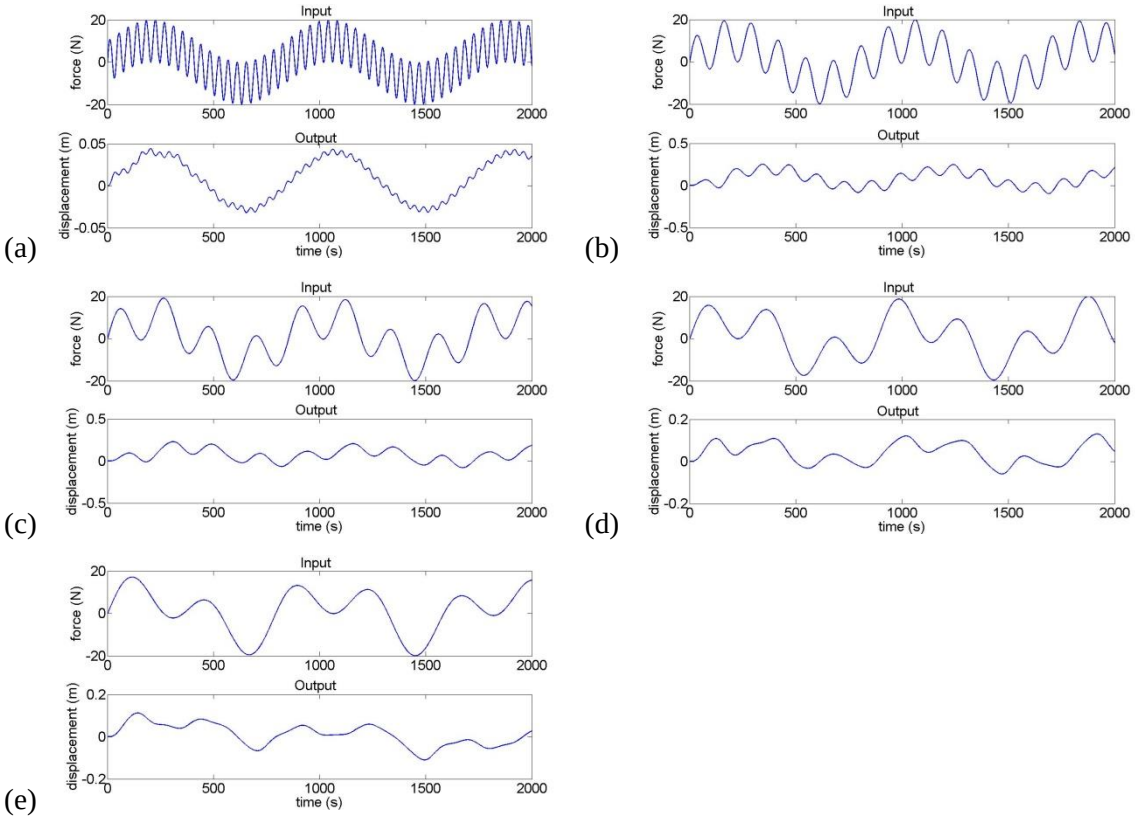

Figure 4.12: Input output plot of multi sinusoidal with amplitude = 10 N, frequency 1 = 3 rad/s and frequency 2 (a) 58.67 rad/s (b) 19.56 rad/s (c) 11.73 rad/s (d) 8.38 rad/s and (e) 6.52 rad/s

4.3.1 Signal without noise

Table 4.10 and Table 4.11 below show the results of the SADE parameter estimation for the first two scenarios with an input signal frequency 1 of 17.6 rad/s and 8 rad/s respectively. As mentioned above, the mean estimated parameter is the average from the total of 100 runs (5 sets of 20 runs each). Both showed an excellent estimation with all of the runs giving very low MSE in 1000 generations. The best estimated parameter for frequency 1 of 17.6 rad/s corresponded to an MSE of 1.46E-29 from set 5 and the best estimated parameter for frequency 1 of 8 rad/s corresponded to an MSE of 3.06E-29 from set 2. As seen in the tables, both had mean estimated parameters (MEP) exactly similar to the real parameter values.

The results of the SADE estimation with frequency 1 = 3 rad/s are shown in Table 4.12. Although the mean estimated parameters are not exactly the same as the real parameter values, the estimation is still an excellent estimation. Even when using signals with frequencies not at the natural frequency of the underlying linear system, with a multi sinusoidal input signal, the results still manage to give a good estimation values comparable to the random input data and single sinusoidal input data estimation. Additionally, over a total of 100 runs, the MSE was brought to a very low level as well. The best estimated parameter corresponds to MSE value of 1.49E-29 coming from set 3.

With multi sinusoidal input, only the data from multi sinusoidal of frequency 1 = 17.6 rad/s and frequency 2 = 58.67 rad/s (set 1) could be fitted with a linear model with an MSE below 5, the other sets could not fit a linear model with good estimates. With frequency 1 = 8 rad/s and frequency 1 = 3 rad/s, the linear model was unable to be estimated with a good fit for all sets here. This shows that multi sinusoidal input data resulted in a unique data that could only be identified with the correct model selection. This counters the disadvantage of using reverse parameter estimation method which suffers from local minima/maxima when using general data.

The linear fitting for frequency 1 = 17.6 rad/s and frequency 2 = 58.67 rad/s (set 1) had an MSE of 1.10 with an Improvement Ratio of 7.51E+28. The high Improvement Ratio indicates that it is worth selecting the Bouc-Wen model over the linear model as the predicted model for the parameter

estimation exercises. Figure 4.13 below shows the output plot comparison for the true system, the estimated Bouc-Wen system and the estimated linear system for the above multi sinusoidal input. It can be seen that the Bouc-Wen and true system are an exact match whilst the linear system has a slight discrepancy. This is the only Improvement Ratio calculated and comparison plot shown, as the other sets did not produce an acceptable estimate for linear fitting. This observation is a good point compared to the random excitation and single sinusoidal excitation investigation previously where linear fitting is always possible. It can be said that the model output data due to the multi sinusoidal inputs is almost exclusive for Bouc-Wen model, meaning that the nonlinearity of the system plays an important role and nonlinear parameters are significant to the parameter estimation algorithm.

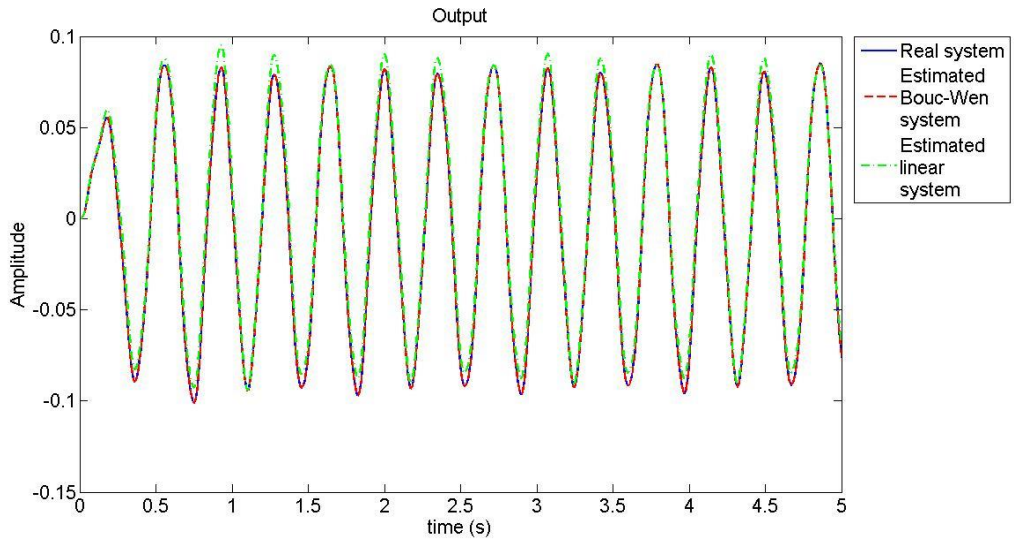

Figure 4.13: Output response plot of real and estimated systems for multi sinusoidal inputs with frequency 1= 17.6 rad/s frequency 2 = 58.67 rad/s both with amplitude of 10 N

	Real Parameter	Best Estimated Parameter	% Error	Mean Estimated Parameter	Standard Deviation
m	1	1	0	1	2.31E-08
c	0.7037	0.7037	0	0.7037	8.54E-07
k	309.51	309.51	0	309.51	4.44E-05
α	0.01	0.01	0	0.01	8.60E-09
A	1	1	0	1	1.07E-07
β	150	150	0	150	2.93E-05
γ	20	20	0	20	8.42E-05

Table 4.10: Estimation with sinusoidal inputs with amplitude = 10 N and freq1 = 17.6 rad/s

	Real Parameter	Best Estimated Parameter	% Error	Mean Estimated Parameter	Standard Deviation
m	1	1	0	1	1.84E-08
c	0.7037	0.7037	0	0.7037	1.56E-07
k	309.51	309.51	0	309.51	7.90E-05
α	0.01	0.01	0	0.01	1.62E-09
A	1	1	0	1	2.56E-07
β	150	150	0	150	4.25E-05
γ	20	20	0	20	9.48E-06

Table 4.11: Estimation with sinusoidal inputs with amplitude = 10 N and freq1 = 8 rad/s

	Real Parameter	Best Estimated Parameter	% Error	Mean Estimated Parameter	Standard Deviation
m	1	1	0	0.9999	7.82E-04
c	0.7037	0.7037	0	0.7039	4.40E-03
k	309.51	309.51	0	311.0477	7.68E+00
α	0.01	0.01	0	0.01	3.16E-06
A	1	1	0	0.9955	2.19E-02
β	150	150	0	150.7682	3.80E+00
γ	20	20	0	20.0767	5.71E-01

Table 4.12: Estimation with sinusoidal inputs with amplitude = 10 N and freq1 = 3 rad/s

4.3.2 Signal with noise

Noise was added to the output signals via simulated white noise using a random signal with amplitude equal to a percentage of the output signal root mean square value (RMS). The simulated white noise was added at levels of 5% RMS, 10% RMS, 15% RMS and 20% RMS for frequency 1 = 3 rad/s and subsequently for frequency 1 = 17.6 rad/s, similar to the previous section with a single sinusoidal excitation. Here, the frequency 1 of 8 rad/s excitation frequency signal sets were not investigated as in the previous subsection since its results were very similar to the 17.6 rad/s excitation frequency parameter estimation and would not provide additional value to the investigation. Figure 4.14 and Figure 4.15 show the output signal with noise levels of 5% and 20% of the output's RMS output for all five sets of signal with frequency 1 = 3 rad/s where (a) to (e) represents set 1 to set 5 respectively.

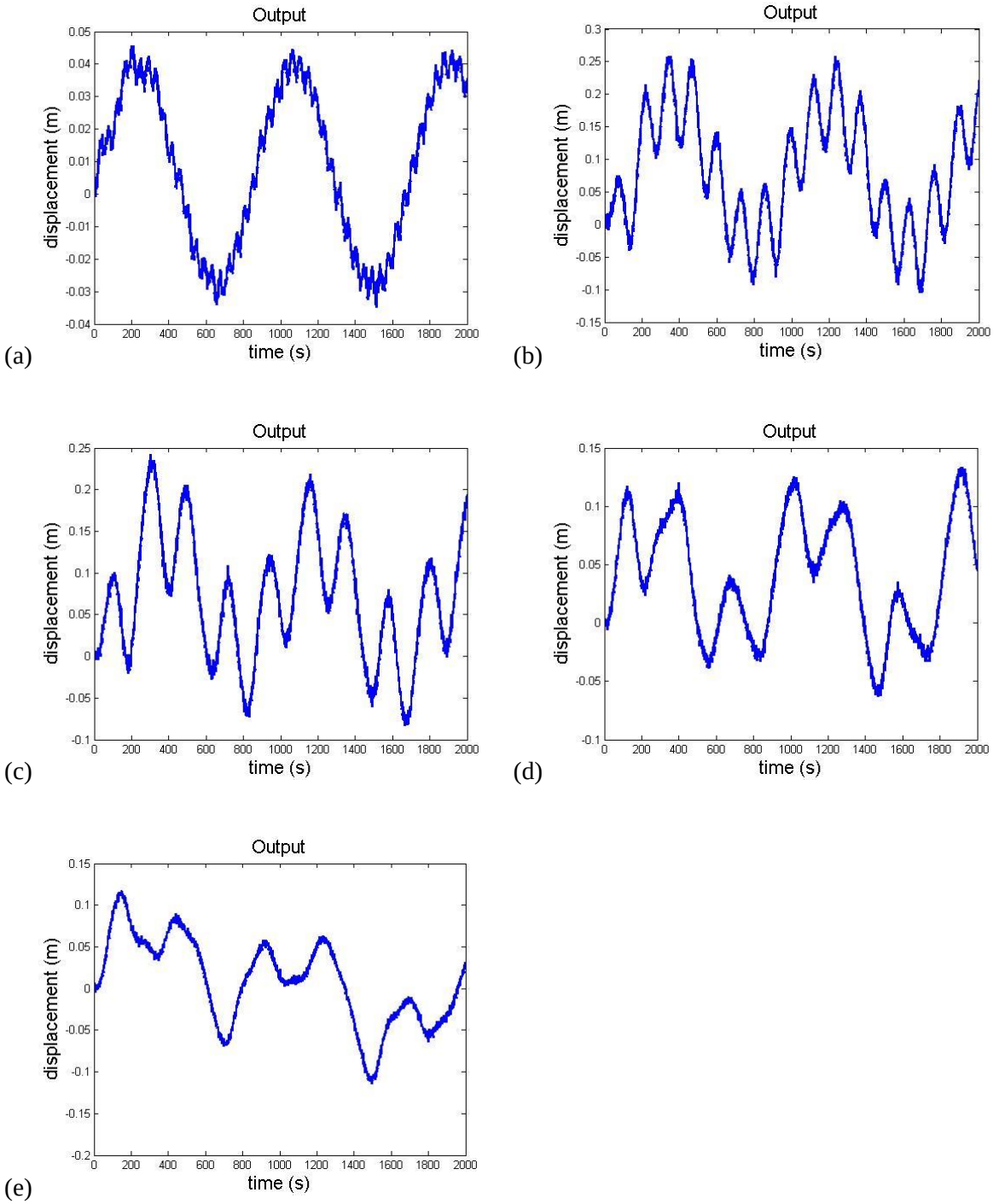

Figure 4.14: Output response plot of sinusoidal input with amplitude = 10 N and frequency 1 = 3 rad/s and frequency 2 (a) 58.67 rad/s (b) 19.56 rad/s (c) 11.73 rad/s (d) 8.38 rad/s and (e) 6.52 rad/s with 5% RMS noise

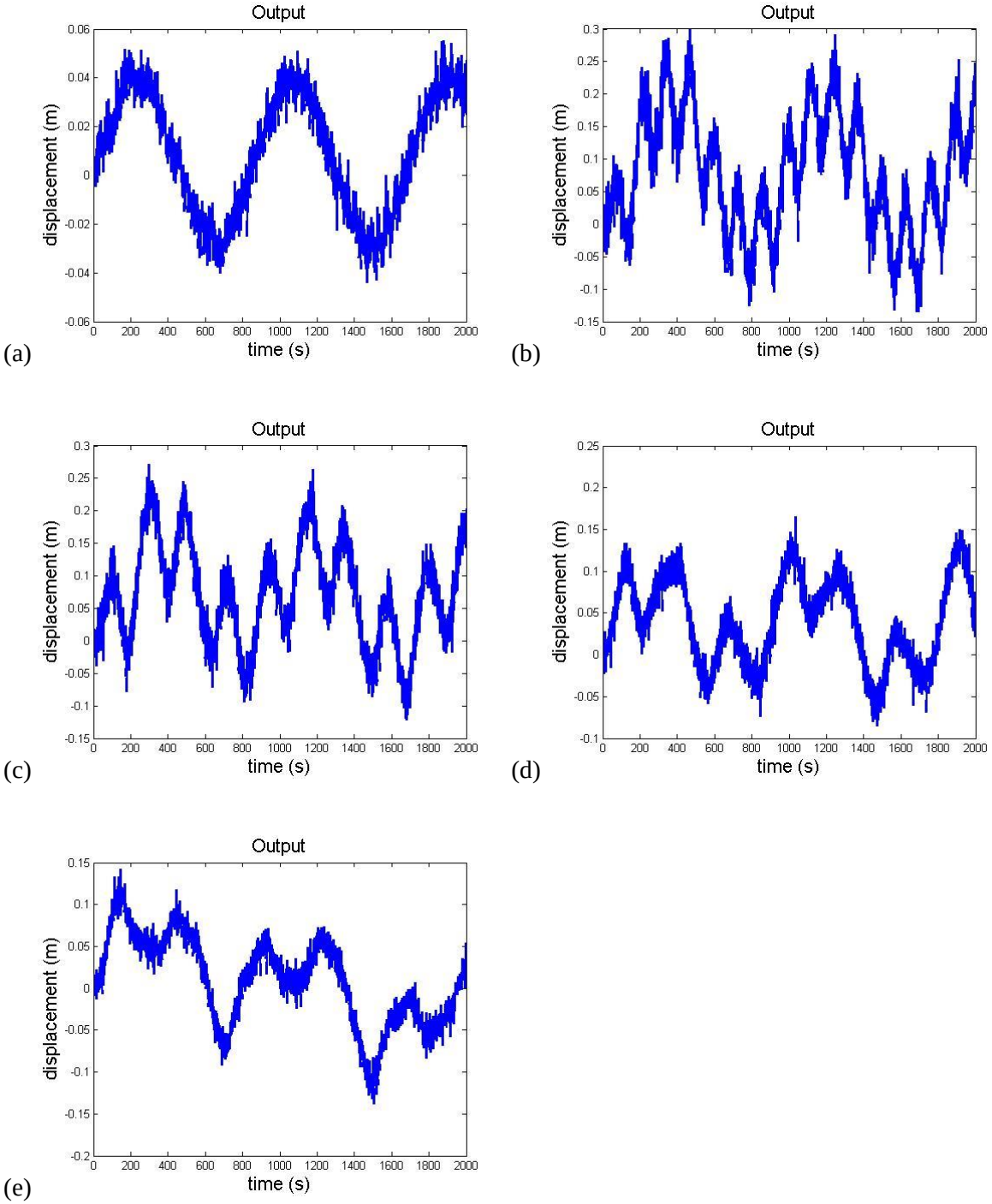

Figure 4.15: Output response plot of sinusoidal input with amplitude = 10 N and frequency 1 = 3 rad/s and frequency 2 (a) 58.67 rad/s (b) 19.56 rad/s (c) 11.73 rad/s (d) 8.38 rad/s and (e) 6.52 rad/s with 20% RMS noise

The results of parameter estimation with the addition of noise can be seen in Table 4.13. As the noise level increases, the estimated values of k, α, β and γ increase, while the other parameters do not show any discernible pattern. As the noise level increases, the standard deviation for parameters m, α, and A decrease, showing a more precise estimation whilst the standard deviation for parameters k, β and γ

increase, showing a more flexible estimation. In this case, the former group of estimated parameters can be said to play a more important role in defining the model with an increasing noise level. By getting these parameters right, the main body of the predicted model would have been satisfied, giving more flexibility to the other parameters to fit to the added noise, although the estimated parameter values are still close to their respective actual values.

Table 4.14 shows the MSE value for the noise levels. It also shows the sets success and failure status of the sets, where success means that at least one run managed to obtain an MSE of less than 5. As can be expected, the MSE value increases as the noise level increases. Up until a 15% RMS noise level, all five sets were successful, while at 20% RMS, only the first set was successful. This was due to the particular combination with frequency 2 value of 58.67 rad/s which still gave good excitation above the noise level. This gives sufficient incentive for the estimation algorithm SADE to identify the nonlinear parameters. At 25% RMS level, all sets failed to give estimates with an MSE less than 5.

	Noise = 5% RMS		Noise = 10% RMS		Noise = 15% RMS		Noise = 20% RMS	
	MEP	SD	MEP	SD	MEP	SD	MEP	SD
m	0.9993	3.40E-03	0.9985	3.00E-03	0.9928	6.80E-03	0.9985	4.39E-04
c	0.7088	2.45E-02	0.6895	4.39E-02	0.7837	1.28E-01	0.6988	1.70E-03
k	310.2929	2.08E+00	316.2839	1.13E+01	316.1786	1.14E+01	319.7268	1.94E+01
α	0.0100	1.07E-05	0.0100	2.88E-05	0.0101	2.57E-04	0.0280	1.60E-03
A	0.9967	6.30E-03	0.9800	3.55E-02	0.9695	3.42E-02	0.9747	5.65E-02
β	150.7626	2.60E+00	152.8707	6.50E+00	152.3013	6.49E+00	159.8336	1.02E+01
γ	19.0069	1.85E+00	20.3522	3.76E+00	21.1089	5.38E+00	30.0000	1.08E-10

Table 4.13: Estimation with sinusoidal inputs with amplitude = 10 N and frequency 1 = 3 rad/s with noise

		Noise = 5% RMS	Noise = 10% RMS	Noise = 15% RMS	Noise = 20% RMS
mean MSE		0.3758	1.4508	3.2479	4.5854
min MSE		0.2666	1.0146	2.5097	4.5854
max MSE		0.4670	1.7937	3.8780	4.5854
Set	1	Yes	Yes	Yes	Yes
	2	Yes	Yes	Yes	No
	3	Yes	Yes	Yes	No
	4	Yes	Yes	Yes	No
	5	Yes	Yes	Yes	No

Table 4.14: MSE value from estimation and status of set success or failure in estimation with noise at amplitude = 10 N and frequency 1 = 3 rad/s

Figure 4.16 shows the plot of the real parameter system output with noise against the predicted system output at the 20% RMS level for the five sets of signal. Since the parameter estimation was only successful with set 1, Figure 4.16 (b) to Figure 4.16(e) do not show a good prediction. The MSE between the real system with noise and the predicted system for set 2, set 3, set 4 and set 5 are 12.5506, 18.6420, 7.8194 and 5.9472 respectively. The complexity introduced to the signal due to choice of frequencies for the sets may have led to the signal being overwhelmed by the 20% RMS level of noise where the signal noise ratio is unsuitable for parameter estimation compared to the simpler output signal of set 1.

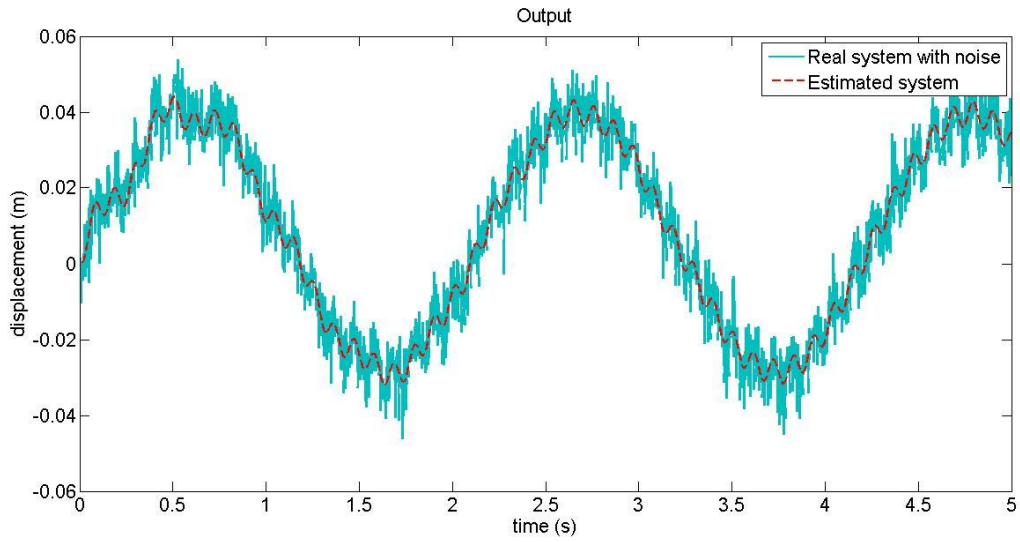

(a) Set 1

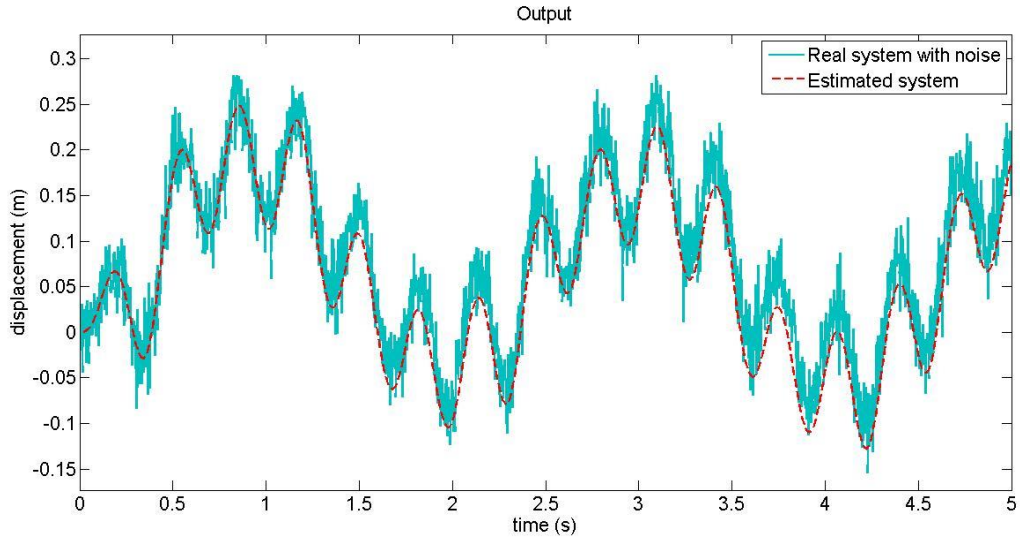
Output
Real system with noise
Estimated system
displacement (m)
time (s)
0.3
0.25
0.2
0.15
0.1
0.05
0
-0.05
-0.1
-0.15
0
0.5
1
1.5
2
2.5
3
3.5
4
4.5
5

(b) Set 2

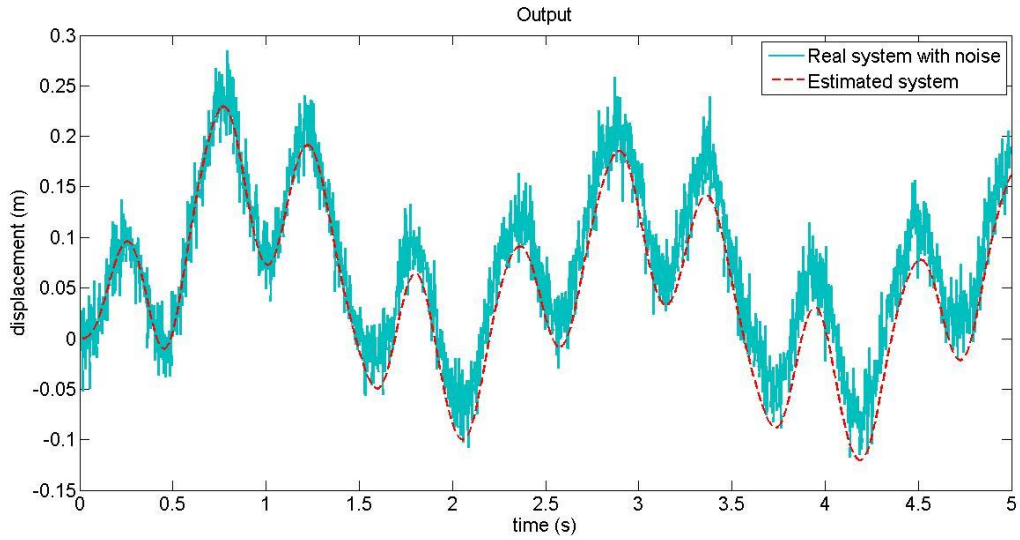
Output
Real system with noise
Estimated system
displacement (m)
time (s)
0.3
0.25
0.2
0.15
0.1
0.05
0
-0.05
-0.1
-0.15
0
0.5
1
1.5
2
2.5
3
3.5
4
4.5
5

(c) Set 3

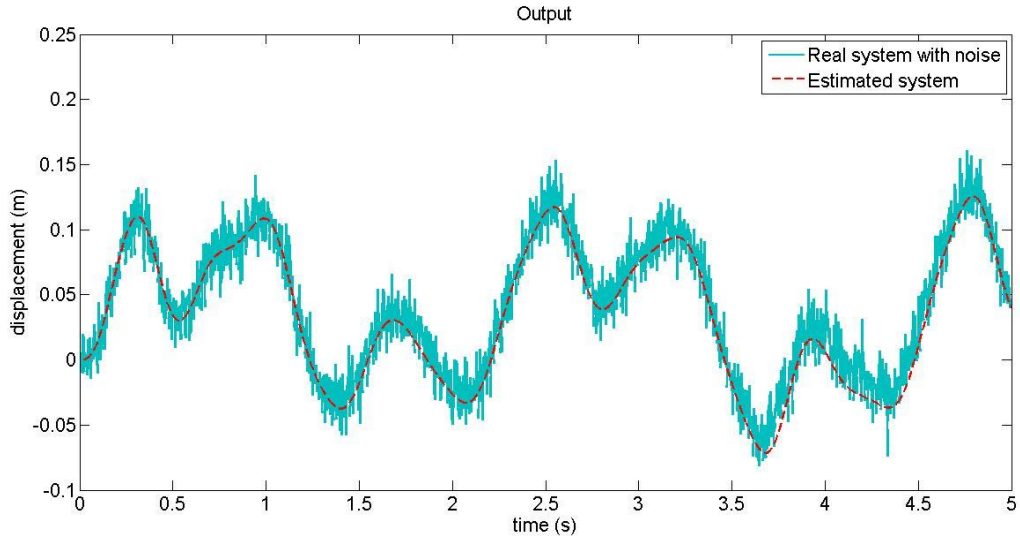

(d) Set 4

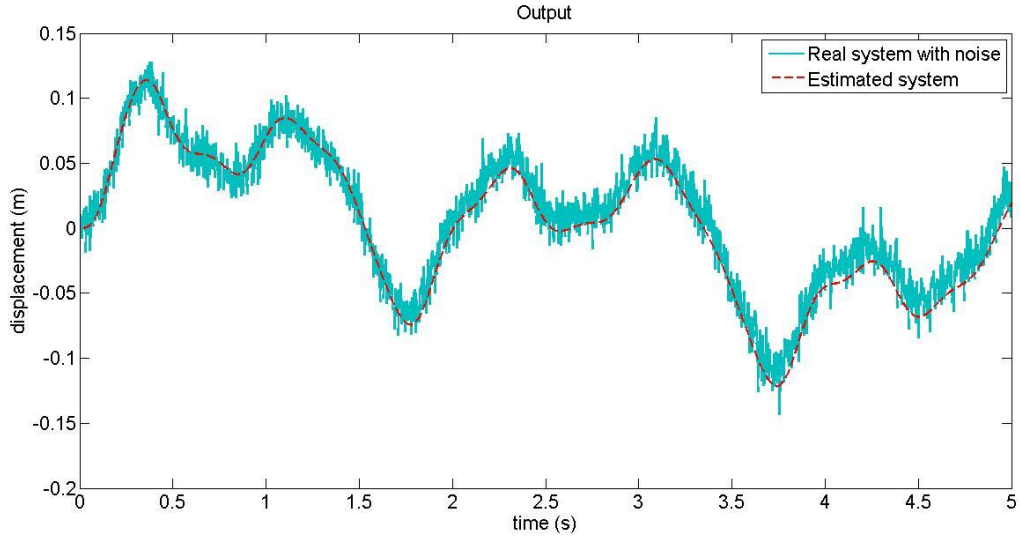

(e) Set 5

Figure 4.16: Output response plot of real system with noise against estimated system at 20% RMS

For frequency 1 = 17.6 rad/s, the estimated parameters are given in Table 4.15 for a noise level of 5% RMS to 20% RMS. There are no clear patterns for all estimated parameter value except that the estimated nonlinear parameters tend to stay close to the real system parameter values with slightly wider standard deviations when compared with the results from frequency 1 = 3 rad/s. This, again, may be due to the super harmonics being introduced by the 3 rad/s excitation frequency which forces the parameter estimation algorithm SADE to obtain parameter estimates to be as accurate as possible for the 3 rad/s excitation frequency sets.

The standard deviation trends are similar to the previous results where parameters *m*, *c*, α, and *A* show small standard deviations while the parameters *k*, β and γ have higher standard deviations throughout. The increasing or decreasing trends relative to the increasing noise level are however not seen here.

In Table 4.16, the MSE values for the estimation are shown. The values here are all lower than the previous estimation MSE with only one set having failed to obtain an MSE below 5 for the parameter estimation with a 20% RMS noise level. However this does not necessarily say that the estimated parameters are better than the previous estimated parameters.

Although the MSE with excitation frequency 1 of 17.6 rad/s is better than that of excitation frequency of 3 rad/s, the standard deviation trends show that the prediction of the latter is more precise. This can be caused by the sets of the 3 rad/s excitation frequency having a more complex output signal with nonlinear features which are easily identified by the parameter estimation algorithm. These nonlinear features penalised the parameter estimation MSE but reward the parameter estimation algorithm with a more precise estimate, hence the narrow standard deviation. In terms of nonlinear parameter estimation, having a complex signal (given there is still nonlinearity present) is a good way forward. However, there needs to be a balance between complexity and information availability from the signal in order to avoid a massively complex signal which can introduce linearisation as does a random signal.

	Noise = 5% RMS		Noise = 10% RMS		Noise = 15% RMS		Noise = 20% RMS	
	MEP	SD	MEP	SD	MEP	SD	MEP	SD
m	0.9950	3.70E-03	1.0027	9.10E-03	0.9974	1.14E-02	0.9911	6.50E-03
c	0.7213	2.59E-02	0.6995	1.18E-01	0.6914	1.37E-01	0.8888	6.96E-02
k	312.2068	3.96E+00	317.4403	1.32E+01	317.9186	1.47E+01	305.1580	3.86E+00
α	0.0102	3.38E-04	0.0101	2.23E-04	0.0104	7.10E-04	0.0100	1.20E-14
A	0.9894	1.43E-02	0.9747	3.08E-02	0.9718	4.28E-02	0.9998	3.60E-04
β	151.3120	2.89E+00	155.0094	8.58E+00	155.2393	8.28E+00	144.3081	3.87E+00
γ	21.9564	4.22E+00	17.3786	1.04E+01	20.8000	7.30E+00	24.3336	5.18E+00

Table 4.15: Estimation with sinusoidal inputs with amplitude = 10 N and frequency 1 = ω_n with noise

		Noise = 5% RMS	Noise = 10% RMS	Noise = 15% RMS	Noise = 20% RMS
mean MSE		0.2868	1.1490	2.5609	3.8671
min MSE		0.2429	0.9676	2.1523	4.1441
max MSE		0.3649	1.5151	3.4072	4.7523
Set	1	Yes	Yes	Yes	Yes
	2	Yes	Yes	Yes	Yes
	3	Yes	Yes	Yes	Yes
	4	Yes	Yes	Yes	No
	5	Yes	Yes	Yes	Yes

Table 4.16: MSE value from estimation and status of set success or failure in estimation with noise at amplitude = 10 N and frequency 1 = ω_n

4.4 **Chirp input**

With Matlab and Simulink, chirp input was used to generate simulated data for parameter estimation using SADE. The reason in moving to chirp input was mainly the issue with the selection of frequency combination for the multi sinusoidal input. A chirp input was relatively easy to specify when compared with the multi sinusoidal input. In the case of the chirp input, only the amplitude and range of frequency needs to be specified. Chirp input will provide a complete range of frequencies excited but in a concentrated manner, in terms of total energy of the input, the energy will be concentrated at a single frequency at any moment in time.

In this case, the amplitude was set at 10 N in line with the previous investigations using sinusoidal input where 10 N was an acceptable level of forcing. The signal frequency sweep was set across 1 to 25 rad/s to include the undamped natural frequency of the underlying linear model of 17.6 rad/s. The input and output signal can be seen in Figure 4.17 below. SADE was allowed to run for 1000 generations for each of the 100 runs.

The data from the chirp input could not be fitted with the linear model with a good MSE. The best linear fitting returned an MSE of 13.9950. Figure 4.18 shows the output response plot of the real system against the estimated linear system. It can be seen that the linear fitting struggled more towards the higher forcing frequency level. With this result, the Improvement Ratio does not need to

be calculated. In the context of this thesis, this is a good outcome, whereby using chirp input resulted in nonlinearity in the output that could not be estimated using the linear model which shows uniqueness of the data produced. This gives higher confidence in the estimated parameter outcome.

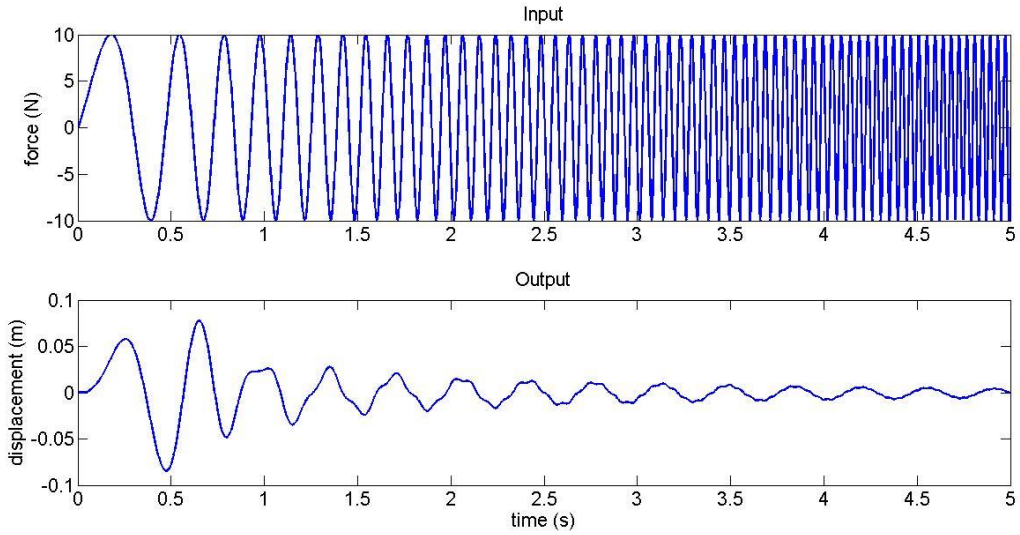

Figure 4.17: Plot of input excitation and output response for chirp input with amplitude = 10 N across 1 to 25 rad/s

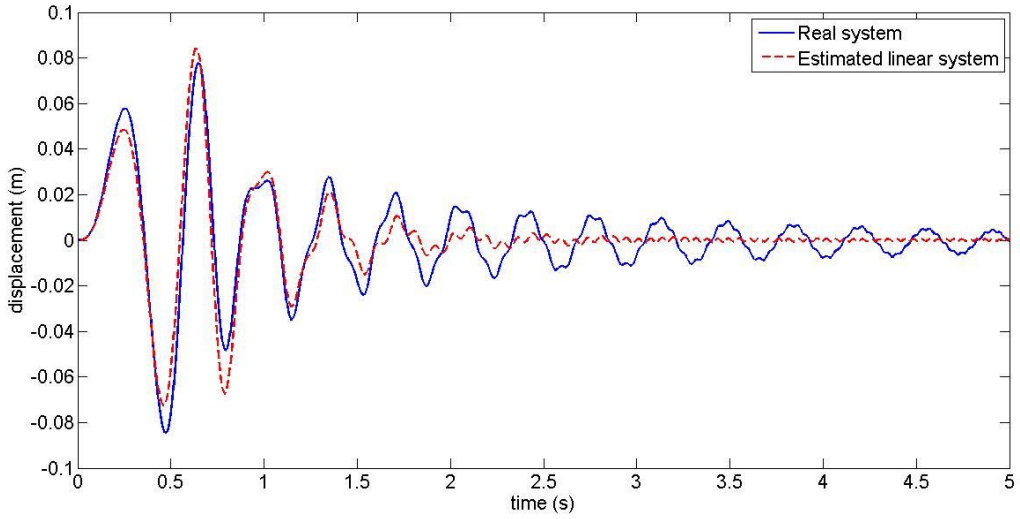

Figure 4.18: Output response plot for real system against estimated linear system

4.4.1 Signal without noise

Table 4.17 shows the nonlinear parameter estimation results. The parameter estimation was very good with all 100 runs successfully returning very low MSE values. The best estimated parameter here

corresponds to an MSE of 1.45E-22. The mean estimated parameter was a very good estimate for both linear and nonlinear parameters.

	Real Parameter	Best Estimated Parameter	% Error	Mean Estimated Parameter	Standard Deviation
m	1	1	0	0.9999	4.64E-04
c	0.7037	0.7037	0	0.7021	4.80E-03
k	309.51	309.51	0	327.7547	1.83E+01
α	0.01	0.01	0	0.0108	3.10E-03
A	1	1	0	0.9463	5.09E-02
β	150	150	0	159.5608	9.77E+00
γ	20	20	0	20.7099	1.43E+00

Table 4.17: Estimation with chirp input with amplitude = 10 N across 1 to 25 rad/s

4.4.2 Signal with noise

Noise was added to the output signal via simulated white noise using a random signal with amplitude equal to a percentage of the output signal root mean-square value (RMS). Simulated white noise was added at levels of 5% RMS, 10% RMS, 15% RMS and 20% RMS. Figure 4.19 and Figure 4.20 shows the signal output at 5% RMS and 20% RMS respectively.

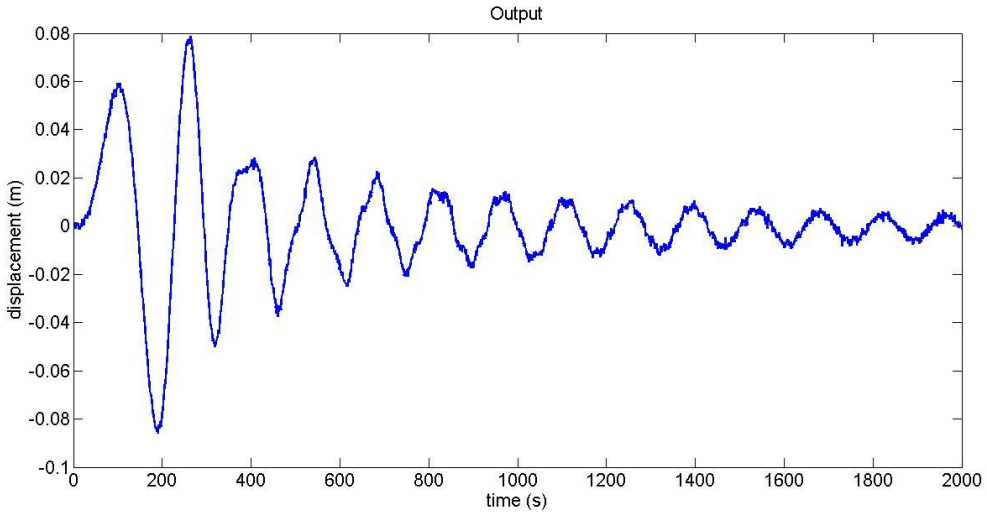

Figure 4.19: Output plot of chirp input with amplitude = 10 N across 1 to 25 rad/s with noise at 5% RMS

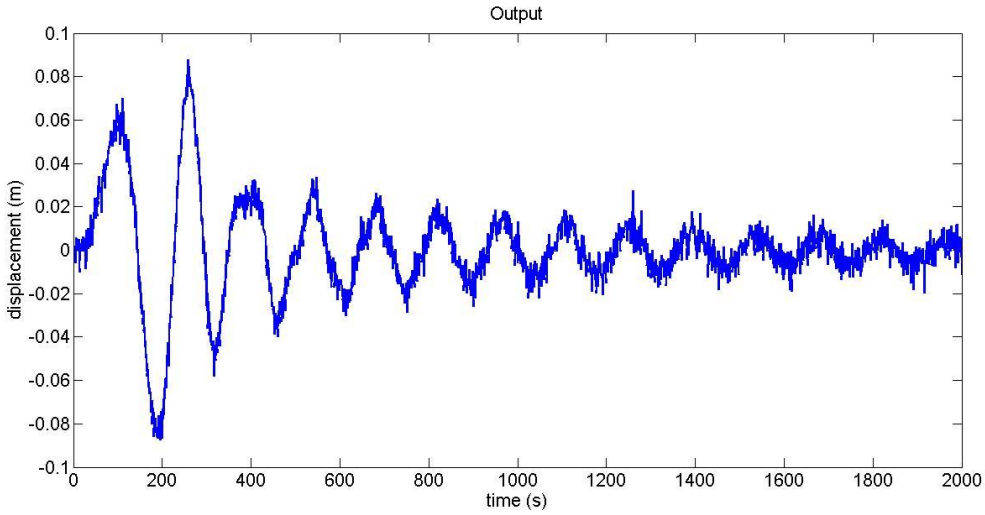

Figure 4.20: Output plot of chirp input with amplitude = 10 N across 1 to 25 rad/s with noise at 20% RMS

With chirp input, noise up to the level of 20% RMS still allowed the parameter estimation algorithm SADE to return an estimation with an MSE of less than 5 as can be seen in Table 4.18. This is compared to the result with sinusoidal input, where only the signal having a frequency at a factor of 3 to the undamped natural frequency of the underlying linear system (set 1), was successful. This indicates that the parameter estimation using the chirp input may be more robust in the presence of noise.

The standard deviation trends were similar for all parameters except γ which showed a low standard deviation compared to results from multi sinusoidal input which was always higher. This may be caused by the chirp input providing additional information in the data that can be picked up by the parameter estimation algorithm specifically for γ compared to when using the multi sinusoidal input data. The other standard deviation for parameters m, c, α and A were always low whilst the standard deviation for parameters k and β remained higher, similar to previous observations.

Figure 4.21 shows the plot of the real parameter output with noise against predicted parameters at the 20% RMS level. As shown by the MSE, the estimated system is a good prediction of the real system.

	Noise = 5% RMS		Noise = 10% RMS		Noise = 15% RMS		Noise = 20% RMS	
	MEP	SD	MEP	SD	MEP	SD	MEP	SD
m	1.0005	7.31E-04	1.0009	2.57E-08	0.9979	3.67E-09	0.9999	6.47E-09
c	0.7079	1.50E-03	0.6994	1.49E-07	0.6791	1.22E-08	0.6572	2.40E-08
k	317.4950	8.53E+00	309.7121	8.10E-06	340.2437	1.60E+01	353.4057	2.12E+01
α	0.0102	4.95E-04	0.0100	1.26E-15	0.0217	1.00E-03	0.0242	1.50E-03
A	0.9754	2.59E-02	1.0000	2.66E-11	0.9069	4.35E-02	0.8743	5.38E-02
β	154.3039	4.52E+00	150.0441	3.24E-05	173.7392	8.34E+00	185.8453	1.14E+01
γ	19.9781	3.00E-01	19.7610	2.27E-06	16.6563	8.00E-01	14.9064	9.18E-01
MSE	0.242		0.9284		2.2292		3.9196	

Table 4.18: Estimation with chirp input with amplitude = 10 N across 1 to 25 rad/s with noise

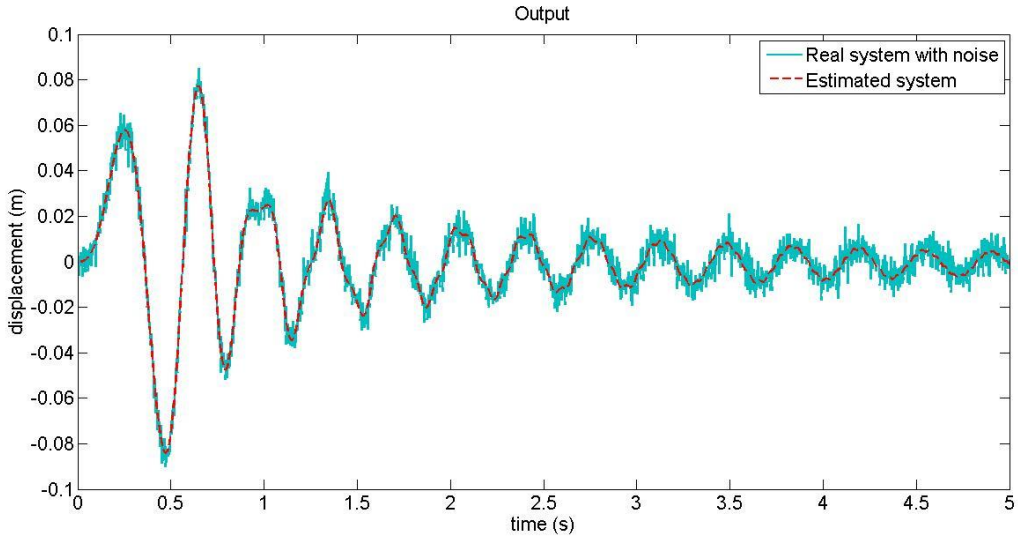

Figure 4.21: Output response of real system with noise against estimated system at 20% RMS

4.5 **Comparing sinusoidal and chirp signal parameter estimation**

In this section, the estimated systems that were identified in the previous sections were used to fit the estimated systems to the data from other input types. This was conducted to investigate the robustness of the estimated system when the real system was subjected to other types of input.

The estimated parameters from the multi sinusoidal input estimation (given in Table 4.13 and Table 4.15) and chirp estimation (given in Table 4.18) at a noise level of 10% RMS and 20% RMS were taken and the estimated system was evaluated against the data from other signal types at the same

noise level. The comparison MSE are presented in Table 4.19 and Table 4.20 for 10% RMS noise system and 20% RMS noise system respectively.

These comparison tables show that the estimated system using multi sinusoidal and chirp input both are robust enough for parameter estimation even when subjected to other types of input. The table also shows that using the estimated system from chirp input with 10% RMS noise results in the best MSE for data from multi sinusoidal, chirp and random input. For the 20% RMS noise chirp estimated system, it still gave the best estimate for chirp and random input types although it was not the best compared to the other two estimated systems for multi sinusoidal input estimation.

	MSE			
	Sinusoidal		Chirp	Random
Estimated system	Frequency 1 = 3 rad/s	Frequency 1 = 17.6 rad/s		
Sine frequency 1 = 3 rad/s	2.6783	2.2819	0.3794	1.2872
Sine frequency 1 = 17.6 rad/s	1.5459	1.2118	1.0336	2.8528
Chirp	1.4984	1.1482	0.0004	1.0050

Table 4.19: MSE value against other input types at 10% RMS noise by fitting estimated system from 10% RMS level

	MSE			
	Sinusoidal		Chirp	Random
Estimated system	Frequency 1 = 3 rad/s	Frequency 1 = 17.6 rad/s		
Sine frequency 1 = 3 rad/s	4.2190	3.9955	3.8642	4.5362
Sine frequency 1 = wn	4.1269	4.3604	4.3439	4.4126
Chirp	4.3975	4.1371	3.7983	3.8011

Table 4.20: MSE value against other input types at 20% RMS noise by fitting estimated system from 20% RMS level

4.5.1 MSE sensitivity for different input

A study was conducted to investigate the variation of the MSE value when only one parameter of the Bouc-Wen model was varied for the different input signal types to determine the sensitivity of the parameter estimation algorithm MSE with the different input types of data. The MSE for the three types of input were plotted on the same figure. This was conducted to further investigate the different types of input, random, multi sinusoidal and chirp input sensitivity to each of the parameters of the model. Observations were made on how the MSE was affected by changes of each parameter

separately. A rapid change in MSE would show better parameter estimation accuracy for the type of inputs used showing high sensitivity of the parameter estimation algorithm towards any change in the parameter value.

Initially, the parameter α was investigated at both low input amplitude and high input amplitude. The low amplitude was 0.1 N for all input types, while the high amplitude was 10 N for chirp and multi sinusoidal input and 100 N for the random input. This was in line with previous work where random input was shown to have less nonlinearity present at amplitude of 10 N.

Figure 4.22 and Figure 4.23 shows the MSE against the parameter α at low and high amplitude respectively. In both figures, multi sinusoidal input is seen as most sensitive to the variation of parameter α, where α is the switch between linear and nonlinear for the Bouc-Wen model. At low amplitude, random and chirp input show almost no MSE changes. Both signals neglected sensitivity towards the change in α, while with multi sinusoidal signal, changes in α affected the MSE value very slightly, thus rewarding the parameter estimation algorithm for accuracy. However the effect was very small and is almost negligible. This was due to the low amplitude excitation data providing data with a mostly linear behaviour. In the high amplitude data in Figure 4.23, a more significant effect on the MSE is seen with changes in parameter α for both multi sinusoidal and chirp input. Random input still showed less sensitivity towards changes in the α parameter.

The following figures only show the response at high amplitude to avoid repetition as similar behaviour was seen at the low amplitude i.e. little sensitivity for all parameters.

Figure 4.24 to Figure 4.27 show the MSE against the linear parameters *m*, *c*, *k* and *A*. With these parameters, a more sensitive MSE reaction to parameter change was seen with random input, followed by chirp input and finally multi sinusoidal input. In Figure 4.25, the value of the MSE of the multi sinusoidal input with respect to changes in parameter *c* was still under 5 up to the value of about 1.94.

Figure 4.28 and Figure 4.29 show the MSE against nonlinear parameters β and γ. Here, it can be seen that the random input was the less sensitive to the variation in the nonlinear parameter while it was

very rewarding for finding the linear parameters. Chirp was the most rewarding to the optimization algorithm with a sharper increase in MSE with changing nonlinear parameters.

The MSE sensitivity investigations showed that for linear parameter estimation, random input was the best choice of input signal for data collection. Random input gave a variety of forcing frequencies that would result in good data for linear parameter estimation. However the linearisation effect due to the use of a random signal was a disadvantage for nonlinear parameter estimation. As shown here, multi sinusoidal and chirp input provide more satisfactory data for nonlinear parameter estimation with higher sensitivity to the nonlinear parameters.

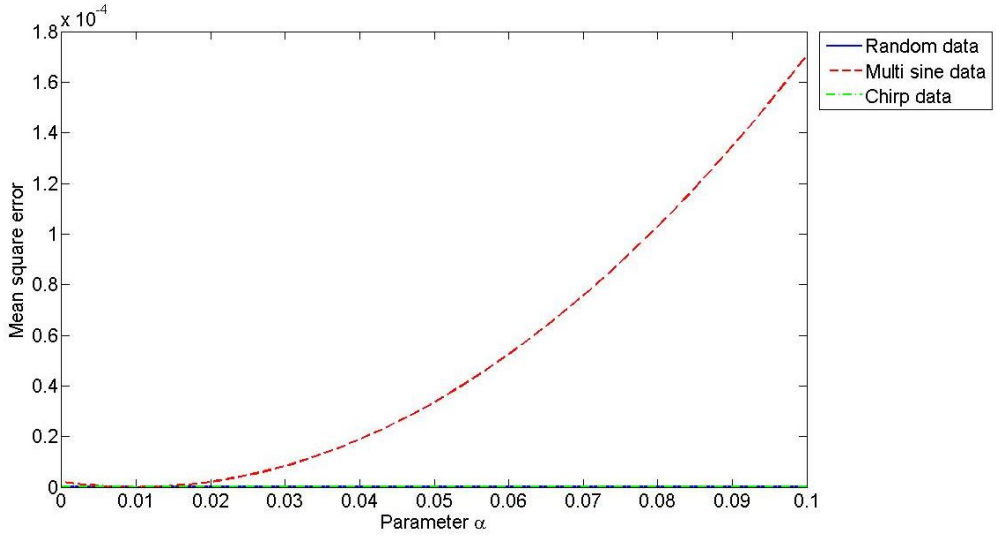

Figure 4.22: MSE against parameter α with low amplitude input

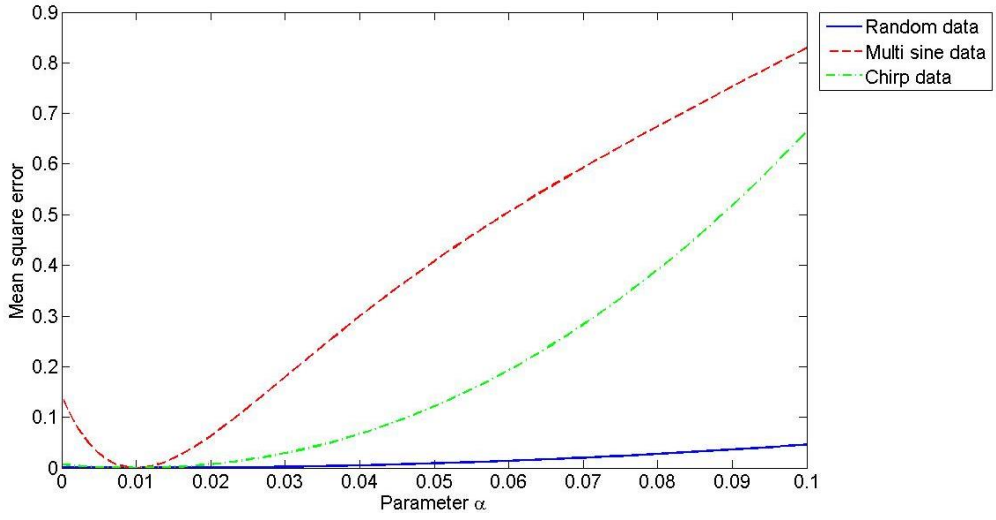

Figure 4.23: MSE against parameter α with high amplitude input

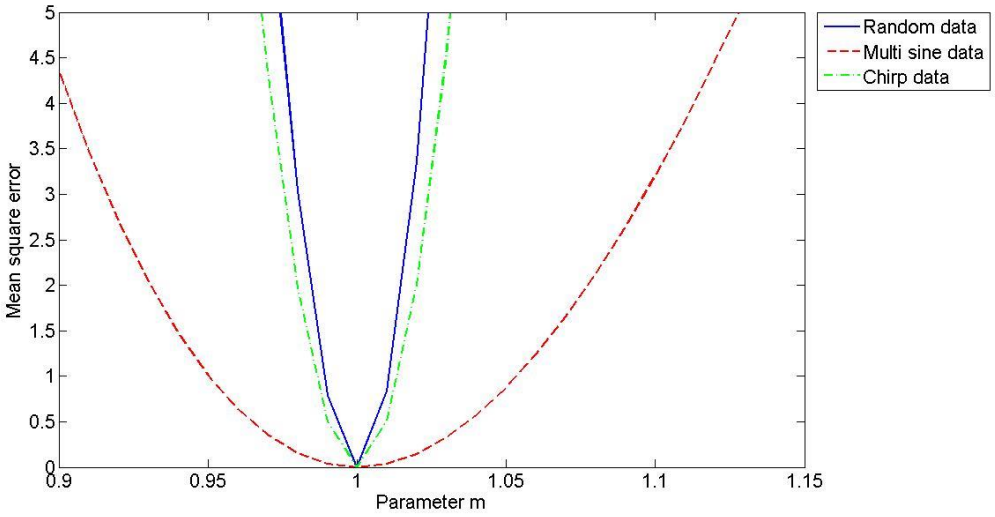

Figure 4.24: MSE against parameter m with high amplitude input

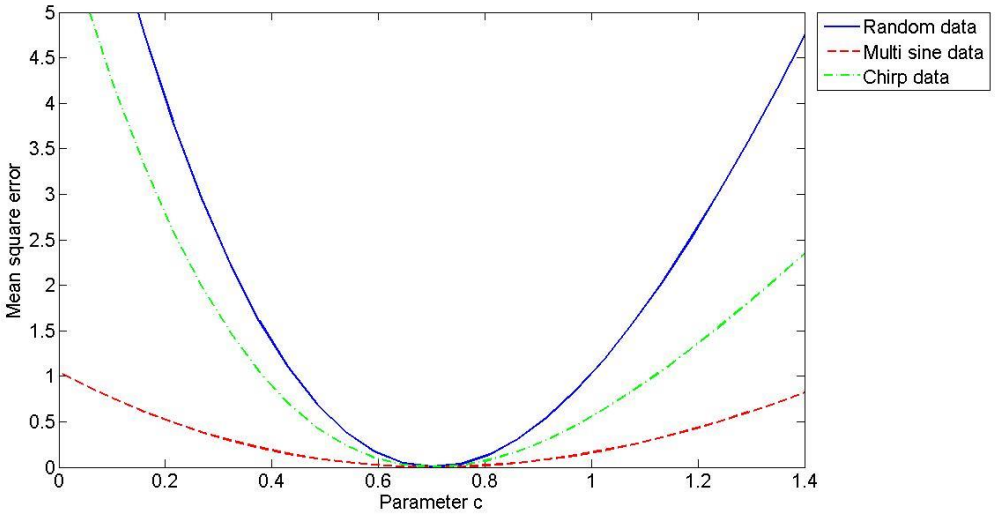

Figure 4.25: MSE against parameter c with high amplitude input

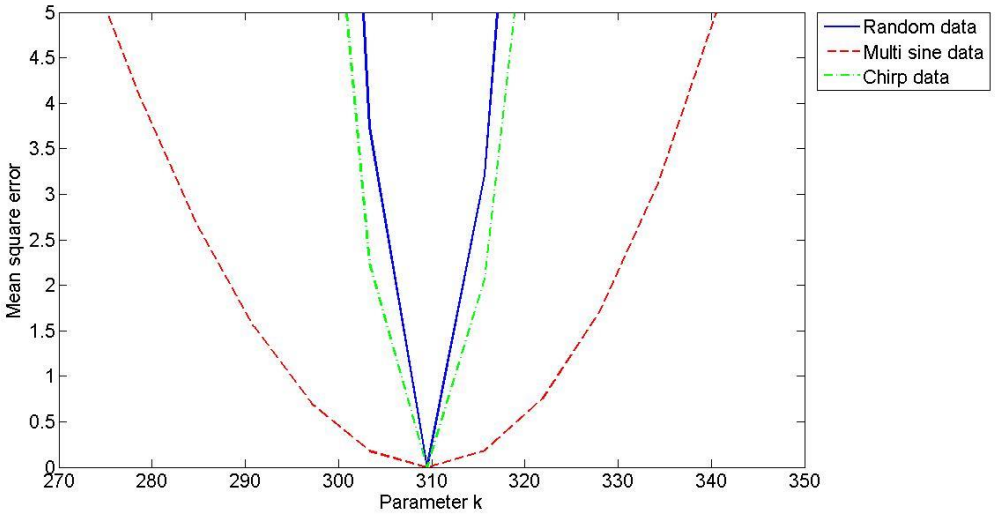

Figure 4.26: MSE against parameter k with high amplitude input

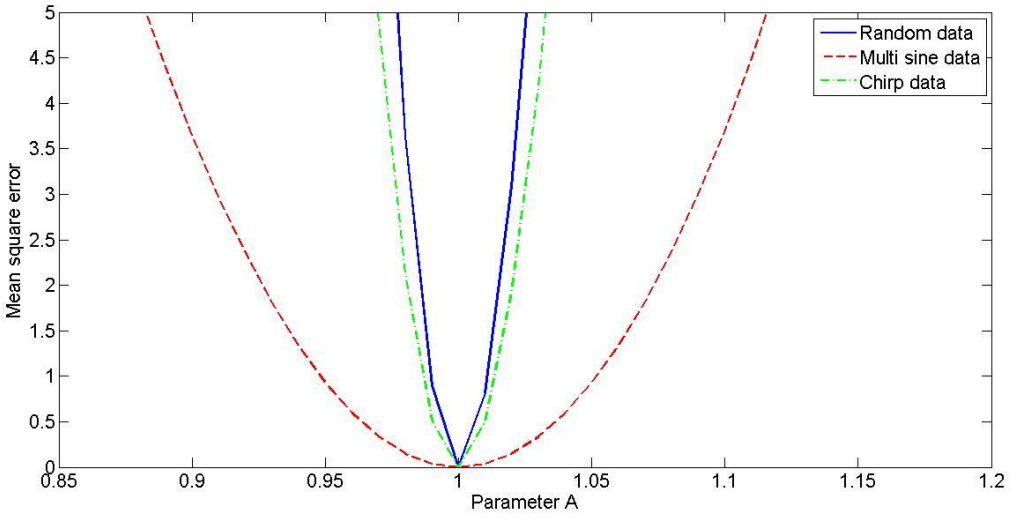

Figure 4.27: MSE against parameter A with high amplitude input

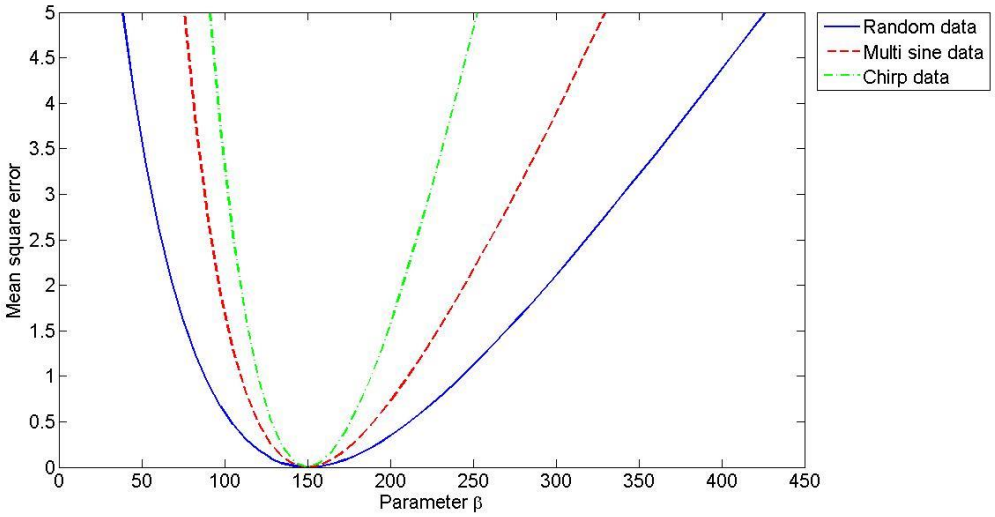

Figure 4.28: MSE against parameter β with high amplitude input

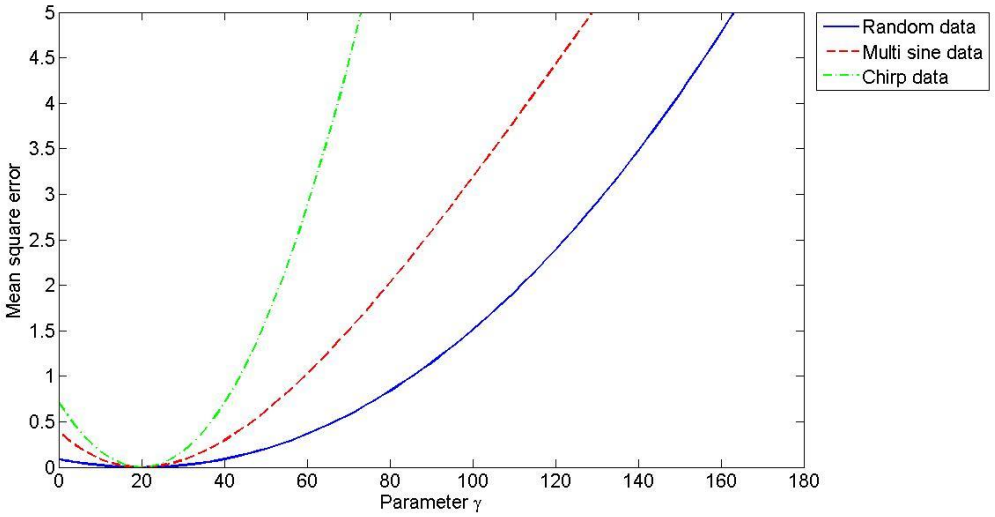

Figure 4.29: MSE against parameter γ with high amplitude input

4.6 **Discussion**

In this chapter, SADE was again used as the parameter estimation algorithm for the investigations. Parameter estimation exercises were conducted using single and multi sinusoidal input signals and using a chirp input signal. A variety of combinations of sinusoidal signal were used in the investigation to understand the effects of frequency choices on parameter estimation. The sinusoidal

input frequency choice in this thesis had been done such that the first part of the combine signal was the control signal which is pre-selected. The other part of the signal frequency was chosen randomly with criteria that it is not multiple or fraction of the first frequency to create a diverse input. From the results in this chapter, it was shown that using first frequency at the undamped natural frequency of the underlying linear system yields almost similar estimates compared to the 'trial and error' frequencies of 3 rad/s and 8 rad/s.

It was found that a sinusoidal signal combination with one of the frequencies at the undamped natural frequency of the underlying linear system (17.6 rad/s) and 8 rad/s gave almost perfect mean estimated parameters without the presence of noise. It is expected that other frequency combinations would allow good parameter estimation as well, as long as it provides sufficient information of the system. A combination of multiples of the frequency, for example ω and 2ω, may not be as useful since the addition or difference of the frequency and the harmonics could clash, reducing the amount of significant information in the signal. Thought should be given into making the choice of frequencies to be used so as to maximise the useful information for parameter estimation purposes.

The investigation was extended to include the presence of noise using frequency 1 = 17.6 rad/s and frequency 1 = 3 rad/s. For a noise level of up to 15% of the output RMS, good estimation was obtained for all sinusoidal combinations. At 20% RMS, for frequency 1 = 3 rad/s, only the first set of combinations manage to bring the MSE value down to less than 5, while others failed. However, with frequency 1 = 17.6 rad/s, only one set failed to give good MSE.

Using a chirp signal, excellent estimation was obtained without the presence of noise. With the introduction of noise, the estimation was still good for a noise level of up to 20% of the output RMS. This was a very positive outcome since the setup of chirp was relatively easy with only the amplitude parameter to be set and it produced good parameter estimation results.

The estimated parameters with noise for multi sinusoidal and chirp input were used to compare with other known real parameter system of sinusoidal, chirp and random type signals. They produced a good MSE estimation against the sinusoidal, chirp and random signal even at 20% RMS noise. This

means that the system estimated using data from the multi sinusoidal and chirp, would work well even when subjected to other types of input showing robustness of the estimated system.

Multi sinusoidal input and chirp input both were shown to be good input for providing data for nonlinear parameter estimation. They both resulted in a reliable estimation that could be used to predict system even with other type of input. The requirements for multi sinusoidal input however required a more particular choice in the design of frequency combinations. A bad frequency combination could result in information loss for the signal from the sum and difference of the frequencies themselves or the harmonic sets which may lead to multi sinusoidal input becoming the worst choice of input signal. A simpler chirp signal may be the best type of input signal for designing data collection experiments for nonlinear parameter estimation for the particular system investigated here and this is expected to be so for other nonlinear systems as well.

For the Improvement Ratio, for investigations without noise for single sinusoidal input, similar to the random input, the range of values of the Improvement Ratio for low amplitude was around 1.16E7 to 5.28E9, while Improvement Ratio for high amplitude data was around 1.66E23 to 2.84E22. For the multi sinusoidal data, the Improvement Ratio was at a higher value of around 7.51E28. The Improvement Ratio for multi sinusoidal was much higher since it gave a more complicated signal that gave a higher incentive to identify the right nonlinear model. This in turn gave higher accuracy for the right model selection compared to a simple linear system.

In the presence of noise, the Improvement Ratio for single sinusoidal data estimation gave a higher confidence with 0 to 0.0008 Improvement Ratios shown for the low amplitude level of 0.1 N data and 0.3 to 4.88 Improvement Ratios shown for the 10 N amplitude data. For the multi sinusoidal and chirp input, no Improvement Ratio was calculated as the linear model could not be fitted with good estimates to both sets of data at 10 N forcing amplitude. This showed that the use of multi sinusoidal and chirp input results in data that was highly nonlinear that could not be estimated with a linear model of m, c and k. This would give a very high confidence that the predicted model was fittingly nonlinear.

In chapter 3 and 4, the Self-adaptive Differential Evolution (SADE) optimisation algorithm has been used to compare the different signal types in a parameter estimation sense. In the next chapter an alternative approach to parameter estimation will be investigated. The Volterra representation will be investigated for use of nonlinear parameter estimation and to further investigate the behaviour of the Bouc-Wen hysteretic model.

Chapter 5

5 Volterra series representation on polynomial model

5.1 **Introduction**

The previous two chapters have shown the benefits of using harmonic excitation in nonlinear parameter identification through the use of optimisation using Self-Adaptive Differential Evolution (SADE). An alternative approach to parameter identification is investigated in this chapter and in the following chapter, with the use of the Volterra Series.

In this chapter, the concept will be demonstrated on a number of nonlinear systems with polynomial nonlinearities. This chapter serves to introduce and show the concept of the Volterra series approximation to guide the reader into the following chapter. The use of the Volterra series approximation on polynomial systems as shown here will be directly applied to the Bouc-Wen hysteretic model in the next chapter to demonstrate new findings in the Bouc-Wen behaviour. The basics of the Volterra representation are not discussed in full detail here. However the equations used will be introduced briefly before being applied to the identification of the parameters.

Firstly, the linear parameters for the polynomial model are identified without the addition of noise. This is then repeated in the presence of noise. Next, the nonlinear parameters are identified using the Volterra series representation, again without noise and then in the presence of noise. Finally, the effect of noise is investigated further relative to the nonlinear parameters.

5.2 **Background study**

The Volterra series representation is currently accepted as an established method for the analysis of nonlinear systems. The application in terms of nonlinearity identification and system response prediction has generated a lot of interest in the series. This is done by measuring the Volterra kernels and kernel transforms.

In 1880, Vito Volterra came out with a functional form of the Taylor series that is now known as the Volterra series. His work can be found in his book [58] which shows the general theory of the continuous series. The early work was a very extensive mathematical description of the series and only showed the first potential in nonlinear system characterization with the work of Norbert Wiener in 1942 in his report [59]. He showed that the summation of Volterra kernels or individual terms in the series represented the output of a nonlinear system. A summary of the development period of the theory on the Volterra series can be found in a survey paper in [60].

Soon, work on the Volterra series mostly revolved around identifying the kernels and its Fourier transform. There were many attempt in this area, resulting in many publications. One of the proposed methods realized in 1971 was described in [61], which used multi sinusoidal testing to obtain the Volterra kernels, known as harmonic probing, resulting in exact terms for the kernels. Only after 12 years, was a publication on the successful application of the method was published for a loudspeaker application [62]. Although the result was poor, it managed to obtain the second frequency response function (FRF) of the loudspeaker. Up to the third order kernel transform, termed as the higher order FRF (HFRF) was found using the harmonic probing technique in 1991 [63].

The limitation of the functional series was also well documented in [64] regarding the convergence problem of the series and in [65] regarding the range of validity of the series. Further to the

convergence problem a look at harmonics excitation limits of the method was presented in [66] and further investigated in [67] with a new criterion proposed. Again in 2011, an extension to the convergence criterion was proposed in [68] by the Billings research group that would give the upper convergence region limit with more accuracy than the previously proposed criteria.

Some early applications of the Volterra series in physiological studies were documented in the book [69]. In the harmonic probing method, a lot of literature has been published on the application of parametric studies, modelling and system identification. In [70], harmonic probing was used in bilinear oscillator identification for structural elements. A modified Volterra harmonic probing technique was used successfully in the simulation of nonlinear bridge aerodynamics in [71] where two cases were looked at the first being a numerical simulation of the bridge and the second was an experimental study in a wind tunnel environment. Some more recent work includes [72] which used Volterra representation in bluff-body aerodynamics nonlinear system analysis and [73] in the dynamic response prediction of a slender marine structure under random white noise (ocean waves).

5.3 **Volterra series**

5.3.1 Time domain and frequency domain representation

The Volterra series is an infinite functional series which can be generally written in the time domain as Equation 5.1 for a nonlinear system given a single input *x(t)* which produces an output *y(t)*. The term $h_1(\tau_1)$, $h_2(\tau_1, \tau_2)$, $h_3(\tau_1, \tau_2, \tau_3), \ldots, h_n(\tau_1, \tau_2, \tau_{3,\ldots,} \tau_n)$ are known as the first, second, third,…, nth order Volterra kernels.

$$y(t) = y_1(t) + y_2(t) + y_3(t) + \cdots + y_n(t) + \cdots \tag{5.1}$$

where

$$y(t) = \int_{-\infty}^{+\infty} d\tau_1 h_1(\tau_1) x(t-\tau_1)$$

$$+ \int_{-\infty}^{+\infty} \int_{-\infty}^{+\infty} d\tau_1 d\tau_2 \, h_2(\tau_1, \tau_2) x(t-\tau_1) x(t-\tau_2)$$

$$+ \int_{-\infty}^{+\infty} \int_{-\infty}^{+\infty} \int_{-\infty}^{+\infty} d\tau_1 d\tau_2 \, d\tau_3 h_2(\tau_1, \tau_2, \tau_3) x(t-\tau_1) x(t-\tau_2) x(t-\tau_3)$$

$$+ \cdots + \int_{-\infty}^{+\infty} \ldots \int_{-\infty}^{+\infty} d\tau_1 \ldots d\tau_n \, h_1 \ldots h_n (\tau_1, \ldots, \tau_n) \prod_{i=1}^{n} x(t-\tau_i) + \cdots \quad (5.2)$$

In general, the n[th] order term of the response is given by

$$y_n(t) = \int_{-\infty}^{+\infty} \ldots \int_{-\infty}^{+\infty} d\tau_1 \ldots d\tau_n \, h_1 \ldots h_n (\tau_1, \ldots, \tau_n) \prod_{i=1}^{n} x(t-\tau_i) \quad (5.3)$$

For a linear system, $y(t) = y_1(t)$ is also called a convolution integral or Duhamel's integral. Taking the Fourier transform of the convolution integral will give the expression in the frequency domain for the linear system response given by Equation 5.4 which will be used for linear parameter estimation.

$$Y(\omega) = \int_{-\infty}^{+\infty} dt \, e^{-i\omega t} \int_{-\infty}^{+\infty} d\tau \, h(\tau) x(t-\tau) = \int_{-\infty}^{+\infty} d\tau \, h(\tau) \int_{-\infty}^{+\infty} dt \, e^{-i\omega t} x(t-\tau)$$

$$= \int_{-\infty}^{+\infty} d\tau \, h(\tau) \; X(\omega) e^{-i\omega t}$$

$$= H(\omega) X(\omega) \quad (5.4)$$

The frequency domain representation of the whole Volterra series as in Equation 5.1 will be of the form

$$Y(\omega) = Y_1(\omega) + Y_2(\omega) + Y_3(\omega) + \cdots + Y_n(\omega) + \cdots \quad (5.5)$$

The $Y_1(\omega)$ component will be the same as the response for the linear system which is expressed in Equation 5.4. The derivation for the higher-order components is more complicated. This requires the use of Higher-order Frequency Response Function (HFRF) of the Volterra kernels $H_n(1,\ldots,\omega)$, n=1,…, ∞ as a multidimensional Fourier transform of the kernels. The Fourier transform of $y_2(t)$ expression yields

$$Y_2(\omega) = \int_{-\infty}^{+\infty}\int_{-\infty}^{+\infty} d\tau_1 d\tau_2 h_2(\tau_1,\tau_2) \int_{-\infty}^{+\infty} dt\ e^{-i\omega t}\left\{\left(\frac{1}{2\pi}\right)\int_{-\infty}^{+\infty} d\omega_1\ e^{-i\omega(t-\tau_1)}X(\omega_1)\right\}$$

$$\times\left\{\left(\frac{1}{2\pi}\right)\int_{-\infty}^{+\infty} d\omega_2\ e^{-i\omega(t-\tau_2)}X(\omega_2)\right\}$$

rearranging and using the fact that

$$\delta(\omega-\omega_1-\omega_2) = \left(\frac{1}{2\pi}\right)\int_{-\infty}^{+\infty} dt\ e^{-i(\omega-\omega_1-\omega_2)t}$$

the expression becomes

$$Y_2(\omega) = \left(\frac{1}{2\pi}\right)\int_{-\infty}^{+\infty}\int_{-\infty}^{+\infty} d\omega_1 d\omega_2 \delta(\omega-\omega_1-\omega_2) H_2(\omega_1,\omega_2)X(\omega_1)X(\omega_2)$$

$$= \left(\frac{1}{2\pi}\right)\int_{-\infty}^{+\infty} d\omega_1 H_2(\omega_1,\omega-\omega_1)X(\omega_1)X(\omega-\omega_1)$$

Now, the complete expression for the Volterra series representation in frequency domain for a response is

$$Y(\omega) = H_1(\omega)X(\omega) + \left(\frac{1}{2\pi}\right)\int_{-\infty}^{+\infty} d\omega_1 H_2(\omega_1,\omega-\omega_1)X(\omega_1)X(\omega-\omega_1)$$

$$+\left(\frac{1}{2\pi}\right)^2\int_{-\infty}^{+\infty}\int_{-\infty}^{+\infty} d\omega_1 d\omega_2 H_3(\omega_1,\omega_2,\omega-\omega_1-\omega_2)\ \times X(\omega_1)X(\omega_2)X(\omega-\omega_1-\omega_2)$$

$$+\left(\frac{1}{2\pi}\right)^{n-1}\int_{-\infty}^{+\infty}\dots\int_{-\infty}^{+\infty} d\omega_1\dots d\omega_{n-1}\, H_n(\omega_1,\dots,\omega_{n-1},\omega-\omega_1-\dots-\omega_{n-1})$$

$$\times X(\omega_1)\dots X(\omega_{n-1})X(\omega-\omega_1-\cdots-\omega_{n-1}) \qquad (5.6)$$

where the nth order term of the response in the frequency domain can be written as

$$Y_n(\omega) = \left(\frac{1}{2\pi}\right)^{n-1}\int_{-\infty}^{+\infty}\dots\int_{-\infty}^{+\infty} d\omega_1\dots d\omega_{n-1}\, H_n(\omega_1,\dots,\omega_{n-1},\omega-\omega_1-\dots-\omega_{n-1})$$

$$\times X(\omega_1)\dots X(\omega_{n-1})X(\omega-\omega_1-\cdots-\omega_{n-1})$$

5.3.2 Harmonic probing

Harmonic probing is a method used to determine the analytical form of HFRFs. The method relies on the use of harmonic input to the Volterra series. To find the analytical form of HFRF, a probing equation is substituted into the equation of motion. For H_1, the probing equation is as Equation 5.7 and Equation 5.8. The probing equation for H_2 is given by Equation 5.9 and Equation 5.10, whilst Equation 5.11 and Equation 5.12 show the general probing expressions. For further information of harmonic probing, the reader can refer to Bedrosian and Rice [61] and Billings two part paper [74], [75].

$$x_{p1}(t) = e^{i\Omega t} \tag{5.7}$$

$$y_{p1}(t) = H_1(\Omega)e^{i\Omega t} \tag{5.8}$$

$$x_{p2}(t) = e^{i\Omega_1 t} + e^{i\Omega_2 t} \tag{5.9}$$

$$y_{p2}(t) = H_1(\Omega_1)e^{i\Omega_1 t} + H_1(\Omega_2)e^{i\Omega_2 t} + H_2(\Omega_1, \Omega_2)e^{i(\Omega_1+\Omega_2)t} \tag{5.10}$$

$$x_{pn}(t) = e^{i\Omega_1 t} + \cdots + e^{i\Omega_n t} \tag{5.11}$$

$$y_{pn}(t) = \sum_{i=1}^{i=n}\sum_{1}^{q} l!\, H_1(\Omega, \dots, \Omega)e^{i\Omega_1 t} \tag{5.12}$$

5.3.3 Volterra series response to sinusoidal input

The exponential form of a sinusoidal wave is $x(t) = Xsin(\Omega t) = \frac{X}{2i}\left\{e^{i\omega t} - e^{-i\omega t}\right\}$ which may be considered as the difference of two ideal harmonics. Due to the interaction between the two harmonic terms, the response at a any harmonic is attributable to an infinite number of HFRFs. The Fourier transform of the input gives:

$$X(\omega) = \frac{\pi X}{2i}\{\delta(\omega - \Omega) - \delta(\omega + \Omega)\} \tag{5.13}$$

Substituting the input to the general Volterra response in the frequency domain of Equation 5.6 yields

$$Y(\omega) = 2\pi H_1(\omega)\left\{\frac{X}{4i}\delta(\omega - \Omega) - \frac{\mathrm{X}}{4\mathrm{i}}\delta(\omega + \Omega)\right\}$$

$$+2\pi\int_{-\infty}^{+\infty} d\omega_1 H_2(\omega_1, \omega-\omega_1)\left\{\frac{X}{4i}\delta(\omega_1-\Omega)-\frac{X}{4i}\delta(\omega_1+\Omega)\right\}$$

$$\times\left\{\frac{X}{4i}\delta(\omega-\omega_1-\Omega)-\frac{X}{4i}\delta(\omega-\omega_1+\Omega)\right\}$$

$$+2\pi\int_{-\infty}^{+\infty}\int_{-\infty}^{+\infty} d\omega_1 d\omega_2 H_3(\omega_1,\omega_2,\omega-\omega_1-\omega_2)\left\{\frac{X}{4i}\delta(\omega_1-\Omega)-\frac{X}{4i}\delta(\omega_1+\Omega)\right\}$$

$$\times\left\{\frac{X}{4i}\delta(\omega_2-\Omega)-\frac{X}{4i}\delta(\omega_2+\Omega)\right\}$$

$$\times\left\{\frac{X}{4i}\delta(\omega-\omega_1-\omega_2-\Omega)-\frac{X}{4i}\delta(\omega-\omega_1-\omega_2+\Omega)\right\}$$

$$+\cdots+2\pi\int_{-\infty}^{+\infty}\ldots\int_{-\infty}^{+\infty} d\omega_{1\ldots} d\omega_{\mathrm{n}-1} H_{\mathrm{n}}(\omega_1,\ldots,\omega_{\mathrm{n}-1},\omega-\omega_1-\cdots-\omega_{\mathrm{n}-1})$$

$$\times\left\{\frac{X}{4i}\delta(\omega_1-\Omega)-\frac{X}{4i}\delta(\omega_1+\Omega)\right\}\ldots\left\{\frac{X}{4i}\delta(\omega_{n-1}-\Omega)-\frac{X}{4i}\delta(\omega_{n-1}+\Omega)\right\}$$

$$\times\left\{\frac{X}{4i}\delta(\omega-\omega_1-\ldots-\omega_{n-1}-\Omega)-\frac{X}{4i}\delta(\omega-\omega_1-\ldots-\omega_{n-1}+\Omega)\right\}$$

$$+\cdots \tag{5.14}$$

By using the property of symmetry of the HFRF, the equation can be generalised as

$$y(t)=AH_1(\Omega_A)e^{i\Omega_A t}+BH_1(\Omega_B)e^{-i\Omega_B t}$$

$$+A^2H_2(\Omega_A,\Omega_A)e^{i2\Omega_A t}+2ABH_2(\Omega_A,\Omega_B)e^{i(\Omega_A+\Omega_B)t}+B^2H_2(\Omega_B,\Omega_B)e^{i2\Omega_B t}$$

$$+A^3H_3(\Omega_A,\Omega_A,\Omega_A)e^{i3\Omega_A t}+3A^2BH_3(\Omega_A,\Omega_A,\Omega_B)e^{i(2\Omega_A+\Omega_B)t}$$

$$+3AB^2H_3(\Omega_A,\Omega_B,\Omega_B)e^{i(\Omega_A+2\Omega_B)t}+B^3H_3(\Omega_B,\Omega_B,\Omega_B)e^{i3\Omega_B t}+\cdots \tag{5.15}$$

where $= B = \frac{X}{4i}$, $\Omega_A = +\Omega$ and $\Omega_B = -\Omega$ for sinusoidal input

5.4 **Polynomial Nonlinear System**

The nonlinear system to be discussed is the polynomial model represented by a Duffing oscillator with linear, quadratic and cubic damping and stiffness as shown in Figure 5.1 with the equation of motion given by Equation 5.16. The polynomial model in this chapter will use the parameters given in Table 5.1 for single nonlinearity systems throughout. This corresponds to the undamped natural frequency of the underlying linear system of 100 rad/s and damping ratio of the underlying linear system, given by, $\zeta = \frac{c}{2\omega_n m}$ of 0.1.

$$m\ddot{y} + c\dot{y} + ky + c_2\dot{y}^2 + c_3\dot{y}^3 + k_2y^2 + k_3y^3 = x(\mathrm{t}) \tag{5.16}$$

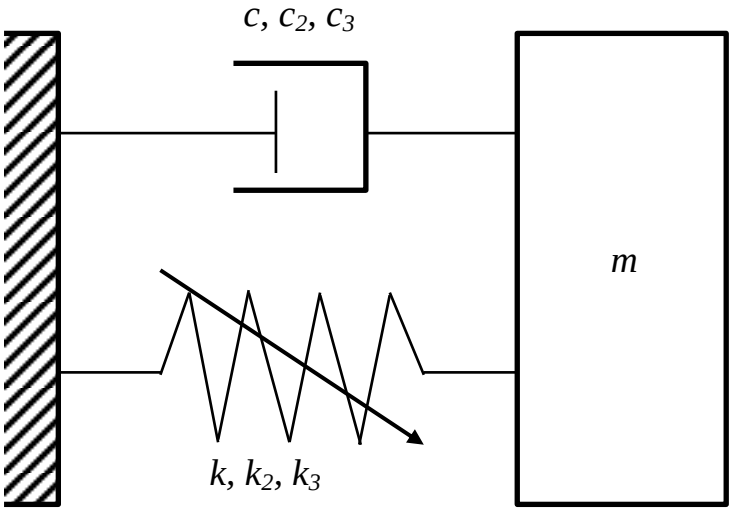

Figure 5.1: SDOF Duffing oscillator: used to introduce HFRF use for parameter estimation with harmonic excitation for polynomial model

Parameter	Value	Units
m	1	kg
c	20	Ns/m
k	1E4	N/m
c_2	150	Ns^2/m^2
c_3	1000	Ns^3/m^3
k_2	1E6	N/m^2
k_3	5E9	N/m^3

Table 5.1: Parameters for polynomial model for single nonlinearity system

In order to find the first order FRF, H_1, probing Equation 5.7 and Equation 5.8 and the first and second derivatives of Equation 5.7 were substituted into the equation of motion Equation 5.16 for an example polynomial system. The coefficients of $e^{i\Omega t}$ were then equated to yield

$$H_1(\Omega) = \frac{1}{k - m\Omega^2 + i\Omega c} \tag{5.17}$$

With simplification of the general Volterra expression in Equation 5.6, taking only the first-order term, the response is given by $Y(\omega) = X(\omega)H_1(\omega)$. Substituting this response into Equation 5.17 above, yields Equation 5.18, which can then be used to the estimate linear parameters of a polynomial system.

$$\Lambda_1(\Omega) = \frac{Y(\Omega)}{X(\Omega)} = \frac{1}{k - m\Omega^2 + i\Omega c} \tag{5.18}$$

As the order increases, the derivation becomes more complicated with more terms to handle. However the basis of the method is similar in which substitution of the probing equation will yield the required expressions. For the second order FRF, H_2, probing Equation 5.9 and Equation 5.10 with first and second derivatives of Equation 5.9 are substituted and the coefficients of $e^{i(\Omega_1+\Omega_2)t}$ were extracted, leading to

$$H_2(\Omega_1, \Omega_2) = -[k_2 + (i\Omega)^2 c_2] \frac{H_1(\Omega_1)H_1(\Omega_2)}{m(\Omega_1+\Omega_2)^2 + ic(\Omega_1+\Omega_2) + k_1}$$

or

$$H_2(\Omega_1, \Omega_2) = -[k_2 + (i\Omega)^2 c_2] H_1(\Omega_1+\Omega_2) H_1(\Omega_1) H_1(\Omega_2) \tag{5.19}$$

The third order FRF, H_3, requires probing Equation 5.20 and Equation 5.21. Solving in the same manner as previously yields Equation 5.22.

$$x_{p3}(t) = e^{i\Omega_1 t} + e^{i\Omega_2 t} + e^{i\Omega_3 t} \tag{5.20}$$

$$y_{p3}(t) = H_1(\Omega_1)e^{i\Omega_1 t} + H_1(\Omega_2)e^{i\Omega_2 t} + H_1(\Omega_3)e^{i\Omega_3 t} + 2H_2(\Omega_1, \Omega_2)e^{i(\Omega_1+\Omega_2)t}$$
$$+ 2H_2(\Omega_1, \Omega_3)e^{i(\Omega_1+\Omega_3)t} + 2H_2(\Omega_2, \Omega_3)e^{i(\Omega_2+\Omega_3)t}$$

$$+6H_3(\Omega_1,\Omega_2,\Omega_3)e^{i(\Omega_1+\Omega_2+\Omega_3)t} \tag{5.21}$$

$$H_3(\Omega_1,\Omega_2,\Omega_3) = H_1(\Omega_1+\Omega_2+\Omega_3)\left\{-\frac{2}{3}[k_2+(i\Omega)^2c_2][H_1(\Omega_1)H_2(\Omega_2,\Omega_3)+H_1(\Omega_2)H_2(\Omega_1,\Omega_3)\right.$$

$$\left.+H_1(\Omega_3)H_2(\Omega_1,\Omega_2)]-[k_3+(i\Omega)^3c_3]H_1(\Omega_1)H_1(\Omega_2)H_1(\Omega_3)\right\} \tag{5.22}$$

5.5 **Estimation of linear parameters**

Using the Volterra series, estimation of linear parameters and nonlinear parameters can be done separately as the linear parameter can be estimated independent of the nonlinear parameters based on the separate equations derived from H_1, H_2 and H_3 as shown in the last section. So this section will conduct estimation of the linear parameters before conducting nonlinear parameter estimation in the following section.

In order to estimate the linear parameters of the equation (*m*, *c*, and *k*), the Volterra relationship of the first order FRF, $H_1(\omega)$ of the system can be used in the form of Equation 5.17. As the Volterra series is an infinite functional series that contains an infinite number of terms, Equation 5.17 was obtained after simplification by removing the repetitive harmonics term in the exponential power up to the relevant harmonics. This was applied for the linear parameter case up to the first harmonic (i.e. response at the forcing frequency) and again for the nonlinear polynomial parameter case later up to the third superharmonic (i.e. response at three times the forcing frequency).

With Equation 5.17, the value of *m* and *k* can be obtained from the plot of $\mathrm{Re}(\Lambda_1(\omega)^{-1})$ against ω^2 and value of *c* can be obtained from the plot of $\mathrm{Im}(\Lambda_1(\omega)^{-1})$ against ω. The term $\Lambda_1(\omega)$ is the composite FRF which comes from the estimation of $H_1(\omega)$ using sinusoidal forcing and it is given by $Y(\omega)/X(\omega)$ from analytical calculation of the response signal and input signal to the system. This was obtained from simplification of the general Equation 5.6 with limits of only the first-order term.

5.5.1 System with quadratic damping (c_2) only

In this section, only the quadratic damping system was investigated with the other nonlinear parameters set to zero. This was conducted only for the investigation of the linear parameters and to

investigate the effect of each type of nonlinearity on its own. Hence the system became a single degree of freedom system with the equation of motion,

$$m\ddot{y} + c\dot{y} + ky + c_2\dot{y}^2 = X\sin(\omega t) \tag{5.23}$$

An investigation was conducted at input amplitudes ranging from 1 to 10 as shown in Figure 5.2 and Figure 5.3 below for both the real and imaginary part plot of $\Lambda_1(\omega)^{-1}$ respectively. Straight lines derived from true linear parameter values were also plotted as a reference on the same figure.

It can be seen that there is only a small frequency range around the undamped natural frequency of the underlying linear system for the real part plot that should be avoided when selecting the frequency to be used for linear parameter estimation. In the imaginary part plot there are two areas (around the undamped natural frequency of the underlying linear system and at around half of that) that should be avoided for linear parameter estimation. As the amplitude increases, the disturbance area grows larger as well. This is due to the increase in the effect of nonlinearity that will also increase the distortion of the $\Lambda_1(\omega)^{-1}$ estimates due to the increasing effect of the higher harmonics terms. Values of *m* and *c* can be identified from the gradient of the line in Figure 5.2 and Figure 5.3 respectively whilst *k* is the intersection at y-axis for the former. This can also be done by taking two (or maybe three) points on the line (away from the problem frequencies) that will result in a good straight line and therefore provide a good estimate of *m*, *c* and *k*.

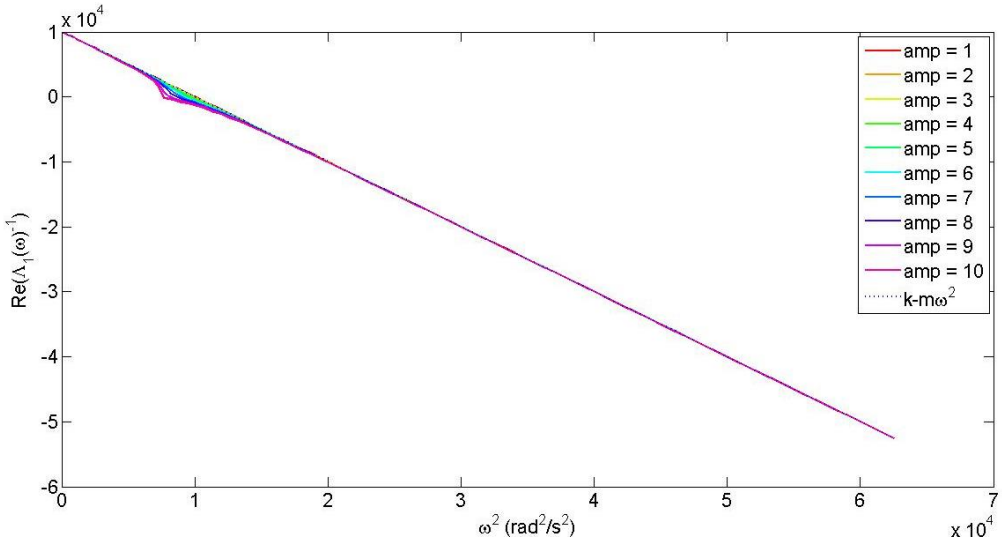

Figure 5.2: Plot of real part of $\Lambda_1(\omega)^{-1}$ against ω^2 for system with quadratic damping (c_2) only

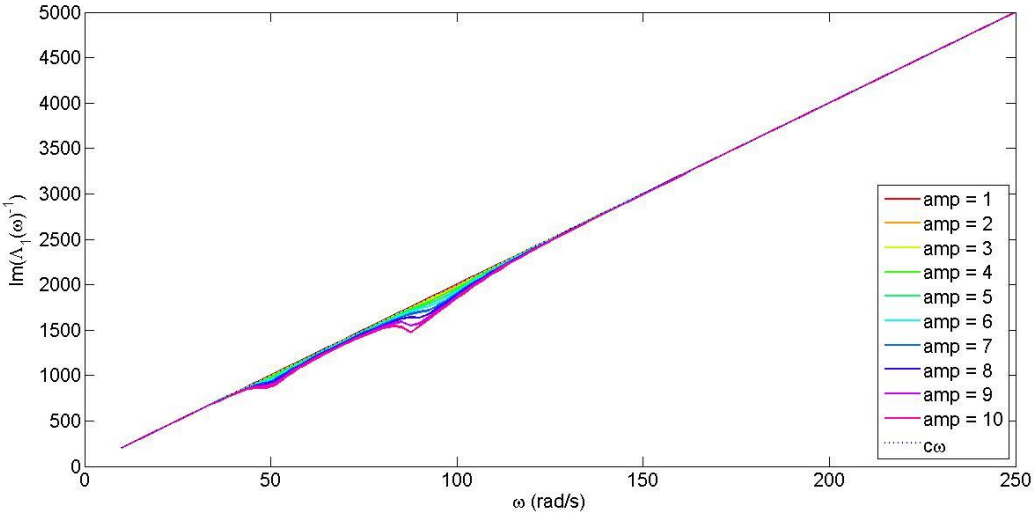

Figure 5.3: Plot of imaginary part of $\Lambda_1(\omega)^{-1}$ against ω for system with quadratic damping (c_2) only

5.5.2 System with cubic damping (c_3) only

In this section, only the cubic damping system was investigated with the other nonlinear parameter set to zero. Hence the system became a single degree of freedom system with the equation of motion:

$$m\ddot{y} + c\dot{y} + ky + c_3\dot{y}^3 = X\sin(\omega t) \tag{5.24}$$

Similar to the previous section, Figure 5.4 and Figure 5.5 show the real and imaginary part plot of $\Lambda_1(\omega)^{-1}$ with increasing amplitude.

For the cubic damping only case, *m* and *k* are easily obtained from the real part plot of $\Lambda_1(\omega)^{-1}$ as a clear straight line can be seen. However for the imaginary plot, the distortion caused by cubic nonlinearity at the undamped natural frequency of the underlying linear system is quite large due to the cubic nature of the nonlinearity. This could affect the value of the linear damping, *c* extracted from the figure when using frequencies above and around the undamped natural frequency of the underlying linear system

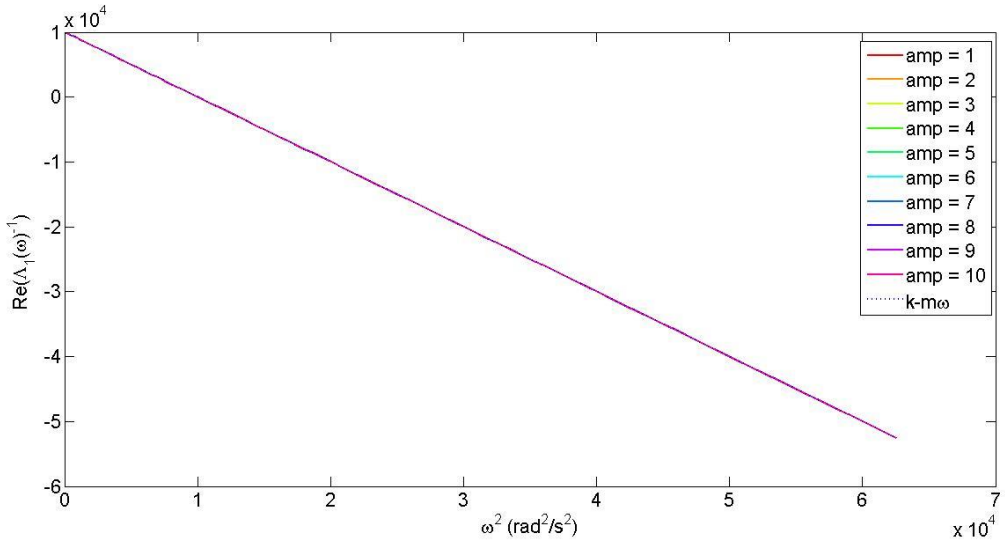

Figure 5.4: Plot of real part of $\Lambda_1(\omega)^{-1}$ against ω^2 for system with cubic damping (c_3) only

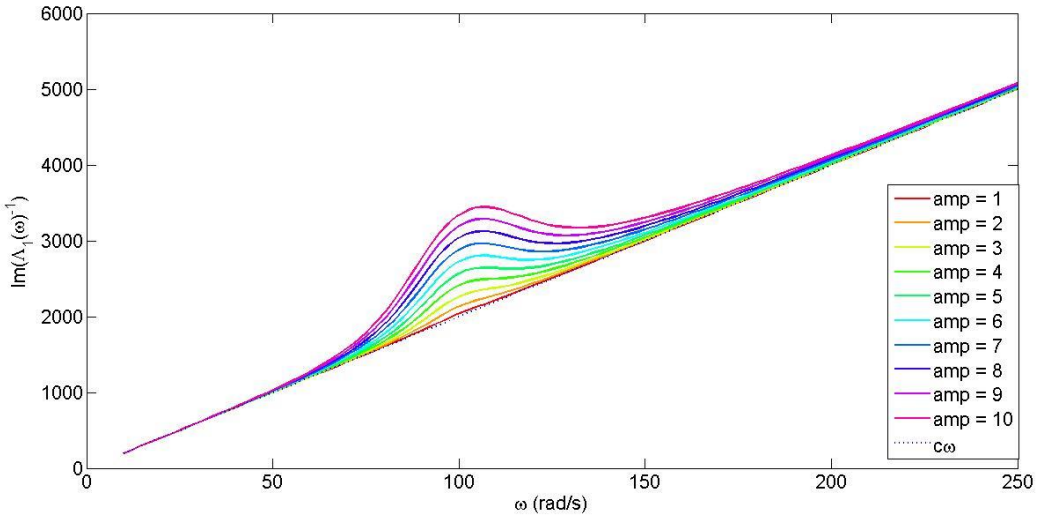

Figure 5.5: Plot of imaginary part of $\Lambda_1(\omega)^{-1}$ against ω for system with cubic damping (c_3) only

5.5.3 System with quadratic stiffness (k_2) only

In this section, only the quadratic stiffness system was investigated with the other nonlinear parameters set to zero. Quadratic stiffness only systems, such as this, may face stability issue due to the quadratic nature of the system at a higher forcing level. Quadratic stiffness would normally not be used independently of cubic stiffness in a real dynamic problem to avoid this stability issue. However, here it is being used only to observe the effect on the estimation of linear parameters. The system became a single degree of freedom system with an equation of motion:

$$m\ddot{y} + c\dot{y} + ky + k_2y^2 = X\sin(\omega t) \tag{5.25}$$

Figure 5.6 and Figure 5.7 show the real and imaginary part plot of $\Lambda_1(\omega)^{-1}$. It is fairly straightforward here to obtain the linear parameter values similar to Section 5.5.1 since the lines are fairly straight on their own. This would be due to the k_2 value which is small relative to the value of k to avoid the stability issue that would occur if using k_2 = 1E7.

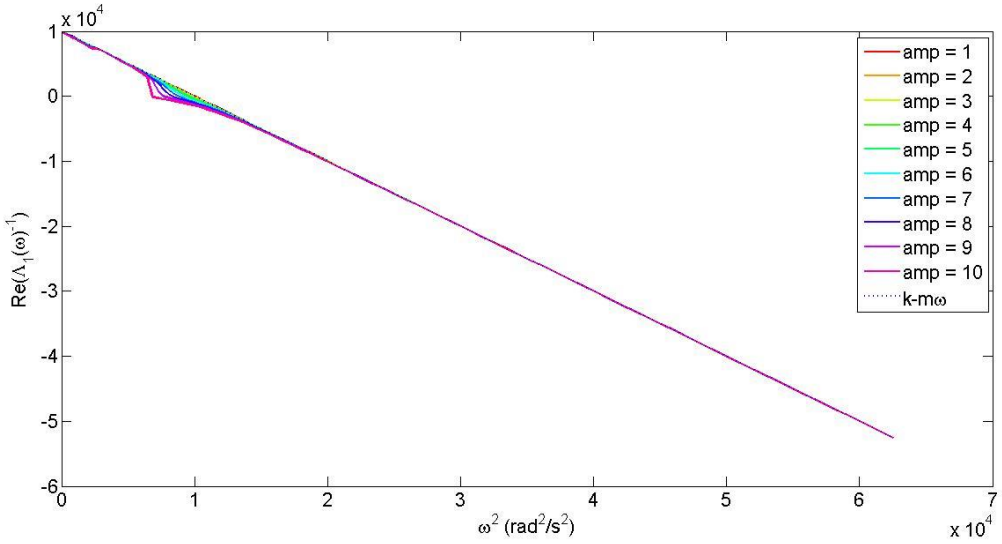

Figure 5.6: Plot of real part of $\Lambda_1(\omega)^{-1}$ against ω^2 for system with quadratic stiffness (k_2) only

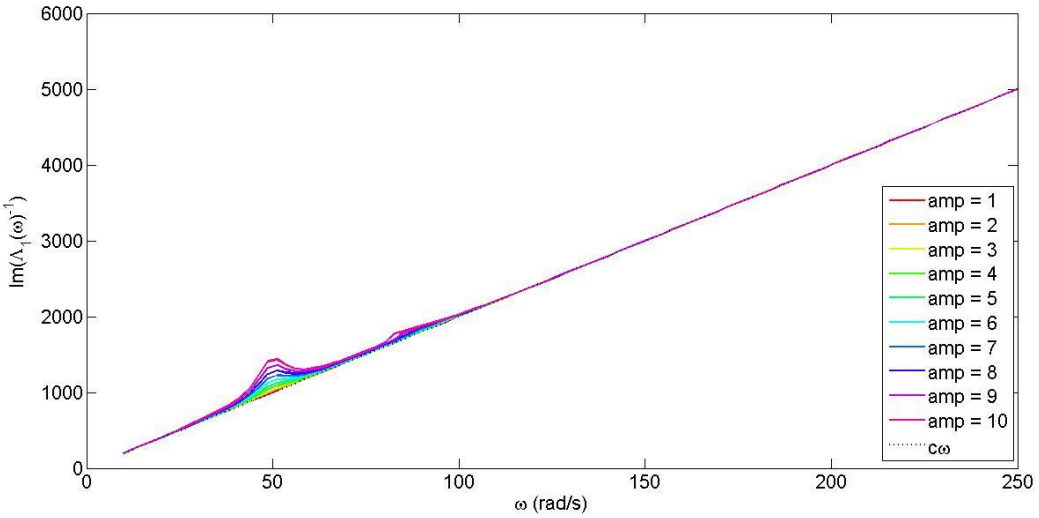

Figure 5.7: Plot of imaginary part of $\Lambda_1(\omega)^{-1}$ against ω for system with quadratic stiffness (k_2) only

5.5.4 System with cubic stiffness (k_3) only

In this section, only the quadratic stiffness system was investigated with the other nonlinear parameters set to zero. Hence the system became a single degree of freedom system with an equation of motion as follows:

$$m\ddot{y} + c\dot{y} + ky + k_3y^3 = X\sin(\omega t) \tag{5.26}$$

For the cubic stiffness case, in Figure 5.8 the low frequency regions introduce inaccuracies in the estimation of *m* and *k*. Nonlinear distortion appears as the amplitude increases in the affected areas around the undamped natural frequency of the underlying linear system and below. Although on a different scale, the effect can be related to cubic damping in Section 5.5.2, where a similar increase in amplitude causes large distortions due to the cubic nature of both systems compared to the effects of the quadratic components.

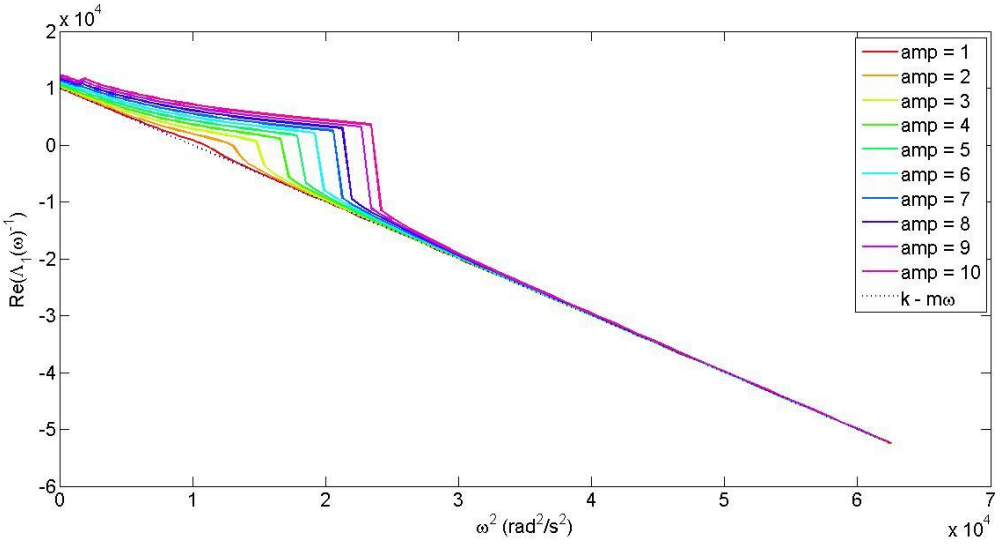

Figure 5.8: Plot of real part of $\Lambda_1(\omega)^{-1}$ against ω^2 for system with cubic stiffness (k_3) only

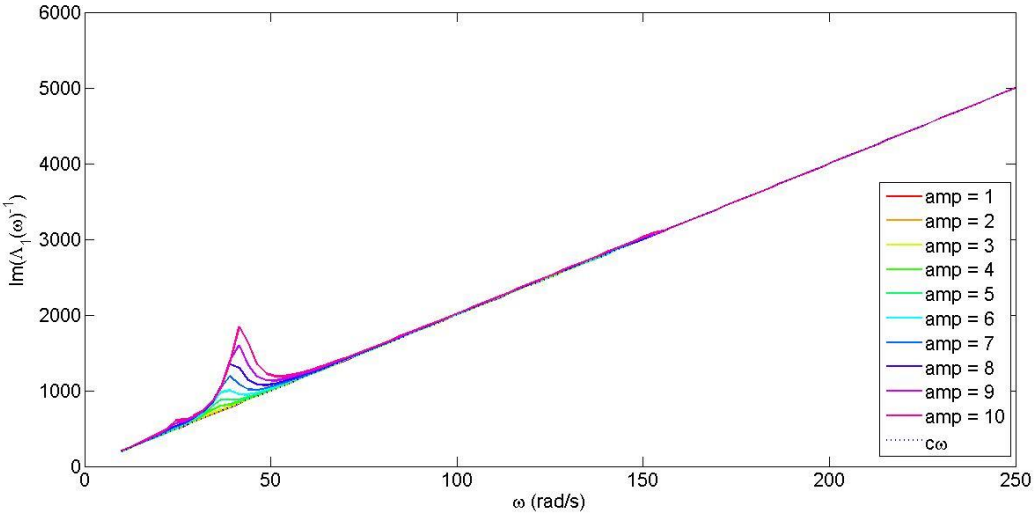

Figure 5.9: Plot of imaginary part of $\Lambda_1(\omega)^{-1}$ against ω for system with cubic stiffness (k_3) only

5.5.5 System with damping and stiffness nonlinearities (c_2, c_3, k_2 and k_3)

Here all four nonlinearities in the above subsections were set to values as shown in Table 5.2 below. The value of k_2 was now set to the appropriate value of 1E7 to have an appropriate response ratio of k_2 to k and k_3.

Parameter	Value	Units
m	1	kg
c	20	Ns/m
k	1E4	N/m
c_2	150	Ns^2/m^2
c_3	1000	Ns^3/m^3
k_2	1E7	N/m^2
k_3	5E9	N/m^3

Table 5.2: Parameters for polynomial model for system with multiple nonlinearities

Figure 5.10 and Figure 5.11 show the real part and the imaginary part plot of system with nonlinear damping, c_2 and c_3, and nonlinear stiffness, k_2 and k_3. The figure shows the combined effect of distortion mainly on the imaginary part plot of Figure 5.11 where the distortion became significantly higher through the presence of all four nonlinear parameters. However, this still allowed estimation

through a similar approach as in the previous subsections with a single nonlinearity using points on the plot in the high frequency region.

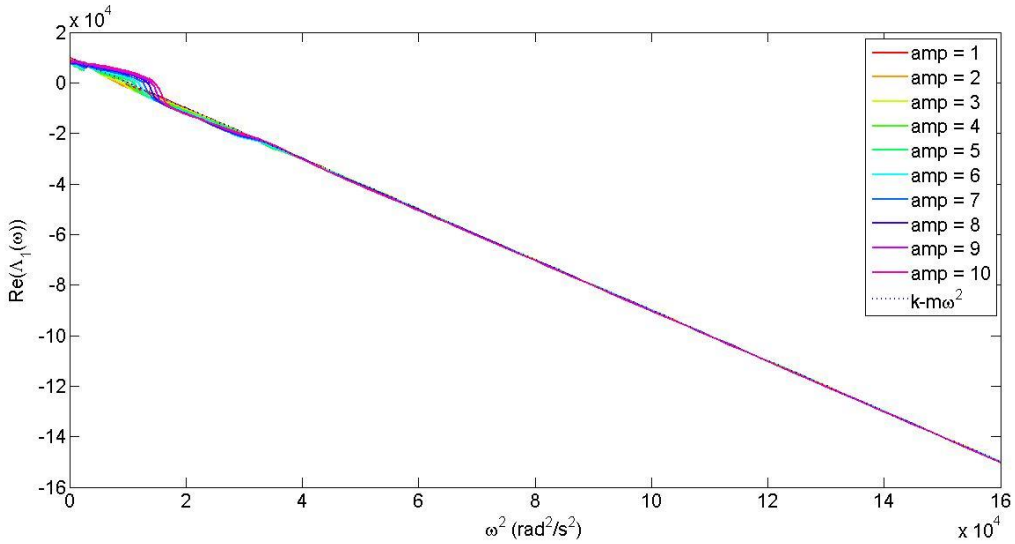

Figure 5.10: Plot of real part of $\Lambda_1(\omega)^{-1}$ against ω^2 for system with all four nonlinearities (c_2, c_3, k_2 and k_3)

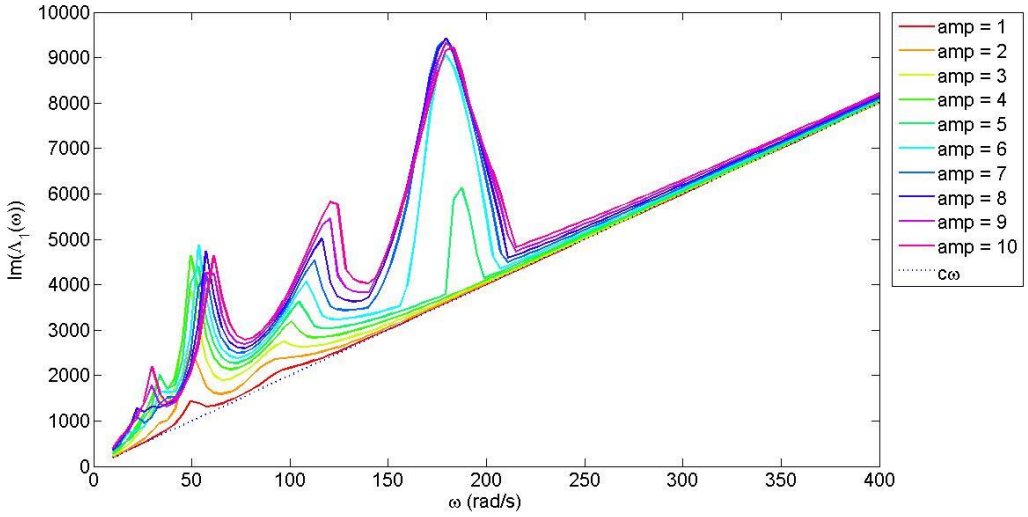

Figure 5.11: Plot of imaginary part of $\Lambda_1(\omega)^{-1}$ against ω for system with all four nonlinearities (c_2, c_3, k_2 and k_3)

5.6 **Estimation of linear parameters in the presence of noise**

To investigate the effect of noise on the Volterra harmonic probing exercise, the same investigations were repeated on the above systems in the presence of simulated noise. Noise was added at two levels

both at a sufficient level to show the effect of noise on parameter estimation. The two levels of noise are given in Table 5.3 below.

Noise level	Low level	High level
Input	1E-3 times amplitude of the input	1E-1 times amplitude of the input
Output	1E-7 times no noise RMS	1E-5 times no noise RMS

Table 5.3: Simulated noise level

The results are shown in Figure 5.12 to Figure 5.31. The effect of noise is generally seen on the imaginary plot more clearly. The reason why the effect of noise on the imaginary part plot is seen as more significant is due to the imaginary part of the response being smaller in magnitude compared to the real part response. The noise generally appears as distortion of the plotted line in the high frequency region of the plot and starts appearing even at a low noise level.

For the real part plot, the noise effect was not seen when subjected to a low noise level, and only very slightly started to show when the noise level was high. This can be seen in Figure 5.14 and Figure 5.18.

The effect of noise here affects the calculations of parameter *m* and *k* only slightly compared to when there was no noise present. However, the value of *c* would be severely altered if using signals with a high frequency. Although that is the case, the value of *c* could still be obtained from the low level frequency region as a gradient can be measured with point on the line at low frequencies (away from the problem region) to the origin instead.

The effect of noise on the estimation lines is more significant on the system with all four nonlinearities as in Figure 5.28 to Figure5.31. Even at the low noise level the high frequency region does not give any good estimation points. This shows that with a full nonlinear system such as this, the noise level must be kept very minimal to obtain an accurate estimation.

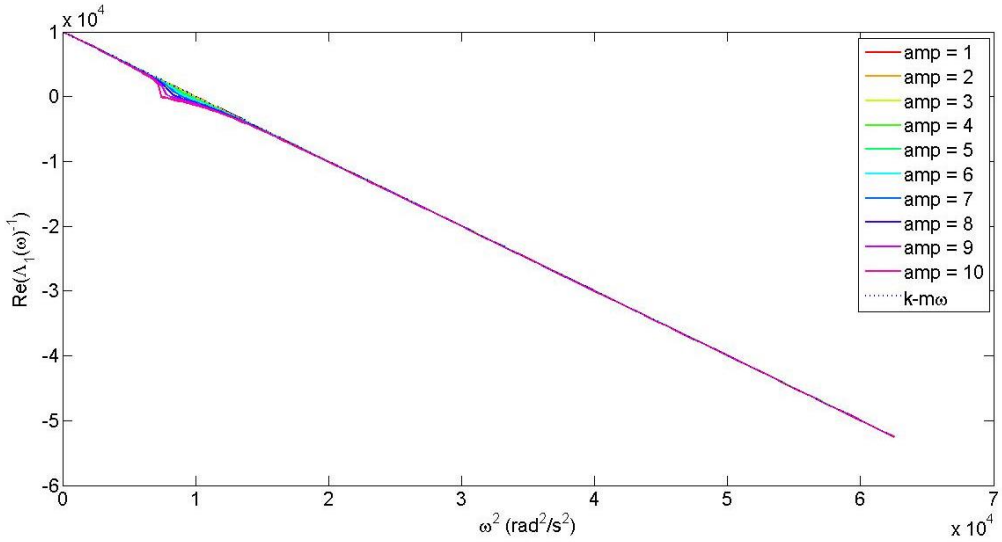

Figure 5.12: Plot of real part of $\Lambda_1(\omega)^{-1}$ against ω^2 for system with quadratic damping (c_2) only with low noise level

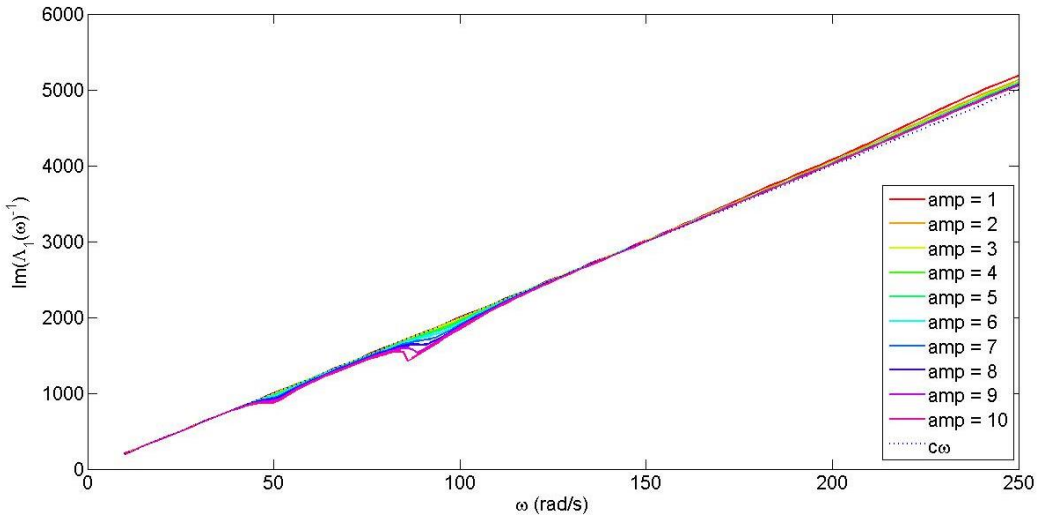

Figure 5.13: Plot of imaginary part of $\Lambda_1(\omega)^{-1}$ against ω for system with quadratic damping (c_2) only with low noise level

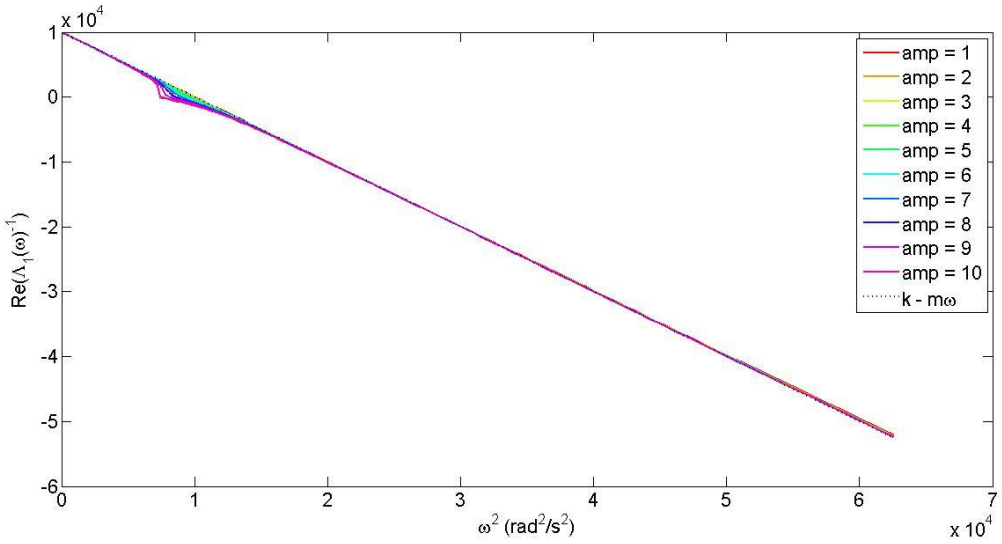

Figure 5.14: Plot of real part of $\Lambda_1(\omega)^{-1}$ against ω^2 for system with quadratic damping (c_2) only with high noise level

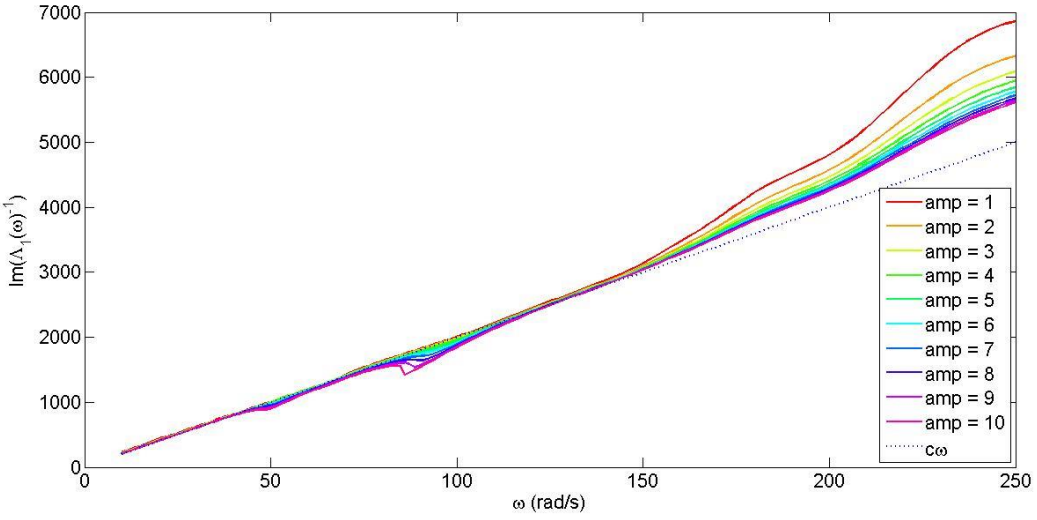

Figure 5.15: Plot of imaginary part of $\Lambda_1(\omega)^{-1}$ against ω for system with quadratic damping (c_2) only with high noise level

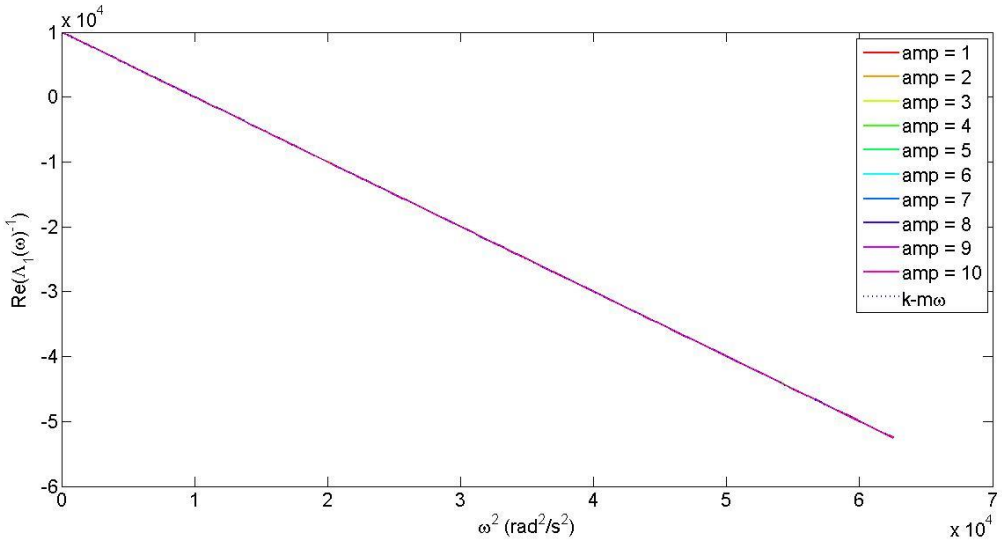

Figure 5.16: Plot of real part of $\Lambda_1(\omega)^{-1}$ against ω^2 for system with cubic damping (c_3) only with low noise level

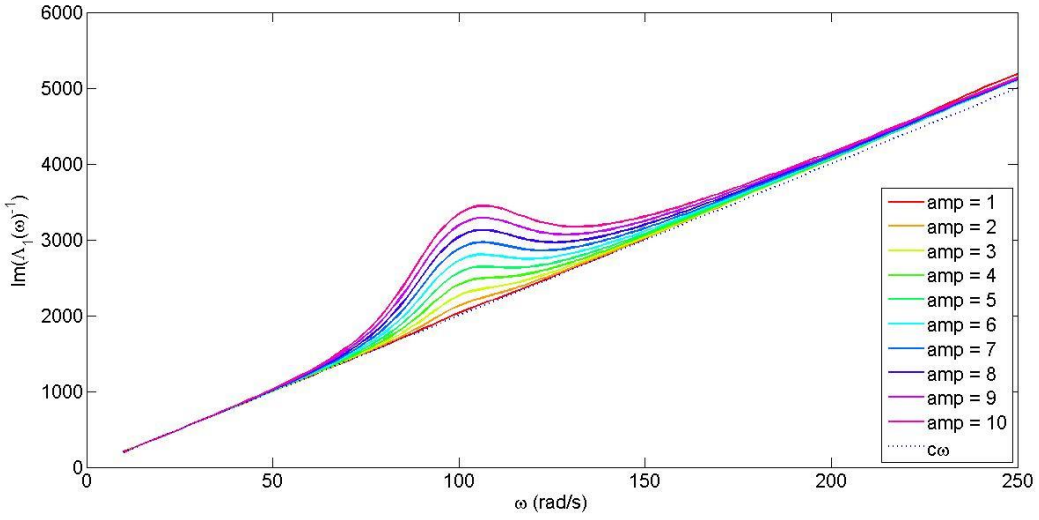

Figure 5.17: Plot of imaginary part of $\Lambda_1(\omega)^{-1}$ against ω for system with cubic damping (c_3) only with low noise level

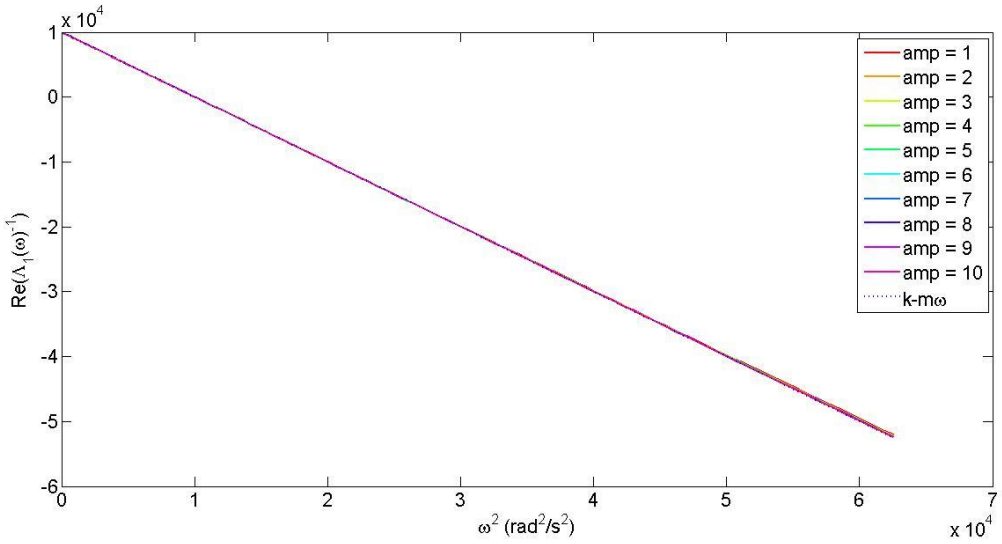

Figure 5.18: Plot of real part of $\Lambda_1(\omega)^{-1}$ against ω^2 for system with cubic damping (c_3) only with high noise level

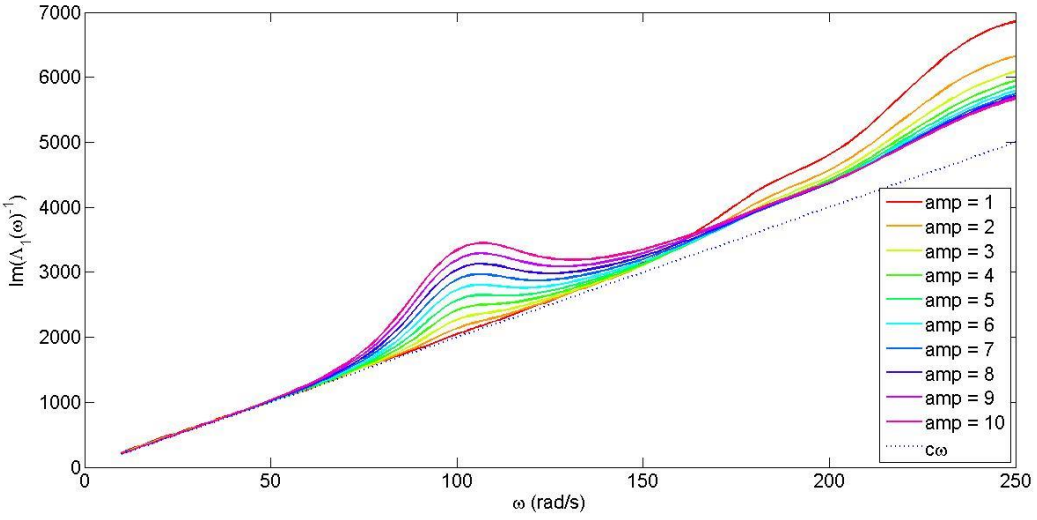

Figure 5.19: Plot of imaginary part of $\Lambda_1(\omega)^{-1}$ against ω for system with cubic damping (c_3) only with high noise level

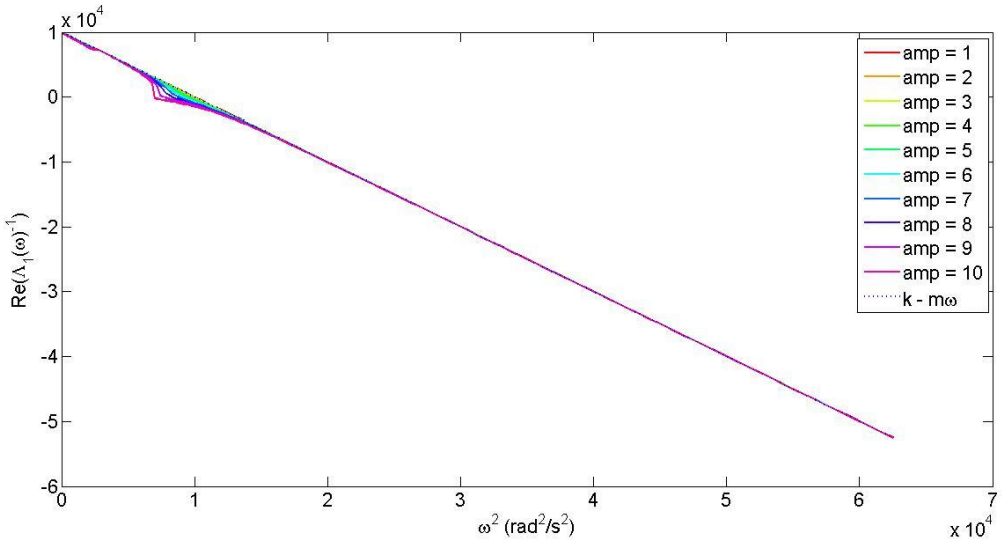

Figure 5.20: Plot of real part of $\Lambda_1(\omega)^{-1}$ against ω^2 for system with quadratic stiffness (k_2) only with low noise level

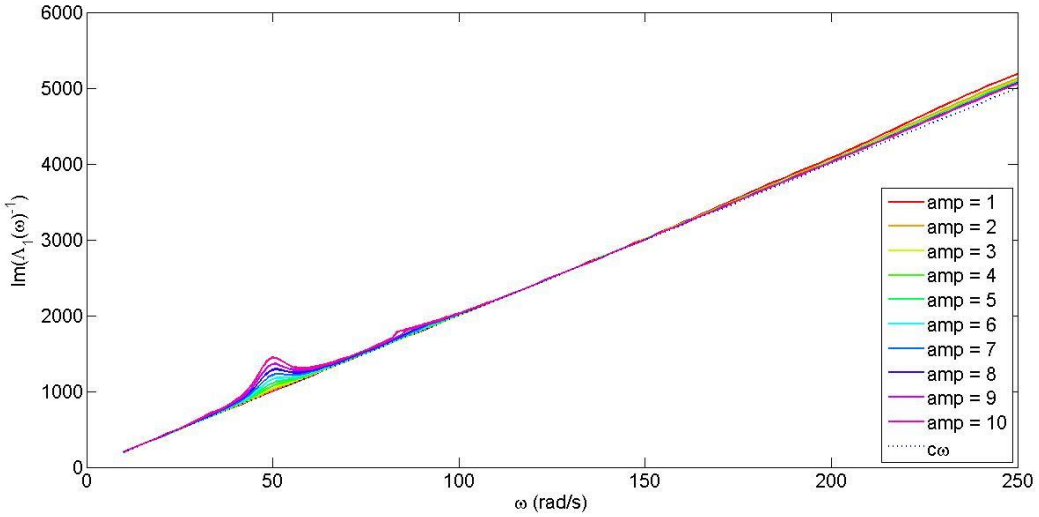

Figure 5.21: Plot of imaginary part of $\Lambda_1(\omega)^{-1}$ against ω for system with quadratic stiffness (k_2) only with low noise level

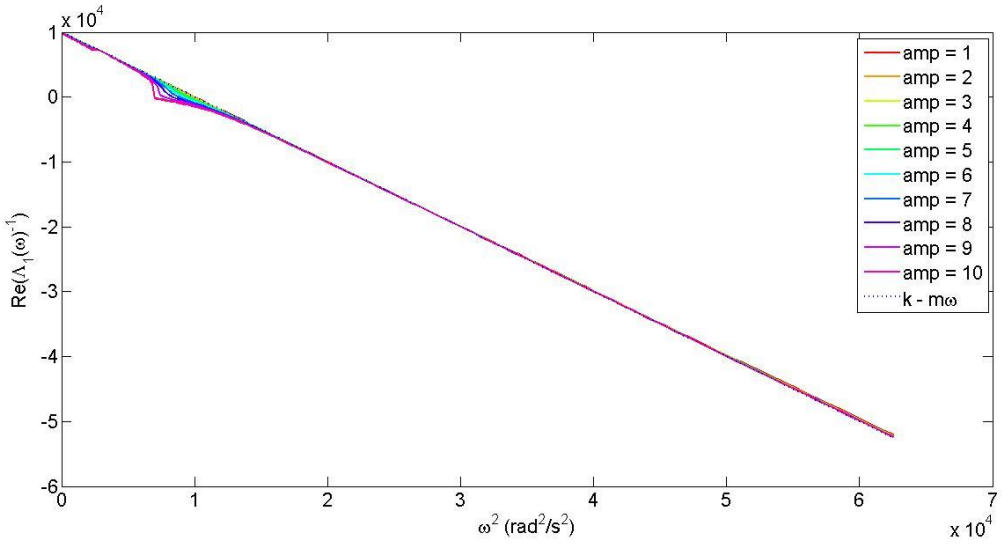

Figure 5.22: Plot of real part of $\Lambda_1(\omega)^{-1}$ against ω^2 for system with quadratic stiffness (k_2) only with high noise level

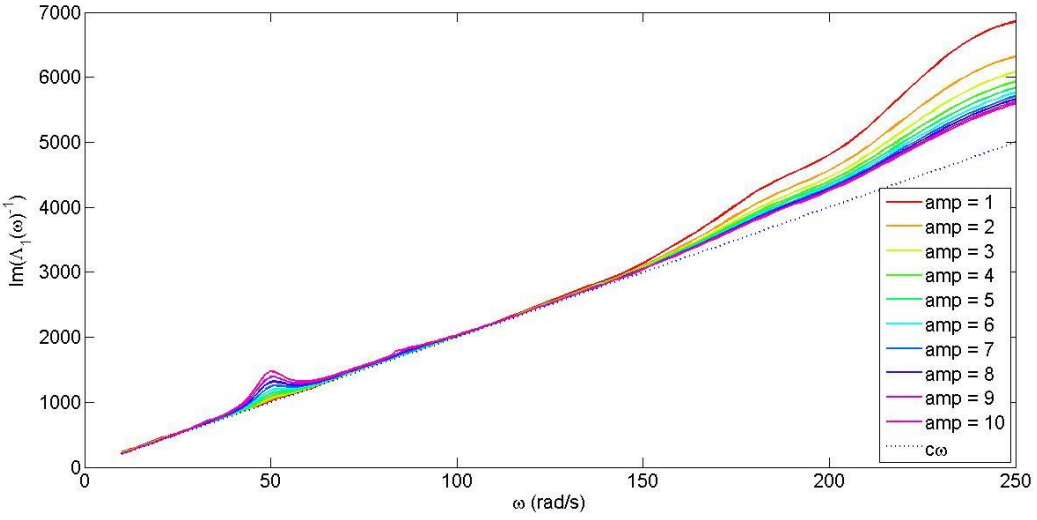

Figure 5.23: Plot of imaginary part of $\Lambda_1(\omega)^{-1}$ against ω for system with quadratic stiffness (k_2) only with high noise level

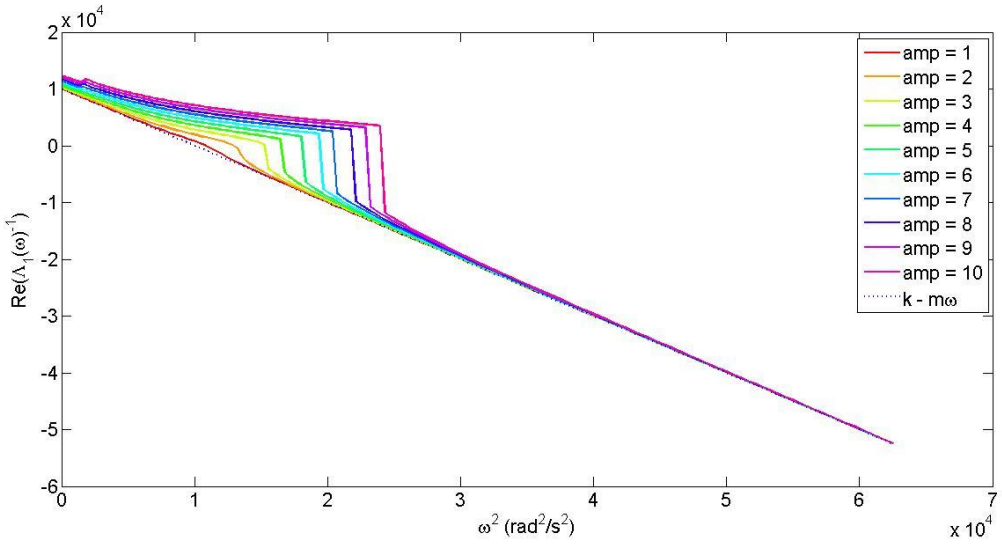

Figure 5.24: Plot of real part of $\Lambda_1(\omega)^{-1}$ against ω^2 for system with cubic stiffness (k_3) only with low noise level

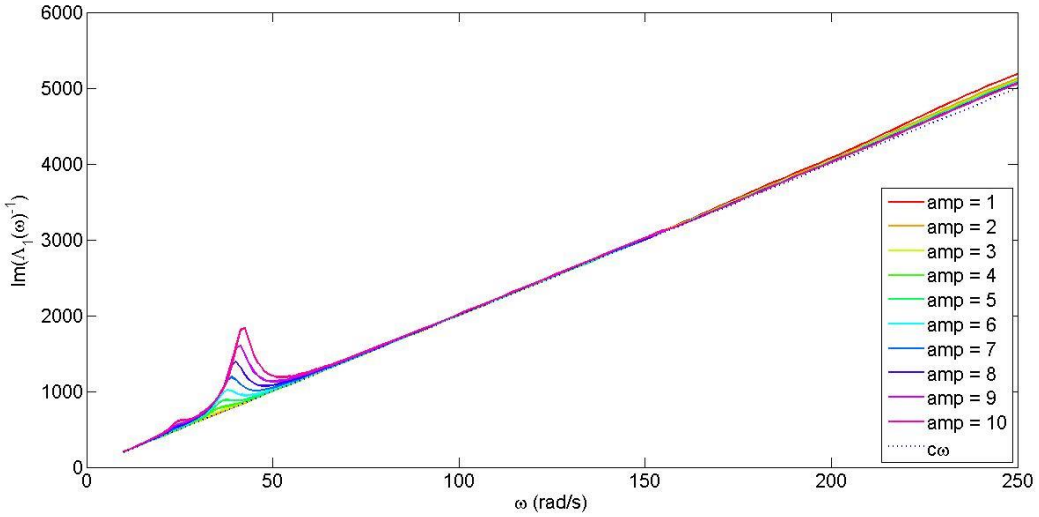

Figure 5.25: Plot of imaginary part of $\Lambda_1(\omega)^{-1}$ against ω for system with cubic stiffness (k_3) only with low noise level

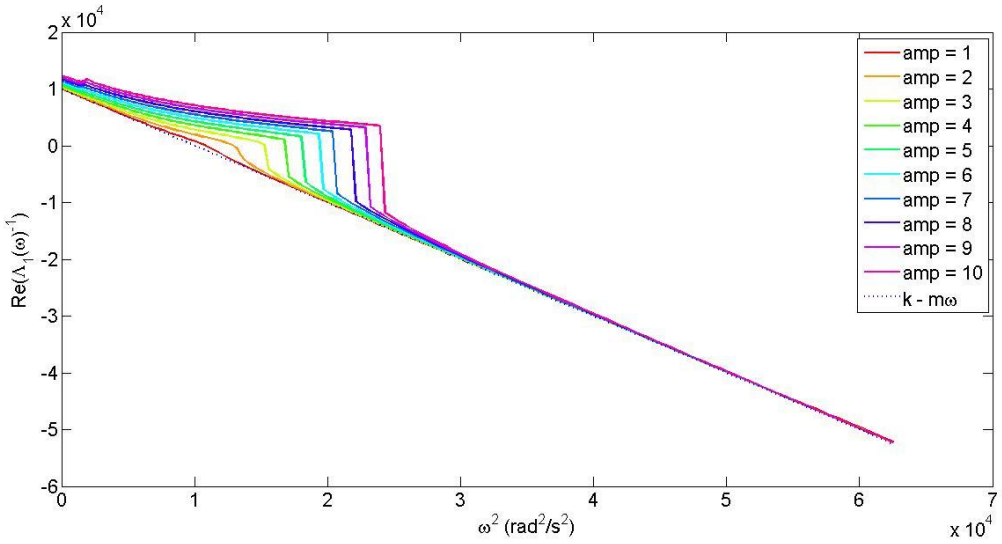

Figure 5.26: Plot of real part of $\Lambda_1(\omega)^{-1}$ against ω^2 for system with cubic stiffness (k_3) only with high noise level

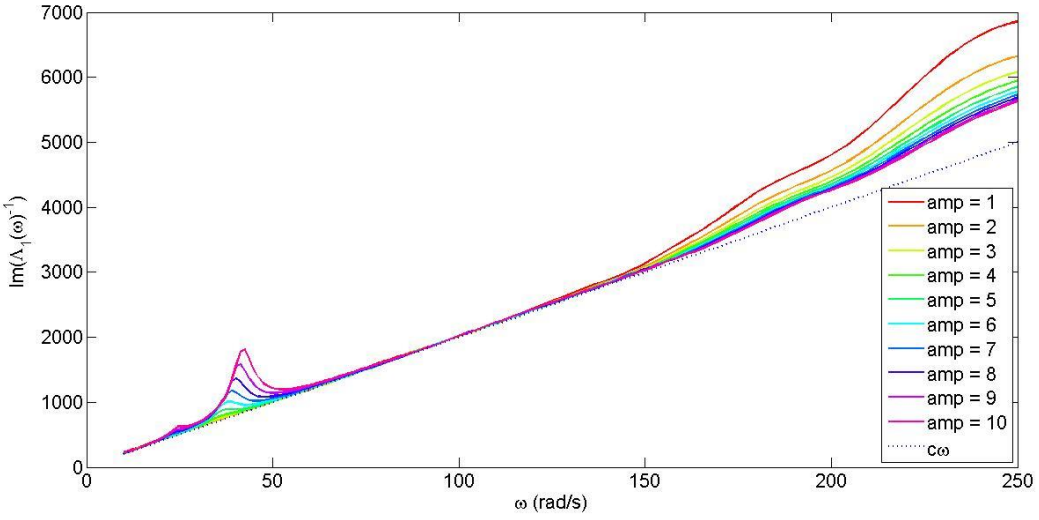

Figure 5.27: Plot of imaginary part of $\Lambda_1(\omega)^{-1}$ against ω for system with cubic stiffness (k_3) only with high noise level

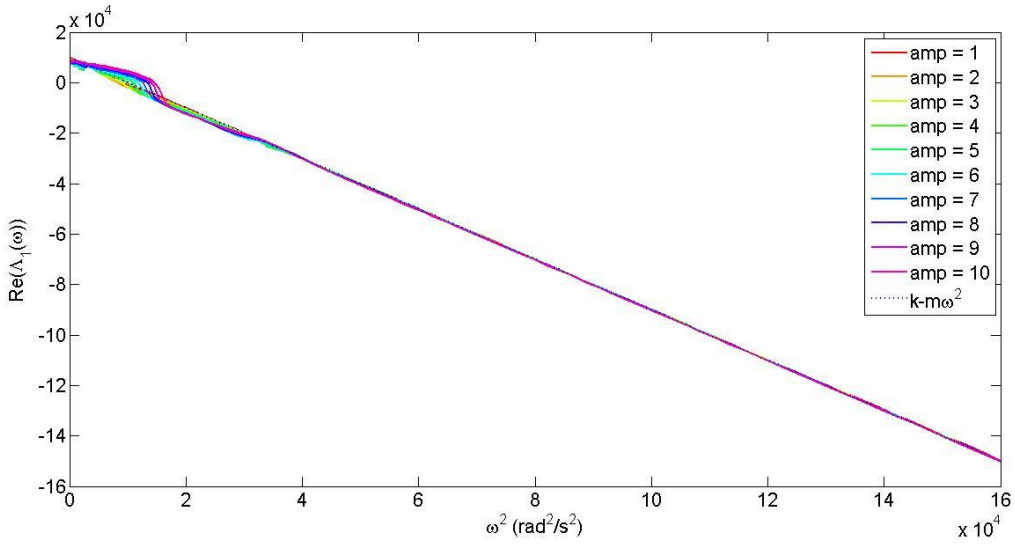

Figure 5.28: Plot of real part of $\Lambda_1(\omega)^{-1}$ against ω for system with all four nonlinearities (c_2, c_3, k_2 and k_3) with low noise level

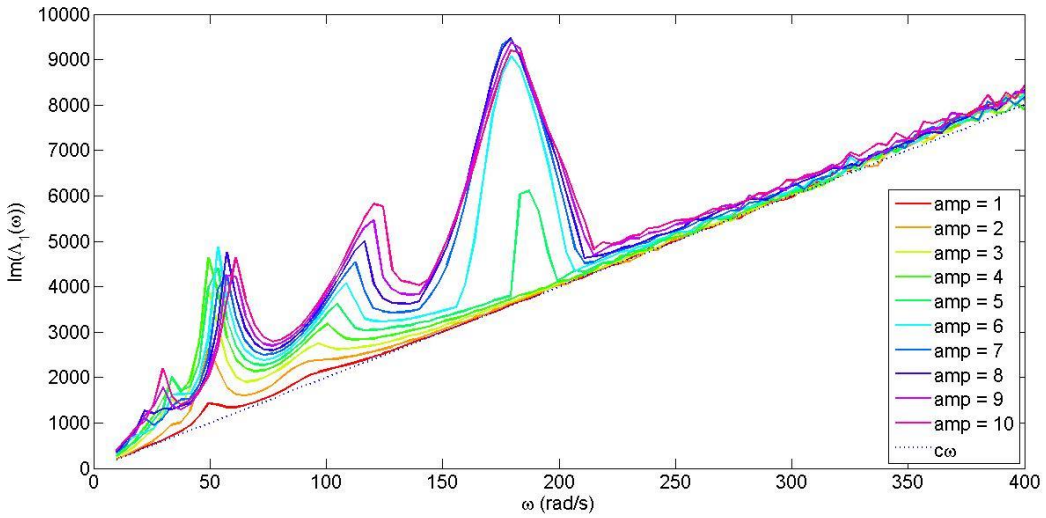

Figure 5.29: Plot of imaginary part of $\Lambda_1(\omega)^{-1}$ against ω for system with all four nonlinearities (c_2, c_3, k_2 and k_3) with low noise level

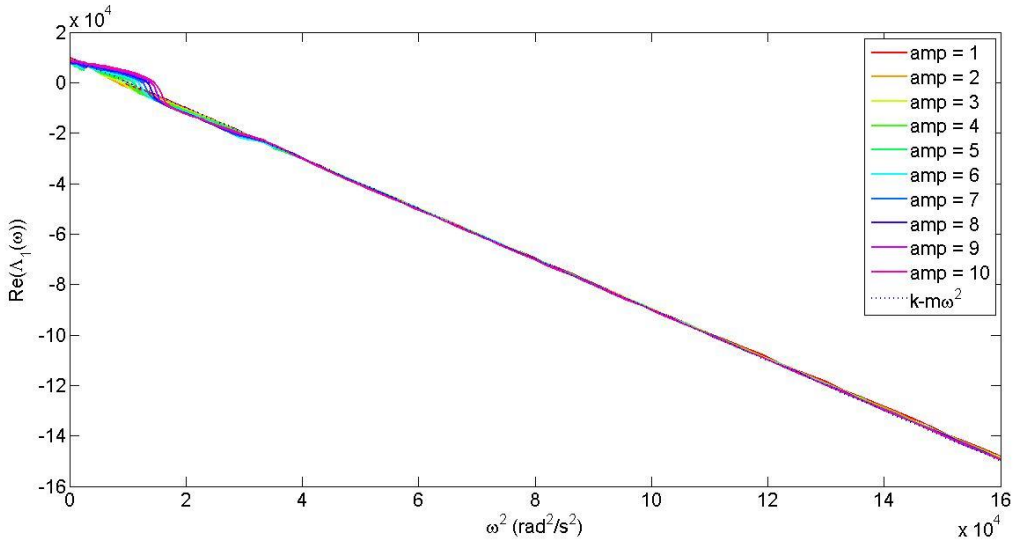

Figure 5.30: Plot of real part of $A_1(\omega)^{-1}$ against ω for system with all four nonlinearities (c_2, c_3, k_2 and k_3) with high noise level

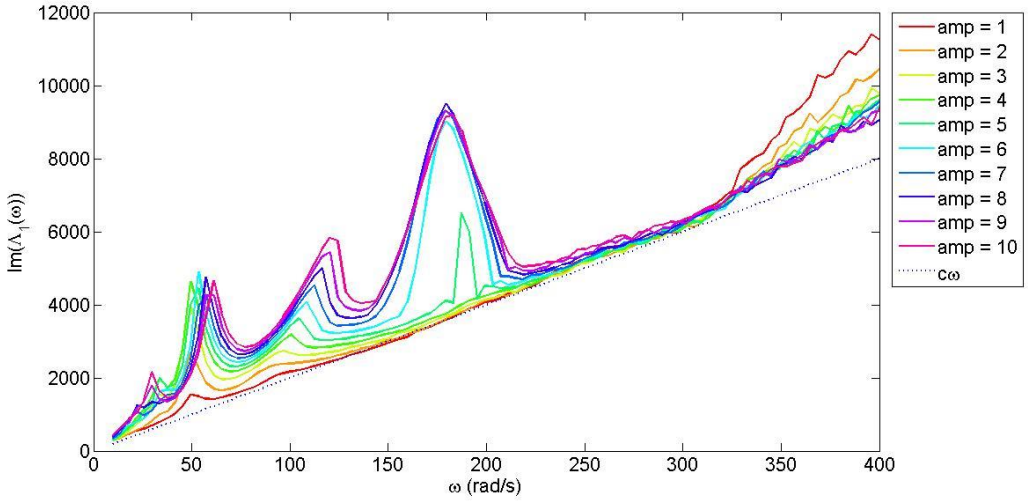

Figure 5.31: Plot of imaginary part of $A_1(\omega)^{-1}$ against ω for system with all four nonlinearities (c_2, c_3, k_2 and k_3) with high noise level

5.7 **Estimation of nonlinear parameters**

After obtaining the values of m, c and k from the above steps, the nonlinear parameter can be examined. In the nonlinear sense, k_2 and c_2 can be estimated from the H_2 relationship while c_3 and k_3 can be estimated from the H_3 relationship given by Equations 5.19 and Equation 5.22.

Using the sinusoidal response as in Equation 5.15 with the HFRF reflection property and applying de Moivre's theorem of the form:

$$\frac{ze^{i\Omega t} - z^* e^{-i\Omega t}}{i} = \frac{|z|e^{i(\Omega t + \angle z)} - |z|e^{-i(\Omega t + \angle z)}}{i} = 2|z|\sin(\Omega t + \angle z)$$

Gives:

$$\begin{aligned} y(t) = {} & X|H_1(\Omega)|\sin\big(\Omega t + \angle H_1(\Omega)\big) \\ & + \frac{X^2}{2}\big\{|H_2(\Omega,\Omega)|\sin\big(2\Omega t + \angle H_2(\Omega,\Omega)\big) + H_2(\Omega,\Omega)\big\} \\ & + \frac{X^3}{4}\big\{|H_3(\Omega,\Omega,\Omega)|\sin\big(3\Omega t + \angle H_3(\Omega,\Omega,\Omega)\big) \\ & \qquad + 3|H_3(\Omega,\Omega,-\Omega)|\sin\big(\Omega t + \angle H_3(\Omega,\Omega,-\Omega)\big) \\ & + \cdots + \frac{X^n}{2^{n-1}} \sum_{m=0}^{m=l(n)} A(n,m)\,|H_n(\Omega,\ldots,\Omega,-\Omega,\ldots-\Omega)| \\ & \qquad \times \sin[(n-2m)\Omega t + \angle H_n(\Omega,\ldots,\Omega,-\Omega,\ldots-\Omega)] + \cdots \end{aligned} \tag{5.27}$$

Equation 5.27 gives the harmonic response for sinusoidal input. To solve for nonlinear parameter estimation, an assumption is made that the first terms in the general Volterra expression given by Equation 5.6 will always dominate at each respective harmonic. So the response at the forcing frequency, ω is $Y(\omega) = X(\omega)H_1(\omega)$. Similarly the first component at 2ω is $Y(\omega,\omega) = \frac{X(\omega)^2}{2}H_2(\omega,\omega)$ and at 3ω the first component is $Y(\omega,\omega,\omega) = \frac{X(\omega)^3}{4}H_3(\omega,\omega,\omega)$. Substituting these with the Equation 5.19 and Equation 5.22 for $H_2(\omega, \omega)$ and $H_3(\omega, \omega, \omega)$ respectively will yield the estimation for the nonlinear parameters. This is given as $\Lambda_2(\omega)$ for the $H_2(\omega, \omega)$ in Equation 5.28 which can be solved for k_2 and c_2 with a real part and imaginary part plot respectively.

$$\frac{2\mathrm{Y}(2\omega)}{\mathrm{X}(\omega)^2} = -[k_2 + (i\omega)^2 c_2]H_1(\omega+\omega)H_1(\omega)H_1(\omega)$$

$$\Lambda_2(\omega) = \frac{2\mathrm{Y}(2\omega)}{\mathrm{X}(\omega)^2 H_1(2\omega)H_1(\omega)^2} = -[k_2 + (i\omega)^2 c_2] \tag{5.28}$$

Solving for the cubic nonlinear parameters is slightly more complicated as there exists the $H_2(\omega, \omega)$ kernel component as well in $\Lambda_3(\omega)$. For an independent cubic system, the equation solves to be much simpler as shown in Equation 5.30 as the absent quadratic terms multiply all of the H_2 terms, removing the term completely.

$$\frac{4\mathrm{Y}(3\omega)}{\mathrm{X}(\omega)^3} = H_1(\omega+\omega+\omega)\left\{-\frac{2}{3}[k_2+(i\omega)^2c_2][H_1(\omega)H_2(\omega,\omega)+H_1(\omega)H_2(\omega,\omega)\right.$$
$$\left.+H_1(\omega)H_2(\omega,\omega)]-[k_3+(i\omega)^3c_3]H_1(\omega)H_1(\omega)H_1(\omega)\right\}$$

$$\Lambda_3(\omega) = \frac{4\mathrm{Y}(3\omega)}{\mathrm{X}(\omega)^3H_1(3\omega)H_1(\omega)^3} + \frac{2H_1(\omega)H_2(\omega,\omega)[k_2+(i\omega)^2c_2]}{\mathrm{X}\ (\omega)^3H_1(\omega)^3} = -[k_3+(i\omega)^3c_3] \qquad (5.29)$$

$$\Lambda_3(\omega) = \frac{4\mathrm{Y}(3\omega)}{\mathrm{X}(\omega)^3H_1(3\omega)H_1(\omega)^3} = -[k_3+(i\omega)^3c_3] \qquad (5.30)$$

5.7.1 System with quadratic damping (c_2) only

With a system with quadratic damping only, the plot of the real part of $\Lambda_2(\omega)$ against ω^2 is shown in Figure 5.32. Since the system is quadratic, the component of c_2 comes from the real part instead of the imaginary part due to the i^2 term. For a system with combination of both c_2 and k_2, this would mean that the y-axis intersect will move from the origin to value of $-k_2$ instead.

The value of c_2 can be extracted from the gradient of the plot. Both low frequency and high frequency signals would yield good estimation of the gradient for all the amplitude shown from 1 to 10.

Frequencies around the undamped natural frequency of the underlying linear system should again be avoided due to the presence of distortion. This distortion is due to the limitations in the assumption that the response at the second harmonic is only due to the $H_2(\omega,\omega)$ term. The distortion in the plotted line is expected to fully vanish only if the whole term in the Volterra series is used for the estimation (which would require infinite terms).

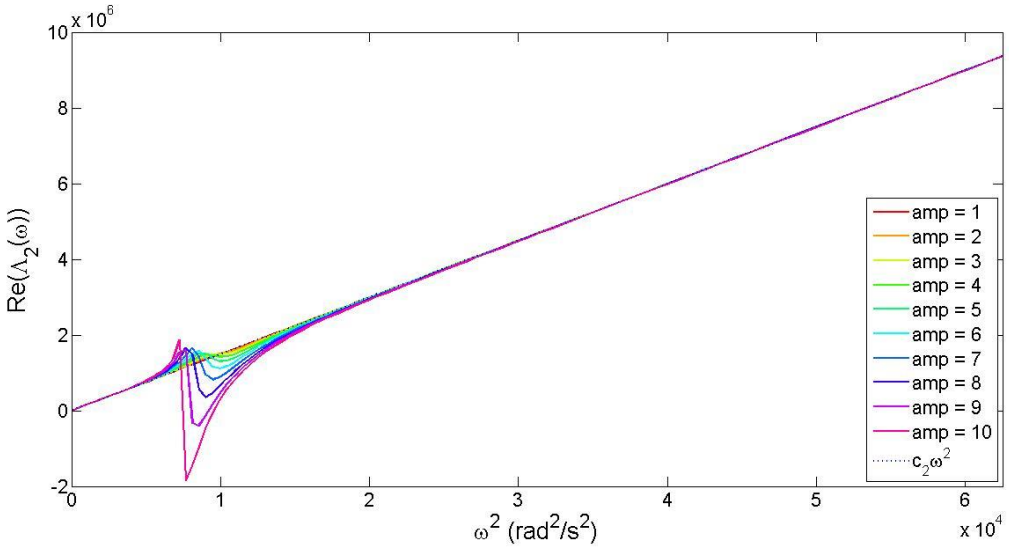

Figure 5.32: Plot of real part of $\Lambda_2(\omega)$ against ω^2 for the estimation of quadratic damping, c_2 only system

5.7.2 System with cubic damping (c_3) only

With the cubic damping only system, Equation 5.30 can be used to estimate the value of c_3. Figure 5.33 shows the plot of the imaginary part of $\Lambda_3(\omega)$ against ω^3. The use of the imaginary part plot is due to the i^3 term in c_3. The value of c_3 can be determined by the gradient of the plot here. Similar to the previous section, value of c_3 can be obtained from the gradient of the line to the origin.

High frequencies will yield good a estimation of the nonlinear parameter across larger regions. However low frequency region have a very limited range that gives a good estimation due to the distortion area spreading quickly as the amplitude increases. Again the distortion is due to the assumption made in only using the first component of $H_3(\omega,\omega,\omega)$ for the estimation. The rapid effect is due to the cubic nature of the system which gets more profoundly affected by the increasing amplitude.

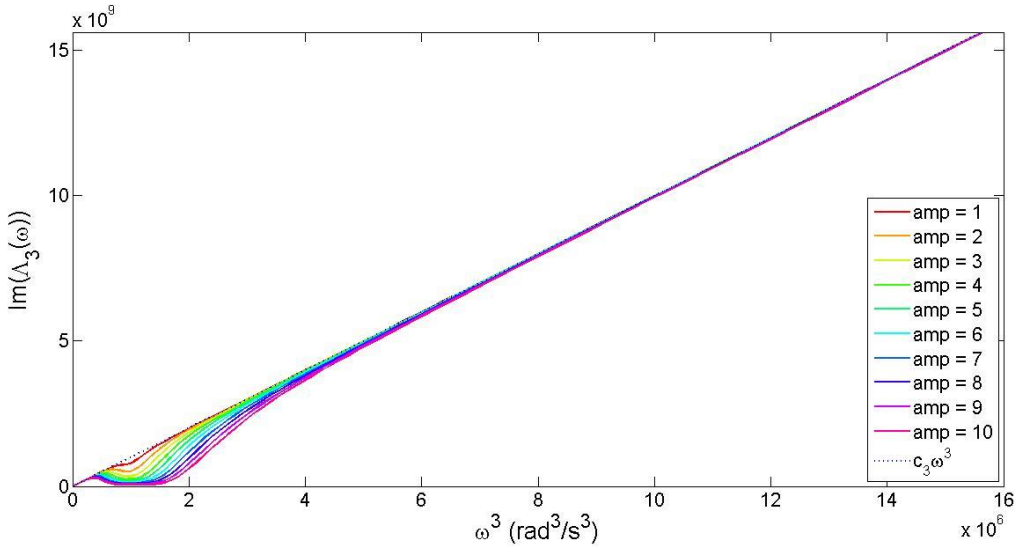

Figure 5.33: Plot of imaginary part of $\Lambda_3(\omega)$ against ω^3 for the estimation of cubic damping, c_3 only system

5.7.3 System with quadratic stiffness (k_2) only

With the quadratic stiffness system, the plot of the real part of $\Lambda_2(\omega)$ against ω is shown in Figure 5.34. This again is an approximation using Equation 5.28. Notice that this is plotted against ω and not ω^3. This allows simpler observations of the frequency value and does not affect the results as it only requires the y-axis intersect for the estimation of the nonlinear parameter k_2. The y-axis intersect from the plot gives the value of $-k_2$. As seen in the plot, a reliable estimation can be obtained only from the high frequency region.

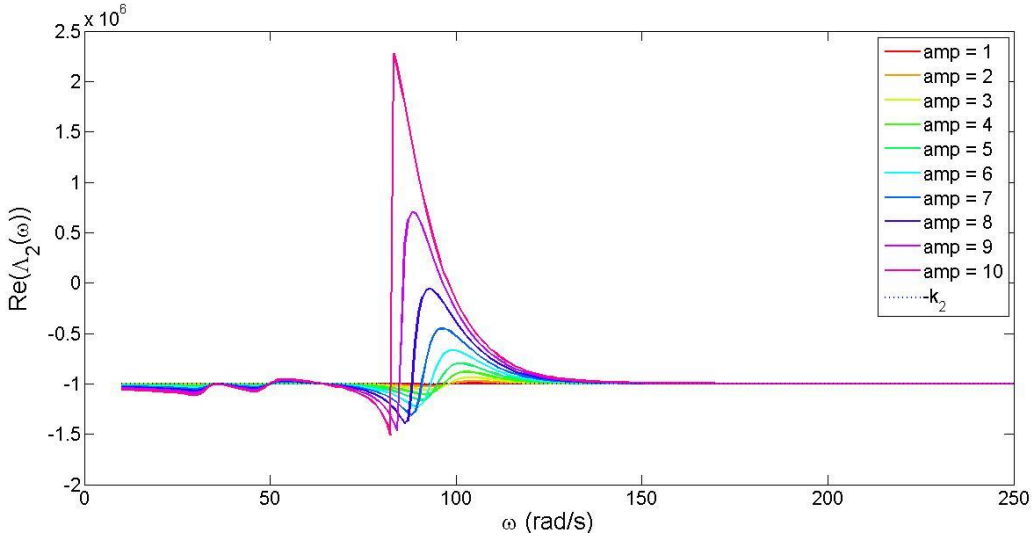

Figure 5.34: Plot of real part of $\Lambda_2(\omega)$ against ω for the estimation of quadratic stiffness, k_2 only system

5.7.4 System with cubic stiffness (k_3) only

For the cubic stiffness system, the plot of the real part of $\Lambda_3(\omega)$ against ω is shown in Figure 5.35. The value of $-k_3$ is the y-intersect of the plot from Equation 5.30. Similar to the k_2 only system, the only reliable estimate is found in the high frequency region where the line converge. The low frequency region suffers from large distortion due to the effects of the assumptions made in using only the first component of the Volterra kernel $H_3(\omega,\omega,\omega)$.

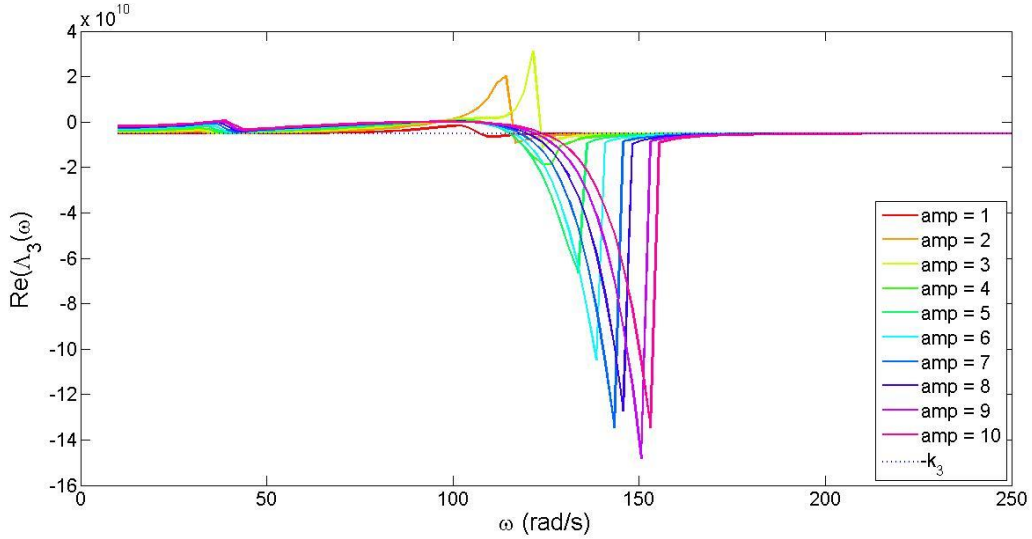

Figure 5.35: Plot of real part of $\Lambda_3(\omega)$ against ω for the estimation of cubic stiffness, k_3 only system

5.7.5 System with damping and stiffness nonlinearities (c_2, c_3, k_2 and k_3)

For the cubic nonlinearities, Equation 5.29 involved $H_2(\omega, \omega)$ which is slightly more complicated but solvable arithmetically with Matlab. The estimation of the nonlinear parameters can be estimated using the plot in Figure 5.36, Figure 5.37 and Figure 5.38 for the quadratic nonlinearities, cubic damping and cubic stiffness respectively. For the quadratic nonlinearities, although both rely on the real part of the $\Lambda_2(\omega)$ plot, the estimation can still be done since the quadratic damping parameter, c_2 relies on the gradient while the quadratic stiffness parameter, k_2 relies on the y-axis intersect of the estimation line.

The estimation for the cubic damping parameter, c_3 works as expected by taking the gradient using point on the plotted line in the high frequency region to the origin. However, the estimation of cubic stiffness parameter, k_3 faces a problem due to the presence of the $H_2(\omega, \omega)$ term in the Equation 5.29.

The presence of $H_2(\omega, \omega)$ term, causes a divergence in the high frequency region where the value for k_3 was obtained for system with single nonlinearity previously.

Figure 5.39 to Figure 5.41 show the real and imaginary plot for system with nonlinear damping only and Figure 5.42 to Figure 5.44 show the real and imaginary plot for system with nonlinear stiffness only. This is to investigate the divergence that occurred for the identification of the cubic stiffness above. The point here in these plots is mainly based on Figure 5.41, where the effect due to the quadratic damping, c_2 causes divergence in the high frequency region for the real part plot of $\Lambda_3(\omega)$ against ω^3. This is the disturbance that causes the problem in estimating the nonlinear parameter k_3 for the system with all four nonlinearities previously. In Figure 5.43, it can be seen that contrary to the effect of $H_2(\omega, \omega)$ on the estimation of cubic stiffness parameter, k_3, the quadratic stiffness parameter, c_3 do not affect the imaginary part plot of $\Lambda_3(\omega)$ against ω^3 which is for the estimation of the cubic damping parameter, c_3 with no divergence shown or any introduction of disturbance in the gradient of the estimation line.

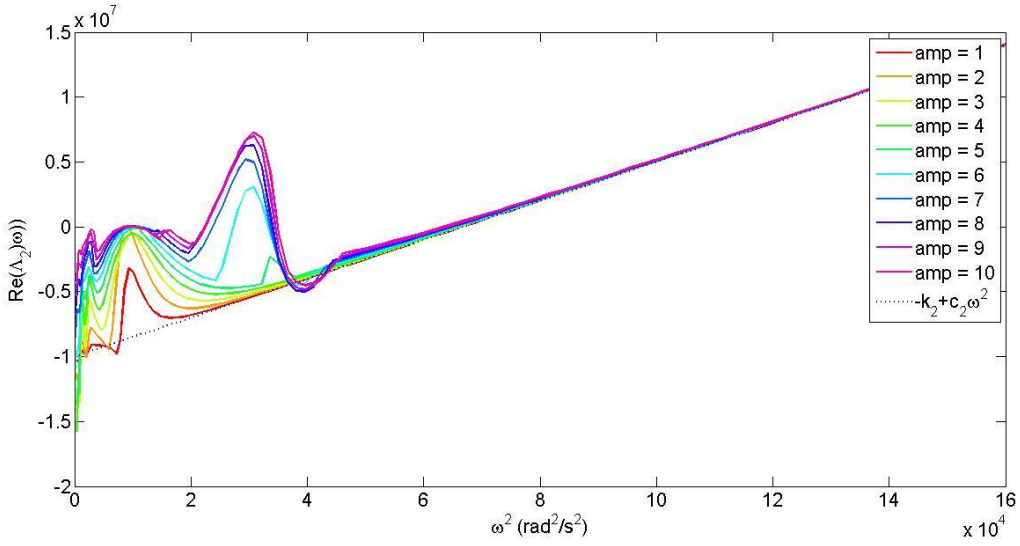

Figure 5.36: Plot of real part of $\Lambda_2(\omega)$ against ω^2 for the estimation of quadratic damping, c_2 and quadratic stiffness, k_2 for system with all four nonlinearities (c_2, c_3, k_2 and k_3)

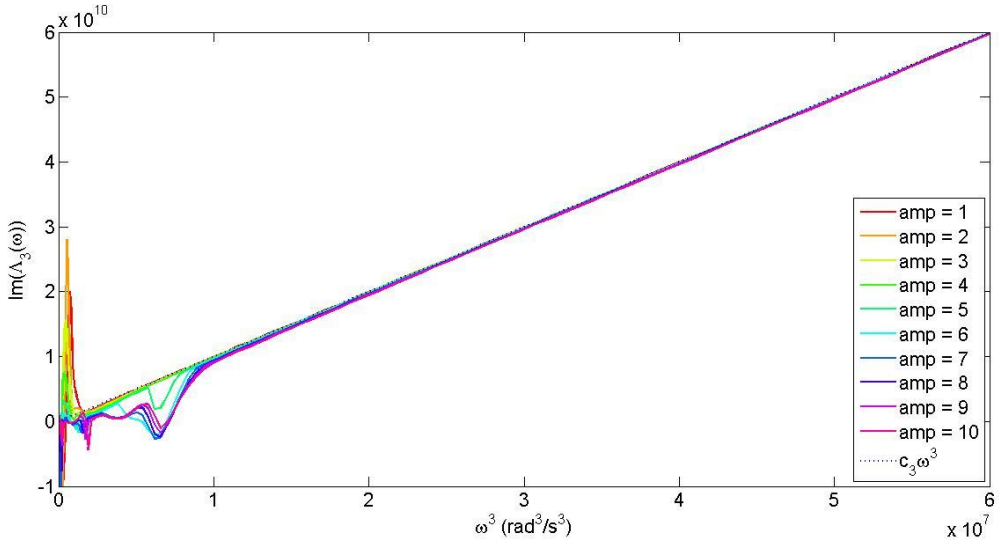

Figure 5.37: Plot of imaginary part of $\Lambda_3(\omega)$ against ω^3 for the estimation of cubic damping, c_3 for system with all four nonlinearities (c_2, c_3, k_2 and k_3)

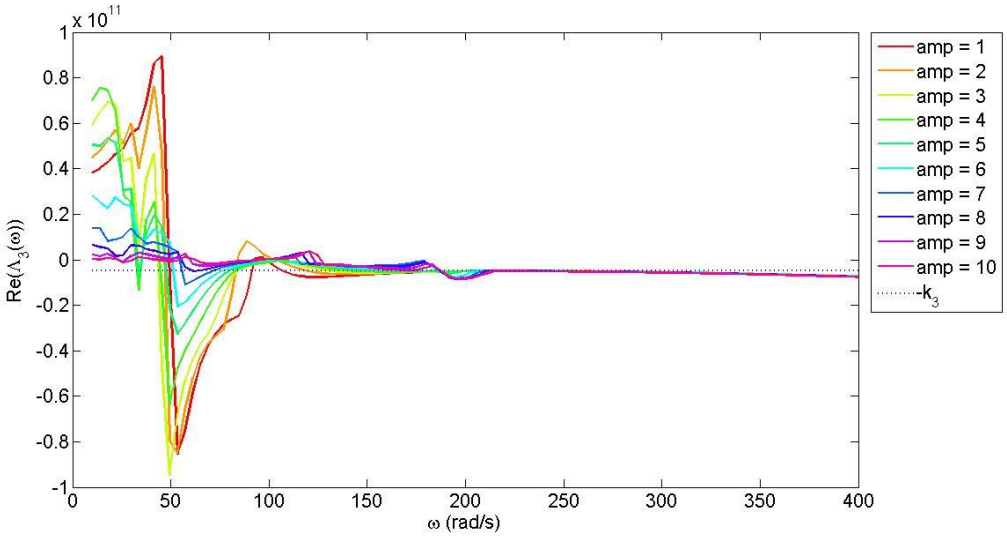

Figure 5.38: Plot of real part of $\Lambda_3(\omega)$ against ω for the estimation of cubic stiffness, k_3 for system with all four nonlinearities (c_2, c_3, k_2 and k_3)

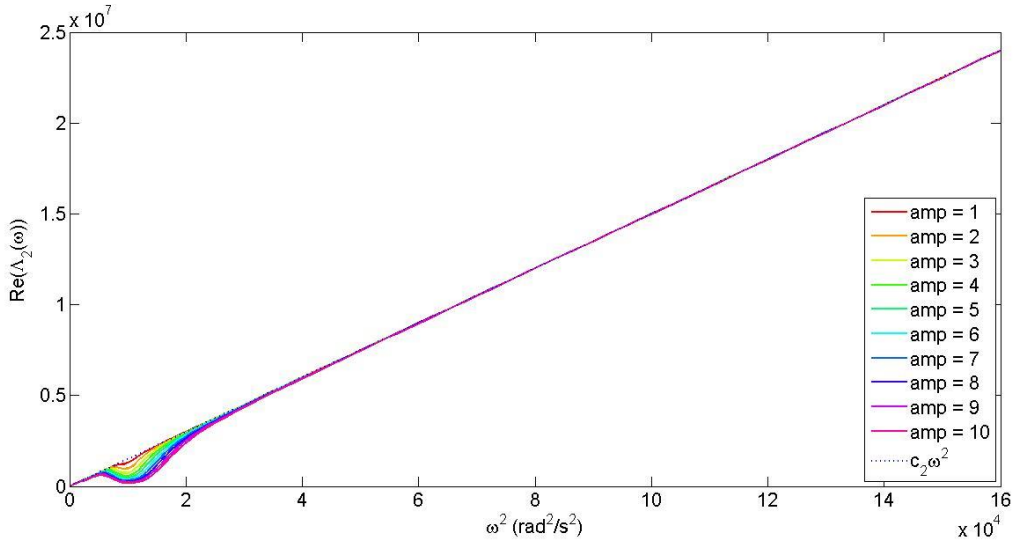

Figure 5.39: Plot of real part of $\Lambda_2(\omega)$ against ω^2 for the estimation of quadratic damping, c_2 for system with both damping nonlinearities (c_2 and c_3)

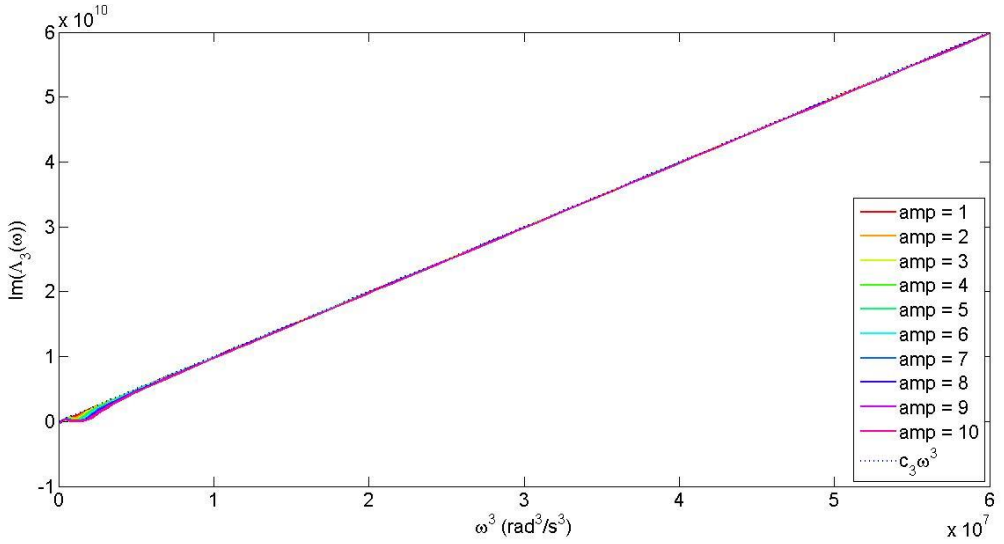

Figure 5.40: Plot of imaginary part of $\Lambda_3(\omega)$ against ω^3 for the estimation of cubic damping, c_3 for system with both damping nonlinearities (c_2 and c_3)

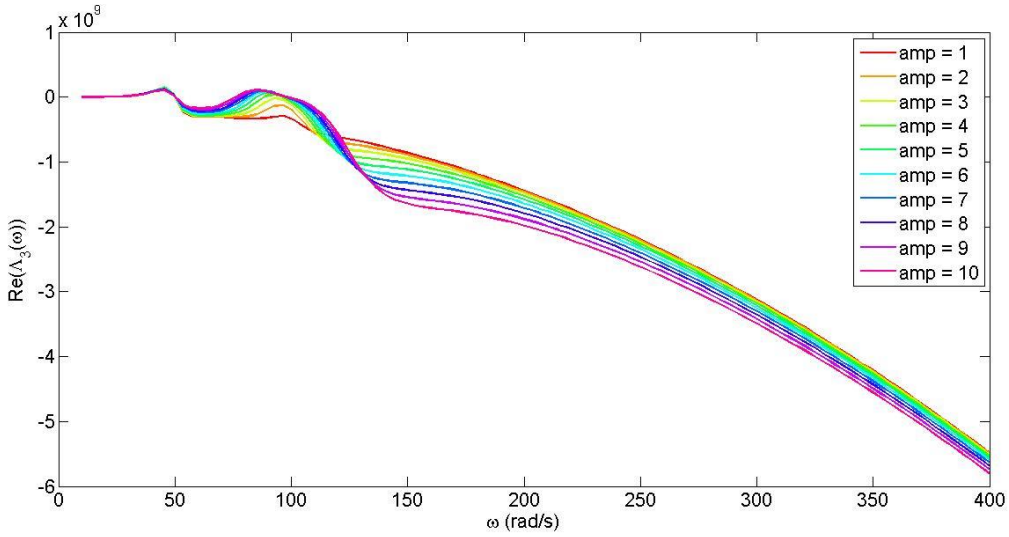

Figure 5.41: Plot of real part of $\Lambda_3(\omega)$ against ω^3 for system with both damping nonlinearities (c_2 and c_3)

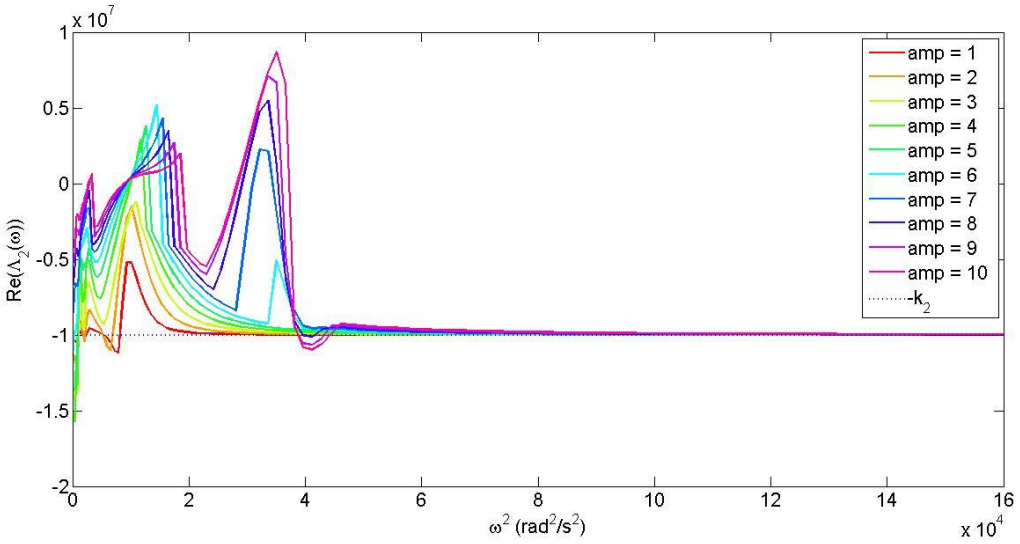

Figure 5.42: Plot of real part of $\Lambda_2(\omega)$ against ω^2 for the estimation of quadratic stiffness, k_2 for system with both stiffness nonlinearities (k_2 and k_3)

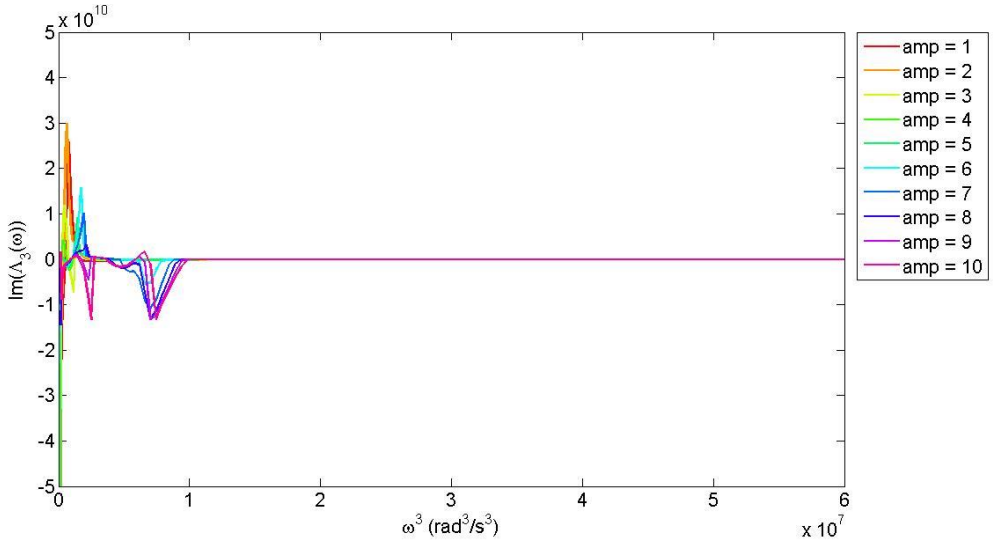

Figure 5.43: Plot of imaginary part of $\Lambda_3(\omega)$ against ω^3 for system with both stiffness nonlinearities (k_2 and k_3)

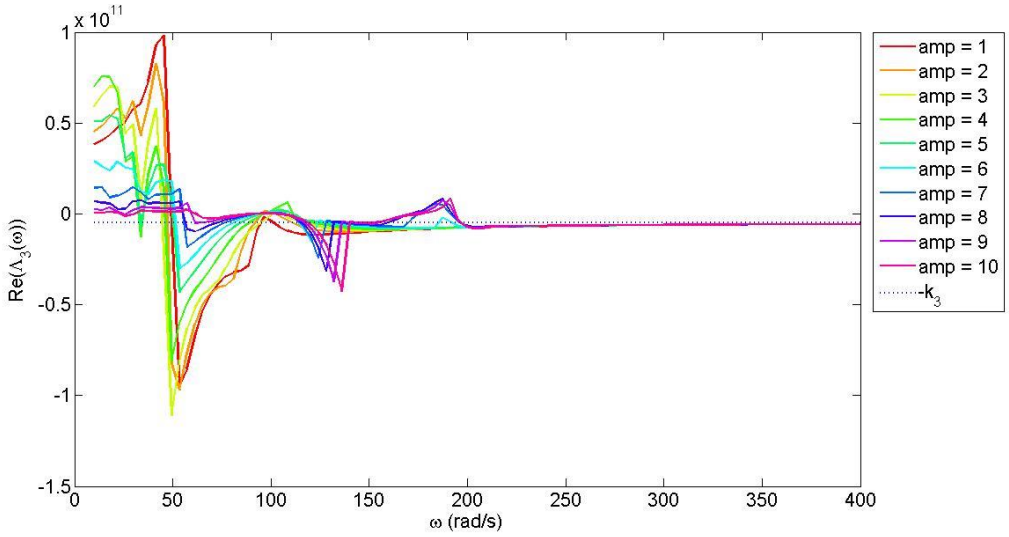

Figure 5.44: Plot of real part of $\Lambda_3(\omega)$ against ω for the estimation of cubic stiffness, k_3 for system with both stiffness nonlinearities (k_2 and k_3)

5.8 **Estimation of nonlinear parameters in the presence of noise**

Noise was added at two levels on the output signal with the first level of noise being low at 1E-7 of the signal RMS value and the other at 1E-5 of the signal RMS value. These are the same output noise levels as used for the linear parameter investigation.

Figures 5.45 to Figure 5.58 show the low level and high level noise plots respectively for the nonlinear parameter comparable to Section 5.6. The noise affected the system similarly to the single nonlinear systems and the system with all four nonlinearities. The attention of the reader is drawn to the fact that the plot for all four nonlinearities in Figure 5.53 to Figure 5.58 show a higher frequency range hence this amplified the noise effect. With the same limited frequency range, a similar effect should be seen.

The low level noise figures show no visible differences. However, when zoomed in closer, it is possible to see a slight deviation mostly around the high frequency region, although this is expected in the presence of noise.

With a higher level of noise, larger deviations could be observed for all the nonlinear polynomial system, again in the high frequency region. The effect of noise is clearly visible in the low amplitude input and improved as the amplitude increases. This results from the fact that at lower amplitude the harmonics of a system would be below the noise level. At higher amplitudes, the amplitude of the higher harmonic peak will be above the noise band.

In the second harmonic plot for c_2 and k_2, the distortion caused by presence of noise is of lesser magnitude compared to the third harmonic. The effect of noise is more prominent in the third harmonic related plot, which is for c_3 and k_3 only systems. In Figure 5.48, significant distortion can be clearly observed for the first three values of low amplitude. In Figure 5.52, the effect is very similar. An increase in amplitude would help to reduce the disturbance of noise in all frequency regions.

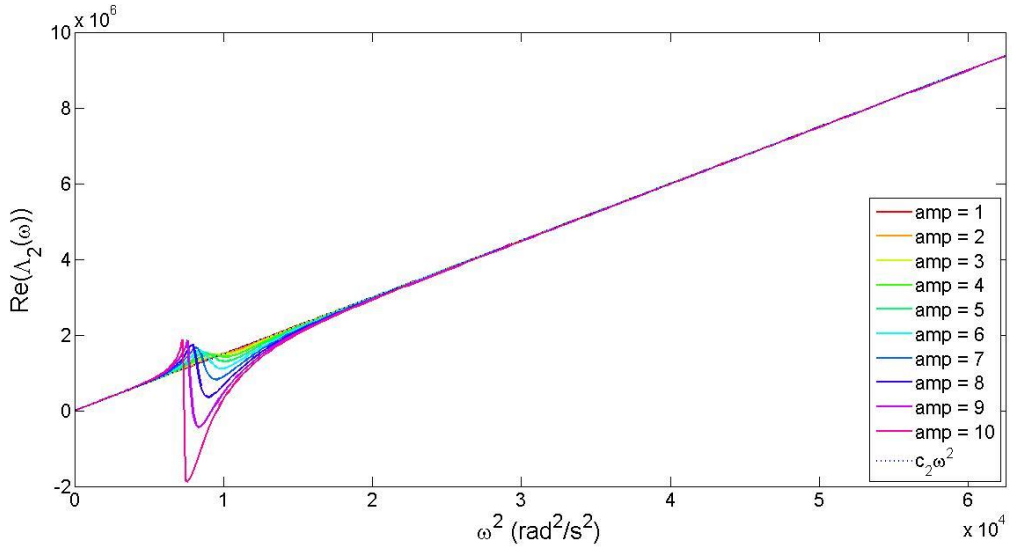

Figure 5.45: Plot of real part of $\Lambda_2(\omega)$ against ω^2 with low level noise for the estimation of quadratic damping, c_2 only system

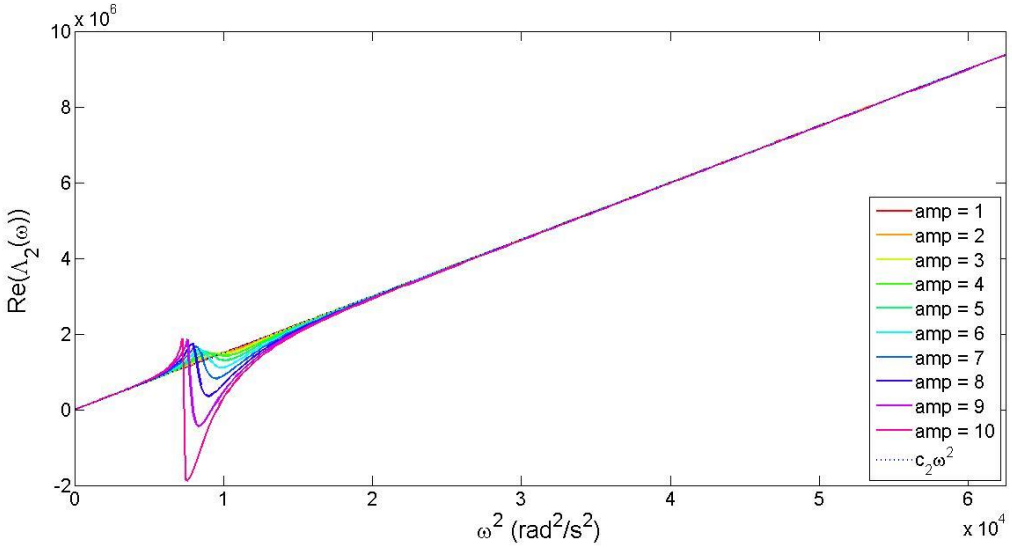

Figure 5.46: Plot of real part of $\Lambda_2(\omega)$ against ω^2 with high level noise for the estimation of quadratic damping, c_2 only system

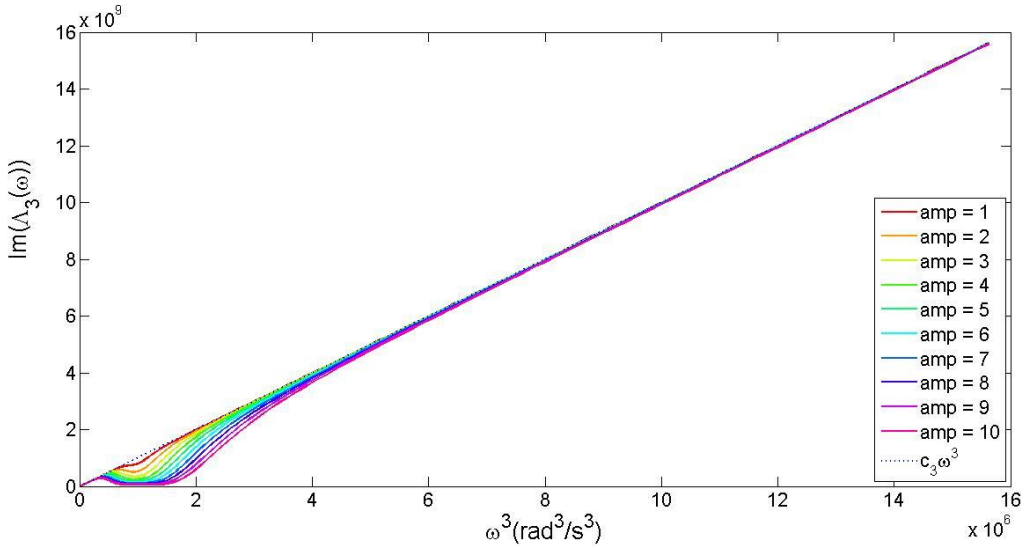

Figure 5.47: Plot of imaginary part of $\Lambda_3(\omega)$ against ω^3 with low level noise for the estimation of cubic damping, c_3 only system

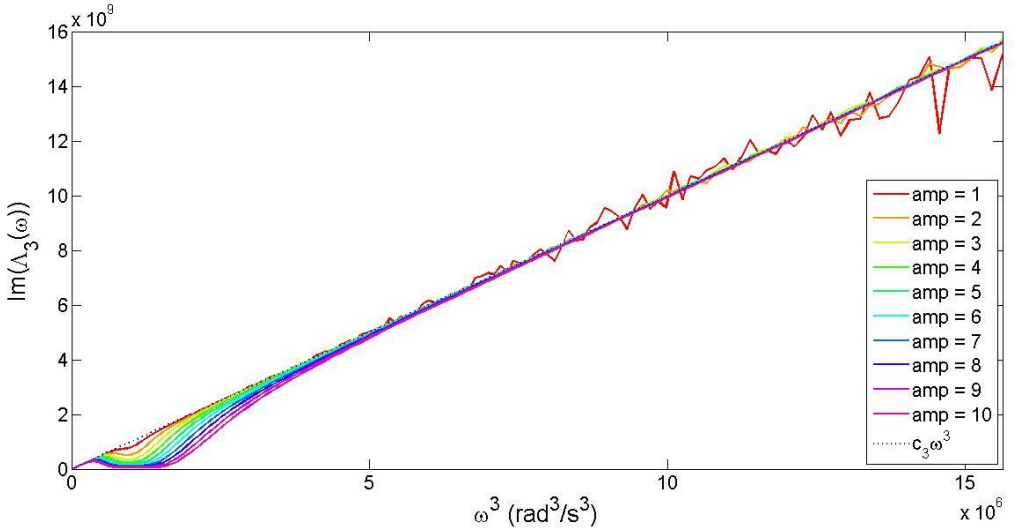

Figure 5.48: Plot of imaginary part of $\Lambda_3(\omega)$ against ω^3 at high level noise for the estimation of cubic damping, c_3 only system

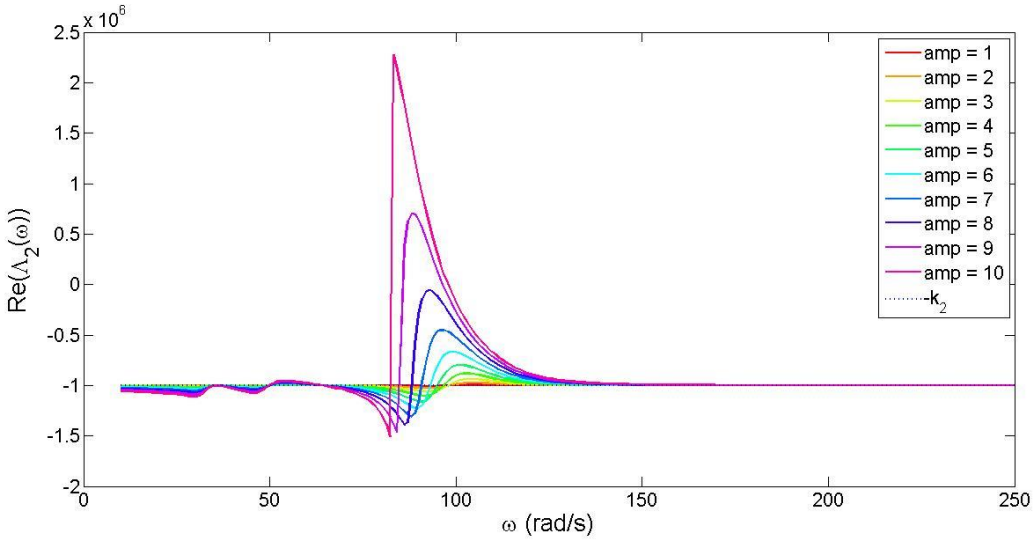

Figure 5.49: Plot of real part of $\Lambda_2(\omega)$ against ω with low level noise for the estimation of quadratic stiffness, k_2 only system

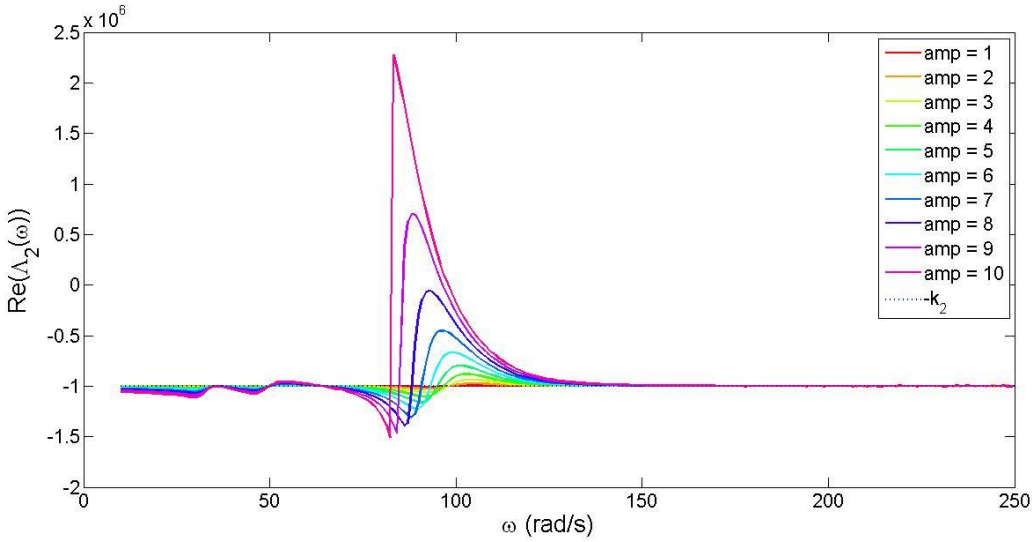

Figure 5.50: Plot of real part of $\Lambda_2(\omega)$ against ω with high level noise for the estimation of quadratic stiffness, k_2 only system

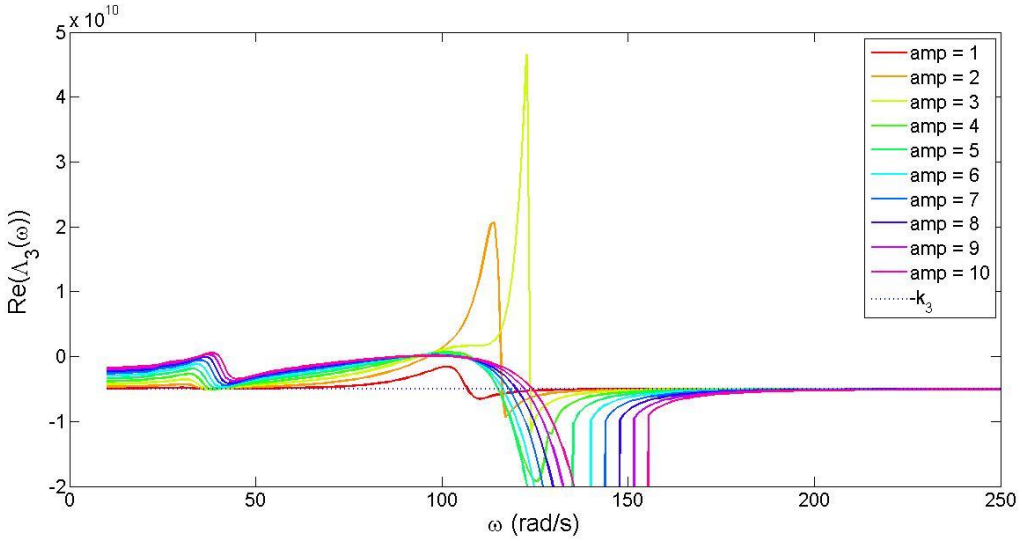

Figure 5.51: Plot of imaginary part of $\Lambda_3(\omega)$ against ω at low level noise for the estimation of cubic stiffness, k_3 only system

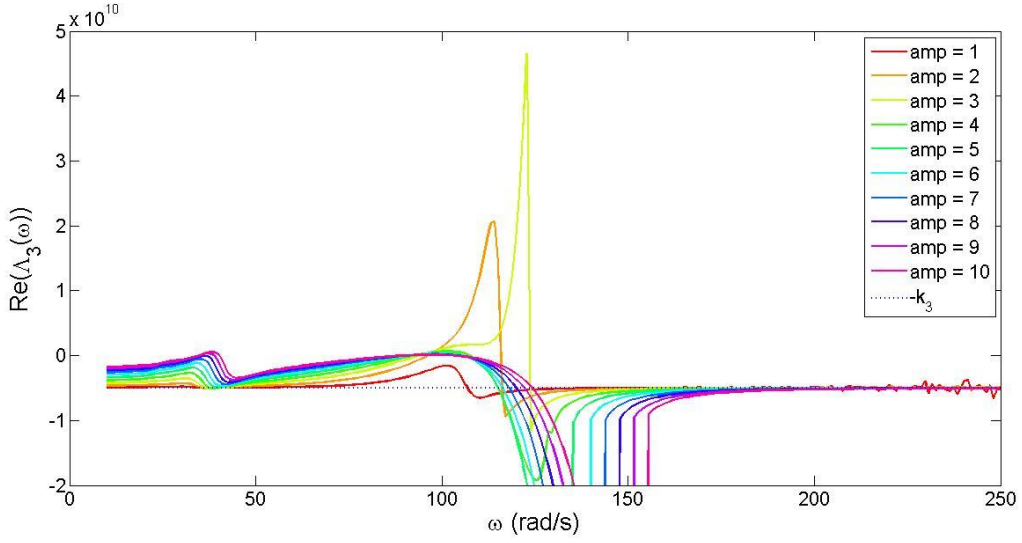

Figure 5.52: Plot of imaginary part of $\Lambda_3(\omega)$ against ω at high level noise for the estimation of cubic stiffness, k_3 only system

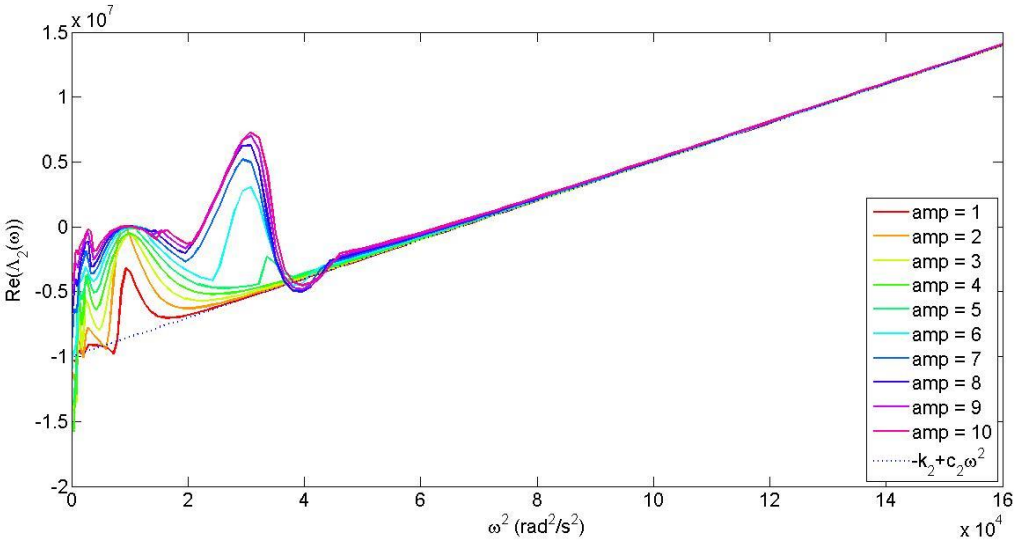

Figure 5.53: Plot of real part of $\Lambda_2(\omega)$ against ω^2 at low level noise for the estimation of quadratic damping, c_2 and quadratic stiffness, k_2 for system with all four nonlinearities (c_2, c_3, k_2 and k_3)

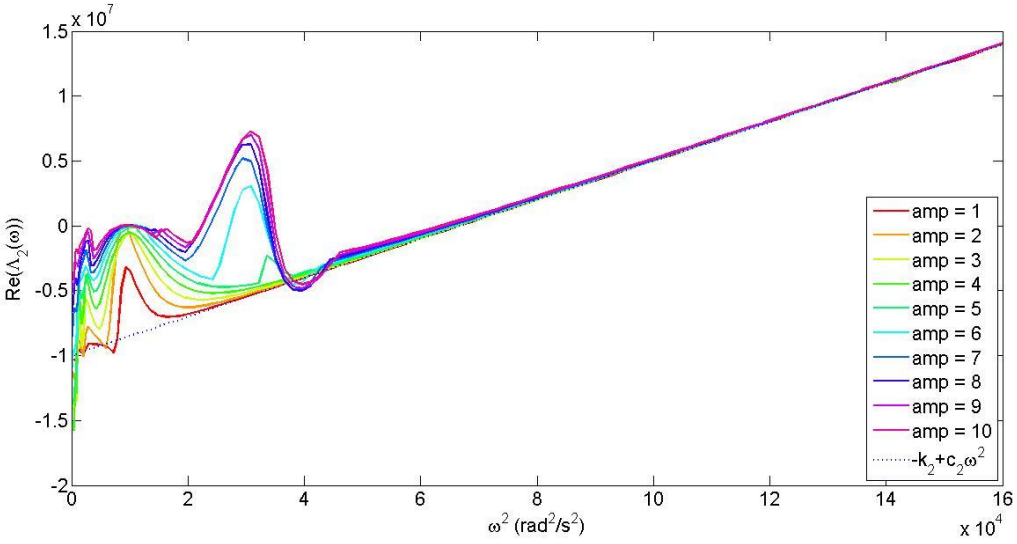

Figure 5.54: Plot of real part of $\Lambda_2(\omega)$ against ω^2 at high level noise for the estimation of quadratic damping, c_2 and quadratic stiffness, k_2 for system with all four nonlinearities (c_2, c_3, k_2 and k_3)

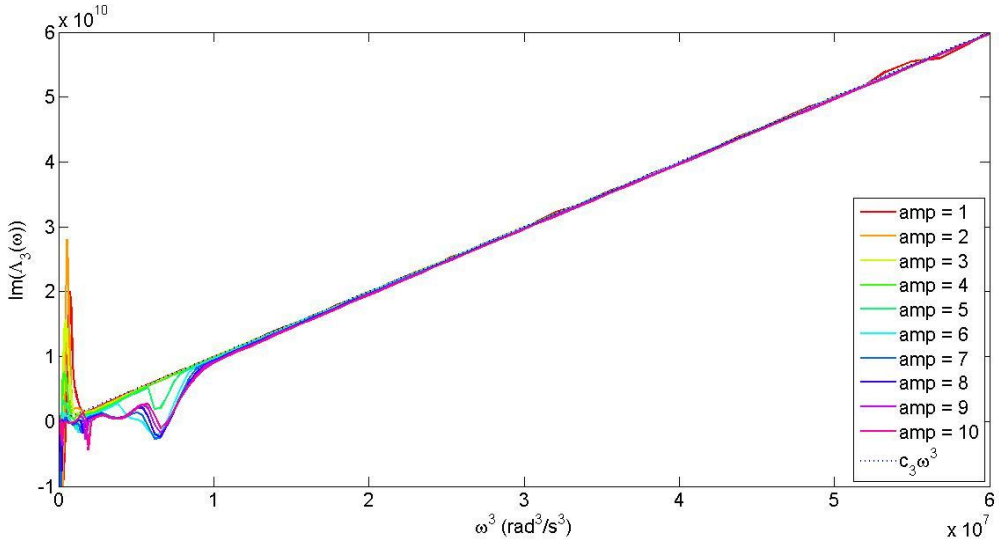

Figure 5.55: Plot of imaginary part of $\Lambda_3(\omega)$ against ω^3 at low level noise for the estimation of cubic damping, c_3 for system with all four nonlinearities (c_2, c_3, k_2 and k_3)

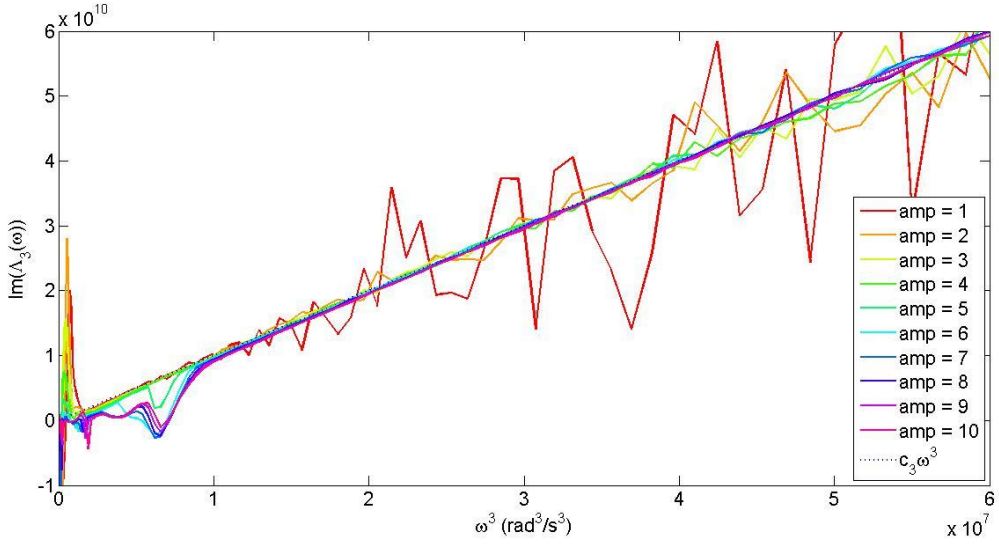

Figure 5.56: Plot of imaginary part of $\Lambda_3(\omega)$ against ω^3 at high level noise for the estimation of cubic damping, c_3 for system with all four nonlinearities (c_2, c_3, k_2 and k_3)

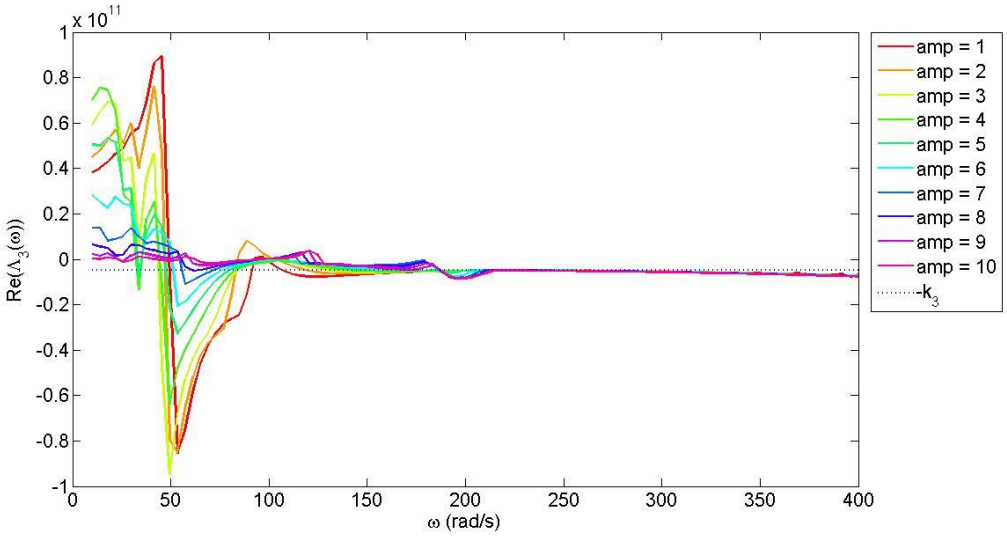

Figure 5.57: Plot of imaginary part of $\Lambda_3(\omega)$ against ω at low level noise for the estimation of cubic stiffness, k_3 for system with all four nonlinearities (c_2, c_3, k_2 and k_3)

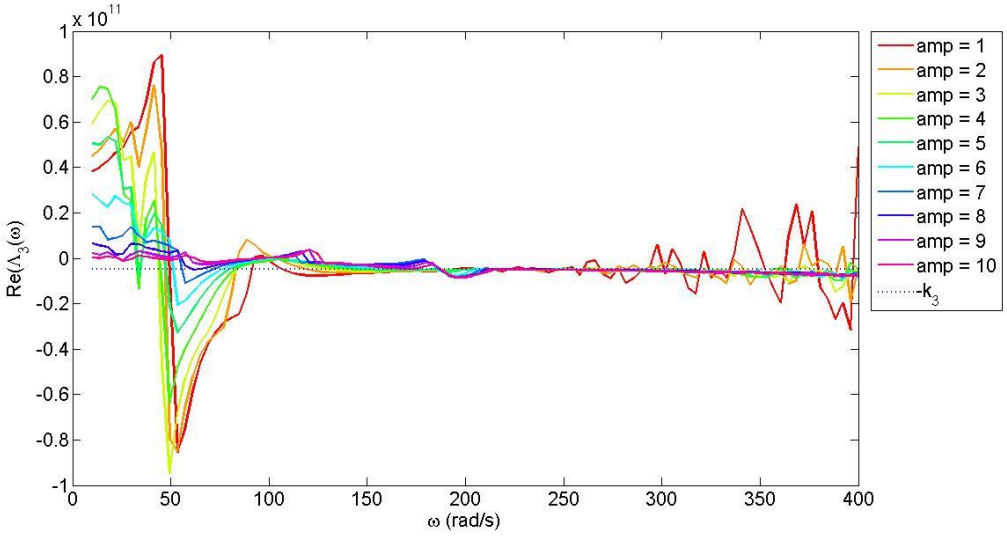

Figure 5.58: Plot of imaginary part of $\Lambda_3(\omega)$ against ω at high level noise for the estimation of cubic stiffness, k_3 for system with all four nonlinearities (c_2, c_3, k_2 and k_3)

5.8.1 Further investigation of the effect of noise on the Volterra series representation

The problems observed in the high frequency region present an issue for obtaining accurate prediction measurements of the nonlinear parameter values from harmonic probing. Looking at Figure 5.59, the frequency spectrum at higher frequency levels showed that, at high frequency, other than the first peak, all the other harmonics were below the noise level. In this case, the higher order harmonic

probing equation would not be reliable as it relies on second and third harmonics for the respective polynomial cases. For example, for the nonlinear parameter estimation of k_3, it depends on the third harmonic as per Equation 5.22 which is not distinguishable from the noise level at high frequencies.

At low frequency and at the undamped natural frequency of the underlying linear system, the effect of noise is slightly less as can be seen from Figure 5.60 and Figure 5.61 respectively. However, in the region of low frequencies and around the undamped natural frequency of the underlying linear system the distortions due to the assumption made of using only the first components of the Volterra kernels do not allow for good estimation even in the absence of noise. In the context of the framework of building nonlinear models, this should guide the choice of input for using Volterra series representation estimation in the design of the experiments stage.

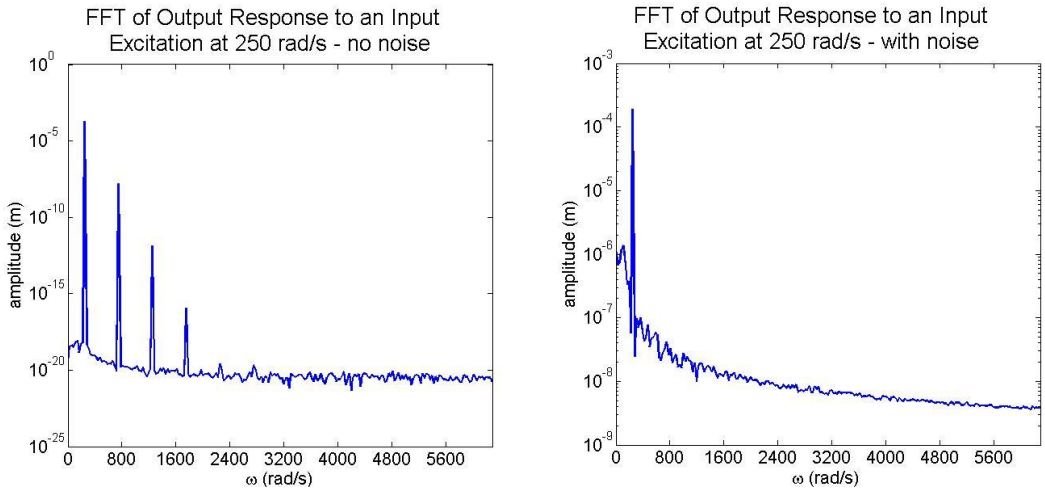

Figure 5.59: Frequency spectrum with probing frequency of 250 rad/s

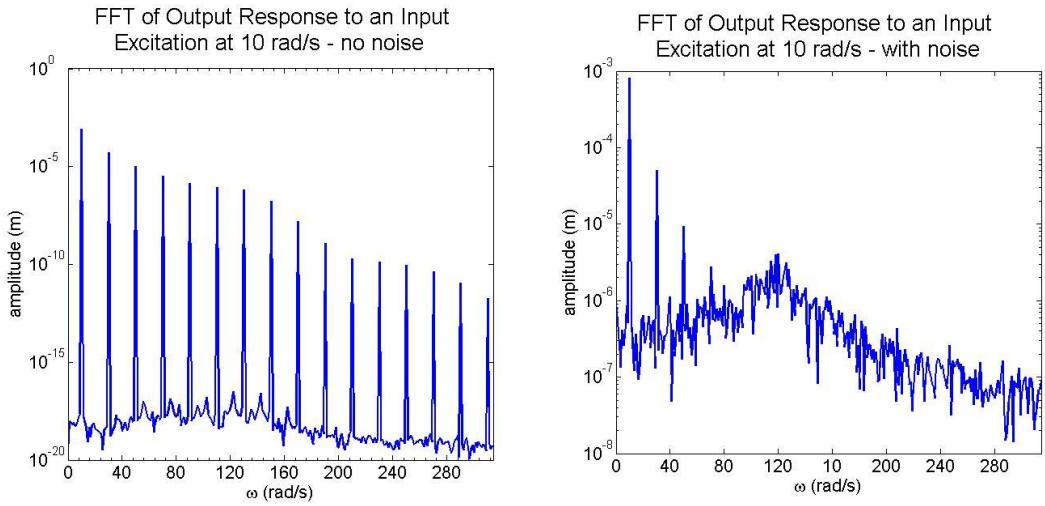

Figure 5.60: Frequency spectrum with probing frequency of 10 rad/s

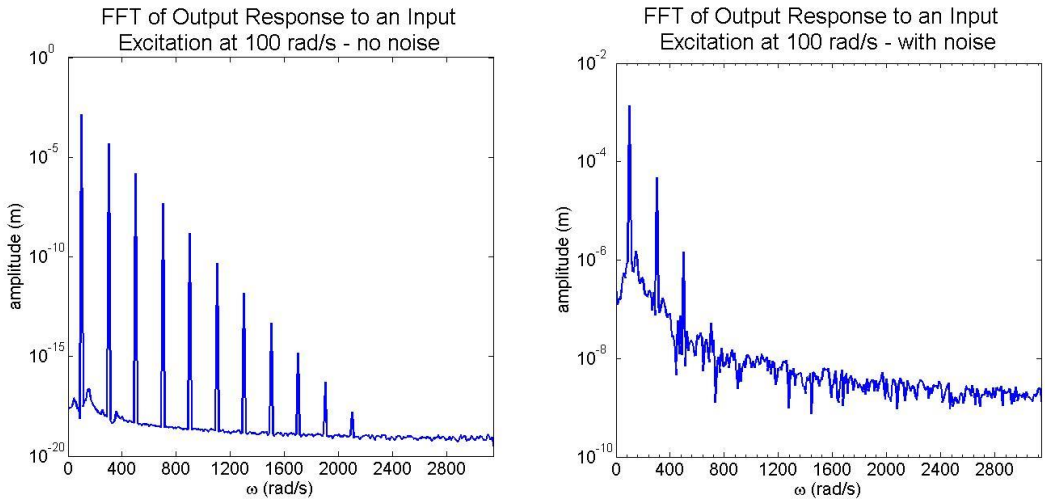

Figure 5.61: Frequency spectrum with probing frequency of 100 rad/s

5.9 **Discussion**

In this chapter, an investigation was conducted into the identification of polynomial model parameters using an approach based on the Volterra series representation. The linear parameters were shown to be independent of the nonlinear parameters when identified this way. For the linear parameters, only the first harmonic (i.e. the response at the forcing frequency) was used whilst the nonlinear parameter required the superharmonics (i.e. response at two times or three times the forcing frequency) for estimation. Observation from the results showed that there are some frequencies which could work well and some that could not due to distortion caused by the assumptions in the estimation steps. Most low frequencies would give less accurate estimation compared to points at frequencies higher than the undamped natural frequency of the underlying linear system. The results also show the distortion of the prediction lines increases as the amplitude increases. However, it can also be observed that higher amplitude gives more tolerance to noise. This should be put into consideration when planning and designing experiments for parameter estimation.

Linear parameter prediction was mostly unaffected in the presence of noise. Noise appears to mostly affect the imaginary part of Λ_1 which is for the calculation of the linear damping parameter, c value. The noise however mostly causes distortion at the high frequency region. The value of the damping

parameter, c can still be obtained by a line drawn from the low level region to the origin to calculate the gradient. For a system with all four nonlinearities, noise significantly affects the estimation. For a system such as this, the noise level should be kept minimal in order to obtain an accurate estimation of the parameters.

The investigation of the nonlinear polynomial parameters shows that the nonlinear parameters can be identified independently from each other. The nonlinear stiffness parameters are estimated from the y-axis intersect and the nonlinear damping parameters are estimated from the gradients of their respective prediction lines of their respective plots. For a system with all four nonlinearities, the estimation of cubic stiffness, k_3 is not possible due to the effect from $H_2(\omega,\omega)$ in the presence of quadratic terms that introduces divergence to the estimation line of the parameter k_3.

For the nonlinear parameters noise also affects mostly the high frequency region similar to the linear cases. This was also shown in the FFT plot where the signal with the high frequency was more affected by noise and lost the harmonics peaks under noise level more easily compared to the low frequency signal. This could introduce inaccuracy in the prediction of the nonlinear parameters.

The combination of the multiple sinusoidal signals such as that used in the previous chapter can also be recommended from the results here with the signal combination having low and high frequency components both with high amplitude. The combination of frequencies, however, should be carefully selected to avoid combinations that could reduce system information such as multiples as discuss in the last chapter.

In the next chapter, the same method that was used here will be applied to the Bouc-Wen model to investigate whether it is possible to use such an approach to predict the parameters of the hysteretic model.

Chapter 6

6 Volterra representation for Bouc-Wen model

6.1 Introduction

In the previous chapter, the feasibility of nonlinear system identification of polynomial nonlinear systems using the Volterra Series approximation was investigated. The Volterra series approximation is intended for nonlinear systems without memory and with smooth nonlinearities.

The Bouc-Wen model however has memory and the nonlinearity is not smooth. That said, the work of the previous chapter will be extended to investigate whether the Volterra approach may be applied to the Bouc-Wen model. The main reason for the work in this chapter is to investigate the odd harmonic behaviour shown by the Bouc-Wen system observed in the Chapter 2. By directly using the Volterra series for the polynomial model on the Bouc-Wen model, the relationship between the two models could be established to find the physical properties of the Bouc-Wen nonlinear parameters β and γ.

Firstly, the estimation of the linear parameters in the Bouc-Wen model is investigated to see if it is comparable to the estimation of the linear parameters of the polynomial model of the previous chapter. Subsequently, the nonlinear parameters of the Bouc-Wen model are investigated. Both will look at the approximation without noise and with noise. Finally, the similarities and differences between the model and the polynomial model behaviour are discussed.

The classic Bouc-Wen model as introduced in chapter 2 is used here. To remind the reader, the relevant equations are shown below. In order to be consistent, the parameters of the Bouc-Wen model are the same as in the previous chapters and are shown below in Table 6.1. Again, these parameters have been obtained from identification of the El Centro 1940 earthquake data with some modification to suit the purpose of the research in this thesis.

$$m\ddot{u} + c\dot{u} + R_T = F(t) \tag{6.1}$$

$$R_T = \alpha k u + (1-\alpha) k z \tag{6.2}$$

$$\dot{z} = A\dot{u} - \beta|\dot{u}||z|^{n-1}z - \gamma\dot{u}|z|^n \tag{6.3}$$

Parameter	Value	Units
m	1	kg
c	0.7037	Ns/m
k	309.51	N/m
A	1	-
α	0.01	1/m
β	150	1/m
γ	20	-
n	2	-

Table 6.1: Parameters for the Bouc-Wen model

6.2 **Estimation of the linear parameters**

With the Volterra relationship of the first order frequency response functions as per Equation 5.18, the linear parameters of the Bouc-Wen model were identified. The input used is also similar to the

previous chapter using sinusoidal input with amplitudes of 1 to 10. Figures 6.1 and Figure 6.2 show the plot of the real part of $\Lambda_1(\omega)$ against ω^2 and the imaginary part of $\Lambda_1(\omega)$ against ω respectively. With reference to the figures, the value of *m*, *c* and *k* can be determined.

Based upon Equation 5.18 of the Volterra relationship for the first order FRF, the mass, *m* and the linear stiffness, *k* may be estimated from the gradient and y-axis intersect respectively of the plot in Figure 6.1. From the figure, a good estimation line of the *m* and *k* value can be obtained both from above or below the underlying linear system undamped natural frequency.

For the linear damping parameter, *c*, the value can be estimated from the gradient of Figure 6.2. Based upon the reference line, the value *c* of can be estimated only at the region of high frequency. The gradient can be drawn from any single point to the origin to obtain an estimation of the parameter *c*.

It has been shown here that the linear parameters of the Bouc-Wen model could be estimated by using the Volterra series representation similar to the polynomial model in the previous chapter. The estimation of the linear parameters is independent of the nonlinear parameters of the model. The method could be used to estimate the linear parameters of the model to understand the basic properties of the system.

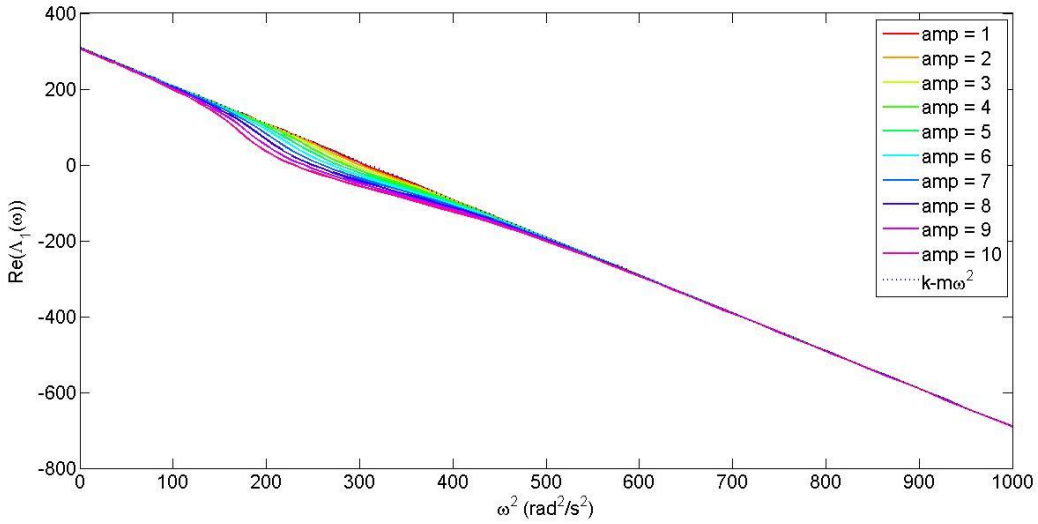

Figure 6.1: Plot of real part of $\Lambda_1(\omega)$ against ω^2 for Bouc-Wen model

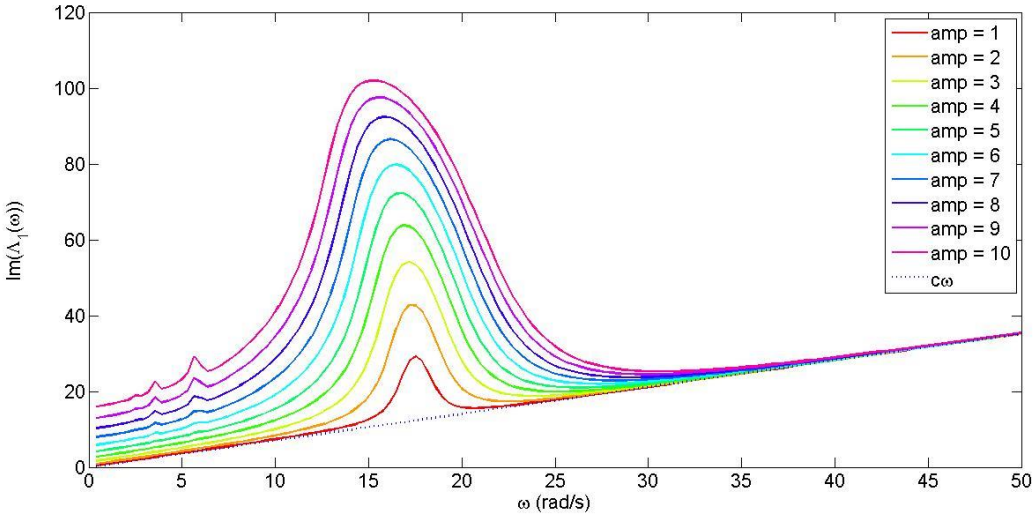

Figure 6.2: Plot of imaginary part of $\Lambda_1(\omega)$ against ω for Bouc-Wen model

6.3 **Estimation of the linear parameters in the presence of noise**

The behaviour of the estimation is investigated in the presence of noise. Noise was added at two levels as per Table 6.2 below. The levels of noise were selected to sufficiently show the effect of noise on the estimation using the Volterra series approximation for the Bouc-Wen model. Figure 6.3 and Figure 6.4 show the low noise level plot while Figure 6.5 and Figure 6.6 show the high noise level plot.

Similarly to the observations made in the previous chapter, the noise affects the imaginary part plot more than the real part plot. The effect of noise also shows mostly at the higher frequency regions. This has been noted in the investigations detailed in the previous chapter with regards to the frequency spectrum, where noise tends to disrupt the harmonic peaks at the higher frequencies, thus appearing to a greater extent in the plots here.

Noise level	Low level	High level
Output	1E-5 times output RMS	1E-2 times output RMS

Table 6.2: Simulated noise levels

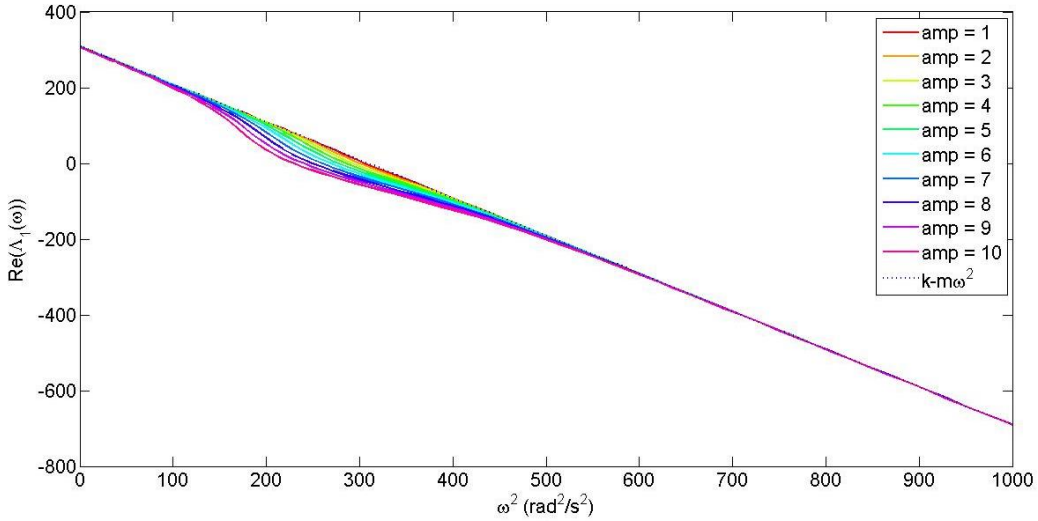

Figure 6.3: Plot of real part of $\Lambda_1(\omega)$ against ω^2 for Bouc-Wen model with low noise level

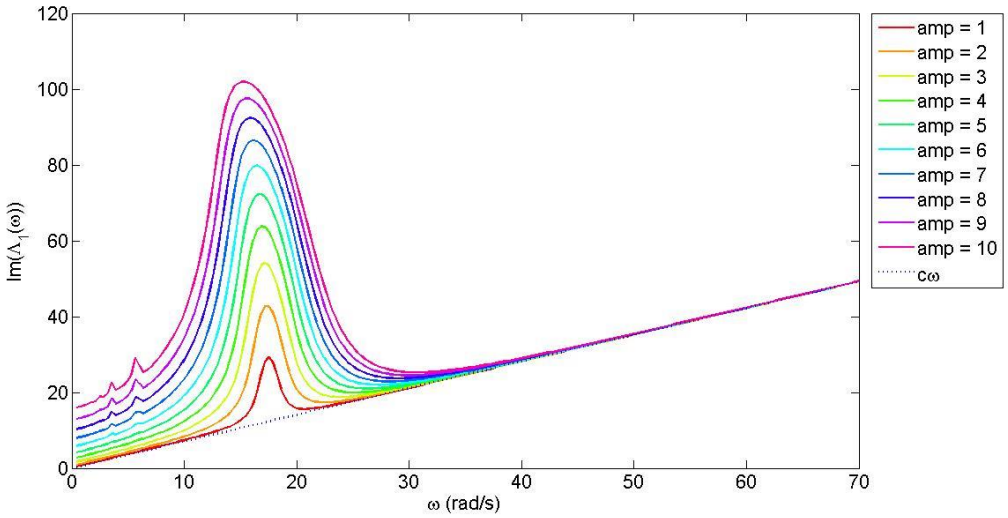

Figure 6.4: Plot of imaginary part of $\Lambda_1(\omega)$ against ω for Bouc-Wen model with low noise level

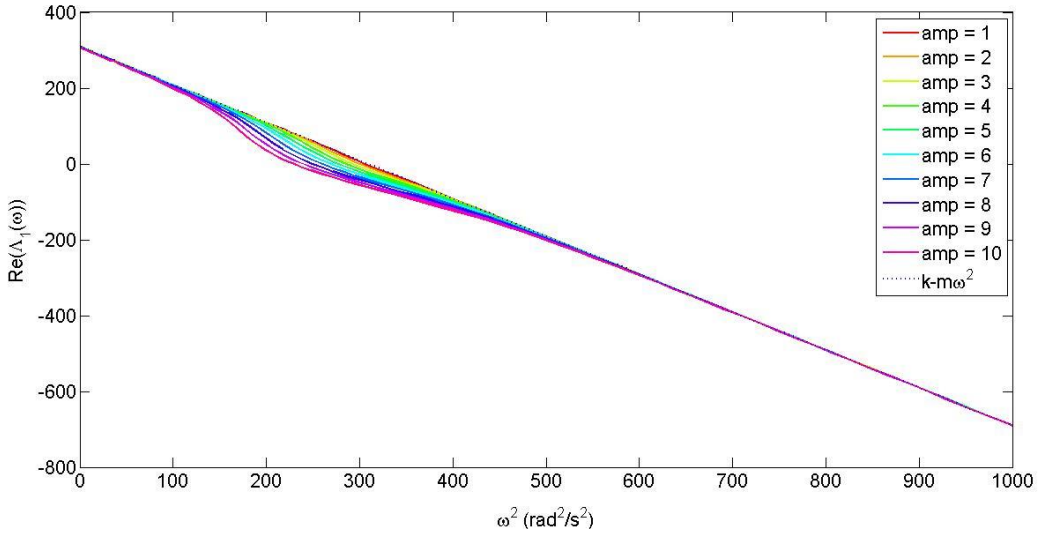

Figure 6.5: Plot of real part of $\Lambda_1(\omega)$ against ω^2 for Bouc-Wen model with low noise level

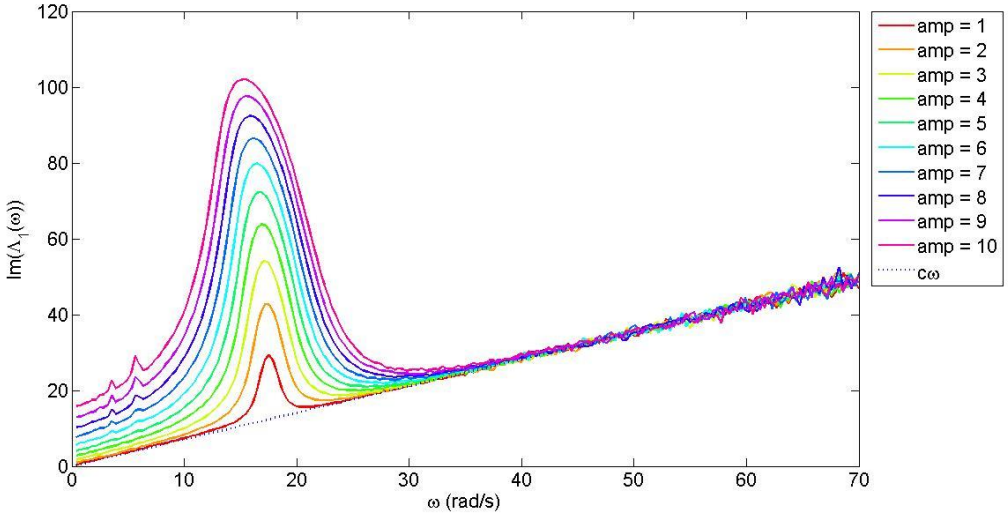

Figure 6.6: Plot of imaginary part of $\Lambda_1(\omega)$ against ω for Bouc-Wen model with low noise level

6.4 **Estimation of the nonlinear parameters**

The investigation here was done without substituting the probing equation into the Bouc-Wen model equation of motion itself which is the reason for not showing any new equations at this point. The complication of the Bouc-Wen equation of motion would make it challenging mathematically. Another reason is the objective to see if the Bouc-Wen model does indeed show any nonlinear

polynomial model behaviour. This could give insights into the behaviour of the Bouc-Wen model comparable to a well-known nonlinear polynomial model.

The Volterra series approximation is not intended for non-smooth systems with memory, such as the Bouc-Wen hysteresis model. That said, there may be some relationship between the Bouc-Wen parameters of the simulated system and the polynomial parameters that can be estimated from the Volterra series parameter estimation.

Using Equation 5.28 and Equation 5.29 for the HFRF of the 2nd and 3rd order harmonics respectively, the relationships between the Bouc-Wen model parameters and the polynomial quadratic and cubic damping and stiffness were investigated. This was conducted by plotting $\Lambda_2(\omega)$ for the quadratic damping and stiffness and plotting $\Lambda_3(\omega)$ for the cubic damping and stiffness similar to that shown in the previous chapter for the polynomial parameters c_2, c_3, k_2 and k_3.

To compare the two models, Figure 6.7 to Figure 6.9 were plotted. Figure 6.7 shows similarities to c_2 and k_2 which would thus show any behaviour of quadratic damping and stiffnes. Figure 6.8 shows similarities to c_3 which would thus show any behaviour of cubic damping and lastly Figure 6.9 shows similarities to k_3 which would thus show any behaviour of cubic stiffness.

The similar behaviour exhibited by the quadratic parameters c_2 and k_2 were practically non-existent as seen in the Figure 6.7. For a non-zero value of c_2, a non-zero gradient would be expected in the plot but this was not observed, whilst a non-zero value of k_2 would result in a non-zero y-axis intersect but again in the figure, the y-axis intersect value was close to zero. This has been shown in Chapter 3 in the frequency spectrum plot where the specific system of parameters for the Bouc-Wen model used here only showed odd harmonics and the 2nd harmonics and other even harmonics were not present.

In Figure 6.8, a non-zero gradient is expected for a non-zero c_3 but this was not observed, showing the lack of cubic damping behaviour for the Bouc-Wen system. However, the value of the y-axis intersect was not zero, as seen in the similar plot for the polynomial model.

Figure 6.9, shows a similar result to that exhibited by the polynomial k_3 model in the previous chapter. A y-axis intersect exists showing that nonlinear stiffness behaviour was present in the Bouc-Wen model. The y-axis intersect can be taken from the higher frequency region where the line is constant as observed in the plot for cubic stiffness where the higher frequency shows the right value for k_3 in the previous chapter. However the value cannot be related to a single Bouc-Wen parameter and warrants further investigation.

For the cubic case, due to the presence of the y-axis intersect observed in the imaginary part plot in Figure 6.8 that was not previously seen in the similar polynomial plot in the previous chapter, an extension to the expressions is proposed. This is in order to fit the Bouc-Wen model to the polynomial model expression. The y-axis intersect relationship can be described as general Equation 6.4 extended from Equation 5.29 in the previous chapter or extended from Equation 5.30 to yield Equation 6.5 for an independent cubic system.

$$\Lambda_3(\omega) = \frac{4\mathrm{Y}(3\omega)}{\mathrm{X}(\omega)^3 H_1(3\omega) H_1(\omega)^3} + \frac{2H_1(\omega)H_2(\omega,\omega)[k_2+(i\omega)^2 c_2]}{\mathrm{X}\ (\omega)^3 H_1(\omega)^3} = -[k_3 + iP_{BW} + (i\omega)^3 c_3] \qquad (6.4)$$

$$\Lambda_3(\omega) = \frac{4\mathrm{Y}(3\omega)}{\mathrm{X}(\omega)^3 H_1(3\omega) H_1(\omega)^3} = -[k_3 + iP_{BW} + (i\omega)^3 c_3] \qquad (6.5)$$

where P_{BW} is a parameter or combination of parameters of the Bouc-Wen model

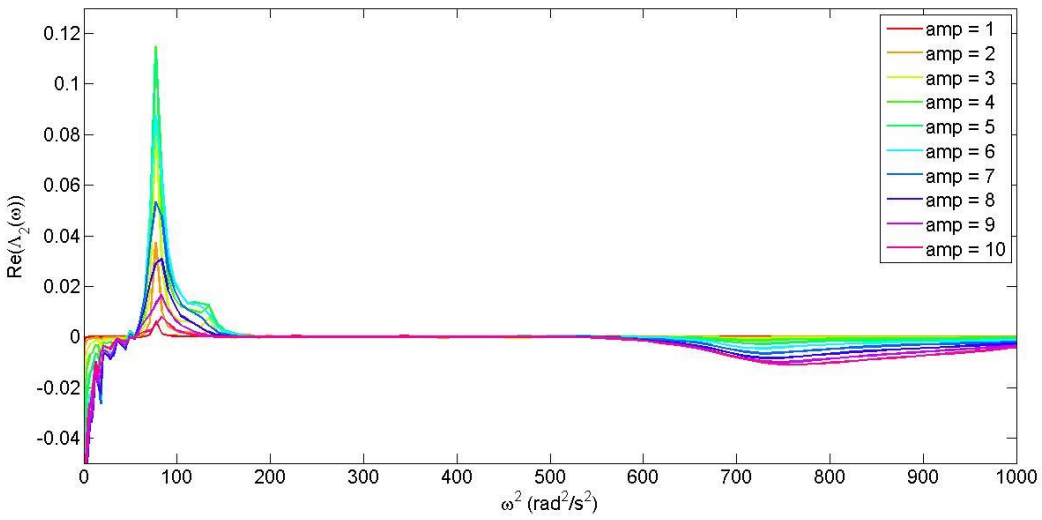

Figure 6.7: Plot of real part of $\Lambda_2(\omega)$ against ω^2 as reference to polynomial c_2 and k_2

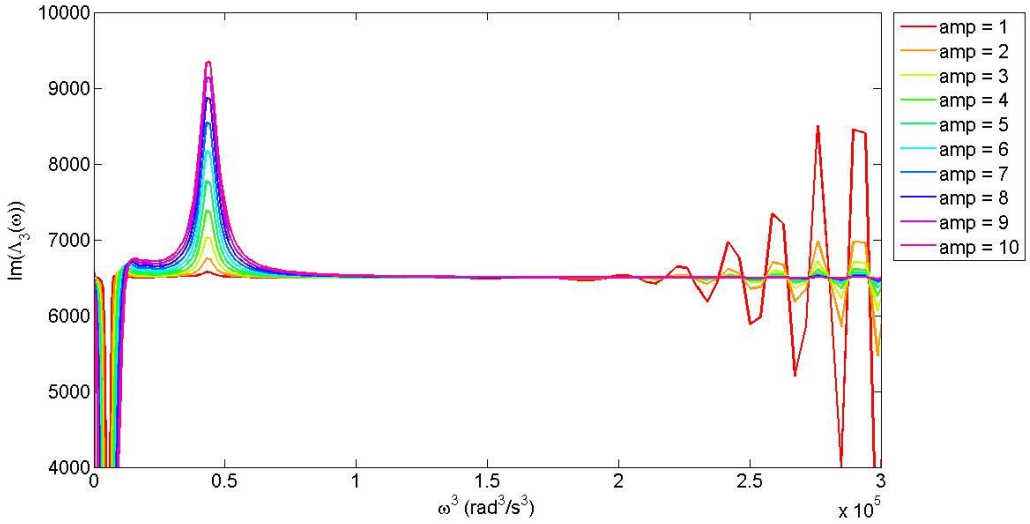

Figure 6.8: Plot of imaginary part of $\Lambda_3(\omega)$ against ω^3 as reference to polynomial c_3

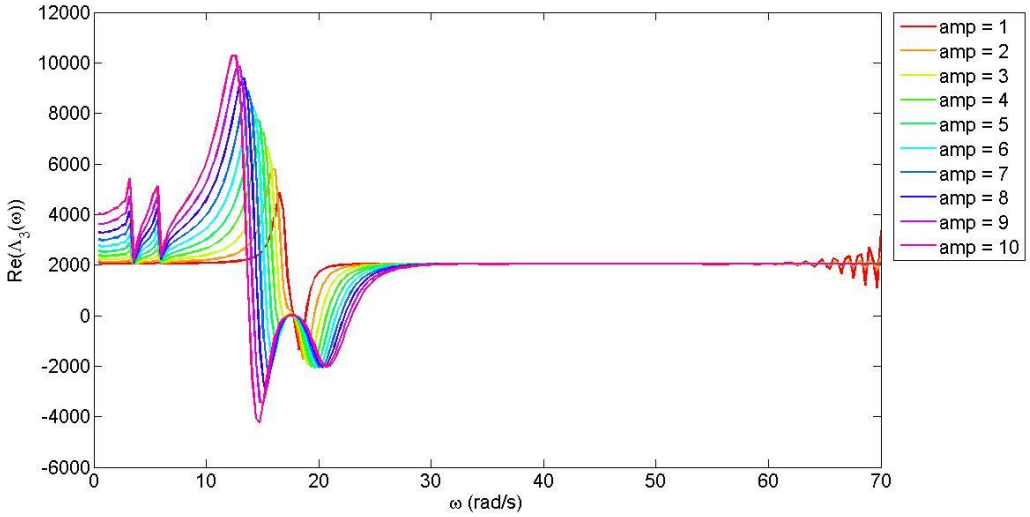

Figure 6.9: Plot of real part of $\Lambda_3(\omega)$ against ω as reference to polynomial k_3

6.4.1 Further investigation on nonlinear parameters

In order to better understand the relationship between the Volterra expressions plotted in the previous section and the Bouc-Wen model parameters, further investigations was conducted. Here for the plot of the imaginary part, only the ω was used instead of the ω^3 to make it easier to view the frequency range. This did not affect the plot as per Equation 6.4 due to the value being independent of the frequency. Observations were mainly made at the high frequency region since it was the best point for

estimation of the nonlinear parameters using the Volterra approximation for the Bouc-Wen system and polynomial system in the previous chapter.

Figure 6.10 and Figure 6.11 show the imaginary and real part plot of $\Lambda_3(\omega)$ against ω with varying parameter α value. At the higher frequency region it can be seen that α affected the $\Lambda_3(\omega)$ almost linearly for both the imaginary and real part. The relationship is inversely proportional, as α increases then $\Lambda_3(\omega)$ decreases until a value of zero at α=1.00, where the equation is linear and only a straight line is observed. This can be related directly to the equation since α is a ratio of the nonlinearity in the Bouc-Wen equation of motion.

Figure 6.12 and Figure 6.13 show the imaginary and real part plot of $\Lambda_3(\omega)$ against ω with varying parameter β value. In the imaginary part plot, an increase in β increases the y-axis intersect taken from the higher frequency region in the figure. With every 50 increase in parameter β, the $Im(\Lambda_3(\omega))$ value increases by around 2170 and this is very much linear up to a β value of 250 corresponding to a $Im(\Lambda_3(\omega))$ of 10880. However, the physical meaning of these values requires further investigation. Meanwhile in the real part plot, the change due to changing β is very small with an almost negligible increase. This appears to show that β does not contribute much to the nonlinear stiffness properties of the model.

For γ, the effect is the reverse from β. Figure 6.14 and Figure 6.15 show the imaginary and real part plot of $\Lambda_3(\omega)$ against ω with varying γ parameter value. Here the imaginary part plot shows that changes in parameter γ do not contribute to changes in the $Im(\Lambda_3(\omega))$ value. Parameter γ inhibits the nonlinear stiffness properties as seen in Figure 6.15 where an increase in parameter γ leads proportionately to an increase in the value of $Re(\Lambda_3(\omega))$. Every increasing parameter γ value of 20 increases the $Re(\Lambda_3(\omega))$ value by around 2040. This is almost the value of γ/α.

Figure 6.16 and Figure 6.17 sum up the varying value of β and γ with the imaginary and real part of $\Lambda_3(\omega)$ respectively. Parameter β only affects the imaginary part while parameter γ affects the real part for the y-axis intersect of the 3D plots.

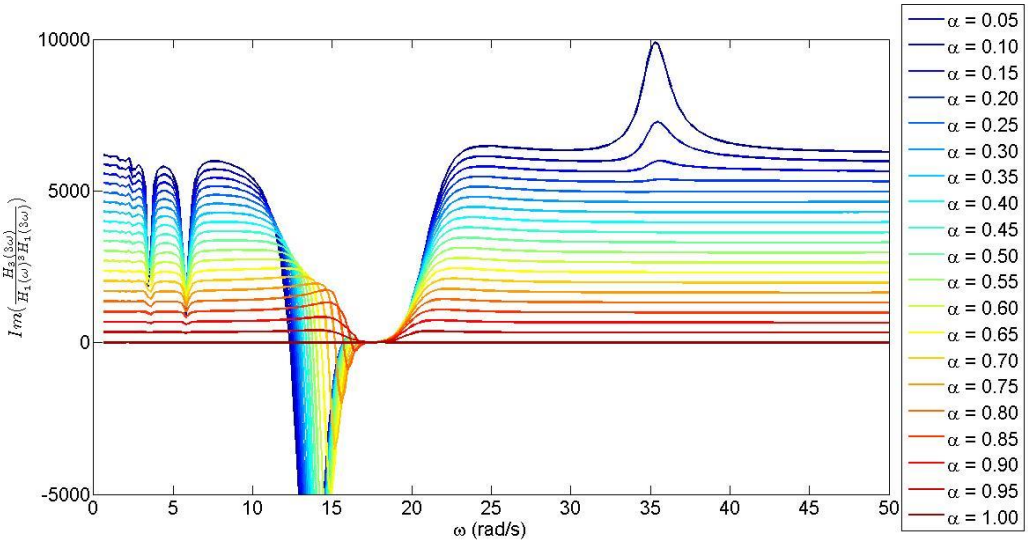

Figure 6.10: Plot of imaginary part of $\Lambda_3(\omega)$ against ω with varying α

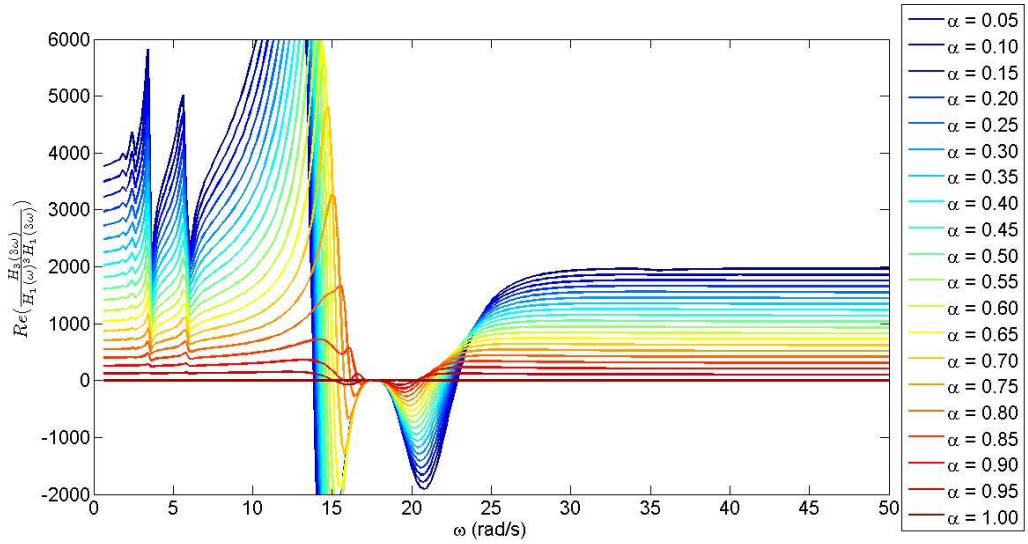

Figure 6.11: Plot of real part of $\Lambda_3(\omega)$ against ω with varying α

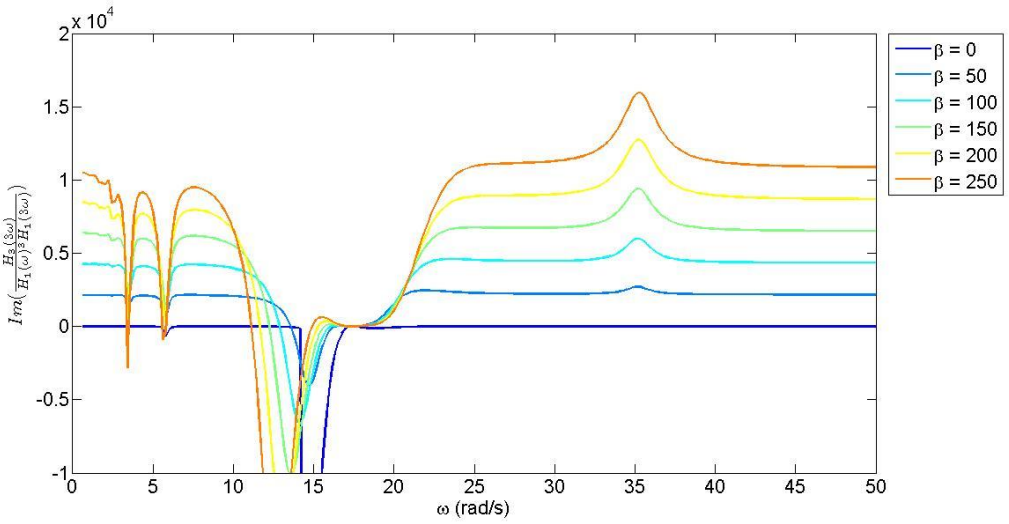

Figure 6.12: Plot of imaginary part of $\Lambda_3(\omega)$ against ω with varying β

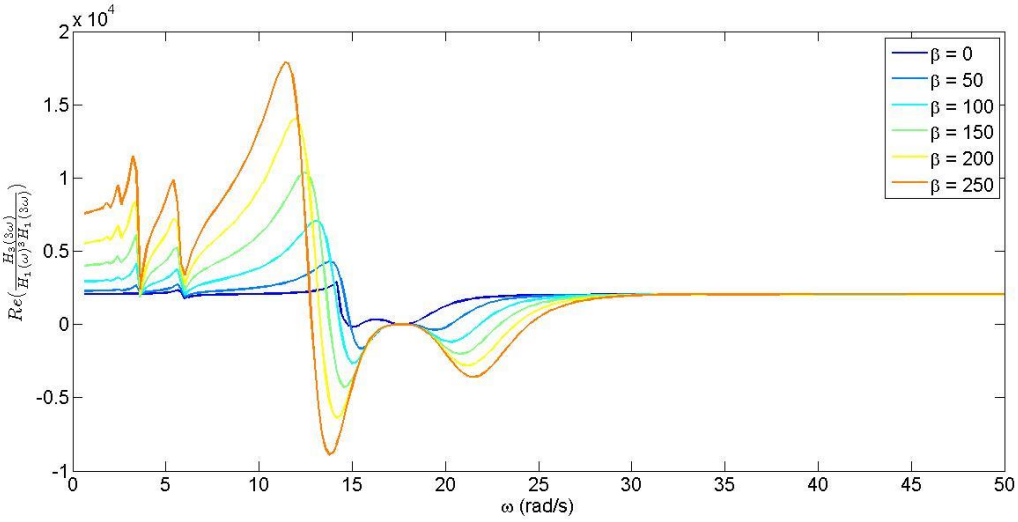

Figure 6.13: Plot of real part of $\Lambda_3(\omega)$ against ω with varying β

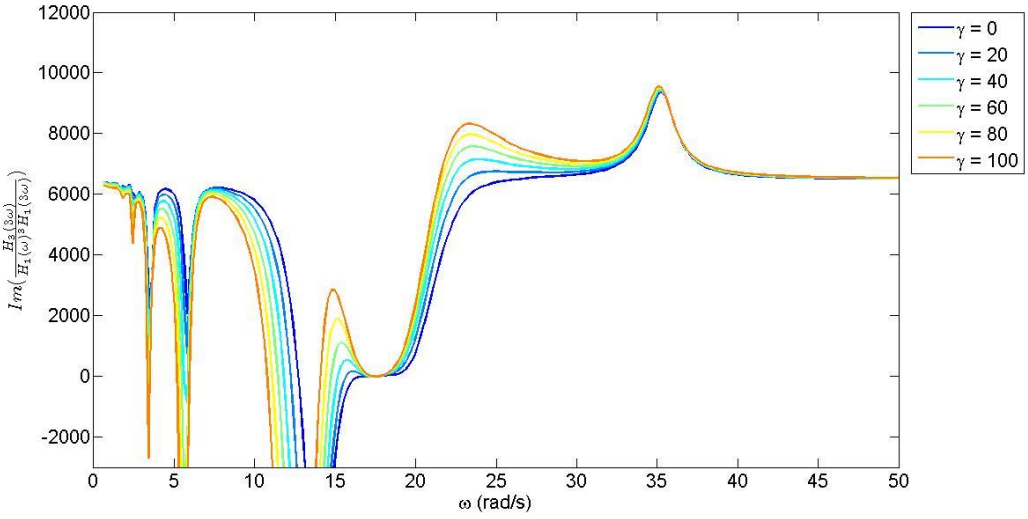

Figure 6.14: Plot of imaginary part of $\Lambda_3(\omega)$ against ω with varying γ

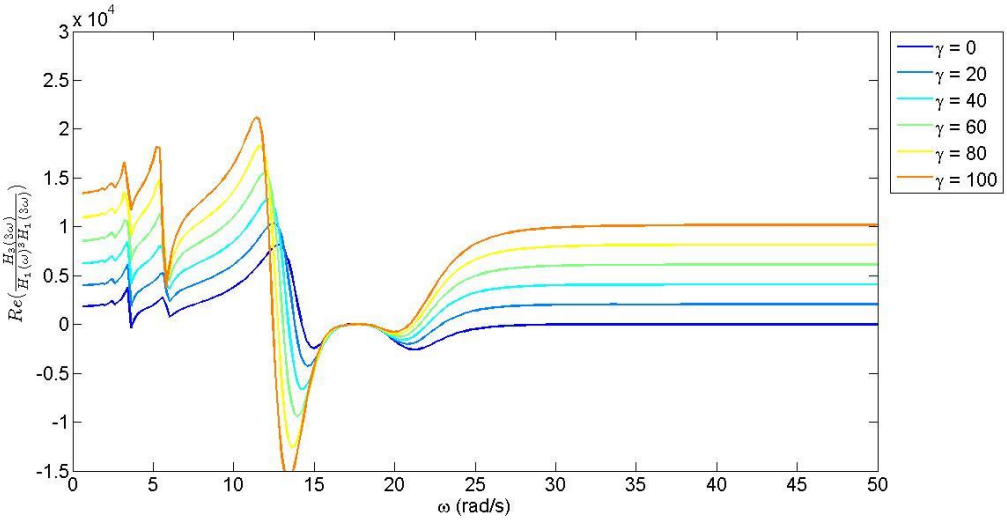

Figure 6.15: Plot of real part of $\Lambda_3(\omega)$ against ω with varying γ

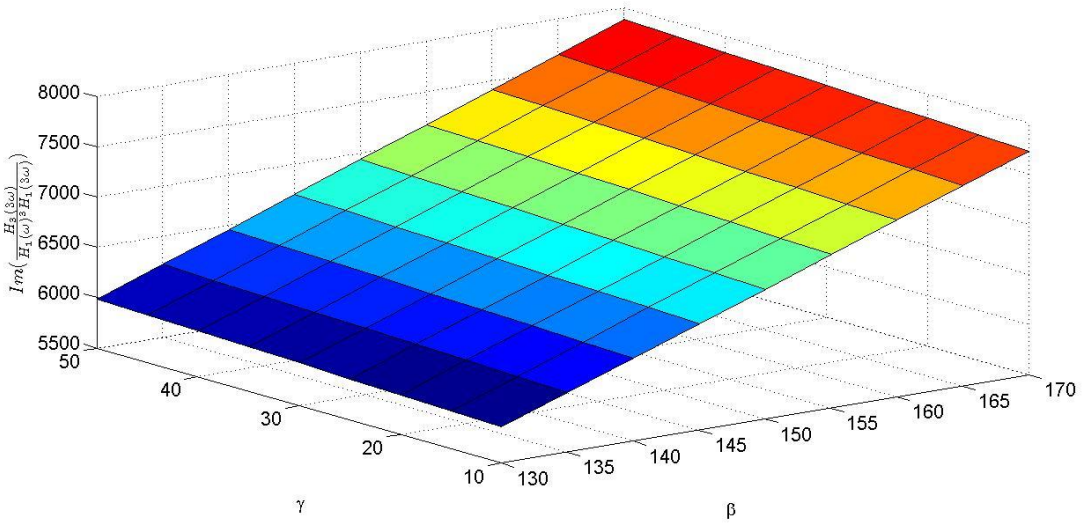

Figure 6.16: Plot of imaginary part of $\Lambda_3(\omega)$ against ω with varying β and γ

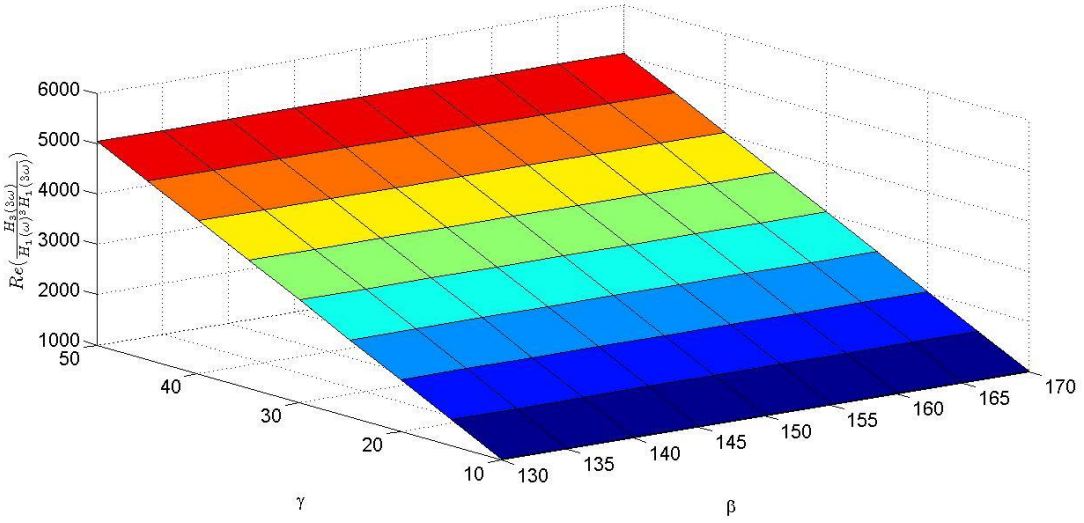

Figure 6.17: Plot of real part of $\Lambda_3(\omega)$ against ω with varying β and γ

6.5 **Estimation of nonlinear parameters in the presence of noise**

In the presence of noise, the estimation of the nonlinear parameter for the Bouc-Wen hysteresis model using the Volterra series approximation of the polynomial model would not give a good estimation. The effect of noise is very high especially at the higher frequency regions which are used as the parameter estimation points. Figure 6.18 to Figure 6.20 show the estimation plot with a noise level of 1E-7 times output RMS. Even at a very low noise level, the line deviations caused by noise effect is clearly seen.

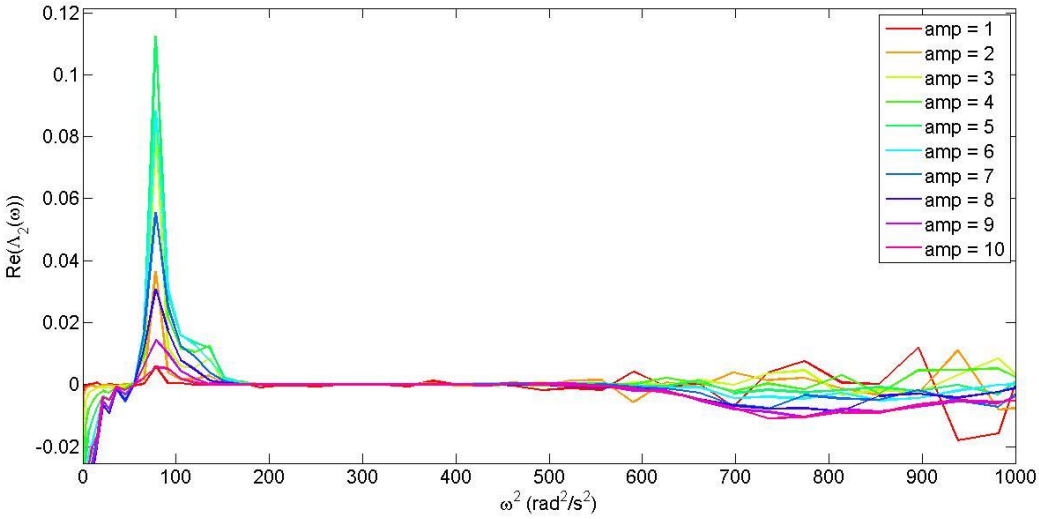

Figure 6.18: Plot of real part of $\Lambda_2(\omega)$ against ω^2 as reference to polynomial c_2 and k_2

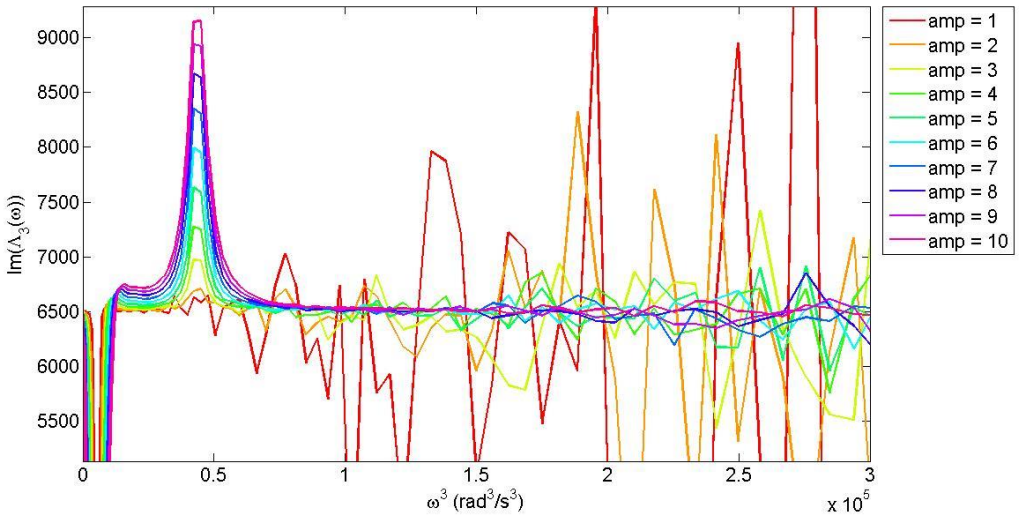

Figure 6.19: Plot of imaginary part of $\Lambda_3(\omega)$ against ω^3 as reference to polynomial c_3

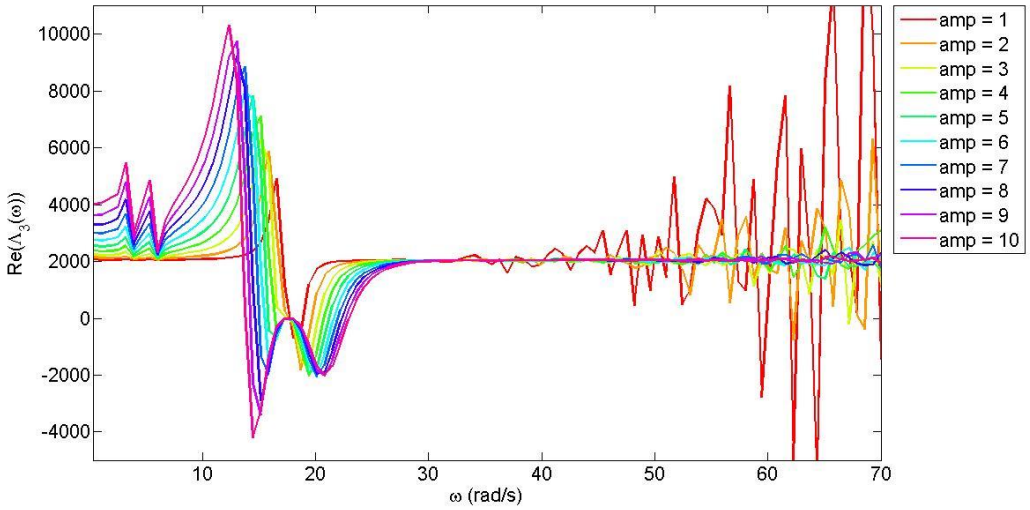

Figure 6.20: Plot of real part of $\Lambda_3(\omega)$ against ω as reference to polynomial c_2 and k_2

6.6 **Discussion**

In this chapter, the Volterra series approximation equation that was used for the polynomial model was applied to the Bouc-Wen model. Both the linear and nonlinear parameters of the Bouc-Wen model were investigated. This is a novel method of parameter estimation introduced in this thesis by using the Volterra series approximation to a nonlinear model with memory such as the Bouc-Wen model.

In the linear parameter investigation, it was shown that the linear parameters could be obtained without knowing the nonlinear parameter. This was similar to the polynomial model, where the linear parameters were independent of the nonlinear parameters and could be identified using the 1st harmonic Volterra series approximation. The linear parameters estimation for the Bouc-Wen model works well considering that the equation used was derived from harmonic probing of a polynomial model.

For the nonlinear parameters, using the equations from the polynomial Volterra series approximation showed that the specific system of the Bouc-Wen model used here was absent of the even harmonics, which agrees with the FFT observations of Chapter 2. Only the odd harmonics were seen, and only the nonlinear cubic stiffness behaviour could be observed directly. Nonlinear cubic damping related to

the polynomial c_3 was not observed although there were values in the imaginary part plot of the 3rd harmonics observed as a y-axis intersect to the plot.

Noise affected the linear parameter estimation in a similar manner to the polynomial model linear parameter estimation in the previous chapter. However, for the nonlinear parameter estimation, even in the presence of a very low level of noise, the estimation would yield inaccurate values. The effect of noise was too large and appeared mostly at the higher frequency regions where the estimation points were generally taken.

The relationship between the nonlinearity expression and the Bouc-Wen model parameters was investigated separately by varying the Bouc-Wen parameters and analysing the imaginary and real part plot. The parameter α that was the ratio in the equation of motion played a role in both the imaginary and the real part plot. The nonlinear stiffness property was shown to be associated with the parameter γ only, while parameter β was linked to the imaginary part plot that contributed to the y-axis intersect value found previously in the c_3 relationship proposed by Equation 6.4 and Equation 6.5 but of unknown physical properties. These equations are also a novel finding in this thesis which tries to relate the Bouc-Wen model to a well understood reference that is the nonlinear polynomial model.

The Volterra series approximation method has been used here to observe polynomial behaviour in the Bouc-Wen model of hysteresis. The assumption made that allows the linear parameters to be estimated independently from the nonlinear parameters may prove useful in model building. It would allow the Volterra series approximation to be used as an initial estimation method to only identify the linear parameters and reduce the number of parameters to be identified by another parameter identification algorithm. It could also be used to counter-check or as proofing of estimated linear parameters using the advantage of independent linear parameter estimation from the nonlinear parameters of a system.

Chapter 7

7 Conclusions and Future Work

7.1 **Conclusions**

The fitness-for-purpose of nonlinear system identification has been shown to be affected by the choice of input data. The first novelty in this thesis is the comparison of different levels and different types of input signal for generating simulated data with respect to the accuracy of nonlinear system identification.

Using an unsuitable amplitude level for the input signal in nonlinear system identification should be avoided. For the Bouc-Wen hysteretic system, a low amplitude level was repeatedly shown to produce a system that has a very low presence of nonlinear behaviour. The nonlinear behaviour was suppressed under these conditions due to the system not being sufficiently excited. This situation could easily lead to systems that are not exclusive, which means that the wrong predicted systems could be identified as having a good fit. In this thesis, almost all low amplitude systems investigated could be fitted with by a predicted linear system with a good MSE.

It was widely believed that random input covered a wide range of frequencies, hence this was the main reason the method was widely used in linear system identification. However it has been shown here that random input produces simulated training data which provides information which is not focused on bringing out the nonlinearity behaviour of a system. This linearisation effect originating from the use of random input has also been previously revealed in Section 2.6.5 of the book listed in reference [9]. Sinusoidal input on the other hand, results in higher nonlinear behaviour in a system due to the total energy distribution compared to the random input. It would be possible to relate between input and output by observing the system harmonics to further understand the system as well. However, this requires an operational frequency at the undamped natural frequency of the underlying linear system to trigger this useful feature - easily obtained in most cases but maybe a hindering obstacle for some purposes. Another observed input signal was the chirp input which resulted in higher nonlinear behaviour and with a relatively simple setup. With the requirement to specify only a sweeping range of frequencies, – which should cross the undamped natural frequency of the underlying linear system– chirp training data resulted in the best estimated parameter for the Bouc-Wen model using SADE.

The findings here can be related to the proposed framework for building a nonlinear model, where the importance of properly setting the correct specification of model performance requirements is stressed. By performing identification of the nonlinear system in the expected working environment, the system safety can be guaranteed which will enable the system to work as required in a similar environment. Cost is saved by not having to repeat experiments since the working environment is already known. Hence all scenarios would have been considered when planning the experiments for the system identification data. Cost can also be saved when the system needs to only work in a low excitation environment. With that knowledge there is no need to employ experiments for higher excitation or extreme conditions which may lead to increase the investigation cost.

The other conclusion that was made in this thesis was that by only relying on the MSE, a false confidence could be generated without identifying the correct system. The MSE could potentially be misleading when identifying a system based on *immature* training data. A proposed novel

Improvement Ratio, based on comparison with a linear fit MSE was used in this thesis to improve confidence against the linearisation effect. It helps to improve confidence by giving a comparative ratio of improvement for a predicted nonlinear system against a fitted linear system.

In this thesis an Improvement Ratio with a factor of 7 to 10 is considered low, whilst a factor of over 20 is considered as good for a clean signal without noise. The Improvement Ratio has been successfully shown for all input types without noise. In the presence of noise, the Improvement Ratio shows a clearer result. For a low level of amplitude estimation, the Improvement Ratio was small at around 0.001 to no improvement shown. This showed that whilst the MSE may indicate a good estimation has been obtained, the Improvement Ratio reveals that the training data had very little, if any, presence of nonlinearity. When using a higher amplitude excitation for the input, a better Improvement Ratio can be obtained, giving a higher confidence of the presence of nonlinearity in the training data which would allow for accurate estimation of the nonlinear parameters.

Another key observation concerning the identification of a system with noise is that only the systems that show linearisation would yield an Improvement Ratio as the other systems were not able to identify a linear system with a good fit. The fact that an Improvement Ratio is not obtained already gives high confidence that the system identified is exclusive and is the correct predicted nonlinear system. The Improvement Ratio used in this thesis has proved useful in increasing confidence in the parameter estimation. It could be useful especially in cases where the training data was not obtained by the researcher conducting their own experiments or the data is from an unknown input.

A Volterra series approximation was used on the polynomial model to identify system parameters. It has been shown that the linear and nonlinear parameters could be identified separately as both were independent of one another due to the assumptions made as part of the Volterra series approximation which separates the harmonic terms in the series. It was also shown that the presence of noise really affected the Higher-order FRF (HFRF) plot especially around the high frequency ranges. This caused a problem with the identification of the nonlinear parameters of the model.

The Volterra representation was then used for identifying the parameters of the Bouc-Wen model based on harmonic probing of the polynomial model. This is a novel method of nonlinear system identification whereby the Volterra series approximation is normally used for systems without memory. However, in this thesis the method was successfully used on a hysteretic system successfully to determine the physical properties of the nonlinear parameters. Some future work needs to be carried out to determine the exact values of the nonlinear parameters.

It has been shown for the Bouc-Wen hysteretic system that the linear parameters were all similarly independent from the nonlinear parameters. The specific Bouc-Wen model with the parameters used here was determined as showing only odd harmonics. The nonlinear parameter γ contributed to changes in the HFRF in the real plane and showed behaviour similar to that identified for cubic stiffness of a polynomial model. On the other hand, parameter β contributed only in the imaginary part of the Volterra HFRF, but without an associated physical attribute of the polynomial model. The assumption made that allows the linear parameter to be estimated independently from the nonlinear parameter may prove useful in the general practice of model building. It could allow the Volterra series approximation to be used as an initial estimation tool to only identify the linear parameters and reduce the number of parameters to be identified by another parameter identification algorithm. It could also be used to counter-check or as proofing of the estimated linear parameters using the advantage of independent linear parameter estimation from the nonlinear parameters of a system.

Other observations in the thesis include the use of extended data for nonlinear system identification using SADE. The use of extended data was determined to not contribute to any improvement in nonlinear system identification when working with data with noise. It was concluded that it is unnecessary to use a larger amount of sampling data for SADE compared to using a smaller amount of sampling data in the real environment where noise is always expected.

On the self-adaptive aspect of SADE, a pattern was observed which showed that SADE did improve the efficiency of the parameter estimation. The ability of SADE to change the preference of the mutation strategies and the values of the hyperparameters crossover ratio and mutation factor allowed

SADE to provide a faster and more efficient parameter estimation value. SADE initially adapts to search in a wider search space until it determines the best value. Then it starts to restrict the search to a more limited search space in order to allow higher accuracy estimation. Although the search space is restricted, the algorithm always allows some search in the full search space and forces this to be evaluated to avoid falling into false minima. This was done seamlessly when the algorithm was run and a similar behaviour observed every time the algorithm was used.

7.2 **Future Works**

The findings in this thesis are something that the author feels is important for the model building and system identification community. However some further work is warranted in order to produce a comprehensive guide to system identification.

Some immediate future works that could contribute to the findings here include investigating training data behaviour on other nonlinear models. The same method that was used here could be directly applied to compare the different training data with different nonlinear models. The results would be expected to either agree with the input choices given in this work, or give way to a guide on input selection for different types of nonlinearity.

Similarly it should be possible to work with different optimization algorithm choices and multi degrees-of-freedom (MDOF) system. The different optimisation algorithm could contribute to refining the Improvement Ratio value. A hybrid input type could also be incorporated, for example sinusoidal, chirp and random combinations with ascending amplitude. This would hopefully capture all the necessary system behaviour and this could result in a better predicted model.

A longer scale research could be dedicated to exploring an additional suitable reference or baseline model for the Improvement Ratio. This could result in extending the confidence level of system identification significantly rather than only relying on one measure of success.

The work on the Volterra series approximation could include generating equation for specific Bouc-Wen equations of motion to allow estimation of nonlinear parameters of the model. The use of other

Volterra kernels could also be explored since currently only the first term is used for estimation which results in much distortion in the estimation lines. With the use of more kernel terms, the distortion would be expected to reduce, which would result in more accurate predictions.

7.3 **Final remarks**

The larger idea behind this thesis was to lay out a best practice framework for nonlinear system identification as a guide for new users coming to the field, and to promote further discussion on the matter. Only some parts of the framework were discussed in this thesis which focussed on looking at the initial stages. The work here has shown that the selection of input for producing data for system identification is important for cost saving and to gain confidence in the predicted model. These were in terms of initial planning in setting up a proper aim of system identification or model building, obtaining proper training data for parameter estimation and finishing off with questioning the obtained predicted model obtained to determine its real meaning and whether it is representative of the real system that was identified. The main objective of system identification should be to have a reliable and fit-for-purpose predicted model that would be useful in the real environment.

With the predicted nonlinear model that results from identification using demanding data that really punishes optimisation mistakes and rewards the correct identification, it should be possible to have a higher confidence in the predicted model to be used in the real working environment and would have the confidence to determine the suitable range of operational conditions for the predicted model.

With the findings given here, the author hopes that this can promote further discussion on the matter. It is also a hope to see that this method can be further improved to be comprehensive, similar to the axioms used in structural health monitoring [76] and the acknowledged guide in neural network [77].

8 Bibliography

[1] D. Kimball, “The Nuclear Testing Tally,” 2015. [Online]. Available: https://www.armscontrol.org/factsheets/nucleartesttally.

[2] D. Kimball, “Nuclear Weapons: Who Has What at a Glance,” 2015. [Online]. Available: http://www.armscontrol.org/factsheets/Nuclearweaponswhohaswhat.

[3] “The Simulation Program,” *The Laser Megajoule*, 2016. [Online]. Available: http://www-lmj.cea.fr/en/simulation-program/index.htm.

[4] F. A. Ghaith and M. F. Haque, “Elastodynamic Modeling and Simulation of the AIRBUS A380 Wing,” in *Volume 8: 26th Conference on Mechanical Vibration and Noise*, 2014, vol. 8, p. V008T11A078.

[5] O. Nelles, *Nonlinear System Identification: From Classical Approaches to Neural Networks and Fuzzy Models*. Springer Science & Business Media, 2001.

[6] R. Strauss, *Neurobiological Models of the Central Complex and the Mushroom Bodies*. 2014.

[7] P. Lynch, “The origins of computer weather prediction and climate modeling,” *J. Comput. Phys.*, vol. 227, no. 7, pp. 3431–3444, Mar. 2008.

[8] Z. Toth and E. Kalnay, “Ensemble Forecasting at NCEP and the Breeding Method,” *Mon. Weather Rev.*, vol. 125, no. 12, pp. 3297–3319, Dec. 1997.

[9] K. Worden and G. R. Tomlinson, *Nonlinearity in Structural Dynamics - Detection, Identification and Modelling*. 2001.

[10] G. Kerschen, K. Worden, A. F. Vakakis, and J.-C. Golinval, “Past, present and future of nonlinear system identification in structural dynamics,” *Mech. Syst. Signal Process.*, vol. 20, no. 3, pp. 505–592, 2006.

[11] W. Heylen, S. Lammens, and P. Sas, *Modal Analysis Theory and Testing*. Leuven: KUL Press, 1997.

[12] S. R. Ibrahim and E. C. Mikulcik, “Time domain identification of standing wave parameters in gas piping systems,” *J. Sound Vib.*, vol. 60, no. 1, pp. 21–31, Sep. 1978.

[13] J. S. Juang and R. S. Pappa, “An eigensystem realization algorithm for modal parameter identification and model reduction,” *AIAA J. Guid. Control Dyn.*, vol. 12, pp. 620–627, 1985.

[14] P. Van Overschee and B. De Moor, *Subspace Identification for Linear Systems: Theory, Implementation, Applications*. Dordrecht, 1996.

[15] B. Peeters, H. Van Der Auweraer, and P. Guillaume, “The PolyMAX frequency domain method: a new standard for modal parameter estimation,” *Shock Vib.*, vol. 11, pp. 395–409, 2004.

[16] T. K. Caughey, “Equivalent linearisation techniques,” *J. Acoust. Soc. Am.*, vol. 35, pp. 1706–1711, 1963.

[17] M. F. Abdul Azeez and A. F. Vakakis, “Numerical and experimental analysis of a continuous overhung rotor undergoing vibro-impacts,” *Int. J. Non. Linear. Mech.*, vol. 34, no. 3, pp. 415–435, May 1999.

[18] E. A. Jackson, *Perspectives of Nonlinear Dynamics:* CUP Archive, 1992.

[19] R. L. Anderson, J. Harnad, and P. Winternitz, “Systems of ordinary differential equations with nonlinear superposition principles,” *Phys. D Nonlinear Phenom.*, vol. 4, no. 2, pp. 164–182, Jan. 1982.

[20] M. Gevers and L. Ljung, “Optimal experiment designs with respect to the intended model application,” *Automatica*, vol. 22, no. 5, pp. 543–554, Sep. 1986.

[21] S. F. Masri and T. K. Caughey, “A Nonparametric Identification Technique for Nonlinear Dynamic Problems,” *J. Appl. Mech.*, vol. 46, no. 2, pp. 433–447, 1979.

[22] M. Feldman, “NON-LINEAR FREE VIBRATION IDENTIFICATION VIA THE HILBERT TRANSFORM,” *J. Sound Vib.*, vol. 208, no. 3, pp. 475–489, Dec. 1997.

[23] T. Söderström and P. Stoica, *System identification*. Prentice Hall, 1989.

[24] L. Ljung and L. Guo, “Classical model validation for control design purposes,” *Math. Model. Syst.*, vol. 3, no. 1, pp. 27–42, Jan. 1997.

[25] K. Worden and G. Manson, “On the identification of hysteretic systems. Part I: Fitness landscapes and evolutionary identification,” *Mech. Syst. Signal Process.*, vol. 29, pp. 201–212, 2012.

[26] A. Mohd Mustafah, G. Manson, and K. Worden, “Identification of hysteretic systems using self-adaptive optimisation,” in *ISMA2012-USD2012 Conference*, 2012.

[27] C. R. Farrar and K. Worden, *Structural Health Monitoring [electronic resource] : A Machine Learning Perspective*. 2013.

[28] T. O`Shaughnessy, “Unemployment Hysteresis and Capacity,” University of Oxford, Department of Economics, Oct. 2001.

[29] S. Neaime and N. Colton, *Money and Finance in the Middle East: Missed Opportunities or Future Prospects*. Emerald Group Publishing, 2005.

[30] J. A. Ewings, “On hysteresis in the relation of strain to stress,” in *Advancement of Science, report of the 59th meeting*, 1890.

[31] S. Chikazumi, *Physics of magnetism*. New York: Wiley, 1964.

[32] A. (Augusto) Visintin, *Differential models of hysteresis*. Heidelberg ; New York: Springer-Verlag, 1994.

[33] X. Zhu and X. Lu, "Parametric identification of Bouc-Wen model and its application in mild steel damper modeling," in *Procedia Engineering*, 2011, vol. 14, pp. 318–324.

[34] G. C. Foliente, "Hysteresis Modeling of Wood Joints and Structural Systems," *J. Struct. Eng.*, vol. 121, no. 6, pp. 1013–1022, Jun. 1995.

[35] I. V. Kolin, V. G. Markov, T. I. Trifonova, and D. V. Shukhovtsov, "Hysteresis in the static aerodynamic characteristics of a curved-profile wing," *Tech. Phys.*, vol. 49, no. 2, pp. 263–266, Feb. 2004.

[36] F. Ikhouane, V. Mañosa, and J. Rodellar, "Dynamic properties of the hysteretic Bouc-Wen model," *Syst. Control Lett.*, vol. 56, no. 3, pp. 197–205, 2007.

[37] R. Bouc, "Forced Vibration of Mechanical Systems with Hysteresis," in *Proceedings of 4th Conference Nonlinear Oscillation*, 1967, p. 315.

[38] R. Bouc, "Mathematical model for hysteresis," 1971.

[39] Y.-K. Wen, "Method for Random Vibration of Hysteretic Systems," *J. Eng. Mech. Div.*, vol. 102, no. 2, pp. 249–263, 1976.

[40] T. T. Baber and Y.-K. Wen, "Random Vibration Hysteretic, Degrading Systems," *J. Eng. Mech. Div.*, vol. 107, no. 6, pp. 1069–1087, 1981.

[41] T. T. Baber and M. N. Noori, "Random Vibration of Degrading, Pinching Systems," *J. Eng. Mech.*, vol. 111, no. 8, pp. 1010–1026, Aug. 1985.

[42] N. M. Kwok, Q. P. Ha, M. T. Nguyen, J. Li, and B. Samali, "Bouc-Wen model parameter identification for a MR fluid damper using computationally efficient GA," *ISA Trans.*, vol. 46, no. 2, pp. 167–179, 2007.

[43] S. Talatahari, A. Kaveh, and N. Mohajer Rahbari, "Parameter identification of Bouc-Wen model for MR fluid dampers using adaptive charged system search optimization," *J. Mech. Sci. Technol.*, vol. 26, no. 8, pp. 2523–2534, 2012.

[44] W. Wang, P.-Q. Xia, and C.-Y. Liu, "Experimental modeling of MR dampers based on Bouc-Wen function," *Zhendong Gongcheng Xuebao/Journal Vib. Eng.*, vol. 19, no. 3, pp. 296–301, 2006.

[45] O. Gomis-Bellmunt, F. Ikhouane, and D. Montesinos-Miracle, "Control of Bouc-Wen hysteretic systems: Application to a piezoelectric actuator," in *2008 13th International Power Electronics and Motion Control Conference, EPE-PEMC 2008*, 2008, pp. 1670–1675.

[46] M. Rakotondrabe, “Bouc-Wen modeling and inverse multiplicative structure to compensate hysteresis nonlinearity in piezoelectric actuators,” *IEEE Trans. Autom. Sci. Eng.*, vol. 8, no. 2, pp. 428–431, 2011.

[47] S. Xiao and Y. Li, “Dynamic compensation and control for piezoelectric actuators based on the inverse Bouc–Wen model,” *Robot. Comput. Integr. Manuf.*, vol. 30, no. 1, pp. 47–54, 2014.

[48] H. Zhang, G. C. Foliente, Y. Yang, and F. Ma, “Parameter identification of inelastic structures under dynamic loads,” *Earthq. Eng. Struct. Dyn.*, vol. 31, no. 5, pp. 1113–1130, May 2002.

[49] T. Sireteanu, M. Giuclea, and A. M. Mitu, “Identification of an extended Bouc–Wen model with application to seismic protection through hysteretic devices,” *Comput. Mech.*, vol. 45, no. 5, pp. 431–441, Jan. 2010.

[50] M. V. Sivaselvan and A. M. Reinhorn, “Hysteretic Models for Deteriorating Inelastic Structures,” *J. Eng. Mech.*, vol. 126, no. 6, pp. 633–640, Jun. 2000.

[51] A. E. Charalampakis and V. K. Koumousis, “A Bouc–Wen model compatible with plasticity postulates,” *J. Sound Vib.*, vol. 322, no. 4–5, pp. 954–968, May 2009.

[52] “El Centro Earthquake.” [Online]. Available: http://www.vibrationdata.com/elcentro.htm. [Accessed: 12-Nov-2015].

[53] A. K. Chopra and E. E. R. Institute, *Dynamics of structures, a primer*. Earthquake Engineering Research Institute, 1995.

[54] F.-G. Fan and G. Ahmadi, “Seismic responses of secondary systems in base-isolated structures,” *Eng. Struct.*, vol. 14, no. 1, pp. 35–48, Jan. 1992.

[55] “Map of Strong Motion Stations for El Centro Earthquake of 18 May 1940.” [Online]. Available: http://www.strongmotioncenter.org/cgi-bin/CESMD/iqrStationMap.pl?ID=ElCentro_18May1940.

[56] K. Worden and W. E. Becker, “On the identification of hysteretic systems. Part II: Bayesian sensitivity analysis and parameter confidence,” *Mech. Syst. Signal Process.*, vol. 29, pp. 213–227, 2012.

[57] C. M. Bishop, *Neural Networks for Pattern Recognition*. Oxford: Clarendon Press, 1995.

[58] V. Volterra, *Theory of functionals and of integral and integro-differential equations*. 1959.

[59] N. Wiener, “Response of a Nonlinear Device to Noise,” 1942.

[60] J. F. Barrett, “The Use of Functionals in the Analysis of Non-linear Physical Systems†,” *J. Electron. Control*, vol. 15, no. 6, pp. 567–615, Dec. 1963.

[61] Bedrosian E and Rice S. O., “Output properties of Volterra systems (nonlinear systems with memory) driven by harmonic and Gaussian inputs,” *Proceedings of the IEEE*, vol. 59, no. 12. pp. 1688–1707, 1971.

[62] S. Boyd, Y. Tang, and L. Chua, “Measuring Volterra kernels,” *IEEE Trans. Circuits Syst.*, vol. 30, no. 8, 1983.

[63] D. M. Storer and G. R. Tomlinson, “Higher Order Frequency Response Functions and their relation to practical structures,” in *Proceedings of the International Modal Analysis Conference - IMAC*, 1991, vol. 2, pp. 1206–1214.

[64] J. F. Barrett, “The Use of Volterra Series to Find Region of Stability of a Non-linear Differential Equation†,” *Int. J. Control*, vol. 1, no. 3, pp. 209–216, Mar. 1965.

[65] G. Palm and T. Poggio, “The Volterra Representation and the Wiener Expansion: Validity and Pitfalls,” *SIAM J. Appl. Math.*, vol. 33, no. 2, pp. 195–216, 1977.

[66] G. R. Tomlinson, G. Manson, and G. M. Lee, “A Simple Criterion for Establishing an Upper Limit to the Harmonic Excitation Level of the Duffing Oscillator using the Volterra Series,” *J. Sound Vib.*, vol. 190, no. 5, pp. 751–762, Mar. 1996.

[67] Z. K. Peng and Z. Q. Lang, “On the convergence of the Volterra-series representation of the Duffing’s oscillators subjected to harmonic excitations,” *J. Sound Vib.*, vol. 305, no. 1–2, pp. 322–332, 2007.

[68] L. M. Li and S. A. Billings, “Analysis of nonlinear oscillators using Volterra series in the frequency domain,” *J. Sound Vib.*, vol. 330, no. 2, pp. 337–355, Jan. 2011.

[69] P. Z. Marmarelis and V. Z. Marmarelis, *Analysis of physiological systems : the white-noise approach*. New York: Plenum Press, 1978.

[70] A. Chatterjee, “Identification and parameter estimation of a bilinear oscillator using Volterra series with harmonic probing,” *Int. J. Non. Linear. Mech.*, vol. 45, no. 1, pp. 12–20, Jan. 2010.

[71] T. Wu and A. Kareem, “Simulation of nonlinear bridge aerodynamics: A sparse third-order Volterra model,” *J. Sound Vib.*, vol. 333, no. 1, pp. 178–188, Jan. 2014.

[72] T. Wu and A. Kareem, “A nonlinear analysis framework for bluff-body aerodynamics: A Volterra representation of the solution of Navier-Stokes equations,” *J. Fluids Struct.*, vol. 54, pp. 479–502, Apr. 2015.

[73] Y. Kim, “Prediction of the dynamic response of a slender marine structure under an irregular ocean wave using the NARX-based quadratic Volterra series,” *Appl. Ocean Res.*, vol. 49, pp. 42–56, Jan. 2015.

[74] S. A. Billings and K. M. Tsang, “Spectral analysis for non-linear systems, Part I: Parametric non-linear spectral analysis,” *Mech. Syst. Signal Process.*, vol. 3, no. 4, pp. 319–339, Oct. 1989.

[75] S. A. Billings and K. M. Tsang, “Spectral analysis for non-linear systems, Part II: Interpretation of non-linear frequency response functions,” *Mech. Syst. Signal Process.*, vol. 3, no. 4, pp. 341–359, Oct. 1989.

[76] K. Worden, C. R. Farrar, G. Manson, and G. Park, “The fundamental axioms of structural health monitoring,” *Proc. R. Soc. A Math. Phys. Eng. Sci.*, vol. 463, no. 2082, pp. 1639–1664, Jun. 2007.

[77] L. Tarassenko, *A guide to neural computing applications*. London: Arnold, 1998.

[78] K. Worden and G. R. Tomlinson, “Experimental study of a number of nonlinear SDOF systems using the restoring force surface method,” in *Proceedings of the International Modal Analysis Conference - IMAC*, 1991, vol. 1, pp. 757–764.

[79] C. M. Richards and R. Singh, “IDENTIFICATION OF MULTI-DEGREE-OF-FREEDOM NON-LINEAR SYSTEMS UNDER RANDOM EXCITATIONS BY THE ‘REVERSE PATH’ SPECTRAL METHOD,” *J. Sound Vib.*, vol. 213, no. 4, pp. 673–708, Jun. 1998.

[80] D. E. Adams and R. J. Allemang, “A FREQUENCY DOMAIN METHOD FOR ESTIMATING THE PARAMETERS OF A NON-LINEAR STRUCTURAL DYNAMIC MODEL THROUGH FEEDBACK,” *Mech. Syst. Signal Process.*, vol. 14, no. 4, pp. 637–656, Jul. 2000.

[81] K. Price and R. Storn, “Differential Evolution,” *Dr. Dobb’s Journal*, 1997. [Online]. Available: http://www.drdobbs.com/database/differential-evolution/184410166. [Accessed: 03-Jun-2015].

[82] A. K. Qin and P. N. Suganthan, “Self-adaptive Differential Evolution Algorithm for Numerical Optimization,” in *2005 IEEE Congress on Evolutionary Computation*, 2005, vol. 2, pp. 1785–1791.

[83] J. Kennedy and R. Eberhart, “Particle Swarm Optimization,” *Proc. IEEE Int. Conf. Neural Networks IV*, pp. 1942–1948, 1995.

[84] Y. Shi and R. Eberhart, “A modified particle swarm optimizer,” in *1998 IEEE International Conference on Evolutionary Computation Proceedings. IEEE World Congress on Computational Intelligence (Cat. No.98TH8360)*, 1998, pp. 69–73.

[85] M. Dorigo, “Optimization, Learning and Natural Algorithms,” *Ph.D. Thesis, Politec. di Milano, Italy*, 1992.

[86] M. Dorigo, V. Maniezzo, and A. Colorni, “Ant system: optimization by a colony of cooperating agents.,” *IEEE Trans. Syst. Man. Cybern. B. Cybern.*, vol. 26, no. 1, pp. 29–41, Jan. 1996.

[87] N. Perisic, P. L. Green, K. Worden, and P. H. Kirkegaard, *Topics in Modal Analysis, Volume 7*. New York, NY: Springer New York, 2014.

[88] R. Storn and K. Price, “Differential Evolution – A Simple and Efficient Heuristic for global Optimization over Continuous Spaces,” *J. Glob. Optim.*, vol. 11, no. 4, pp. 341–359.

[89] K. Price, R. Storn, and J. Lampinen, *Differential Evolution: A Practical Approach to Global Optimization*. Springer, 2005.

[90] W. L. Price, “Global optimization by controlled random search,” *J. Optim. Theory Appl.*, vol. 40, no. 3, pp. 333–348, Jul. 1983.

[91] J. A. Nelder and R. Mead, “A Simplex Method for Function Minimization,” *Comput. J.*, vol. 7, no. 4, pp. 308–313, 1965.

[92] L. S. Nelson and D. M. Olsson, “The Nelder-Mead Simplex Procedure for Function Minimization,” *Technometrics*, vol. 17, no. 1, pp. 45–51, 1975.

[93] H.-P. P. Schwefel, *Evolution and Optimum Seeking: The Sixth Generation*. John Wiley & Sons, Inc., 1993.

[94] J. Lampinen and I. Zelinka, “Mechanical engineering design optimization by differential evolution,” in *New ideas in optimization*, D. Corne, M. Dorigo, and F. Glover, Eds. McGraw-Hill Ltd., UK, 1999, pp. 127–146.

[95] J. Vesterstrom and R. Thomsen, “A comparative study of differential evolution, particle swarm optimization, and evolutionary algorithms on numerical benchmark problems,” in *Proceedings of the 2004 Congress on Evolutionary Computation (IEEE Cat. No.04TH8753)*, 2004, vol. 2, pp. 1980–1987.

[96] T. Krink and S. Paterlini, “Differential evolution and particle swarm optimisation in partitional clustering,” in *Proceedings of the 2004 Congress on Evolutionary Computation*, 2004.

[97] R. Joshi and A. C. Sanderson, “Minimal representation multisensor fusion using differential evolution,” *IEEE Trans. Syst. Man, Cybern. - Part A Syst. Humans*, vol. 29, no. 1, pp. 63–76, 1999.

[98] B. Růžek and M. Kvasnička, “Differential Evolution Algorithm in the Earthquake Hypocenter Location,” *Pure Appl. Geophys.*, vol. 158, no. 4, pp. 667–693, Apr. 2001.

[99] R. K. Ursem and P. Vadstrup, “Parameter identification of induction motors using differential evolution,” in *The 2003 Congress on Evolutionary Computation, 2003. CEC ’03.*, 2003, vol. 2, pp. 790–796.

[100] M. J. Reddy and D. N. Kumar, “Multiobjective Differential Evolution with Application to Reservoir System Optimization,” *J. Comput. Civ. Eng.*, vol. 21, no. 2, pp. 136–146, Mar. 2007.

[101] H. Yousefi, H. Handroos, and A. Soleymani, “Application of Differential Evolution in system identification of a servo-hydraulic system with a flexible load,” *Mechatronics*, vol. 18, no. 9, pp. 513–528, Nov. 2008.

[102] N. Henderson, W. F. Sacco, N. E. Barufatti, and M. M. Ali, “Calculation of Critical Points of Thermodynamic Mixtures with Differential Evolution Algorithms,” *Ind. Eng. Chem. Res.*, vol. 49, no. 4, pp. 1872–1882, Feb. 2010.

[103] J. Novo, J. Santos, and M. G. Penedo, “Multiobjective differential evolution in the optimization of topological active models,” *Appl. Soft Comput.*, vol. 13, no. 6, pp. 3167–3177, Jun. 2013.

[104] S. Talatahari, A. H. Gandomi, X.-S. Yang, and S. Deb, “Optimum design of frame structures using the Eagle Strategy with Differential Evolution,” *Eng. Struct.*, vol. 91, pp. 16–25, May 2015.

[105] V. L. Huang, A. K. Qin, and P. N. Suganthan, “Self-adaptive Differential Evolution Algorithm for Constrained Real-Parameter Optimization,” in *2006 IEEE International Conference on Evolutionary Computation*, 2006, pp. 17–24.

[106] R. Gämperle, S. D. Müller, and P. Koumoutsakos, “A Parameter Study for Differential Evolution,” in *WSEAS Int. Conf. on Advances in Intelligent Systems, Fuzzy Systems, Evolutionary Computation*, 2002, pp. 293–298.

[107] J. Brest, V. Zumer, and M. S. Maucec, “Self-Adaptive Differential Evolution Algorithm in Constrained Real-Parameter Optimization,” in *2006 IEEE International Conference on Evolutionary Computation*, 2006, pp. 215–222.

Appendix A

Differential Evolution

Parameter estimation for nonlinear models can be conducted via many methods that have been discussed in much of the literature. Some examples in the literature are [21], [22], [78], [79] and [80]; a more general description concerning some of the methods can be found in [10]. The best approach for one type of nonlinearity may often be inapplicable to many other types of nonlinearity. For simple problems which have only one local minimum or maximum, a gradient-based method may be the most applicable. This method will iteratively find the minimum, depending on the set conditions. However, when faced with a more complex problem with multiple local minima or maxima with many flat surfaces in the search space, a simple gradient based method may be insufficient. Here, the use of population-based algorithms is usually more successful. Some examples of established methods of population based optimization are differential evolution [81], [82], particle swarm optimization [83], [84] and ant colony optimisation [85], [86].

In this thesis, the differential evolution (DE) method is used as the optimisation algorithm. DE is an algorithm which is based on the Darwinian evolution principle with the fundamentals of natural selection, namely, mutation, crossover and survival of the fittest. It is a population based method with multiple starting points that can cater for the optimisation of a multi modal problem. Since the Bouc-Wen model used in this thesis is a nonlinear model, a simple linear estimation algorithm would not suffice. The DE algorithm had been used successfully in many academic papers with a wide range of applications and is relatively simple to use and relatively easy to code using Matlab. The author and the Dynamic Research Group at University of Sheffield have also had previous experience in using the differential evolution algorithm [26], [25], [87].

The Differential Evolution algorithm was originally proposed by Storn and Price [88] and it is well explained in their book [89] with example application of DE on 12 subjects. Since the introduction in 1995[88][88][88][88][87][87][86][85][85][85], DE is very well accepted and has been proven in competitions such as IEEE's International Contest on Evolutionary Optimization (ICEO) over the two following years.

DE works by having multiple trial vectors all over the search space termed as parent vectors in this thesis. Then another set of random population of vector is selected from the current population. The random vectors are then mutated or recombined. Unlike Controlled Random Search [90] and Nelder-Mead [91], [92] which uses reflections and Evolution Strategies [93], which uses a predefined probability density function, DE uses a scaled difference of two randomly generated trial vectors. These random vectors are then further crossed with the initial parent vector. The random vectors and parent vectors are then compared via objective functions and the winners move on to be the next generation parent vectors. This is illustrated more clearly in figure A.1.

DE can be found in much of the literature since its introduction. This includes the performance evaluation of DE, comparative studies of DE against other optimisation algorithms and the application of DE in many fields of research. One example of a performance assessment study is in Lampinen and Zelinka [94] in 1999, who compared DE with ten other optimisation algorithms. Three test problems were set up for a gear train, pressure vessel and coil spring. DE performed very well posting new alternative solutions for the gear train problem. DE also posted the best result for three cases of the pressure vessel variations and beating the previous best objective function value for the coil spring problem.

Some comparative studies of DE have compared DE with other optimization techniques such as particle swarm optimisation (PSO) and the Genetic Algorithm (GA). Such literature includes [95] where DE was quoted as outstanding, reliable, robust and easy to manipulate while in [96], DE was found to be superior on the harder test problems.

DE has also been applied in many fields of research with new publications being published every year. There are too many to be listed here in this thesis. Some examples are selected from 1999 to 2015. In [97], DE was used successfully for analysing information on visual and tactile sensors for sensing object shape and orientation. In [98], an earthquake epicentre was found using DE from the seismographic data reported by multiple stations. DE was also used in parametric identification of two induction motor models in [99]. In [100], the ability of DE in multi-objective interdependence

problems was utilised in a reservoir system optimization problem. An agreeable solution between a simulated and a real system was found using DE in applications for a servo-hydraulic system with a flexible load as shown in [101]. DE was also shown to be able to find multiple solutions in the prediction of critical thermodynamic mixtures of different petroleum fluids in [102].

Some new DE variants and hybrids have also been introduced. In [103], for the optimisation of topological active nets (TAN), a type of deformable model was introduced which can be solved by minimisation of objective functions. DE was incorporated with other well established optimisation algorithms as a hybrid optimisation algorithm that resulted in faster search with minimised initial decisions. In [104], a more recent paper published in 2015 DE was combined with the Eagle Strategy as ES-DE, in the minimisation of steel frame weight. A variant used in this thesis was the Self-Adaptive Differential Evolution introduced in [105] which allows multiple strategy and adaptation of hyperparameters of the original DE.

The procedure with the evolution strategy that was proposed initially is illustrated in Figure A.1. DE was based on the fundamentals of biologically inspired natural selection i.e. mutation, crossover and survival of the fittest. DE works by evolving a parent matrix of potential solutions using a mutation strategy and mutation factor, Fr (where $0 < Fr < 1$). The parameters from both the parent matrix and mutant matrix are combined by using a crossover ratio, Cr, thus creating a more diverse trial matrix. Vectors from the parent matrix or the trial matrix are then selected on lowest objective function value calculated by a normalised mean-square error between the actual response and the response using the predicted parameters. This is repeated every generation until a suitably low objective function value is achieved or until a maximum number of generations have been reached.

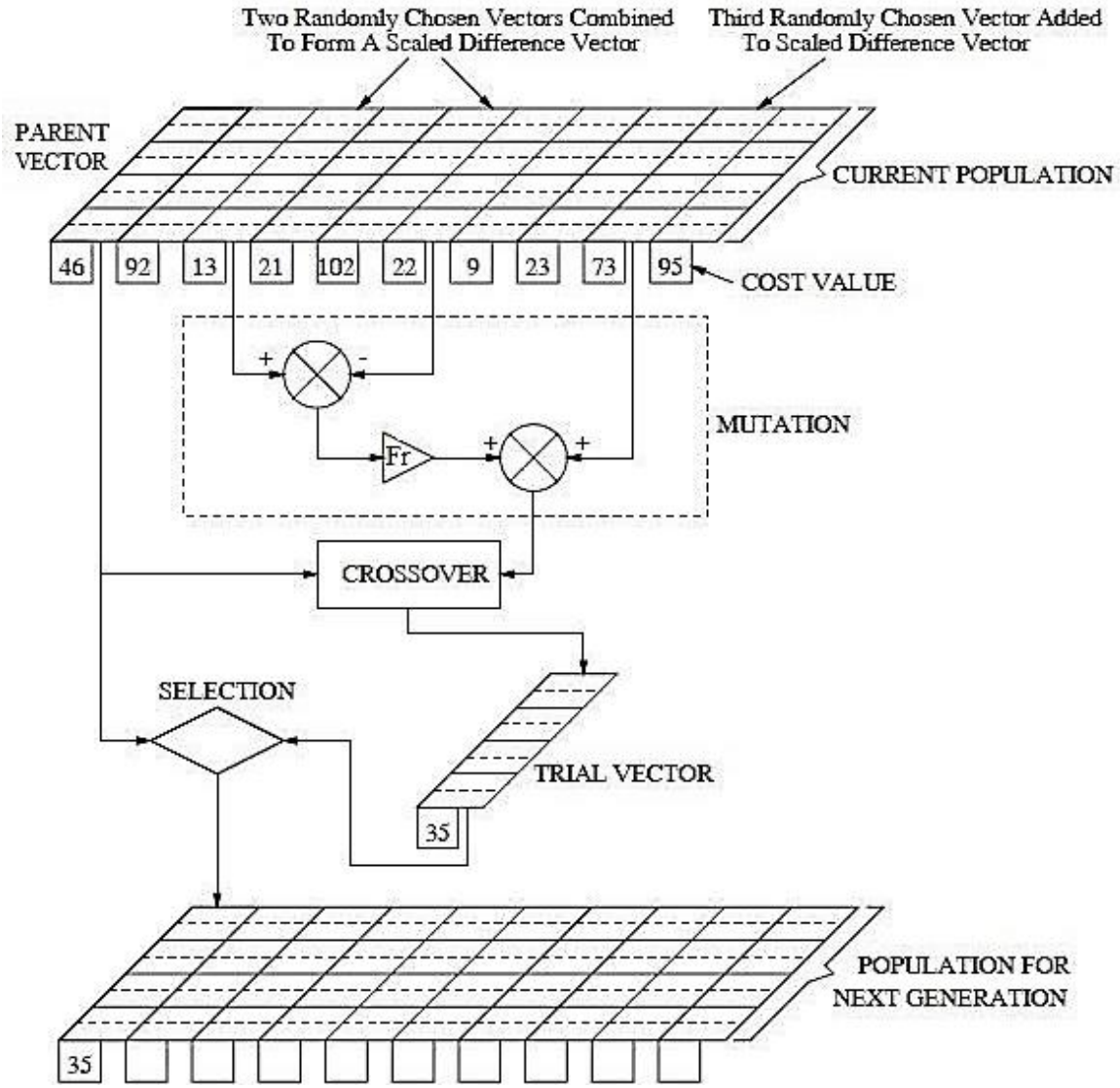

Figure A.1: Schematic of Differential Evolution with Rand/1 Strategy.

In [81], DE was initially introduced with only one strategy which was Rand/1 that can also be seen illustrated in Figure A.1. In the paper, for DE, some starting values or hyperparameters have to be determined before running the algorithm. These are the population size, mutation factor (*Fr*) and crossover ratio (*Cr*). A suggested optimum value for population size is 5 times the dimensions. The maximum value for *Fr* was empirically determined to be 1.2. However the optimum value was suggested to be between 0.4 to 1.0. Since *Fr* and *Cr* must be determined beforehand, it was suggested that the user tries different value of *Fr* and *Cr* to determine the suitable value to be used for any function.

DE works by evolving a parent matrix of potential solutions using a mutation strategy and mutation factor to create a mutant matrix. The parameters from both the parent matrix and mutant matrix are then pooled by a crossover ratio to generate a more diverse trial matrix. Vectors from the parent matrix or the trial matrix are then evaluated through the model to be identified to obtain the model response. Selection is then made based on an objective function value calculated by a normalised mean-square error between the system's real response of the system and the predicted system response (parent and trial response). The objective function could be something that is to be minimised or maximised depending on the system. This thesis uses the minimisation objective function. This is repeated every generation until a suitably low objective function value is achieved or until a maximum number of generations have been reached, whichever comes first.

The process flow for DE is given in Figure A.2 and explained in the following sections.

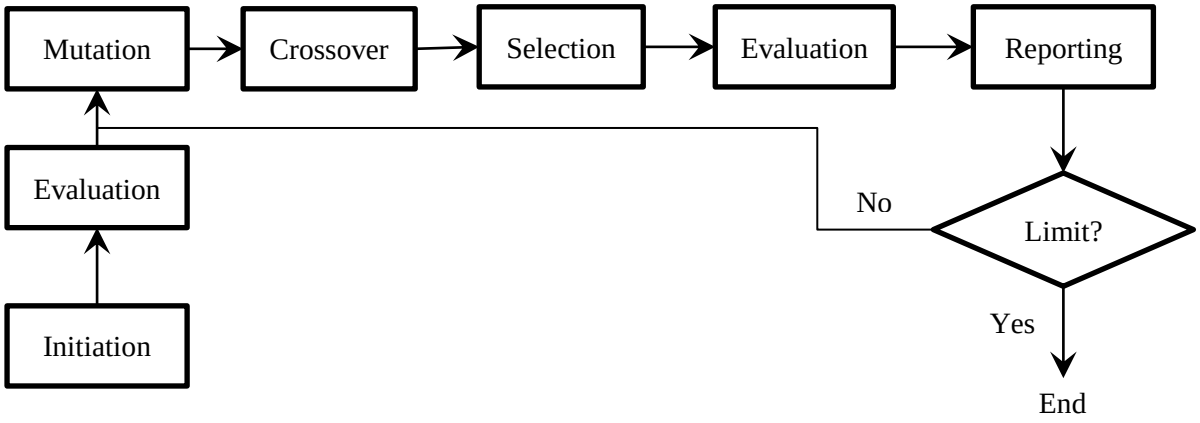

Figure A.2: Differential Evolution process flow

A.1 Initiation

Initially a parent matrix of a population of *N D*-dimensional vectors is generated randomly within a lower and upper limit for each of the parameters to be identified. The value of D depends on the number of parameters to be identified and the value will vary depending on the model itself. The upper and lower limit is usually set for a known system by physical limitations. For an unknown system where parameters cannot be related to a physical attributes or physical limitations, this can be estimated to capture the system optimum. The algorithm will still work even when the lower and

upper limit are not set, however the process will be expected to take a longer time to find the optimum value. This range of lower and upper limits can be set to restrict the search space if desired. This will contain the algorithm to search only within the lower and upper limit and will return the border value whenever the limit is breached. For the classic Bouc-Wen model the parent matrix will have D = 7, which is the number of parameters in the classic Bouc-Wen model. In this thesis the population size is set to be 5 times the dimensions ($N = 5*D$). This is to keep the balance between large populations/fewer generations versus smaller populations/many generations. There will be an optimal setting to give fewest overall functions evaluation, on average. This will depend upon application but population sizes between $3*D$ and $10*D$ are generally recommended [88], [106].

A.2 Evaluation

The vectors that were created in the population matrix are evaluated to give a fitness vector or cost vector (maximisation or minimisation). This will evaluate the chosen model with parameters from the vectors to give a predicted response from the model. This process is the real application dependant part of the algorithm and may be very time-consuming.

The objective functions will then be evaluated via a normalised mean-square error function from the real response against the predicted response. The objective function in this thesis is the cost function as it is a minimisation problem as shown in Equation A.1. A cost value of less than 5 shows that the parameter estimation is good and a value of less than 1 is considered as excellent [25].

$$cost = \frac{100}{N\sigma_{u^2}} \sum_1^N (u_i - u_{REAL_i})^2 \tag{A.1}$$

Where N is the total number of population
σ_u is the variance of real response
u_i is the predicted response
u_{REAL_i} is the real response

A.3 Mutation

A mutation matrix is then created from the parent matrix using mutation strategies. Mutation is the creation of different variations of the solution with values close to the parent vector by mixing multiple random parent vectors, best parent vectors or current parent vectors with each other and including a multiplier of the mutation factor, *Fr*. The mutation matrix will then be used in the crossover procedure to give diversity to the trial vectors.

In [81], DE was initially introduced with only one mutation strategy which is Rand/1 as illustrated in Figure A.1. Five of the earlier mutation strategies for DE are given below [105], [107].

Rand/1 : $v_{i,G} = x_{r_1,G} + Fr(x_{r_2,G} - x_{r_3,G})$

Rand/2 : $v_{i,G} = x_{r_1,G} + Fr\left(x_{r_2,G} - x_{r_3,G}\right) + Fr(x_{r_4,G} - x_{r_5,G})$

Best/1 : $v_{i,G} = x_{best,G} + Fr(x_{r_1,G} - x_{r_2,G})$

Best/2 : $v_{i,G} = x_{best,G} + Fr\left(x_{r_1,G} - x_{r_2,G}\right) + Fr(x_{r_3,G} - x_{r_4,G})$

Current to Best/1 : $v_{i,G} = x_{i,G} + Fr\left(x_{best,G} - x_{r_i,G}\right) + Fr(x_{r_1,G} - x_{r_2,G})$

Where $v_{i,G}$ is the current trial vector (*i*th row) at generation G

$x_{r_1,G}$ to $x_{r_5,G}$ are randomly chosen vectors from the parent matrix at generation G

$x_{best,G}$ is the best vector from parent matrix that gives the lowest objective function value at generation G

$x_{i,G}$ is the current vector from the parent matrix (*i*th row) at generation G

A.3 Crossover

To create diversity in the trial matrix, a population of trial vectors is created from combinations of two vectors which are the parent vectors and the mutation vectors, and is obtained via a crossover process. This process is imitating nature where a child inherits both DNA from the mother and father. In this

work uniform crossover {0,1} is used. Uniform crossover decides which of the two vectors, contributes to each chromosome of the trial vector by a series of D – 1 binomial experiments. Each experiment is mediated by a crossover ratio, *Cr* (where $0 < Cr < 1$). If a randomly generated number from the uniform distribution is less than *Cr*, the trial vector takes its parameters from the mutation vector. Otherwise the parameter comes from the parent vector. So if $Cr = 1$, the trial vector will always come from the mutation vector, whilst when $Cr = 0$, the trial vector will always come from the parent. To avoid non-mixing or stagnant generation, even with $Cr = 0$, at least one value in the trial vector will always be drawn from the mutation vector pool.

A.4 Selection

Selection is when a new population matrix for the next generation is created. The winner between the parent vectors and trial vectors dependent on the objective function score will move forward to be part of the parent vectors in the next generation population matrix.

A.5 Self-Adaptive Differential Evolution

Self-Adaptive Differential Evolution (SADE) is an extension of DE. It was introduced in 2005 in a special session on real parameter optimisation of the IEEE Congress on Evolutionary Computation [82]. The rationale behind SADE is that it has the ability to alter its behaviour mid-operation, in order to improve its efficiency and overall chances of successfully finding the global optimum for a particular problem. It achieves this by using multiple mutation strategies and automatically selects the best strategies during different periods of the optimisation. The mutation factor, *Fr* and crossover ratio, *Cr* are also allowed to change for improved efficiency. The mutation strategies, Fr and Cr behaviours are recorded during the reporting process to be assessed and then altered to adapt for this purpose.

As discussed above, optimisation with DE requires the specification of two hyperparameters, *Cr* and *Fr* and the selection of one of the strategies of mutations. The success of the technique will be dependent upon the choice of values. In the case of Self-Adaptive Differential Evolution (SADE), the expectations using this method is that the hyperparameters will gradually adapt themselves from the

initial values to a value which gives a better survival rate of the trial matrix. In the code, *Cr* and *Fr* are started at the suggested value of 0.5 and 0.9. These are then updated every 10 generations to allow fair amount of successful values and does not burden the algorithm with rapid changes in the hyperparameters. The updating is done by selecting all successful values of *Cr* and *Fr*, which are the values of *Cr* and *Fr* that results in an improved solution - where the trial vector wins over the parent vector. The mean of all the successful values is taken as the value of *Cr* and *Fr* for the next 10 generations.

As for the strategies, SADE allows several strategies to be employed. This thesis uses the same four mutation strategies that were used in [25]:

Rand/1 : $v_{i,G} = x_{r_1,G} + Fr(x_{r_2,G} - x_{r_3,G})$

Rand/2 : $v_{i,G} = x_{r_1,G} + Fr\left(x_{r_2,G} - x_{r_3,G}\right) + Fr(x_{r_4,G} - x_{r_5,G})$

Current to Best/2 : $v_{i,G} = x_{i,G} + Fr\left(x_{best,G} - x_{r_i,G}\right) + Fr\left(x_{r_1,G} - x_{r_2,G}\right) + Fr\left(x_{r_3,G} - x_{r_4,G}\right)$

Current to Rand/1 : $v_{i,G} = x_{i,G} + Fr\left(x_{r_3,G} - x_{r_i,G}\right) + Fr\left(x_{r_1,G} - x_{r_2,G}\right)$

The mutation strategies will initially be selected using a "roulette-wheel" approach with each strategy having equal probability of selection. After a set amount of generations, (this thesis uses 20 initial generations), the probability of each of the strategies will be recalculated according to the number of successful trials for that strategy divided by the number of times that strategy was selected, thereby giving a bias towards the most successful strategies. After the first initial update, the strategy probabilities are updated at every generation according to Equation (A.2).

$$p_i = \frac{S_i success}{S_i success + S_i fail} \tag{A.2}$$

For illustration on how DE suffers from poor choice of hyperparameter and a limited mutation strategy compared to SADE which is able to adapt, 20 runs of DE and SADE was used to estimate the parameter values of a Bouc-Wen model. The hyperparameter settings for DE are as suggested in

Reference [25], with *Cr* = 0.5 and *Fr* = 0.9. For the SADE *Cr* and *Fr* are started with the same values. The maximum generations are limited to 1000 to give ample time for both algorithms to work.

Both DE and SADE yielded good estimates with low objective functions, as expected. Figure A.3(a) and Figure A.3(b) show how the DE and SADE perform to reduce the mean population cost and best population cost against the number of generations respectively. The plots are limited to a cost value below 5 MSE, which demonstrates good parameter estimation. The plots show that for this particular model, both DE and SADE would quickly drop to below a cost value of 5 MSE within 50 generations. DE then starts to take hundreds of generations to find another solution that improves the cost value. For DE, although the mean cost decreases gradually, the best cost starts to plateau. SADE on the other hand, does not show this 'lag' in finding the next solution and keeps improving rapidly. This is where the *Cr*, *Fr* and strategy choices are adapting to help the algorithm to expedite the estimation process.

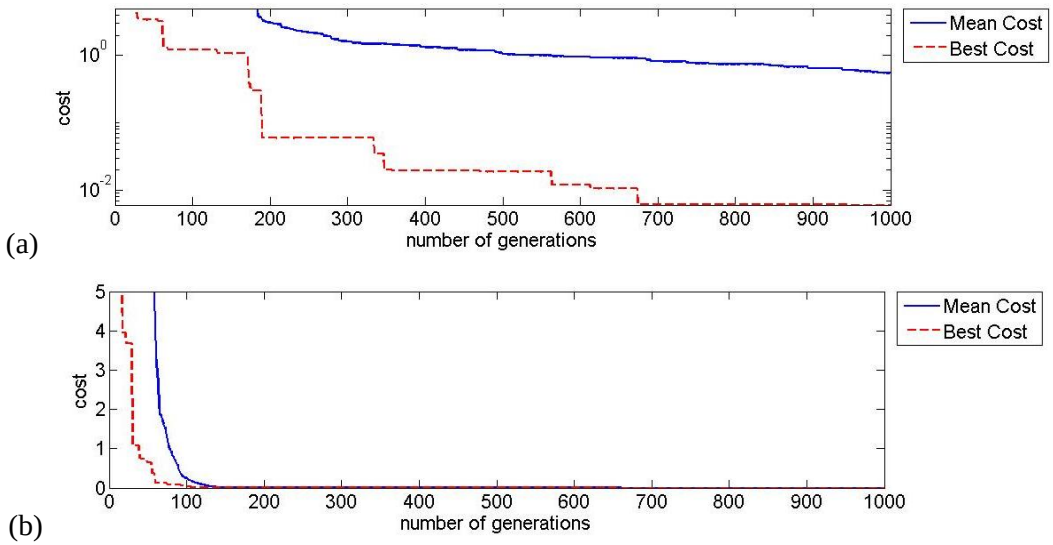

Figure A.3: (a) Differential evolution cost plot (b) Self-adaptive differential evolution cost plot